

**Investigating mechanisms of
aggrephagy flux using small molecules:
Potential implications in
neurodegeneration**

**Thesis submitted for the degree of
DOCTOR OF PHILOSOPHY**

by

S N Suresh



Autophagy Laboratory

Molecular Biology and Genetics Unit

Jawaharlal Nehru Centre for Advanced Scientific Research

Bangalore- 560064 (INDIA)

February, 2018

CERTIFICATE

This is to certify that work described in this thesis entitled “**Investigating mechanisms of aggrephagy flux using small molecules: Potential implications in neurodegeneration**” is the result of investigations carried out by Mr. S N Suresh in Autophagy lab, Molecular Biology and Genetics Unit, Jawaharlal Nehru Centre for Advanced Scientific Research, Bangalore, India, under my guidance and that the results presented here have previously not formed the basis for the award of any other diploma, degree or fellowship

RAVI MANJITHAYA
(Research Supervisor)

Associate Professor
Molecular Biology and Genetics Unit
Associate Faculty, NeuroScience Unit
Jawaharlal Nehru Centre for Advanced Scientific Research
Jakkur, Bangalore 560 064 INDIA

Date:

DECLARATION

I hereby declare that the thesis entitled “**Investigating mechanisms of aggrephagy flux using small molecules: Potential implications in neurodegeneration**” is an authentic record of research work carried out by me, under the guidance of Dr. Ravi Manjithaya at Autophagy lab, Molecular Biology and Genetics Unit, Jawaharlal Nehru Centre for Advanced Scientific Research, Bangalore.

In keeping with the norm of reporting scientific observations, due acknowledgement has been given whenever work based on the findings of other investigators has been cited. Any omission owing to oversight or misjudgement is regretted.

S N Suresh

Bangalore, India.

Date:

To

My family....

Acknowledgement

This work was made possible only with the tremendous and overwhelming support from many generous people.

First, I am extremely fortunate to have Dr. Ravi Manjithaya as my research supervisor who has been an extremely motivating, enthusiastic scientific guide. I am thankful to him for providing the intellectual freedom, cultivating scientific rigor. I am deeply indebted to him for training me all aspects of science such as framing the research problem, designing and executing experiments, troubleshooting, writing and publishing manuscripts. I still remember my experiment when I joined the lab was to perform 50 PCR reactions simultaneously with him. I can recollect many such incidents. There are all memories that I will always cherish! He has been extremely supportive and positive during all my low times (from my health to unjustified criticism from editors and reviewers) and never let my moral go down. He not only inspires you with his scientific abilities but also with his people management skills.

I want to thank all my enthusiastic collaborators: Dr. Phalguni Anand Alladi (NIMHANS), Dr. James Clement Chelliah, Dr. Govindaraju and Dr. Taslim Syed Arif (C-CAMP) to make this work possible.

I want to thank Aparna ma'am for her sincere efforts towards reading this entire thesis and manuscripts so patiently and providing suggestions. I thank Aditya for making the lab dinners and outings so pleasant with his presence. I want to thank Dr. G R Ramesh sir for teaching me how to use pipette and introducing me to the benchwork (This environment is totally new as I was from B.Sc agriculture background). My first year training period by him during Integrated PhD has immensely helped me to cope with the lab projects. He would patiently forgive all our trivial mistakes in experiments and correcting them.

I want to thank Prof. Hemalatha Balaram for accommodating me in her laboratory for my lab rotation project.

I am grateful to Prof. Sheeba Vasu for being my external examiner and providing the constructive inputs for my work.

I thank the present and past chairperson of MBGU: Prof. Ranga Uday Kumar and Prof. Anuranjan Anand for creating the vibrant scientific environment in our department.

I had an opportunity to interact with Prof. MRS Rao and immensely thankful to him for critical inputs and suggestions for my work. I acknowledge all MBGU faculties: Prof. Namita Surolia, Prof. Tapas Kumar Kundu, Prof. Maneesha Inamdar and Prof. Kaustuv Sanyal for their course works and their suggestions during annual work presentation.

I want to thank Dr. Aravinda Chavalmame who taught me the cell culture, animal work and giving the experimental suggestions. He is very meticulous and always an inspiration. I enjoyed the numerous brainstorming sessions with him over coffee.

I thank Dr. Malini Pillai for her cell culture tips due to her immense experience. She is very knowledgeable like Dr. Aravinda and had a wonderful discussions on a range of topics.

I am immensely thankful to Vidyadhara and Aphan from NIMHANS for their help in animal work. Without them, animal work would not have been possible.

I want to thank Dr. Sreedevi for her friendly gesture and our temple visits.

I want to thank immensely Dr. Lakshmi ma'am for her timely help in many aspects: motivating, attending my thesis colloquium rehearsals, scientific discussions and giving critical inputs for my thesis.

I had an opportunity to work with Shashank Rai, Abhik Paul and Meenakshi and their help is acknowledged.

I want to thank my junior Veena for being critical in my work presentations and her suggestions.

I want to acknowledge trainees and lab rotation students with whom I enjoyed teaching: Neha, Kanika, Greg, Anindita and Swati.

I want to thank all present and past members of autophagy lab for creating a lively environment: Gaurav, Piyush, Sunaina, Somya, Vishwa, Anushka, Banu, Cuckoo, Mirudhula, Vidya, Dr. Mamta, Srikanth, Shreyas, Lakshmeesha, Arpitha, Pallabi, Lalitha, Amol, Sarika, Dr. Mayur, Vijay.

I want to thank Ramjee for his timely help and maintaining wellness of the lab.

I thank MBGU-FACS facility and their associated personnel's: Prof. Ranga Uday Kumar (FACS In-Charge), Dr. Uttara, Swaroopa and Dr. Narendra.

I want to thank Dr. Prakash and Vasanth from animal house facility for their immense help in conducting our animal experiments.

I want to thank MBGU confocal facility and Suma ma'am.

I want to thank JNCASR hostel, library, Dhanvantari, administrative and academic sections for their indispensable role in completing my tenure.

I am immensely thankful to JNCASR for funding throughout my tenure.

I thank all my batchmates: Sunaina, Vikas, Lakshmi, Shweta, Surubhi, Amrutha, Malini, Arpit and Vijayanthi.

I thank all my JNCASR friends: Gopal, Kiruthika, Gowsica, Prabhu, Ram, Vijay A, Lakshmeesha, Amrutha, Vijay J.

I thank all my MBGU and NSU friends and colleagues for their inputs and fruitful interactions.

My sincere apologies to friends and people if I miss any of your names in my acknowledgement.

I want to thank all my undergraduate friends for their moral support.

Last but not the least, I am extremely lucky and fortunate to have such a supportive parents, brother, sister in law and Kanishya and without whom my journey till now would not have been possible. I can't thank them enough for that. I want to thank Ramee who has been extremely supportive throughout my journey and I am deeply indebted for his encouragement especially during all my tough and low points of my life.

I thank Almighty God for making everything possible.

S N Suresh

TABLE OF CONTENTS

Abbreviations	i
Synopsis	v
List of publications and patents	xi
Chapter 1: Introduction	1
Chapter 2: Materials and methods	41
Chapter 3: A novel autophagy modulator 6-Bio ameliorates SNCA/α-synuclein toxicity	55
Chapter 4: Modulation of autophagy by a small molecule inverse agonist of ERRα is neuroprotective	95
Chapter 5: Novel small molecule autophagy modulators AGK2 and PD180970 are neuroprotective	135
Chapter 6: A novel small molecule autophagy modulator TGR 63 ameliorates Parkinsonism	161
Chapter 7: Rationally designed peptidomimetic modulators of $a\beta$ toxicity in Alzheimer's disease	183
Chapter 8: Summary and future directions	193
Reprints of publications	203
Permission letter from journal for image replication	244

Abbreviations

A ₆₀₀	Absorbance at 600 nm
AD	Alzheimer disease
ALS	Amylotrophic lateral sclerosis
3-MA	3-methyladenine
A ₆₀₀	absorbance at 600 nm
DA	dopamine
GFP	green fluorescent protein
HRP	horseradish peroxidase
i.p.	intraperitoneally
LOPAC Compounds	Library of Pharmacologically Active Compounds
MAP1LC3B/LC3B beta	microtubuleassociated protein 1 light chain 3 beta
MPTP tetrahydropyridine	1-methyl-4-phenyl-1,2,3,6- tetrahydropyridine
PD	Parkinson disease
Pep A	pepstatin A
RFP	red fluorescent protein
SD	standard deviation
SNpc	substantia nigra pars compacta
TH	tyrosine hydroxylase
CMA	Chaperone mediated autophagy

DTT	Dithiothretol
FDA	Food and drug administration
GFP	Green fluorescent protein
GM	Growth medium
HD	Huntington disease
HTS	High-throughput screen
PD	Parkinson disease
RFP	Red fluorescent protein
SD	Standard deviation
SEM	Standard error mean

Thesis Synopsis

Investigating mechanisms of aggrephagy flux using small molecules: Potential implications in neurodegeneration

Submitted by

S N Suresh

Autophagy Laboratory

Molecular Biology and Genetics Unit

Jawaharlal Nehru Centre for Advanced Scientific Research

Jakkur, Bangalore-560064, India

Thesis Advisor: Dr. Ravi Manjithaya

Investigating mechanisms of aggrephagy flux using small molecules: Potential implications in neurodegeneration

Introduction

Macroautophagy (herein autophagy) is an evolutionarily conserved intracellular degradation pathway that delivers cytoplasmic contents to vacuole/lysosome for its effective clearance. It is an essential pathway to maintain the cellular proteostasis and overall homeostasis. Autophagy is also crucial to protect the cells from accumulation of misfolded toxic protein aggregates. Thus, aggrephagy is a specific autophagy pathway that selectively captures protein aggregates to enable them for lysosomal mediated degradation¹. Presence of toxic protein aggregates is the hallmark of many neurodegenerative diseases such as Alzheimer's, Parkinson's, Huntington's and Amyotrophic lateral sclerosis². These misfolded protein aggregates are toxic, and the consequence of this cytopathic effect is even more profound in the case of neurons as they are mostly non-dividing and also indispensable. One of the cellular mechanisms to tag the misfolded protein aggregates is to get them ubiquitinated. These are then recognized by adaptor proteins such as p62, NBR1, NDP52, optineurin and tollip². These adaptors bind to ubiquitinated aggregates(cargo) at one end and LC3 (autophagy protein) at the other end, aiding formation of autophagosomes. The autophagosomes then sequester these aggregates from the cytoplasm and eventually fuse with lysosome to degrade the captured cargo.

Aim and scope of the study

In neurodegeneration, autophagy is dysfunctional as protein aggregates trap autophagy proteins with them². Also, autophagy functionality declines with age and might contribute to late onset of neurodegeneration³. Interestingly, the autophagy knock out (*Atg5^{-/-}*) mice manifest neurodegeneration as they accumulate ubiquitin positive protein aggregates in different regions of the brain with concomitant motor deficits. On the other hand, the increase of autophagy flux (e.g., through overexpression of *Atg5*) displays enhanced clearance of p62 adaptor (and presumably its cargo such as ubiquitinated protein aggregates) with concomitant extension of life span of mice significantly⁴. Pharmacological upregulation of autophagy mitigates the

proteotoxicity and is beneficial in neurodegeneration⁵. Although proof-of-principle experiments exist, several vital questions remain unanswered, such as, what stage of autophagy is rate limiting or crucial pertaining to clearance of the toxic protein aggregates. Thus, further studies to probe the mechanisms of autophagy are essential to realize the therapeutic potential of this pathway in curbing neurodegeneration.

With this background, we set our aims for our study with following objectives,

1. Screening and identifying small molecule autophagy modulators using proteotoxicity models.
2. Elucidate the mechanisms of autophagy using these small molecules.
3. Evaluate the neuroprotective potential of small molecules in preclinical mouse model of Parkinson's disease (PD).

The chapters are divided to address these important questions in the field of autophagy and neurodegeneration.

Chapter 1 is a review of literature about the role of autophagy and autophagy in proteotoxicity related diseases such as neurodegeneration. In these disorders, in addition to the toxic accumulation or overproduction of protein aggregates, autophagy is dysfunctional and detailing its underlying causes is essential to understand these disease manifestations. Detailed description of autophagy pathway and its regulation during pathological conditions will be discussed. Importantly, the upregulation of autophagy by either genetic or pharmacological means to combat neurodegeneration by clearing the toxic protein aggregates is also highlighted. In the end, the current and future directions of this burgeoning field is summarized.

Chapter 2 describes materials and methods involved in this study.

Chapter 3 describes a novel autophagy modulator, 6-Bio and its potential to ameliorate SNCA/ α -synuclein toxicity. Parkinson disease is a life-threatening neurodegenerative movement disorder with unmet therapeutic intervention. We have identified a small molecule autophagy modulator, 6-Bio that shows clearance of toxic SNCA/ α -synuclein (a protein implicated in synucleopathies) aggregates in yeast and mammalian cell lines. 6-Bio induces autophagy and dramatically enhances autolysosome formation resulting in SNCA degradation. Importantly, when tested in

a preclinical mouse model of PD, 6-Bio also induced autophagy in dopaminergic neurons of mice midbrain with a concomitant decrease in toxic protein aggregates. Furthermore, immunohistology and behavior analyses revealed a neuroprotective function for 6-Bio. Overall, these results suggest that 6-Bio could be a potential therapeutic candidate for protein conformational disorders.

Chapter 4 illustrates a new function for estrogen related receptor alpha ($ERR\alpha$) in aggrephagy. $ERR\alpha$ negatively regulates autophagy and its small molecule inverse agonist (XCT 790) is neuroprotective. We initially identified XCT 790 in a screen for small molecule modulators for aggrephagy, that cleared α -synuclein aggregates in an autophagy dependent, but an MTOR independent manner. Interestingly, this mTOR independent XCT 790 modulation of autophagy is not mediated by AMPK. $ERR\alpha$ keeps autophagy flux in check by inhibiting autophagosome formation. XCT 790 modulates autophagosome formation in an $ERR\alpha$ dependent manner as validated by over expression (autophagy inhibited) and RNAi mediated knockdown (autophagy induced) approaches. Furthermore, we show that in a basal state, $ERR\alpha$ is localized on to the autophagosomes and upon autophagy induction by XCT 790, this localization is lost and is accompanied with an increase in autophagy flux. Additionally, in a preclinical mouse model of PD, XCT 790 exerted neuroprotective effects in the dopaminergic neurons of brain by inducing autophagy to clear toxic protein aggregates and ameliorated motor co-ordination deficits.

Chapter 5 is about the autophagy modulator TGS 63 that is neuroprotective and attempts at its target identification. Through a small molecule screen, we identified a small molecule C1, that mitigates α -synuclein and β -amyloid mediated toxicities in yeast models of proteotoxicity. SAR (Structure Activity Relationship) studies of C1 identified TGS 63 as the most potent small molecule that curbs proteotoxicity in autophagy-dependent manner. It induces autophagy in nutrient-rich conditions, augments starvation-induced autophagy and clears toxic protein aggregates. In mammalian cells, TGS 63 induces autophagy flux, by promoting autolysosome formation in an MTOR independent manner. Furthermore, TGS 63 is neuroprotective by inducing autophagy to clear toxic protein aggregates in the preclinical mouse model of PD. It also ameliorates the behavioral deficits observed in the mouse model of PD. As the target of TGS 63 is unknown, using click chemistry

based methods, we have identified a specific subset of proteins that interact with TGS 63. Further attempts at validating the potential target(s) is described.

Chapter 6 describes the role of two small molecules AGK2 and PD 180970 in modulating autophagy in various models such as yeast, mammalian cells and mouse. In a yeast model of proteotoxicity, these small molecules rescue the α -synuclein mediated toxicity in an autophagy dependent manner. Like in yeast, they induce autophagy flux in mammalian cells. PD 180970 enhances autophagosomes formation whereas AGK2 induced autolysosome formation. They were also cytoprotective towards the SH-SY5Y neuroblastoma cells when challenged with α -synuclein mediated toxicity. In the preclinical mouse model of PD, PD 180970 is neuroprotective as it mitigates the motor co-ordination impairments by inducing autophagy to degrade the toxic misfolded protein aggregates in brain.

Chapter 7 is about peptidomimetic modulators of Amyloid Beta ($A\beta$) toxicity in Alzheimer's disease through autophagy. This chapter describes the investigation of peptidomimetics in modulating autophagy in the yeast model of β -amyloid proteotoxicity. The peptidomimetics were designed to solubilize β -amyloid *in vitro*, and we tested for their solubilizing ability in the yeast cells that overexpress β -amyloid. Initial results reveal that these peptidomimetics curb the β -amyloid mediated toxicity in an autophagy dependent manner. Microscopic analyses revealed that, these peptidomimetics clear toxic β -amyloid aggregates in the wild-type cells overexpressing β -amyloid but not in the autophagy mutant. Toxic oligomers and aggregates are substrates for autophagy. Our results suggest that the fibrils solubilized by peptidomimetics could be degraded by autophagy mechanistically to alleviate the β -amyloid toxicity.

Chapter 8 encompasses overall discussion of the work described in the preceding chapters and proposes future directions. In summary, we identified several novel small molecule autophagy modulators such as 6-Bio, XCT 790, AGK2, PD180970 and TGS 63. By employing these small molecules, we unveiled new molecular players such as $ERR\alpha$ and $GSK3\beta$ in autophagy. Surprisingly, both of these negatively regulate autophagy that might be a prerequisite to maintain a steady state of basal autophagy flux during normal growing conditions. We attempted to identify the target of TGS 63 that might uncover a new player for autophagy. All the

small molecules are neuroprotective in mouse model of PD. In future, the possible negative regulatory mechanism(s) will be probed further to understand how autophagy is tightly regulated to maintain cellular homeostasis.

References

1. Klionsky DJ. Autophagy: from phenomenology to molecular understanding in less than a decade. *Nat Rev Mol Cell Biol* 2007; 8:931-7.
2. Nixon RA. The role of autophagy in neurodegenerative disease. *Nat Med* 2013; 19:983-97.
3. Hara T, Nakamura K, Matsui M, Yamamoto A, Nakahara Y, Suzuki-Migishima R, Yokoyama M, Mishima K, Saito I, Okano H, et al. Suppression of basal autophagy in neural cells causes neurodegenerative disease in mice. *Nature* 2006; 441:885-9.
4. Pyo JO, Yoo SM, Ahn HH, Nah J, Hong SH, Kam TI, Jung S, Jung YK. Overexpression of Atg5 in mice activates autophagy and extends lifespan. *Nat Commun* 2013; 4:2300.
5. Sarkar S, Perlstein EO, Imarisio S, Pineau S, Cordenier A, Maglathlin RL, Webster JA, Lewis TA, O'Kane CJ, Schreiber SL, et al. Small molecules enhance autophagy and reduce toxicity in Huntington's disease models. *Nat Chem Biol* 2007; 3:331-8.

List of publications:

1) **Suresh SN**, Chavalmane AK, D J V, Yarreiphang H, Rai S, Paul A, Clement JP, Alladi PA, Manjithaya R. A novel autophagy modulator 6-Bio ameliorates SNCA/ α -synuclein toxicity. *Autophagy*. 2017 Jul 3;13(7):1221-1234.

2) Rajasekhar K, **Suresh SN**, Manjithaya R, Govindaraju T. Rationally designed peptidomimetic modulators of $\alpha\beta$ toxicity in Alzheimer's disease. *Sci Rep*. 2015 Jan 30;5:8139.

3) **Suresh SN**, Aravinda K. Chavalmane, Malini Pillai, Veena A, Vidyadhara DJ, Haorei Yarreiphang, Shashank Rai, Abhik Paul, James P Clement, Phalguni Anand Alladi and Ravi Manjithaya. Estrogen related receptor alpha negatively regulates autophagy and its inverse agonist is neuroprotective. (*Manuscript under revision*)

4) **Suresh SN** et al., Novel MTOR independent modulators AGK2 and PD 180970 are neuroprotective through regulating neuroinflammation. (*Manuscript under preparation*)

5) **Suresh SN** et al., A novel small molecule autophagy modulator TGS 63 ameliorates Parkinsonism. (*Manuscript under preparation*)

6) **Suresh SN** et al., Neuroprotective and dopamine derivative of TGS 63, TGS 67 modulates ROS mediated autophagy. (*Manuscript under preparation*)

7) **Suresh SN** et al., Role of autophagy in neurodegeneration. (*Under review, Journal of Genetics*)

8) Kolla Rajasekhar, Nagarjun Narayanaswamy, Piyush Mishra, **Suresh SN**, Manjithaya R. and T. Govindaraju. Synthesis of Hybrid Cyclic Peptoids and Identification of Autophagy Enhancer. *Chem Plus Chem*. 2014 79, 25.

9) Sarika Chinchwadkar, Sreedevi Padmanabhan, Piyush Mishra, Sunaina Singh, **Suresh SN** et al Multifaceted Housekeeping Functions of Autophagy. *J Indian Inst Sci*. 2017. 97:79-94.

Patents:

- 1) Indian Patent Application No. 6596/CHE/2015 Title: Modulator and modulation of autophagy and applications thereof. *Indian patent application filed*.
- 2) Prophylactic and therapeutic intervention for neurodegeneration and associated disorders through reduction of neuroinflammation. *Patent filed*.

Chapter 1

Introduction

Note:

**A part of this chapter is under review for a publication in
*Journal of Genetics.***

Introduction

Neurodegenerative diseases (ND) are life threatening with no cure. One of the main pathophysiological hallmarks of neurodegeneration is the presence of misfolded toxic protein aggregates in neurons¹. Tau/ β -amyloid, α -synuclein, Huntingtin polyQ repeats, fused with sarcoma (FUS)/ TAR DNA-binding protein 43 (TDP43)/ superoxide dismutase (SOD1) are misfolded protein aggregates primarily implicated in Alzheimer's (AD)², Parkinson's (PD)³, Huntington's (HD)⁴ and Amyotrophic lateral sclerosis (ALS)⁵ respectively.

Alzheimer's disease (AD) is the most common form of dementia⁶. AD is characterized by presence of two hallmark features 1) extracellular amyloid plaques and 2) intracellular tau aggregates⁷. The amyloid plaque encompasses toxic, β -amyloid species generated from enzymatic cleavage of amyloid precursor protein (APP)⁸. When tau proteins are hyperphosphorylated by various enzymes, the tau aggregates or neurofibrillary tangles are formed⁹.

Parkinson's disease (PD) is the second most common neurodegenerative disorder¹⁰. Presence of Lewy bodies, primarily composed of misfolded, toxic α -synuclein protein aggregates is a hallmark of PD¹¹. This accumulation of toxic aggregates in dopaminergic neurons of Substantia Nigra pars compacta (SNpc) leads to its death that manifests the pathogenesis^{12, 13}. Most clinical cases of PD are sporadic in nature. Mutations in genes such as SNCA, Parkin, PINK1 (PTEN-induced putative kinase 1) and LRRK2 (leucine-rich repeat kinase 2) also manifests PD¹⁴. The hereditary cases for PD are less profound compared to sporadic ones among populations.

Huntington's disease (HD) is an autosomal dominant disease caused by the abnormal expansion of polyglutamine (CAG) repeats of the Huntingtin (HTT) gene¹⁵. The resultant protein leads to the formation of toxic aggregates in striatum¹⁶. The penetrance of the mutated huntingtin expanded polyQ repeats is very high¹⁷. The gross behavioral symptoms of HD are loss of motor co-ordination and cognitive dysfunction¹⁷. The polyglutamine repeats are around 36 in normal individuals whereas 36 to 130 lead to pathophysiological conditions. The disease is a progressive one with an increase in number of polyglutamine repeats; for instance, higher number of polyglutamine repeats leads to early onset of disease¹⁷.

Lou Gehrig's disease or Amyotrophic Lateral Sclerosis (ALS) is a motor neuron disease caused by the loss of motor neurons in both brain and spinal cord¹⁸. Most clinical cases are reported to be sporadic in nature with ~5-10% cases being genetic¹⁹. This disease is characterized by the presence of protein aggregates such as SOD1/TDP43/FUS¹⁸.

The accumulation of toxic misfolded protein aggregates in neurons exerts toxicity and compromised viability that are commonly associated with cellular pathophysiological phenomena of above-mentioned neurodegeneration¹⁶. The main causes for protein aggregation are rarely genetic but mostly sporadic in nature. Neurons are post-mitotic specialized cells and so cannot divide further to dilute out the aggregates unlike other cell types²⁰. Furthermore, owing to the neuronal specialized shapes such as dendrites and axons, the damaged organelles or misfolded proteins tend to accumulate over time²⁰. Importantly, the neurogenesis event is sparse and thus unable to replace the dead neurons²¹. Considering this, neurons tremendously rely on protein quality control machineries for their maintenance of homeostasis²². Loss of such mechanism can also spontaneously lead to the development of ND²³. Sequestration of other intrinsically disordered proteins into protein aggregates is one of the widely proposed pathophysiological mechanisms underlying aggregate toxicity²⁰. By doing so, the participating proteins in multiple essential cellular pathways are perturbed making the overall homeostasis compromised leading to detrimental effect.

Cellular homeostasis is achieved through a balance of anabolic and catabolic states. Cells possess several quality control mechanisms to identify, correct or remove dysfunctional or potential toxic cellular components such as proteins and organelles. For example, inside cells, at steady state, misfolded proteins are formed continuously and are fixed by chaperones or cleared via the ubiquitin proteasome system and autophagy related pathways²². This maintains the proteostatic equilibrium in cells. Altered cellular states resulting from expression of pathogenic levels or mutant forms of aggregate prone proteins overwhelm these quality control systems and their buildup eventually can result in cell death^{24,25}. This is the fate of brain cells in ND. We discuss this proteostatic central view as a cause for ND and the potential reasons behind the failure of quality control systems with emphasis on an autophagy related pathway, aggregophagy²⁵.

Proteostasis

Protein quality control machineries ensure the proper folding of newly synthesized proteins for their distinct function. This process is critical as 30% of these new proteins are prone to

misfolding²⁶. The cellular quality control measures include unfolding, refolding and/or degradation of the misfolded proteins²⁴. Not surprisingly, failure of protein quality control poses a threat to the cellular vitality²². This qualitative process of maintaining the homeostasis of intracellular pool of functional and “healthy” proteins is called proteostasis. Proteostasis as a function for cell survival becomes even more critical for those cells such as neurons that cannot divide and thus dilute out the toxic protein aggregates²². In addition, with age, the neuronal proteostatic machineries become incompetent and prone for accumulation of damaged organelles and misfolded proteins^{27,28}.

The presence of misfolded proteins activate chaperones to unfold and refold them in an ATP-dependent manner. Misfolded proteins induce heat shock response (HSR) and heat shock (HS) transcription factor HSF-1 that includes the upregulation of heat shock cognate protein (Hsc70)²⁹. The aim of enhancing chaperone expression and its activity is to prevent protein aggregation. In certain scenarios, when protein aggregates overwhelm chaperone capacity, the available chaperones themselves get trapped in protein aggregates^{30,31}. Subsequently, these events also aggravate disease pathogenesis. An additional mechanism that has been recently described, identifies misfolded proteins as early as they are translating and then marks them for degradation. Such nascent misfolded polypeptides are ubiquitinated at K-48 residue as a degradation mark in a process termed as cotranslational ubiquitination (CTU)³². The polypeptide with this mark will be acted upon by proteasome for its effective degradation. CTU happens within the active translation complexes³².

At the organellar level, accumulation of misfolded proteins inside lumen of endoplasmic reticulum (ER) induces ER stress, which triggers one of the vital cellular adaptive mechanisms known as unfolded protein response (UPR)³³. UPR leads to suppression of active protein translation, increases ER chaperone accumulation to unfold and/or degrade these proteins to ameliorate the proteotoxicity³⁴. Postmortem brain analyses of AD, PD and HD have revealed the correlation of UPR markers with protein aggregation and onset of disease pathogenesis³⁵.

The fate of misfolded proteins not refolded by chaperones is marked for degradation through ubiquitin-proteasome system (UPS) and/or autophagy. UPS degrades ubiquitinated, soluble and short-lived proteins. The target protein is tagged by ubiquitin through three enzymatic, namely ubiquitin-activating (E1), -conjugating (E2) and -ligating (E3) reactions³⁶. Ubiquitin is attached through its carboxyl residue to a specific lysine residue through isopeptide linkage. One ubiquitin molecule is a target for another ubiquitin

molecule and forms a polyubiquitin chain at its lysine residues at 48, 63 or at N-terminal methionine residue³⁷. The polyubiquitin signal at K48 serves as a proteasome degradation signal whereas K63 and N-terminal methionine signals serve other functions³⁷. It is also proposed that K63 polyubiquitination may target a protein to autophagy but the exact mechanism is unclear.

UPS has been shown to degrade several neurodegenerative disease related proteins such as tau, SOD1 and α -synuclein³⁶. Inhibiting UPS causes disease related proteins to aggregate and form inclusion bodies inside cells. Thus, UPS is essential for cells to prevent toxic protein aggregate formation³⁸. It is believed that larger aggregates that cannot be resolved by UPS are substrates of the autophagy machinery.

Aggrephagy: definition and modes

In 1960s, the Nobel laureate Christian De Duve observed double membrane vesicles entrapping intracellular organelles and proteins and coined the term “self-eating” or autophagy³⁹. Nobel laureate Yoshinori Ohsumi tapped the power of yeast genetics to elucidate the molecular mechanisms governing autophagy and contributed to discovering its conserved nature from yeast to mammals⁴⁰.

Depending on the distinct molecular mechanisms, autophagy is broadly classified into three types: Macroautophagy, Microautophagy and Chaperone mediated autophagy (CMA). Macroautophagy is the most extensively studied process that has an indispensable role in maintaining cellular and organismal homeostasis. During macroautophagy, a phagophore or isolation membrane is formed and expands to form double membrane autophagosomes that engulfs cellular cargoes. These cargoes are parts of cytosol constituting superfluous organelles, pathogenic organisms, misfolded protein aggregates and/or damaged mitochondria⁴¹. These autophagosomes fuse with lysosomes to form autolysosomes and eventually degrade its intraluminal cargoes. The degraded entities result in building blocks that are recycled back to the cytosol for fueling other cellular pathways. Apart from randomly sequestering portions of cytosol for degradation (general autophagy), macroautophagy can be highly selective in the cargoes it captures. The selective autophagy pathway that is involved in clearance of misfolded protein aggregates is called aggrephagy²⁵. Here, misfolded proteins that are tagged by ubiquitin are recognized by adaptor proteins such as p62, NBR1 and NDP52 which in turn recruit autophagy proteins such as LC3 to facilitate selective capture (**Fig. 1**).

Thus, aggrephagy is a prominent defense mechanism against misfolded protein aggregate mediated cellular toxicity. Microautophagy is the direct uptake of cargo by lysosomes through membrane invagination. It can also occur through transportation of cargo through late endosomes that is dependent on the chaperone Hsc70. Chaperone Mediated Autophagy (CMA) is the selective degradative process of proteins that involves Hsc70 but is a vesicle independent process. During CMA, the target protein is recognized by Hsc70 through a specific amino acid motif, KFERQ and delivered to lysosome by interacting with LAMP2A in an ATP-dependent manner.

Neurodegeneration model systems as tools to study aggrephagy

Numerous model systems have been utilized to study the aggrephagy and modulate it to clear the protein aggregates. It is important to note that the cellular proteostatic machineries are conserved from simple yeast to higher model such as rodents. I will brief the different model systems used to understand the neurodegeneration pathogenesis with a special emphasis on autophagy.

Yeast

The budding yeast (*Saccharomyces cerevisiae*) is a simple yet powerful tool to study the cellular pathophysiological mechanisms underlying the protein toxicity⁴². It recapitulates the toxicity of protein aggregates as that of neurons. This is because the fundamental cellular features and vital cellular pathways are conserved⁴³. For instance, the membrane-bound organelles such as mitochondria, Golgi, lysosome, endoplasmic reticulum and so on exist in yeast. More importantly, the unfolded protein response is conserved as that of the mammalian cells. The major advantages of yeast are short doubling time, existence of genetic sources, amenable to genetic manipulation and scalable to high throughput genetic and chemical screens. Also, around 3500 genes are found to be homologues to the ones in human cells^{44,45}. Pioneering work by Susan Lindquist and her colleagues have shown that yeast cells expressing aggregate prone genes and their variants that have been identified in ND have been used to understand their pathobiology⁴⁶. The fact that ER-Golgi trafficking defect due to α -synuclein overexpression, can lead to cellular toxicity was first noted in yeast and further validated in mammalian cells^{47,48}. Several studies including ours have identified novel peptidomimetics and small molecule autophagy modulators that ameliorate ND related aggregate proteotoxicity^{43,49,50}. Some of the obvious limitation of the yeast

model is that it cannot recapitulate the complexities of neuronal network and multicellularity that is present at the organ level.

Drosophila melanogaster

It is a multicellular eukaryote that exhibits both histological and behavioral phenotype associated with neurodegeneration. Flies expressing the proteins such as α -synuclein, β -amyloid, polyglutamine repeats and tau recapitulate many of the histological and behavioral disease phenotypes associated with neurodegeneration⁵¹. In this model, the toxic proteins are overexpressed in retina leading to rough-eye phenotype that forms a platform, which is used extensively for genetic and chemical screens⁵². The advantages of working with flies are short doubling time, multicellularity, availability of genetic resources and ability to express proteins in a tissue-specific manner. Also, the fly model can unravel the basic pathophysiological mechanisms underlying neurodegeneration. It is often used synergistically with another disease model to validate the basic mechanisms. For e.g. a small molecule screen performed on fly model identified mGLUR5 (GPCR) as a druggable target that is abundantly expressed in brain⁵³. Recently, regulation of protein QPCT (glutaminyl cyclase) has been shown to curb neurodegeneration symptoms in fly model and mammalian cells⁵⁴.

Caenorhabditis elegans

It is one of the widely used models to study neurodegeneration for more than a decade. Pros are the availability of genetic resources for this tiny transparent animal where all 302 neurons are mapped for their interactions and their short generation time⁵⁵. Genetic strains were constructed that express toxic protein aggregates such as A β , α -synuclein, TDP43 and polyglutamine repeats in either whole body or tissue specific manner. They not only form visible aggregates but also show the behavior phenotype such as paralysis. Numbers of genetic and chemical screens were conducted to identify modulators that rescue the behavioral phenotype. This led to identification of small molecules that cleared toxic protein aggregates and were further validated in higher model systems⁵⁶. Successful genetic screens too have identified many genes such as LRRK2, the reduction of its kinase activity rescued the dopaminergic deficit motor phenotype⁵⁷. Various regulators of HSR have been tested in the worm model to treat proteotoxicity. Its transparent tissue enables for high content imaging. More importantly, they also show typical ageing symptoms making them

an ideal tool to investigate a comprehensively, the interplay of metabolism, ageing and neurodegeneration^{58,59}.

Rodents

It has been one of the widely used models by neurobiology researchers. They often mimic the diverse ND symptoms at both histological and behavioral level. The main advantages are availability and amenable to genetic manipulation that allows researchers to express the protein at endogenous levels in tissue specific manner. Till date, this model has provided significant insights into basic pathophysiological mechanisms of ND and continues to serve as a preclinical drug-testing model for PD, AD, HD and ALS^{60,61}.

The occurrence of neurodegeneration is majorly a sporadic event with poorly understood etiological basis. However, in familial cases of AD, PD, HD and ALS, the genetic mutation(s) are the underlying causes of disease phenotypes and these can be recapitulated in animal models to a great extent.

Mutations in APP and presenilin 1 or 2 genes result in an autosomal dominant form of AD⁶². Recently, a very robust mouse model, 5xFAD, having five familial AD mutations, causing relatively early and aggressive presentation of AD, has been widely used as compared to other models. It recapitulates the following disease phenotypes: β -amyloidosis, plaques, neurite dystrophy, dendritic spine loss, neuroinflammation, neuronal loss and age-dependent cognitive decline. Limitations of these models include the following: a) evidences from positron-emission tomography (PET) suggest that mouse plaques are significantly different from humans biochemically, and b) the neuronal loss is not profound as that of humans⁶².

For the PD model, the transgenics are generated that express causative mutant genes such as α -synuclein, PARKIN, PINK1 and PARK7¹⁴. α -synuclein transgenic mice exhibit Lewy bodies that is the histopathological hallmark of PD. These animals exert age-related progressive movement deficits which is associated with dopaminergic neuronal loss. However, transgenic mutants generated with other mutations do not exert dopaminergic neuronal loss significantly⁶³.

Mutations in genes such as TARDP (TDP-43), FUS and SOD1 drive the familial forms of ALS¹⁸. Mice transgenics overexpressing wild type or mutant TDP-43 proteins cause TDP-43 inclusion bodies and loss of motor neurons with behavioral impairments. In addition,

mice overexpressing mutant SOD-1 develops inclusion bodies, neuronal loss, gliosis, tremor, hindlimb paralysis with significant reduction in lifespan⁶⁴.

Expanded polyglutamine repeats (>36) of Huntingtin gene causes HD. Myriad of transgenic mice with expanded polyQ repeats like R6/1, R6/2 and N171-Q82 have been generated that recapitulate the symptoms of HD. All these models develop aggregate inclusions, neuronal loss and motor-coordination deficits⁶⁵. The most profound HD mouse model is R6/2 that shows aggregate inclusions (around one month), behavioral impairments (~2 months) and eventually dies in 3-4 months of age⁶⁶.

iPSC

iPSC technology enables researchers to generate human specific, disease relevant cell types such as neurons directly from patient fibroblasts. The advancement of gene editing techniques such as CRISPR-Cas9 has simplified genetic knock out/in studies in iPSC-derived neurons to understand the pathogenesis of neurodegeneration. The potential of this model system to shed light on basic disease pathology mechanisms is massive⁵⁶. iPSC lines for AD, PD, Niemann-Pick disease type C and ALS disease have been generated for their biological investigations⁶⁷⁻⁶⁹. Consequently, genetic or small molecule screens can be performed using iPSC. The current limitations are: 1) hurdle in scaling up for high throughput screening due to their relative slow propagation rates, 2) extensive and time-consuming neuronal differentiation protocols. However, they can be used to validate the data generated from non-human disease models. For example, yeast screen yielded the NAB2 compound where it rescued the disease phenotype and validated its disease modifying mechanisms in iPSC⁶⁹.

Current understanding on the mechanistic insights of aggrephagy

These and other model systems have contributed immensely to unravel molecular aspects of the process of aggrephagy and how aggrephagy is perturbed by various protein aggregates is detailed below.

Substrate recognition

Protein aggregate (substrate) recognition by receptors/adaptors such as Alfy, p62/SQSTM1, Optineurin and Cue5/Tollip, is one of the first steps of autophagy for its clearance⁷⁰. The selectivity of autophagic cargo depends on specific receptors/adaptors that recognize it by degradation marks. Autophagic receptors bind to the ubiquitinated substrates through their respective domains to capture the aggregates. They also tether them to autophagic protein

like LC3 to enable autophagosome formation around the aggregates. The brief description pertaining to autophagic receptors are as follows:

Alfy: This multidomain scaffolding protein recognizes ubiquitinated protein aggregates for their clearance. It contains the following domains: 1) Pleckstrin homology (PH)-BEACH domain that binds to p62, 2) FYVE domain for PI3P binding, and 3) WD40 repeats that interacts with Atg5. It colocalizes with ubiquitin positive p62 aggregates⁷¹. It stabilizes the LC3 and p62 interaction and also recruits Atg5 for the formation of autophagosomes that facilitate huntingtin polyQ aggregate clearance⁷².

p62/SQSTM1: p62 is the adaptor for aggrephagy⁷³, mitophagy⁷⁴, pexophagy⁷⁵ and xenophagy⁷⁶. It possesses several domains namely: 1) UBA domain that binds ubiquitin, 2) PB1 domain for aggregation of cargoes, and 3) LC3 Interacting Region(LIR) motif for LC3 binding³⁸. It also has nuclear localization signal (NLS) and nuclear export signal (NES) for nucleocytoplasmic shuttling⁷³. p62 mutations have been linked to sporadic and familial cases of ALS through impaired clearance of TDP-43 and SOD1⁷⁷. In Paget's disease of bone, patients with mutations in p62 are predisposed to ALS, a disease that is characterized by p62 positive inclusions in neurons. Mutant p62 contributes to pathogenesis through multitude of mechanisms and one of them is via over activation of nuclear factor- κ B (NF- κ B) signaling⁷⁸.

Optineurin: It binds to ubiquitinated proteins through its UBA and NF- κ B Essential Modulator (NEMO) domains⁷⁹. On its other end, it binds to LC3 through LIR motif. Genetic mutations of optineurin are also associated with ALS. Optineurin mutation is associated with rare ALS mutations leading to TAR DNA-binding protein 43 (TDP-43) inclusions⁸⁰.

Cue5: Cue5 is a recently identified yeast autophagy receptor that binds to ubiquitin through its CUE domain and Atg8 via its AIM1 and AIM2 motifs⁸¹. Its mammalian homologue is *Tollip* which is essential for the huntingtin polyQ clearance.

Valosin-Containing Protein (VCP): It is a member of AAA+ family of ATPase and is involved in the sorting of ubiquitinated cargoes through endolysosomal pathway. VCP mutation is associated with Paget's disease of bone and Fronto Temporal dementia (FTD). Overexpression or knockdown of VCP in cells leads to appearance of autophagosomes that are immature with accumulation of ubiquitin positive cargoes⁸².

Autophagosome formation

MTOR complex 1 (TORC1) negatively regulates autophagy (**Fig. 1**). Various stimuli in neurons such as ATP, ER stress, and specific amino acids repress TORC1 to activate ULK complex (ULK1, FIP200, ULK2, Atg101 and Atg13)⁸³. Phosphorylation of ULK1 at its active site leads to subsequent phosphorylation of other components of complex for initiating autophagy⁸⁴. Although ULK1 phosphorylation is primarily regulated by TORC1, it can be also independently modulated by AMP-activated protein kinase (AMPK)⁸⁵. Also, ULK1 phosphorylation leads to the translocation of class III PI3 Kinase complex (beclin1, Atg14, Vps15 and Vps34) to isolation membranes (also known as omegasome formation at the ER) by phosphorylating one of its components, AMBRA⁸⁶. Vps34 activity generates phosphatidylinositol-3-phosphate (PI3P) to bind to its effectors such as WIPI1 (WD repeat domain phosphoinositide interacting 1) and WIPI2 (WD repeat domain phosphoinositide interacting 2)⁸⁷. This is to catalyze the ubiquitination like reactions at the isolation membrane that aid autophagosome formation. Atg5-Atg12-Atg16L complex is formed on the isolation membrane in presence of Atg7 and Atg10. This Atg5-Atg12-Atg16L catalyzes the covalent attachment of phosphotidyl ethanolamine to LC3 that facilitates the closure of autophagosome membranes⁸⁸. Atg9 aims to supply membranes for the growing autophagosomes by shuttling from various sources such as endoplasmic reticulum-mitochondria contact sites⁸⁹, Golgi⁹⁰ and plasma membrane⁹¹ to autophagosome formation site. ER has been suggested as a membrane source for autophagosomes formed at synapse but the main source is not yet clear⁹².

In neurons, autophagy induction is still an enigma. Conventionally, the key trigger for autophagy is starvation that induces autophagy in numerous cell types⁹³. However, even 48 hours of starvation did not induce GFP-LC3 puncta in brain but profoundly induced autophagy in the liver⁹⁴. On the other hand, while caloric restriction induced autophagy in cortical, Purkinje and motor neurons, nutrient starvation failed to induce autophagy in cultured hippocampal neurons⁹⁵. These contradicting results may mirror the neuronal specificity in inducing and regulating autophagy. Several studies have shed light about “other” ways of modulating autophagy in the brain.

Recently, it has been shown that neuronal activity such as acute stimuli can trigger autophagy. Upon high frequency stimulation, the Atg8 puncta are increased at neuromuscular junctions (presynapse) in *D. melanogaster*⁹⁶. Although the molecular players and its mechanism(s) are not yet elucidated, calcium signaling can be a key player.

During exocytosis driven action potential, there is a remarkable increase in calcium levels at presynapse⁹⁷. Calcium can either enhance or inhibit autophagy depending on the context and notably calcium responsive proteins are abundant at presynapse. It is noteworthy to mention that investigating calcium-mediated autophagy at presynapse can shed light on the novel mechanistic aspects of neuronal autophagy. Interestingly, the presynaptic resident proteins such as Endophilin A, Bassoon and Synaptojanin 1 regulate autophagy by interacting with autophagy related proteins⁹⁸.

Regulation of protein synthesis by TORC1 is implicated in synaptic plasticity⁹⁹ (**Fig. 2**). However, TORC1 mediated autophagy induction at presynapse has not been studied extensively. Autophagy mediated degradation of GABA receptors and AMPA receptors (that are involved in synaptic plasticity) at post-synapse induce long term depression¹⁰⁰.

In PD model, α -synuclein perturbs Rab1a mediated Atg9 translocation to isolation membrane leading to impairment of omegasome formation⁴⁷. Atg9 trafficking is also abnormal in vacuolar protein sorting-associated protein 35 (VPS35), due to D620N mutation that results in autosomal dominant case of PD¹⁰¹. VPS35 (component of retromer complex) recruits actin nucleation-promoting WASP and Scar homolog (WASH) complex to endosomes. Mutation in VPS35 perturbs this recruitment to cause the abnormal Atg9 trafficking to impair autophagy¹⁰². The E122D Atg5 mutation has been identified in childhood ataxia¹⁰³. This disease is characterized by loss of motor coordination and cerebellar hypoplasia. This mutation decreases the affinity of Atg5 to Atg12 and reduces the autophagosome biogenesis and its flux¹⁰³.

β -propeller protein-associated neurodegeneration (BPAN) and the static encephalopathy of childhood with neurodegeneration in adulthood (SENDA) are caused by *de novo* mutations in WDR45¹⁰⁴ (**Fig. 2**). WDR45 gene encodes WIPI4, the key protein that bridges PI3P production and LC3 lipidation for autophagosome maturation¹⁰⁵. Neuronal specific knockout of WDR45 recapitulates some of the BPAN disease phenotype such as impaired motor coordination, cognitive deficit and axonal swelling with accumulation of ubiquitin positive aggregates¹⁰⁶.

Hexanucleotide repeats in C9ORF72 gene is one of the most common causes of ALS. Different mechanisms have been proposed for this disease pathogenesis and perturbation of autophagy is one of them. C9ORF72 interacts with ULK1 and affects the phagophore initiation complex¹⁰⁷. In addition, C9ORF72 is a part of WD repeat domain 41 (WDR41)

and Smith-Magenis syndrome chromosome region, candidate 8 (SMCR8) complex that is involved in both vesicular trafficking and autophagy. This complex is a guanosine diphosphate (GDP)/guanosine triphosphate (GTP) exchange factor (GEF) that activates the small GTPases Rab39 and Rab8 for autophagosome formation¹⁰⁸.

Wild type huntingtin protein acts as a scaffold for autophagosome formation whereas its mutant fails to recognize the cargo leading to “empty” autophagosomes¹⁰⁹. It also impairs autophagosome transport and further accumulation of autophagic substrates¹¹⁰. Mutant huntingtin interacts with Rhes that is selectively expressed in striatum to inactivate it. Rhes interacts with beclin 1 to induce autophagy by reducing the bcl2-beclin 1 interaction¹¹¹. Furthermore, MTOR is also sequestered in HD and spino-cerebellar ataxia 7 (SCA7)¹¹².

Autophagosome-lysosome fusion

Autophagosomes fuse with lysosomes to generate autolysosomes that digest the toxic protein aggregates. In neurons, autophagosomes generated in axons are transported to the lysosomes that are abundant near perinuclear MicroTubule-Organizing Centre (MTOC). Microtubules and motor proteins such as dynein-dynactin complex are involved in retrograde transport of autophagosomes towards neuronal cell body. Mutations in dynein (axonal Charcot-Marie-Tooth hereditary neuropathy type 2) and dynactin (motor neuron disease) motor protein complexes are implicated in neurodegeneration pathogenesis indicating the importance of retrograde transport of autophagosomes to fuse with lysosomes¹¹³. Interestingly, decreased dynein activity resulted in the accumulation of autophagosomes, autolysosomes and p62 positive inclusions in motor neurons before the onset of symptoms where the neurons degenerate upon clinical manifestations¹¹⁴.

Amphisome formation (a fusion product of endosomes with autophagosome) is perturbed in familial ALS and FTD (Fronto Temporal Dementia) and is associated with loss-of-function mutations in CHMP2B (charged multivesicular body protein 2B). Mutant CHMP2B neurons accumulate ubiquitin positive inclusions by disrupting the activity of ESCRT machinery activity¹¹⁵. Autophagy and endolysosomal pathways have significant crosstalk pertaining to the use of cellular protein machineries. Mutations in an endolysosomal pathway affects autophagy and *vice versa*¹¹⁶. Endosomal maturation protein Rab7 is essential for autophagic flux and its mutation is associated with bone related osteopetrosis (lysosomal perturbation) and neurodegenerative CMT2 (autophagy flux perturbation) diseases¹¹⁷. Furthermore, Rab7 significantly influences lysosome positioning. ALS2 protein

mutation, an activator of Rab5 perturbs ALS2 mediated Rab5 activation that hampers amphisome formation as observed in familial cases of ALS¹¹⁶. Thus, the coordinated crosstalk of endolysosomal and autophagy pathways to clear toxic protein aggregates in healthy cells goes awry in neurodegeneration (**Fig. 1**).

In neuronal specific interferon- β knockout of a transgenic mouse model, the autophagosome-lysosome fusion process is affected with concomitant accumulation of ubiquitin positive inclusion in neurons that lead to motor coordination and behavioral impairments¹¹⁸.

Regulation of lysosomal activity

Autophagosomes fuse with lysosomes for the clearance of its contents (**Fig. 1**). For this process to be efficient, uncompromised lysosomal activity is essential. The lysosomal pH is optimally (~4.5 to 5) maintained by proton pump vacuolar ATPase for the activity of hydrolytic enzymes (proteases, peptidases, lipases and nucleases). Ionic balance of lysosomes is regulated by presence of numerous ion channels (calcium, chloride and potassium). Lysosomal associated membrane protein-1 (LAMP1) and LAMP2 prevents the self-digestion of lysosomes²⁰. The functional integrity of lysosomes is compromised in most neurodegenerative disorders¹¹⁹.

Lysosomes serve as key players in the initial stage of autophagy induction. Upon perceiving the autophagy inducing stimuli, the TORC1 localized on the lysosomal membrane is repressed and that further allows activation of transcription factor EB (TFEB) to translocate to the nucleus. TFEB activates genes involved in lysosomal biogenesis and autophagy process. TORC1 regulation of TFEB is achieved through Rag-GTPase pathway⁹³. TORC1 and TFEB activities are tightly controlled by the presence of intracellular and lysosomal amino acid contents. If amino acids are limiting inside cells, for instance as in starvation, the TORC1 activity is repressed and is followed by translocation of dephosphorylated TFEB to nucleus resulting in upregulation of autophagy. On the other hand, the surplus amino acids lead to reactivation of TORC1 to terminate the autophagy induction¹²⁰. The androgen receptor polyQ repeat mutant (implicated in SBMA), interacts with TFEB and suppresses autophagy at transcription level¹²¹. SCA3 transgenic animals show low levels of sirtuin 1 (deacetylates numerous autophagy and its related proteins), parkin and beclin 1¹²².

Zinc-finger protein with KRAB and SCAN domains 3 (ZKSCAN3) is a repressor of autophagy and has an opposite function to that of TFEB. Inhibition of MTOR enhances

TFEB accumulation in the cytosol. Down regulating ZKSCAN3 induces autophagosome and lysosomal biogenesis¹²³. Apart from this, around 20 different transcription factors are reported to regulate autophagy at gene transcription level depending on the context of stimuli. For instance, p53, forkhead box O3 (FOXO3) and microphthalmia-associated transcription factor (MITF) profoundly affect autophagy gene expression¹²⁴.

Lysosomal storage disorders (LSDs) illustrate the nexus between lysosomal dysfunction and neurodegeneration. In LSDs, the unavailability of functional lysosomal hydrolytic enzymes lead to defective autophagy that manifests disease pathology in brain. In Niemann Pick type C (NPC) disease, the mutations of *NPC1* and/or *NPC2* genes lead to defective cholesterol trafficking where profound autophagic vacuoles are observed in neurons¹²⁵. In neuronal ceroid lipofuscinosis, the mutation in *CLN3* gene reduces autolysosome formation, whereas a Cathepsin D mutation that causes the same disease, decline in lysosomal proteolysis is observed¹²⁶.

Importance of basal autophagy in maintaining neuronal proteostasis

The systemic knockout of essential autophagy genes such as *Atg5* and *Atg7* resulted in neonatal lethality due to starvation^{23,127}.

Interestingly, neuronal specific *Atg5* KO transgenic animals were born normally and also survived neonatal starvation. However, motor behavioral deficits were evident around 14 weeks of age. These animals also displayed partial loss of neurons in cerebellar Purkinje cells and cerebral pyramidal cells. In addition, axonal swelling is noted in various brain sections such as hippocampus, thalamus, pons and reticulate nucleus. Ubiquitin positive inclusions are observed in brain indicating the impaired clearance of proteins by autophagy²³.

In another example of autophagy inhibition specifically in the neurons, neuron specific *Atg7* KO mice were similarly generated. These mice showed retarded growth at P14 and motor behavioral deficits such as tremors and abnormal clasping around P21. Histological analyses revealed cerebral cortex atrophy with complete loss of pyramidal neurons, reduction in Purkinje cells with corresponding increase in glial cells that is a signature of neuronal damage. Ubiquitin positive aggregates are observed at P56 in various brain regions such as cerebral cortex, thalamus, hypothalamus and pontine nuclei. Interestingly, the degree of punctate size is varied across different brain regions indicating the differential response towards ablating autophagy that is governed by multitude of factors such as

intracellular and extracellular milieu, electrical inputs/outputs and on the variation in the levels of autophagy flux across various cell types. Interestingly, the proteasome activity is uncompromised in knockout animals²³.

Systemic overexpression of Atg5, a key autophagy protein in a mice model significantly enhanced the life span of animals by 17.2% through elevated autophagy¹²⁸. Interestingly, the mouse embryonic fibroblasts from Atg5 overexpressing transgenic exert enhanced tolerance to oxidative stress that was autophagy-mediated¹²⁸.

These three studies indicate that basal autophagy is very critical for neuronal proteostasis by degrading the protein aggregates at steady state and manifests neurodegeneration pathogenesis when compromised.

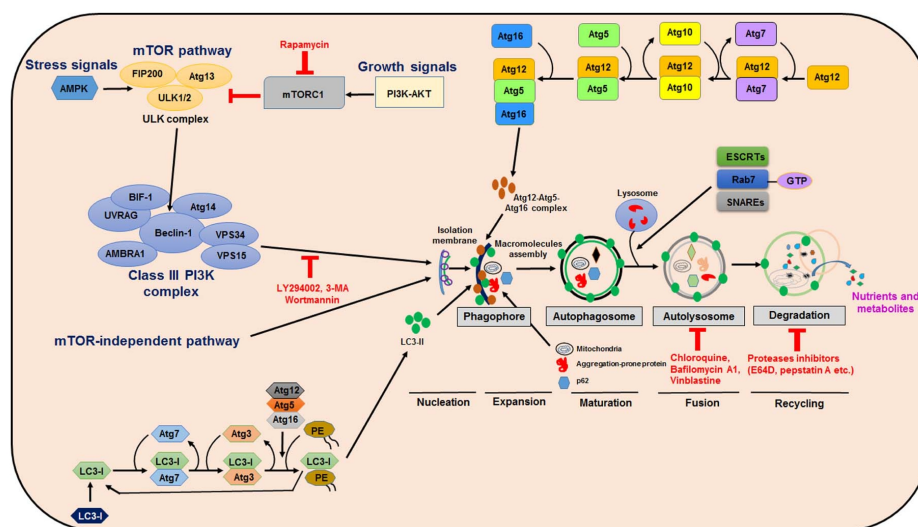


Figure 1. Autophagy pathway. Illustration of the molecular machineries involved in various steps of autophagy. Reproduced this image with permission¹²⁹.

Contribution of dysfunctional mitophagy and CMA in neurodegeneration pathogenesis

Damaged mitochondria generate toxic reactive oxygen species (ROS), one of the crucial factors that assaults cellular protein functions and impair the neuronal health¹³⁰. Damaged and depolarized mitochondria selectively are degraded in a specific autophagic process called mitophagy¹³¹. Mitochondrial associated proteins such as Parkin (E3 ubiquitin ligase), phosphatase and tensin homolog-induced putative kinase 1 (PINK1) regulate mitophagy.

PINK1 is a serine-threonine kinase localized on the mitochondrial outer membrane and is activated upon membrane depolarization and phosphorylates its substrate Parkin. Parkin is an E3-ubiquitin ligase that binds and ubiquitinates exposed mitochondrial membrane proteins and activates a cascade of events that culminate in recruitment of key autophagy proteins such as p62 and LC3 facilitating the mitochondrial clearance¹³¹. Mutations in Parkin and PINK1 are associated with recessive forms of PD, characterized by the neuronal accumulation of damaged mitochondria and that eventually trigger apoptosis either through ROS mediated lysosomal membrane destabilization or through the intrinsic pathway¹³².

Several studies illustrate the function of mitophagy receptors in nervous system. In *parkin* knockout (KO) mice, the mitochondrial activity and synaptic plasticity of striatal neurons is compromised¹³³. *Pink1* and *Parkin* knockout mice also display deficits in mitochondrial respiration in striatum¹³⁴.

LAMP2 and Hsc70 activities decline in dopaminergic neurons of PD patients and in α -synuclein overexpressed transgenic mouse model¹³⁵. LAMP2 and Hsc70 machineries are prerequisite for Chaperone Mediated Autophagy (CMA) and its suboptimal activity hampers CMA progression. Impaired CMA is linked to buildup of toxic protein aggregates such as tau in frontotemporal lobar dementia with ubiquitin inclusions (FTLD-U) and α -synuclein in PD¹³⁶.

Ageing and neurodegeneration

Ageing is one of the most commonly associated factors for decline in proteostasis and onset of neurodegeneration¹³⁷. The impact of ageing on the activity of various protein quality control machineries is discussed below.

Poor cellular energetics owing to ageing-related reduced mitochondrial function and deregulated energy, protein and lipid metabolism constrict the available ATP pool for chaperone activity¹³⁸. This could be one of the reasons for subdued activity of ATP dependent chaperones and concomitant increase in activity of ATP independent chaperones in aged brain¹³⁹. In addition, cargo recognition by chaperones is reduced with ageing. Presence of sustained cellular stress results in holding proteins in metastable states and this then constantly engages chaperones thus acting as a 'sink' for chaperones¹⁴⁰. Age-related modifications on proteins also negatively interfere with efficacy of chaperone activity. For instance, the presence of glycation end products in long-lived proteins hamper the chaperone function¹⁴¹. Though these modifications are identified and repaired by

methionine sulfoxide reductases, their levels too plummet with age¹⁴². Cells thus are known to adapt to such age-related effects by regulating the pool of available chaperones.

Like the studies on chaperones, impact of ageing on proteasome and autophagy has been well explored¹⁴³⁻¹⁴⁵. There are accumulating evidences that enhancing proteasome or autophagy by overexpressing their core components such as proteasomal subunits or core autophagy genes extend the life span of several model organisms by reducing stress burden. In *S. cerevisiae*, down regulating the negative regulator of UPS transcription, Ubr2 levels enhance lifespan¹⁴⁶. In *C. elegans*, lifespan extension is achieved by Rpn6 overexpression and/or caloric restriction (CR)¹⁴⁷. In mouse models, overexpressing insulin like growth factor (IGF1) or CR extends lifespan of animals significantly¹⁴⁸.

In *C. elegans*, the pharmacological up-regulation of autophagy by resveratrol or spermidine extends the lifespan¹⁴⁹. In an elegant study that genetically enhanced autophagy pathway by overexpressing a key autophagy protein (Atg5) extended the life span by 17.2%¹²⁸. Interestingly, these mice cleared ubiquitinated proteins better than the wild type in brain and elsewhere¹²⁸.

Crosstalk of autophagy and UPS

UPS and autophagy pathways were considered independent for a long time. Increasing evidences suggest that ubiquitinated proteins can be a target for both UPS and also autophagy¹⁵⁰. For example, α -synuclein is a substrate for both degradative pathways¹⁵¹. Monomers and dimers of misfolded proteins are proteasome substrates but not larger aggregates, owing to the limitation of the 26S proteasome tunnel size¹⁵². Notably, the higher order aggregate structures block the tunnel and choke the proteasomal structure¹⁵³. Co-chaperone molecules such as C-terminus of Hsp70- interacting protein (CHIP) and Bcl-2-associated athanogene1 (BAG) are one of the first lines of interface between UPS and autophagy¹⁵⁴. These proteins interact with target proteins and direct them for either UPS or autophagy. CHIP has E3 ubiquitin ligase activity that is associated with Hsc70. Its two functional domains namely tetratricopeptide repeat domain for proteasomal degradation and U-box domain is crucial for autophagy-mediated degradation¹⁵⁵.

Presence of polyubiquitin marks in target proteins at specific sites dictate their cellular fates, for example, in general, K48 is for UPS mediated degradation whereas K63 is for autophagy mediated degradation¹⁵⁶. In case of misfolded protein aggregates, the initial K48

signal marked for UPS can be removed by de-ubiquitinase (DUB) and again attached with K63 to direct them for autophagy-mediated degradation¹⁵⁷.

Apart from ubiquitin, the adaptor molecules such as p62 and NBR1 act as switches between UPS and autophagy¹⁵⁷. p62 interacts with ubiquitinated cargo via its ubiquitin-associated (UBA) domain and with LC3 through its LC3 interacting region (LIR). It can also interact with UPS through its ubiquitin-like (UBL) domain. It interacts with NBR1 through PB1 domain and LC3 through LIR motif¹⁵⁷. With these properties, p62 acts as a shuttle between UPS and autophagy depending on various cellular cues.

Histone deacetylase 6 (HDAC6) is associated to microtubules through its interaction with dynein motor proteins. It has BUZ domain that binds to ubiquitin and aids in retrograde transport of proteins to microtubule organizing center (MTOC) near the nucleus periphery where proteasomes are abundant. Furthermore, HDAC6 is also needed for retrograde transport of autophagosomes to MTOC for the degradation of cargo¹⁵⁷.

Transcellular propagation of toxic protein aggregates

Various research groups have demonstrated “prion-like” propagation of disease-associated proteins such as α -synuclein, β -amyloid, tau and polyQ huntingtin across neurons¹⁵⁸.

This discovery of cell-to-cell transfer of protein aggregates is a paradigm shift in understanding the pathogenesis of neurodegeneration. This concept supports the *Braak* hypothesis that explains the spatiotemporal regulation of disease manifestation¹⁵⁹. Braak and his colleagues hypothesized that Lewy bodies traverse from gastrointestinal tract to central nervous system. Earlier view postulated that protein aggregates accumulated in specific regions of the brain, but now it is clear that they also spread across cells or neuronal projections suggesting the spatiotemporal manifestation of disease pathology. For instance, injection of fibrillar toxic species leads to the spreading of aggregates and neuronal death that is directly routed through synapse¹⁶⁰.

The combinatorial factors such as specific neuronal susceptibility in addition to transcellular migration of aggregates may attribute to the disease progression.

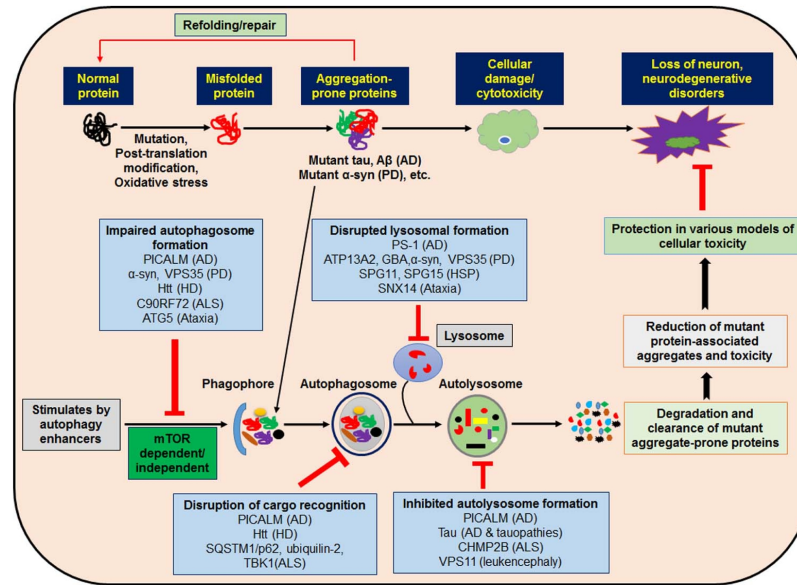


Figure 2. Dysfunctional autophagy in neurodegeneration. The mechanistic aspects underlying the impairment of autophagy flux by various disease associated protein aggregates at selective steps are detailed here. Reproduced with permission¹²⁹.

Therapeutic strategies for ND

Potential disease modifying therapeutic interventions for neurodegeneration includes three different strategies. First, preventing the toxic protein aggregate buildup. For instance, the antisense oligonucleotides ameliorated the amyotrophic lateral sclerosis disease phenotype under preclinical settings and showed significant safety in phase I clinical trial¹⁶¹. Second, dissolving the culminated toxic protein aggregates inside the neurons. Various groups identified small molecules and peptides that can bring about disintegration of the aggregate. This has been a widely used tested for a number of years as a promising anti-neurodegenerative therapeutic. For AD, few small molecule candidates that dissolve the amyloid plaques are currently in the clinical trials in USA and Europe. Third and recent approach is to promote cellular pathways to capture and degrade the protein aggregates by either ubiquitin proteasome (UPS) or autophagy systems. Numerous groups have demonstrated that neurodegeneration could be ameliorated by upregulating the activities of cellular clearance systems such as proteasome or autophagy through small molecules or peptides. Many small molecule screens have been reported that have identified the druggable candidate(s) (target proteins or pathways). For e.g., Rilmenidine, an autophagy

inducer is currently in clinical trial as a HD therapeutic in Europe (European Union Clinical Trial Register website).

Chemical modulation of autophagy

As mentioned earlier, upregulation of autophagy gene expression enhances the longevity of several model organisms¹²⁸. Convincing evidences demonstrate that dysfunctional autophagy contributes to the pathogenesis of neurodegeneration²⁰. Importantly, autophagy has the ability to clear toxic misfolded protein aggregates. Mechanisms that govern degradation of these aggregates is thus a therapeutically attractive target^{50,162}. Numerous studies demonstrated that pharmacological upregulation of autophagy to clear protein aggregates is beneficial in ameliorating neurodegeneration.

MTOR dependent autophagy modulators

MTOR dependent modulators induce autophagy by repressing MTOR and these can be of ATP competitive (e.g., Torin1) or non-ATP competitive (e.g., rapamycin). MTOR can be found in two complexes such as TORC1 (negative regulator of autophagy) and TORC2 (positive regulator of autophagy). Rapamycin and their analogs are relatively safer owing to its non-ATP competitive mode of inhibition. The allosteric TORC1 inhibitor, rapamycin was the first identified small molecule autophagy inducer. Rapamycin interacts with FK506-binding protein 12 (FKBP12) to inhibit the TORC1 activity¹⁶³. Rapamycin has been demonstrated to be neuroprotective in various diseases such as PD, HD, AD and FTD in an autophagy dependent manner¹⁶⁴ (**Fig. 1**). Limited absorption of rapamycin led to the development of its analogs (rapalogs) such as everolimus, temsirolimus, and ridaforolimus. Rapalogs are under rigorous investigation for their therapeutic potential in neurodegeneration. For instance, Food and Drug Administration (FDA) approved everolimus, a rapalog as a tuberous sclerosis therapeutic¹⁶⁵. Torin1, another rapalog inhibits both TORC1 and TORC2 in a concentration dependent manner¹⁶⁶.

There are other classes of modulators that indirectly inhibit MTOR activity. For instance, metformin (Type II diabetes therapeutic) inhibits MTOR through regulating AMPK pathway. Another AMPK activator, Nilotinib also exerts neuroprotection by inhibiting MTOR activity and is currently under phase II clinical trial for PD therapy¹⁶⁷. PI103 belongs to dual MTOR/class III PI3Kinase modulators that inhibit both MTOR and AKT

pathways to induce autophagy. However, due to its rapid *in vivo* metabolism, PI103 is currently unsuitable for neurodegenerative therapy¹⁶⁸.

MTOR independent autophagy modulators

MTOR independent autophagy modulators are those that induce autophagy without repressing the MTOR activity (**Fig. 1**). MTOR being the epicenter for cellular growth signaling whose chronic inhibition exerts significant toxicity. These inhibitors are preferred therapeutically since significant side effects such as impaired wound healing and immunosuppression that are classically associated with MTOR inhibitors can be avoided. Thus, these are also more suited for long-term drug administration. Small molecule screening of FDA approved drugs revealed that several modulators ameliorated neurodegeneration pathogenesis in various model systems in an MTOR independent manner. This study revealed the involvement of two cyclical pathways namely $G\alpha$ /calpain/ Ca^{2+} ¹⁶⁹ and EPAC/cAMP/PLC ϵ /Ins(1,4,5)P3¹⁷⁰ that are important for the MTOR independent clearance of aggregates.

Rilmenidine, an imidazoline receptor inhibitor, enhances autophagy by reducing cAMP levels. It has been shown to ameliorate neurodegeneration in various model systems such as primary neurons and transgenic mouse models of HD. It is important to note that rilmenidine is currently undergoing safety trials for HD in Europe¹⁷⁰.

Other drugs identified to regulate autophagy through the cyclical pathway are lithium, valproic acid and carbamazepine. Carbamazepine and valproic acid repress inositol synthesis, while lithium inhibits inositol monophosphatase to reduce Ins(1,4,5)P3 levels and thus induce autophagy¹⁷⁰.

Modulators of $G\alpha$ /calpain/ Ca^{2+} pathway such as verapamil and amiodarone along with calpain inhibitors such as calpeptin and calpastatin have shown to exert neuroprotective potential by degrading the protein aggregates through an autophagy-mediated mechanism¹⁷⁰.

Trehalose clears α -synuclein and mutant huntingtin protein aggregates in autophagy dependent manner in various model systems¹⁷¹. It has been shown to be neuroprotective in tauopathy models as well¹⁷². It extends life span, curbs motor and cognitive deficits in transgenic HD and ALS mouse models¹⁷³.

Aim and scope of the study

In neurodegeneration, autophagy is dysfunctional as protein aggregates trap autophagy proteins with them. But the mechanistic aspects underlying the impairment of autophagy by protein aggregates is not elucidated clearly. Also, autophagy functionality declines with age and might contribute to late onset of neurodegeneration. Interestingly, the autophagy knockout (Atg5^{-/-}) mice manifest neurodegeneration as they accumulate ubiquitin positive protein aggregates in different regions of the brain with concomitant motor deficits. On the other hand, the increase of autophagy flux (e.g., through over-expression of Atg5) displays enhanced clearance of p62 adaptor (and presumably its cargo such as ubiquitinated protein aggregates) with concomitant extension of life span of mice significantly. Pharmacological up-regulation of autophagy mitigates the proteotoxicity and is beneficial in neurodegeneration. Although proof-of-principle experiments exist, several vital questions remain unanswered, such as, what stage of autophagy is rate limiting or crucial, pertaining to the clearance of toxic protein aggregates. Thus, further studies to probe the mechanisms of autophagy are essential to realize the therapeutic potential of this pathway in curbing neurodegeneration.

With this background, we set the aims for our study with the following objectives,

1. Screening and identifying small molecule autophagy modulators using proteotoxicity models.
2. Elucidate the mechanisms of autophagy using these small molecules.
3. Evaluate the neuroprotective potential of small molecules in a preclinical mouse model of Parkinson's disease (PD).

To address this problem, we employed various model systems of proteotoxicity such as yeast, mammalian cells and mouse. The late Prof. Susan Lindquist (Whitehead Institute, MIT) generated yeast proteotoxicity models by over-expressing disease-associated proteins such as α -synuclein, β -amyloid and FUS. We employed this phenotypic based screening approach, rather than target based, upon considering the disease complexity. Yeast as a proteotoxicity model has the following advantages: 1) it dies when disease associated protein is over-expressed. 2) homologues with vital machineries of mammalian cells such as protein folding and its quality control, UPR, vesicular trafficking, mitochondria, peroxisomes and oxidative stress. 3) short doubling time. 4) available genetic resources and also its 5) genetic manipulation amenability.

'Hits' attained from yeast would be tested in proteotoxicity models of human cells and mouse with a focus on using them as tools to understand autophagy (aggrephagy flux) and also to realize their therapeutic potential.

References

1. Mayo KJ, Cyr DM. Protein aggregation and neurodegeneration. *Methods* 2011; 53:185-6.
2. Ashraf GM, Greig NH, Khan TA, Hassan I, Tabrez S, Shakil S, Sheikh IA, Zaidi SK, Akram M, Jabir NR, et al. Protein misfolding and aggregation in Alzheimer's disease and type 2 diabetes mellitus. *CNS Neurol Disord Drug Targets* 2014; 13:1280-93.
3. Irvine GB, El-Agnaf OM, Shankar GM, Walsh DM. Protein aggregation in the brain: the molecular basis for Alzheimer's and Parkinson's diseases. *Mol Med* 2008; 14:451-64.
4. Arrasate M, Finkbeiner S. Protein aggregates in Huntington's disease. *Exp Neurol* 2012; 238:1-11.
5. Blokhuis AM, Groen EJ, Koppers M, van den Berg LH, Pasterkamp RJ. Protein aggregation in amyotrophic lateral sclerosis. *Acta Neuropathol* 2013; 125:777-94.
6. Rocca WA, Petersen RC, Knopman DS, Hebert LE, Evans DA, Hall KS, Gao S, Unverzagt FW, Langa KM, Larson EB, et al. Trends in the incidence and prevalence of Alzheimer's disease, dementia, and cognitive impairment in the United States. *Alzheimers Dement* 2011; 7:80-93.
7. Bloom GS. Amyloid-beta and tau: the trigger and bullet in Alzheimer disease pathogenesis. *JAMA Neurol* 2014; 71:505-8.
8. Zhang YW, Thompson R, Zhang H, Xu H. APP processing in Alzheimer's disease. *Mol Brain* 2011; 4:3.
9. Lee HG, Perry G, Moreira PI, Garrett MR, Liu Q, Zhu X, Takeda A, Nunomura A, Smith MA. Tau phosphorylation in Alzheimer's disease: pathogen or protector? *Trends Mol Med* 2005; 11:164-9.
10. Alexander GE. Biology of Parkinson's disease: pathogenesis and pathophysiology of a multisystem neurodegenerative disorder. *Dialogues Clin Neurosci* 2004; 6:259-80.
11. Mhyre TR, Boyd JT, Hamill RW, Maguire-Zeiss KA. Parkinson's disease. *Subcell Biochem* 2012; 65:389-455.
12. Spillantini MG, Schmidt ML, Lee VM, Trojanowski JQ, Jakes R, Goedert M. Alpha-synuclein in Lewy bodies. *Nature* 1997; 388:839-40.
13. Double KL. Neuronal vulnerability in Parkinson's disease. *Parkinsonism Relat Disord* 2012; 18 Suppl 1:S52-4.

14. Klein C, Westenberger A. Genetics of Parkinson's disease. *Cold Spring Harb Perspect Med* 2012; 2:a008888.
15. Myers RH. Huntington's disease genetics. *NeuroRx* 2004; 1:255-62.
16. Sieradzan KA, Mann DM. The selective vulnerability of nerve cells in Huntington's disease. *Neuropathol Appl Neurobiol* 2001; 27:1-21.
17. Walker FO. Huntington's disease. *Lancet* 2007; 369:218-28.
18. Boillee S, Vande Velde C, Cleveland DW. ALS: a disease of motor neurons and their nonneuronal neighbors. *Neuron* 2006; 52:39-59.
19. Andersen PM. Genetic factors in the early diagnosis of ALS. *Amyotroph Lateral Scler Other Motor Neuron Disord* 2000; 1 Suppl 1:S31-42.
20. Nixon RA. The role of autophagy in neurodegenerative disease. *Nature medicine* 2013; 19:983-97.
21. Deng W, Aimone JB, Gage FH. New neurons and new memories: how does adult hippocampal neurogenesis affect learning and memory? *Nature reviews Neuroscience* 2010; 11:339-50.
22. Balch WE, Morimoto RI, Dillin A, Kelly JW. Adapting proteostasis for disease intervention. *Science* 2008; 319:916-9.
23. Komatsu M, Waguri S, Chiba T, Murata S, Iwata J, Tanida I, Ueno T, Koike M, Uchiyama Y, Kominami E, et al. Loss of autophagy in the central nervous system causes neurodegeneration in mice. *Nature* 2006; 441:880-4.
24. Sontag EM, Samant RS, Frydman J. Mechanisms and Functions of Spatial Protein Quality Control. *Annual review of biochemistry* 2017; 86:97-122.
25. Hyttinen JM, Amadio M, Viiri J, Pascale A, Salminen A, Kaarniranta K. Clearance of misfolded and aggregated proteins by aggrephagy and implications for aggregation diseases. *Ageing research reviews* 2014; 18:16-28.
26. Mymrikov EV, Daake M, Richter B, Haslbeck M, Buchner J. The Chaperone Activity and Substrate Spectrum of Human Small Heat Shock Proteins. *The Journal of biological chemistry* 2017; 292:672-84.
27. Labbadia J, Morimoto RI. Repression of the Heat Shock Response Is a Programmed Event at the Onset of Reproduction. *Molecular cell* 2015; 59:639-50.
28. Walther DM, Kasturi P, Zheng M, Pinkert S, Vecchi G, Ciryam P, Morimoto RI, Dobson CM, Vendruscolo M, Mann M, et al. Widespread Proteome Remodeling and Aggregation in Aging *C. elegans*. *Cell* 2017; 168:944.

29. Kampinga HH, Craig EA. The HSP70 chaperone machinery: J proteins as drivers of functional specificity. *Nature reviews Molecular cell biology* 2010; 11:579-92.
30. Ankar J, Sistonen L. Regulation of HSF1 function in the heat stress response: implications in aging and disease. *Annual review of biochemistry* 2011; 80:1089-115.
31. Raychaudhuri S, Loew C, Korner R, Pinkert S, Theis M, Hayer-Hartl M, Buchholz F, Hartl FU. Interplay of acetyltransferase EP300 and the proteasome system in regulating heat shock transcription factor 1. *Cell* 2014; 156:975-85.
32. Wang F, Durfee LA, Huibregtse JM. A cotranslational ubiquitination pathway for quality control of misfolded proteins. *Molecular cell* 2013; 50:368-78.
33. Powers ET, Morimoto RI, Dillin A, Kelly JW, Balch WE. Biological and chemical approaches to diseases of proteostasis deficiency. *Annual review of biochemistry* 2009; 78:959-91.
34. Hetz C. The unfolded protein response: controlling cell fate decisions under ER stress and beyond. *Nature reviews Molecular cell biology* 2012; 13:89-102.
35. Hetz C, Mollereau B. Disturbance of endoplasmic reticulum proteostasis in neurodegenerative diseases. *Nature reviews Neuroscience* 2014; 15:233-49.
36. Goldberg AL. Protein degradation and protection against misfolded or damaged proteins. *Nature* 2003; 426:895-9.
37. Kirkin V, McEwan DG, Novak I, Dikic I. A role for ubiquitin in selective autophagy. *Molecular cell* 2009; 34:259-69.
38. Lim J, Yue Z. Neuronal aggregates: formation, clearance, and spreading. *Developmental cell* 2015; 32:491-501.
39. De Duve C, Wattiaux R. Functions of lysosomes. *Annual review of physiology* 1966; 28:435-92.
40. Harnett MM, Pineda MA, Latre de Late P, Eason RJ, Besteiro S, Harnett W, Langsley G. From Christian de Duve to Yoshinori Ohsumi: More to autophagy than just dining at home. *Biomedical journal* 2017; 40:9-22.
41. Zaffagnini G, Martens S. Mechanisms of Selective Autophagy. *Journal of molecular biology* 2016; 428:1714-24.
42. Smith MG, Snyder M. Yeast as a model for human disease. *Current protocols in human genetics* 2006; Chapter 15:Unit 15 6.
43. Khurana V, Lindquist S. Modelling neurodegeneration in *Saccharomyces cerevisiae*: why cook with baker's yeast? *Nature reviews Neuroscience* 2010; 11:436-49.

44. Botstein D, Chervitz SA, Cherry JM. Yeast as a model organism. *Science* 1997; 277:1259-60.
45. Kachroo AH, Laurent JM, Yellman CM, Meyer AG, Wilke CO, Marcotte EM. Evolution. Systematic humanization of yeast genes reveals conserved functions and genetic modularity. *Science* 2015; 348:921-5.
46. Outeiro TF, Lindquist S. Yeast cells provide insight into alpha-synuclein biology and pathobiology. *Science* 2003; 302:1772-5.
47. Cooper AA, Gitler AD, Cashikar A, Haynes CM, Hill KJ, Bhullar B, Liu K, Xu K, Strathearn KE, Liu F, et al. Alpha-synuclein blocks ER-Golgi traffic and Rab1 rescues neuron loss in Parkinson's models. *Science* 2006; 313:324-8.
48. Winslow AR, Chen CW, Corrochano S, Acevedo-Arozena A, Gordon DE, Peden AA, Lichtenberg M, Menzies FM, Ravikumar B, Imarisio S, et al. alpha-Synuclein impairs macroautophagy: implications for Parkinson's disease. *The Journal of cell biology* 2010; 190:1023-37.
49. Rajasekhar K, Suresh SN, Manjithaya R, Govindaraju T. Rationally designed peptidomimetic modulators of abeta toxicity in Alzheimer's disease. *Scientific reports* 2015; 5:8139.
50. Sarkar S, Perlstein EO, Imarisio S, Pineau S, Cordenier A, Maglathlin RL, Webster JA, Lewis TA, O'Kane CJ, Schreiber SL, et al. Small molecules enhance autophagy and reduce toxicity in Huntington's disease models. *Nature chemical biology* 2007; 3:331-8.
51. Kumar A, Singh PK, Parihar R, Dwivedi V, Lakhotia SC, Ganesh S. Decreased O-linked GlcNAcylation protects from cytotoxicity mediated by huntingtin exon1 protein fragment. *The Journal of biological chemistry* 2014; 289:13543-53.
52. Luheshi LM, Tartaglia GG, Brorsson AC, Pawar AP, Watson IE, Chiti F, Vendruscolo M, Lomas DA, Dobson CM, Crowther DC. Systematic in vivo analysis of the intrinsic determinants of amyloid Beta pathogenicity. *PLoS biology* 2007; 5:e290.
53. Chang S, Bray SM, Li Z, Zarnescu DC, He C, Jin P, Warren ST. Identification of small molecules rescuing fragile X syndrome phenotypes in *Drosophila*. *Nature chemical biology* 2008; 4:256-63.
54. Jimenez-Sanchez M, Lam W, Hannus M, Sonnichsen B, Imarisio S, Fleming A, Tarditi A, Menzies F, Dami TE, Xu C, et al. siRNA screen identifies QPCT as a druggable target for Huntington's disease. *Nature chemical biology* 2015; 11:347-54.

55. Nussbaum-Krammer CI, Morimoto RI. *Caenorhabditis elegans* as a model system for studying non-cell-autonomous mechanisms in protein-misfolding diseases. *Disease models & mechanisms* 2014; 7:31-9.
56. Narayan P, Ehsani S, Lindquist S. Combating neurodegenerative disease with chemical probes and model systems. *Nature chemical biology* 2014; 10:911-20.
57. Yao C, Johnson WM, Gao Y, Wang W, Zhang J, Deak M, Alessi DR, Zhu X, Miesel JJ, Roder H, et al. Kinase inhibitors arrest neurodegeneration in cell and *C. elegans* models of LRRK2 toxicity. *Hum Mol Genet* 2013; 22:328-44.
58. Chung K, Crane MM, Lu H. Automated on-chip rapid microscopy, phenotyping and sorting of *C. elegans*. *Nature methods* 2008; 5:637-43.
59. Zhang Y, Yan L, Zhou Z, Yang P, Tian E, Zhang K, Zhao Y, Li Z, Song B, Han J, et al. SEPA-1 mediates the specific recognition and degradation of P granule components by autophagy in *C. elegans*. *Cell* 2009; 136:308-21.
60. Phillips W, Michell A, Pruess H, Barker RA. Animal models of neurodegenerative diseases. *Methods Mol Biol* 2009; 549:137-55.
61. Shekhar S, Vatsa N, Kumar V, Singh BK, Jamal I, Sharma A, Jana NR. Topoisomerase 1 inhibitor topotecan delays the disease progression in a mouse model of Huntington's disease. *Human molecular genetics* 2017; 26:420-9.
62. Sasaguri H, Nilsson P, Hashimoto S, Nagata K, Saito T, De Strooper B, Hardy J, Vassar R, Winblad B, Saido TC. APP mouse models for Alzheimer's disease preclinical studies. *The EMBO journal* 2017; 36:2473-87.
63. Jackson-Lewis V, Blesa J, Przedborski S. Animal models of Parkinson's disease. *Parkinsonism Relat Disord* 2012; 18 Suppl 1:S183-5.
64. Pioro EP, Mitumoto H. Animal models of ALS. *Clin Neurosci* 1995; 3:375-85.
65. Ramaswamy S, McBride JL, Kordower JH. Animal models of Huntington's disease. *ILAR J* 2007; 48:356-73.
66. Mangiarini L, Sathasivam K, Seller M, Cozens B, Harper A, Hetherington C, Lawton M, Trotter Y, Leach H, Davies SW, et al. Exon 1 of the HD gene with an expanded CAG repeat is sufficient to cause a progressive neurological phenotype in transgenic mice. *Cell* 1996; 87:493-506.
67. Kiskinis E, Sandoe J, Williams LA, Boulting GL, Moccia R, Wainger BJ, Han S, Peng T, Thams S, Mikkilineni S, et al. Pathways disrupted in human ALS motor neurons identified through genetic correction of mutant SOD1. *Cell stem cell* 2014; 14:781-95.

68. Ryan SD, Dolatabadi N, Chan SF, Zhang X, Akhtar MW, Parker J, Soldner F, Sunico CR, Nagar S, Talantova M, et al. Isogenic human iPSC Parkinson's model shows nitrosative stress-induced dysfunction in MEF2-PGC1alpha transcription. *Cell* 2013; 155:1351-64.
69. Chung CY, Khurana V, Auluck PK, Tardiff DF, Mazzulli JR, Soldner F, Baru V, Lou Y, Freyzon Y, Cho S, et al. Identification and rescue of alpha-synuclein toxicity in Parkinson patient-derived neurons. *Science* 2013; 342:983-7.
70. Stolz A, Ernst A, Dikic I. Cargo recognition and trafficking in selective autophagy. *Nature cell biology* 2014; 16:495-501.
71. Isakson P, Holland P, Simonsen A. The role of ALFY in selective autophagy. *Cell death and differentiation* 2013; 20:12-20.
72. Filimonenko M, Isakson P, Finley KD, Anderson M, Jeong H, Melia TJ, Bartlett BJ, Myers KM, Birkeland HC, Lamark T, et al. The selective macroautophagic degradation of aggregated proteins requires the PI3P-binding protein Alfy. *Molecular cell* 2010; 38:265-79.
73. Pankiv S, Clausen TH, Lamark T, Brech A, Bruun JA, Outzen H, Overvatn A, Bjorkoy G, Johansen T. p62/SQSTM1 binds directly to Atg8/LC3 to facilitate degradation of ubiquitinated protein aggregates by autophagy. *The Journal of biological chemistry* 2007; 282:24131-45.
74. Geisler S, Holmstrom KM, Skujat D, Fiesel FC, Rothfuss OC, Kahle PJ, Springer W. PINK1/Parkin-mediated mitophagy is dependent on VDAC1 and p62/SQSTM1. *Nature cell biology* 2010; 12:119-31.
75. Kim PK, Hailey DW, Mullen RT, Lippincott-Schwartz J. Ubiquitin signals autophagic degradation of cytosolic proteins and peroxisomes. *Proc Natl Acad Sci U S A* 2008; 105:20567-74.
76. Bah A, Vergne I. Macrophage Autophagy and Bacterial Infections. *Frontiers in immunology* 2017; 8:1483.
77. Fecto F, Yan J, Vemula SP, Liu E, Yang Y, Chen W, Zheng JG, Shi Y, Siddique N, Arrat H, et al. SQSTM1 mutations in familial and sporadic amyotrophic lateral sclerosis. *Archives of neurology* 2011; 68:1440-6.
78. Chamoux E, McManus S, Laberge G, Bisson M, Roux S. Involvement of kinase PKC-zeta in the p62/p62(P392L)-driven activation of NF-kappaB in human osteoclasts. *Biochimica et biophysica acta* 2013; 1832:475-84.

79. Kachaner D, Genin P, Laplantine E, Weil R. Toward an integrative view of Optineurin functions. *Cell cycle* 2012; 11:2808-18.
80. Ito H, Nakamura M, Komure O, Ayaki T, Wate R, Maruyama H, Nakamura Y, Fujita K, Kaneko S, Okamoto Y, et al. Clinicopathologic study on an ALS family with a heterozygous E478G optineurin mutation. *Acta Neuropathol* 2011; 122:223-9.
81. Lu K, Psakhye I, Jentsch S. Autophagic clearance of polyQ proteins mediated by ubiquitin-Atg8 adaptors of the conserved CUET protein family. *Cell* 2014; 158:549-63.
82. Ritz D, Vuk M, Kirchner P, Bug M, Schutz S, Hayer A, Bremer S, Lusk C, Baloh RH, Lee H, et al. Endolysosomal sorting of ubiquitylated caveolin-1 is regulated by VCP and UBXD1 and impaired by VCP disease mutations. *Nature cell biology* 2011; 13:1116-23.
83. Mizushima N. The role of the Atg1/ULK1 complex in autophagy regulation. *Current opinion in cell biology* 2010; 22:132-9.
84. Chan EY, Longatti A, McKnight NC, Tooze SA. Kinase-inactivated ULK proteins inhibit autophagy via their conserved C-terminal domains using an Atg13-independent mechanism. *Molecular and cellular biology* 2009; 29:157-71.
85. Khan SH, Kumar R. Role of an intrinsically disordered conformation in AMPK-mediated phosphorylation of ULK1 and regulation of autophagy. *Molecular bioSystems* 2012; 8:91-6.
86. Di Bartolomeo S, Corazzari M, Nazio F, Oliverio S, Lisi G, Antonioli M, Pagliarini V, Matteoni S, Fuoco C, Giunta L, et al. The dynamic interaction of AMBRA1 with the dynein motor complex regulates mammalian autophagy. *The Journal of cell biology* 2010; 191:155-68.
87. Jaber N, Zong WX. Class III PI3K Vps34: essential roles in autophagy, endocytosis, and heart and liver function. *Annals of the New York Academy of Sciences* 2013; 1280:48-51.
88. Ichimura Y, Kirisako T, Takao T, Satomi Y, Shimonishi Y, Ishihara N, Mizushima N, Tanida I, Kominami E, Ohsumi M, et al. A ubiquitin-like system mediates protein lipidation. *Nature* 2000; 408:488-92.
89. Hamasaki M, Furuta N, Matsuda A, Nezu A, Yamamoto A, Fujita N, Oomori H, Noda T, Haraguchi T, Hiraoka Y, et al. Autophagosomes form at ER-mitochondria contact sites. *Nature* 2013; 495:389-93.
90. Geng J, Klionsky DJ. The Golgi as a potential membrane source for autophagy. *Autophagy* 2010; 6:950-1.

91. Ravikumar B, Moreau K, Jahreiss L, Puri C, Rubinsztein DC. Plasma membrane contributes to the formation of pre-autophagosomal structures. *Nature cell biology* 2010; 12:747-57.
92. Maday S, Holzbaur EL. Autophagosome biogenesis in primary neurons follows an ordered and spatially regulated pathway. *Developmental cell* 2014; 30:71-85.
93. Kim E, Goraksha-Hicks P, Li L, Neufeld TP, Guan KL. Regulation of TORC1 by Rag GTPases in nutrient response. *Nature cell biology* 2008; 10:935-45.
94. Mizushima N, Yamamoto A, Matsui M, Yoshimori T, Ohsumi Y. In vivo analysis of autophagy in response to nutrient starvation using transgenic mice expressing a fluorescent autophagosome marker. *Molecular biology of the cell* 2004; 15:1101-11.
95. Kaushik S, Rodriguez-Navarro JA, Arias E, Kiffin R, Sahu S, Schwartz GJ, Cuervo AM, Singh R. Autophagy in hypothalamic AgRP neurons regulates food intake and energy balance. *Cell metabolism* 2011; 14:173-83.
96. Vanhauwaert R, Kuenen S, Masius R, Bademosi A, Manetsberger J, Schoovaerts N, Bounti L, Gontcharenko S, Swerts J, Vilain S, et al. The SAC1 domain in synaptojanin is required for autophagosome maturation at presynaptic terminals. *The EMBO journal* 2017; 36:1392-411.
97. Rizzoli SO. Synaptic vesicle recycling: steps and principles. *The EMBO journal* 2014; 33:788-822.
98. Vijayan V, Verstreken P. Autophagy in the presynaptic compartment in health and disease. *The Journal of cell biology* 2017; 216:1895-906.
99. Kovacs KA, Steullet P, Steinmann M, Do KQ, Magistretti PJ, Halfon O, Cardinaux JR. TORC1 is a calcium- and cAMP-sensitive coincidence detector involved in hippocampal long-term synaptic plasticity. *Proc Natl Acad Sci U S A* 2007; 104:4700-5.
100. Shehata M, Matsumura H, Okubo-Suzuki R, Ohkawa N, Inokuchi K. Neuronal stimulation induces autophagy in hippocampal neurons that is involved in AMPA receptor degradation after chemical long-term depression. *J Neurosci* 2012; 32:10413-22.
101. Zhou L, Wang W, Hoppel C, Liu J, Zhu X. Parkinson's disease-associated pathogenic VPS35 mutation causes complex I deficits. *Biochimica et biophysica acta* 2017; 1863:2791-5.
102. Zavodszky E, Seaman MN, Moreau K, Jimenez-Sanchez M, Breusegem SY, Harbour ME, Rubinsztein DC. Mutation in VPS35 associated with Parkinson's disease impairs WASH complex association and inhibits autophagy. *Nature communications* 2014; 5:3828.

103. Kim M, Sandford E, Gatica D, Qiu Y, Liu X, Zheng Y, Schulman BA, Xu J, Semple I, Ro SH, et al. Mutation in ATG5 reduces autophagy and leads to ataxia with developmental delay. *Elife* 2016; 5.
104. Haack TB, Hogarth P, Gregory A, Prokisch H, Hayflick SJ. BPAN: the only X-linked dominant NBIA disorder. *International review of neurobiology* 2013; 110:85-90.
105. Zhao YG, Sun L, Miao G, Ji C, Zhao H, Sun H, Miao L, Yoshii SR, Mizushima N, Wang X, et al. The autophagy gene Wdr45/Wipi4 regulates learning and memory function and axonal homeostasis. *Autophagy* 2015; 11:881-90.
106. Saitsu H, Nishimura T, Muramatsu K, Kodera H, Kumada S, Sugai K, Kasai-Yoshida E, Sawaura N, Nishida H, Hoshino A, et al. De novo mutations in the autophagy gene WDR45 cause static encephalopathy of childhood with neurodegeneration in adulthood. *Nat Genet* 2013; 45:445-9, 9e1.
107. Webster CP, Smith EF, Bauer CS, Moller A, Hautbergue GM, Ferraiuolo L, Myszczyńska MA, Higginbottom A, Walsh MJ, Whitworth AJ, et al. The C9orf72 protein interacts with Rab1a and the ULK1 complex to regulate initiation of autophagy. *The EMBO journal* 2016; 35:1656-76.
108. Amick J, Ferguson SM. C9orf72: At the intersection of lysosome cell biology and neurodegenerative disease. *Traffic* 2017; 18:267-76.
109. Martinez-Vicente M, Talloczy Z, Wong E, Tang G, Koga H, Kaushik S, de Vries R, Arias E, Harris S, Sulzer D, et al. Cargo recognition failure is responsible for inefficient autophagy in Huntington's disease. *Nat Neurosci* 2010; 13:567-76.
110. Wong YC, Holzbaur EL. The regulation of autophagosome dynamics by huntingtin and HAP1 is disrupted by expression of mutant huntingtin, leading to defective cargo degradation. *J Neurosci* 2014; 34:1293-305.
111. Subramaniam S, Sixt KM, Barrow R, Snyder SH. Rhes, a striatal specific protein, mediates mutant-huntingtin cytotoxicity. *Science* 2009; 324:1327-30.
112. Jimenez-Sanchez M, Thomson F, Zavodszky E, Rubinsztein DC. Autophagy and polyglutamine diseases. *Prog Neurobiol* 2012; 97:67-82.
113. Ferrucci M, Fulceri F, Toti L, Soldani P, Siciliano G, Paparelli A, Fornai F. Protein clearing pathways in ALS. *Archives italiennes de biologie* 2011; 149:121-49.
114. Sasaki S. Autophagy in spinal cord motor neurons in sporadic amyotrophic lateral sclerosis. *J Neuropathol Exp Neurol* 2011; 70:349-59.
115. Skibinski G, Parkinson NJ, Brown JM, Chakrabarti L, Lloyd SL, Hummerich H, Nielsen JE, Hodges JR, Spillantini MG, Thusgaard T, et al. Mutations in the endosomal

- ESCRTIII-complex subunit CHMP2B in frontotemporal dementia. *Nat Genet* 2005; 37:806-8.
116. Otomo A, Kunita R, Suzuki-Utsunomiya K, Ikeda JE, Hadano S. Defective relocalization of ALS2/alsin missense mutants to Rac1-induced macropinosomes accounts for loss of their cellular function and leads to disturbed amphisome formation. *FEBS letters* 2011; 585:730-6.
117. Tabata K, Matsunaga K, Sakane A, Sasaki T, Noda T, Yoshimori T. Rubicon and PLEKHM1 negatively regulate the endocytic/autophagic pathway via a novel Rab7-binding domain. *Molecular biology of the cell* 2010; 21:4162-72.
118. Ejlerskov P, Hultberg JG, Wang J, Carlsson R, Ambjorn M, Kuss M, Liu Y, Porcu G, Kolkova K, Friis Rundsten C, et al. Lack of Neuronal IFN-beta-IFNAR Causes Lewy Body- and Parkinson's Disease-like Dementia. *Cell* 2015; 163:324-39.
119. Kroemer G, Jaattela M. Lysosomes and autophagy in cell death control. *Nature reviews Cancer* 2005; 5:886-97.
120. Avruch J, Long X, Ortiz-Vega S, Rapley J, Papageorgiou A, Dai N. Amino acid regulation of TOR complex 1. *American journal of physiology Endocrinology and metabolism* 2009; 296:E592-602.
121. Cortes CJ, Ling SC, Guo LT, Hung G, Tsunemi T, Ly L, Tokunaga S, Lopez E, Sopher BL, Bennett CF, et al. Muscle expression of mutant androgen receptor accounts for systemic and motor neuron disease phenotypes in spinal and bulbar muscular atrophy. *Neuron* 2014; 82:295-307.
122. Cunha-Santos J, Duarte-Neves J, Carmona V, Guarente L, Pereira de Almeida L, Cavadas C. Caloric restriction blocks neuropathology and motor deficits in Machado-Joseph disease mouse models through SIRT1 pathway. *Nature communications* 2016; 7:11445.
123. Chauhan S, Goodwin JG, Chauhan S, Manyam G, Wang J, Kamat AM, Boyd DD. ZKSCAN3 is a master transcriptional repressor of autophagy. *Molecular cell* 2013; 50:16-28.
124. Li L, Zviti R, Ha C, Wang ZV, Hill JA, Lin F. Forkhead box O3 (FoxO3) regulates kidney tubular autophagy following urinary tract obstruction. *The Journal of biological chemistry* 2017; 292:13774-83.
125. Elrick MJ, Yu T, Chung C, Lieberman AP. Impaired proteolysis underlies autophagic dysfunction in Niemann-Pick type C disease. *Hum Mol Genet* 2012; 21:4876-87.

126. Nixon RA. Niemann-Pick Type C disease and Alzheimer's disease: the APP-endosome connection fattens up. *The American journal of pathology* 2004; 164:757-61.
127. Komatsu M, Waguri S, Ueno T, Iwata J, Murata S, Tanida I, Ezaki J, Mizushima N, Ohsumi Y, Uchiyama Y, et al. Impairment of starvation-induced and constitutive autophagy in Atg7-deficient mice. *The Journal of cell biology* 2005; 169:425-34.
128. Pyo JO, Yoo SM, Ahn HH, Nah J, Hong SH, Kam TI, Jung S, Jung YK. Overexpression of Atg5 in mice activates autophagy and extends lifespan. *Nature communications* 2013; 4:2300.
129. Rahman MA, Rhim H. Therapeutic implication of autophagy in neurodegenerative diseases. *BMB reports* 2017; 50:345-54.
130. Guo C, Sun L, Chen X, Zhang D. Oxidative stress, mitochondrial damage and neurodegenerative diseases. *Neural Regen Res* 2013; 8:2003-14.
131. Youle RJ, Narendra DP. Mechanisms of mitophagy. *Nature reviews Molecular cell biology* 2011; 12:9-14.
132. Scarffe LA, Stevens DA, Dawson VL, Dawson TM. Parkin and PINK1: much more than mitophagy. *Trends Neurosci* 2014; 37:315-24.
133. Pickrell AM, Youle RJ. The roles of PINK1, parkin, and mitochondrial fidelity in Parkinson's disease. *Neuron* 2015; 85:257-73.
134. Moiso N, Fedele V, Edwards J, Martins LM. Loss of PINK1 enhances neurodegeneration in a mouse model of Parkinson's disease triggered by mitochondrial stress. *Neuropharmacology* 2014; 77:350-7.
135. Lopes da Fonseca T, Villar-Pique A, Outeiro TF. The Interplay between Alpha-Synuclein Clearance and Spreading. *Biomolecules* 2015; 5:435-71.
136. Lynch-Day MA, Mao K, Wang K, Zhao M, Klionsky DJ. The role of autophagy in Parkinson's disease. *Cold Spring Harb Perspect Med* 2012; 2:a009357.
137. Wyss-Coray T. Ageing, neurodegeneration and brain rejuvenation. *Nature* 2016; 539:180-6.
138. Payne BA, Chinnery PF. Mitochondrial dysfunction in aging: Much progress but many unresolved questions. *Biochimica et biophysica acta* 2015; 1847:1347-53.
139. Ciechanover A, Kwon YT. Protein Quality Control by Molecular Chaperones in Neurodegeneration. *Front Neurosci* 2017; 11:185.
140. Yang H, Hu HY. Sequestration of cellular interacting partners by protein aggregates: implication in a loss-of-function pathology. *FEBS J* 2016; 283:3705-17.

141. Gkogkolou P, Bohm M. Advanced glycation end products: Key players in skin aging? *Dermatoendocrinol* 2012; 4:259-70.
142. Moskovitz J. Methionine sulfoxide reductases: ubiquitous enzymes involved in antioxidant defense, protein regulation, and prevention of aging-associated diseases. *Biochimica et biophysica acta* 2005; 1703:213-9.
143. Rubinsztein DC, Marino G, Kroemer G. Autophagy and aging. *Cell* 2011; 146:682-95.
144. Carroll B, Hewitt G, Korolchuk VI. Autophagy and ageing: implications for age-related neurodegenerative diseases. *Essays Biochem* 2013; 55:119-31.
145. Cuervo AM. Autophagy and aging: keeping that old broom working. *Trends Genet* 2008; 24:604-12.
146. Andersson V, Hanzen S, Liu B, Molin M, Nystrom T. Enhancing protein disaggregation restores proteasome activity in aged cells. *Aging (Albany NY)* 2013; 5:802-12.
147. Anton S, Leeuwenburgh C. Fasting or caloric restriction for healthy aging. *Exp Gerontol* 2013; 48:1003-5.
148. van Heemst D. Insulin, IGF-1 and longevity. *Aging Dis* 2010; 1:147-57.
149. Petrovski G, Das DK. Does autophagy take a front seat in lifespan extension? *J Cell Mol Med* 2010; 14:2543-51.
150. Wojcik S. Crosstalk between autophagy and proteasome protein degradation systems: possible implications for cancer therapy. *Folia Histochem Cytobiol* 2013; 51:249-64.
151. Webb JL, Ravikumar B, Atkins J, Skepper JN, Rubinsztein DC. Alpha-Synuclein is degraded by both autophagy and the proteasome. *The Journal of biological chemistry* 2003; 278:25009-13.
152. Myeku N, Metcalfe MJ, Huang Q, Figueiredo-Pereira M. Assessment of proteasome impairment and accumulation/aggregation of ubiquitinated proteins in neuronal cultures. *Methods Mol Biol* 2011; 793:273-96.
153. Holmberg CI, Staniszewski KE, Mensah KN, Matouschek A, Morimoto RI. Inefficient degradation of truncated polyglutamine proteins by the proteasome. *The EMBO journal* 2004; 23:4307-18.
154. Kalia LV, Kalia SK, Chau H, Lozano AM, Hyman BT, McLean PJ. Ubiquitinylation of alpha-synuclein by carboxyl terminus Hsp70-interacting protein (CHIP) is regulated by Bcl-2-associated athanogene 5 (BAG5). *PloS one* 2011; 6:e14695.

155. Smith MC, Scaglione KM, Assimon VA, Patury S, Thompson AD, Dickey CA, Southworth DR, Paulson HL, Gestwicki JE, Zuiderweg ER. The E3 ubiquitin ligase CHIP and the molecular chaperone Hsc70 form a dynamic, tethered complex. *Biochemistry* 2013; 52:5354-64.
156. DePavia A, Jonasch E, Liu XD. Autophagy degrades hypoxia inducible factors. *Mol Cell Oncol* 2016; 3:e1104428.
157. Lilienbaum A. Relationship between the proteasomal system and autophagy. *Int J Biochem Mol Biol* 2013; 4:1-26.
158. Brundin P, Melki R, Kopito R. Prion-like transmission of protein aggregates in neurodegenerative diseases. *Nature reviews Molecular cell biology* 2010; 11:301-7.
159. Rietdijk CD, Perez-Pardo P, Garssen J, van Wezel RJ, Kraneveld AD. Exploring Braak's Hypothesis of Parkinson's Disease. *Front Neurol* 2017; 8:37.
160. Guo JL, Lee VM. Cell-to-cell transmission of pathogenic proteins in neurodegenerative diseases. *Nature medicine* 2014; 20:130-8.
161. Nizzardo M, Simone C, Rizzo F, Ulzi G, Ramirez A, Rizzuti M, Bordoni A, Bucchia M, Gatti S, Bresolin N, et al. Morpholino-mediated SOD1 reduction ameliorates an amyotrophic lateral sclerosis disease phenotype. *Scientific reports* 2016; 6:21301.
162. Rousseaux MW, de Haro M, Lasagna-Reeves CA, De Maio A, Park J, Jafar-Nejad P, Al-Ramahi I, Sharma A, See L, Lu N, et al. TRIM28 regulates the nuclear accumulation and toxicity of both alpha-synuclein and tau. *eLife* 2016; 5.
163. Lorenz MC, Heitman J. TOR mutations confer rapamycin resistance by preventing interaction with FKBP12-rapamycin. *The Journal of biological chemistry* 1995; 270:27531-7.
164. Jahrling JB, Laberge RM. Age-Related Neurodegeneration Prevention Through mTOR Inhibition: Potential Mechanisms and Remaining Questions. *Current topics in medicinal chemistry* 2015; 15:2139-51.
165. Bissler JJ, Kingswood JC, Radzikowska E, Zonnenberg BA, Belousova E, Frost MD, Sauter M, Brakemeier S, de Vries PJ, Berkowitz N, et al. Everolimus long-term use in patients with tuberous sclerosis complex: Four-year update of the EXIST-2 study. *PloS one* 2017; 12:e0180939.
166. Ma N, Liu Q, Zhang L, Henske EP, Ma Y. TORC1 signaling is governed by two negative regulators in fission yeast. *Genetics* 2013; 195:457-68.

167. Karuppagounder SS, Brahmachari S, Lee Y, Dawson VL, Dawson TM, Ko HS. The c-Abl inhibitor, nilotinib, protects dopaminergic neurons in a preclinical animal model of Parkinson's disease. *Scientific reports* 2014; 4:4874.
168. Hassan B, Akcakanat A, Holder AM, Meric-Bernstam F. Targeting the PI3-kinase/Akt/mTOR signaling pathway. *Surgical oncology clinics of North America* 2013; 22:641-64.
169. Cardenas C, Miller RA, Smith I, Bui T, Molgo J, Muller M, Vais H, Cheung KH, Yang J, Parker I, et al. Essential regulation of cell bioenergetics by constitutive InsP3 receptor Ca²⁺ transfer to mitochondria. *Cell* 2010; 142:270-83.
170. Williams A, Sarkar S, Cuddon P, Ttofi EK, Saiki S, Siddiqi FH, Jahreiss L, Fleming A, Pask D, Goldsmith P, et al. Novel targets for Huntington's disease in an mTOR-independent autophagy pathway. *Nature chemical biology* 2008; 4:295-305.
171. Sarkar S, Davies JE, Huang Z, Tunnacliffe A, Rubinsztein DC. Trehalose, a novel mTOR-independent autophagy enhancer, accelerates the clearance of mutant huntingtin and alpha-synuclein. *The Journal of biological chemistry* 2007; 282:5641-52.
172. Schaeffer V, Lavenir I, Ozcelik S, Tolnay M, Winkler DT, Goedert M. Stimulation of autophagy reduces neurodegeneration in a mouse model of human tauopathy. *Brain* 2012; 135:2169-77.
173. Tanaka M, Machida Y, Niu S, Ikeda T, Jana NR, Doi H, Kurosawa M, Nekooki M, Nukina N. Trehalose alleviates polyglutamine-mediated pathology in a mouse model of Huntington disease. *Nature medicine* 2004; 10:148-54.

Chapter 2

Materials and methods

Chemicals and Antibodies

Yeast extract (RM027), peptone (RM667), dextrose (GRM077), galactose (RM101) and amino acids [leucine (GRM054), methionine (GRM200), histidine (RM051) and uracil (RM264)] were purchased from HiMedia. 3-MA (M9281), 6-Bio (B1686), XCT 790 (X4753), PD 180970 (PZ0142), AGK2 (A8231), LOPAC (LO1280), anti-LC3B antibody (L7543), MPTP (methyl-4-phenyl-1, 2, 3, 6-tetrahydropyridine, M0896), DMEM (D5648), DMEM F-12 (D8900), penicillin and streptomycin (P4333), DAB (3, 3'-Diaminobenzidine, D3939), Atto 663 (41176), lysine (L5501) and trypsin EDTA (59418C) were purchased from Sigma-Aldrich. Anti-p-RPS6KB1 T389 antibody (9862) and total RPS6KB1 antibody (9202), anti-p-GSK3B S9 antibody (5558) and total GSK3B antibody (9315), anti-p-EIF4EBP1 T37/46 antibody (2855) and total EIF4EBP1 antibody (9452), anti-LAMP1 antibody (9091) and anti-rabbit IgG, horseradish peroxidase (HRP; 7074) antibody were purchased from Cell Signaling Technology. Anti-TUBB/ β -Tubulin (MA5-16308) and anti-Tdh (MA5-15738) antibodies were purchased from Thermo Scientific. Yeast does not express GAPDH but instead expresses three orthologs (Tdh1/2/3) of the mammalian protein, and that the antibody was raised against recombinant GAPDH (Thermo Scientific). Anti-APP/amyloid beta oligomer/A11 (AB9234) was purchased from Merck Millipore. Anti-Pgk1 (ab 38007) antibody was purchased from Abcam. Anti-GFP (11 814 460 001) antibody was purchased from Roche. Anti TH/tyrosine hydroxylase (N196) antibody was purchased from Santa Cruz Biotechnology. Anti-mouse IgG, HRP (172-1011) antibody was purchased from Bio-Rad. CMAC-Blue (C2110) was purchased from Life Technologies. Bafilomycin A1 (11038) was purchased from Cayman chemical. VECTASTAIN Elite ABC Kit (PK-6200) was purchased from VECTOR laboratories.

Plasmid constructs, siRNA, shRNA and yeast strains

Plasmids used were GFP-Atg8 (pRS316) (gift from Y. Oshumi [Tokyo Institute of Technology]), SNCA-GFP (pRS 306) under the galactose promoter (gift from Paulo Ludovico) and GFP-bA₁₋₄₂ (pRS306). ptfLC3B¹ (gift from Tamotsu Yoshimori; Addgene, 21074), GFP-SNCA² (gift from David Rubinzstein; Addgene, 40822). pLKO.1-GSK3B-#1 was a gift from Alex Toker³ (Addgene, 32496). Scrambled shRNA was a gift from David Sabatini⁴ (Addgene, 1864). ERR α siRNA (L-003403-00) and scrambled siRNA (D-001810-10-05) were procured from Dharmacon.

Yeast media, culture conditions, growth assays and SNCA-GFP aggregate induction

Yeast media used for culturing were YPD (yeast extract, peptone and dextrose) for wild-type (WT) GFP and autophagy mutant strains, SD-Ura (synthetic dextrose [2%] medium without uracil) for culturing the SNCA-GFP strain and the GFP-Atg8-processing assay, SG-Ura (synthetic galactose [2%] medium without uracil) to induce SNCA-GFP expression. All strains were cultured at 30°C and 250 rpm.

Growth assays: In a 384-well plate, appropriate yeast strains were seeded ($A_{600} \sim 0.07$) with or without drugs and incubated (80 μ l, 30°C and 420 rpm) in a multiplate reader (Varioskan Flash, Thermo Scientific, USA) for 48 h with automatic absorbance (A_{600}) recording every 20 min. Growth curves were plotted and analyzed using GraphPad Prism.

Induction of SNCA-GFP aggregates: To induce SNCA-GFP aggregates, the corresponding strains were inoculated in SD-Ura medium. Secondary culture was inoculated from primary inoculum until the absorbance at A_{600} reached 0.8/ml. Cells were washed twice with sterile water and adding SG-Ura for 12 to 16 h induced aggregates.

Small molecule screen

To screen small molecule library LOPAC¹²⁸⁰ in the *S. cerevisiae* SNCA toxicity model, working plates containing 50 μ M drugs in 1.5% DMSO (190 compounds/plate) were prepared in a 384-well format. WT SNCA-GFP with or without small molecules and untreated WT GFP were grown under optimized conditions (80 μ l, 30°C and 420 rpm) for 36 h in a plate reader (Varioskan Flash, Thermo Scientific) in duplicates with automatic absorbance (A_{600}) recording every 20 min. Growth curves of untreated WT GFP and WT SNCA-GFP strains were plotted and mid to late exponential phase time point of untreated WT GFP strain was chosen as reference for data analysis. Its corresponding time point of untreated and drug-treated WT SNCA-GFP strains were plotted separately in a box plot. Small molecules that rescued the growth lag by ≥ 3 SD units of untreated WT SNCA-GFP strain were considered as 'Hits'.

SNCA-GFP degradation assays

To assess SNCA-GFP degradation efficacy by small molecules, after inducing SNCA-GFP aggregate, adding dextrose turned off the galactose promoter. Cells were treated with small

molecule(s) (50 μ M) for 0, 6, 12 and 24 h. Subsequent degradation of SNCA-GFP levels were analyzed using immunoblotting.

Mammalian cell culture

HeLa cells were maintained in DMEM containing 10% fetal bovine serum (Pan-Biotech, P03-6510). Undifferentiated SH-SY5Y cells were maintained in DMEM-F12 containing 10% fetal bovine serum (Life Technologies, 12500062). Cell lines were cultured in the presence of 5% CO₂ at 37°C. To perform autophagy assays, equal numbers of subconfluent HeLa cells were seeded in 6-well dishes, allowed to attach for 24 h, treated with small molecules and/or 3-MA (5 mM) in growth medium for 2 h. For the GFP-SNCA degradation assay, equal numbers of subconfluent SH-SY5Y cells were seeded in 6-well dishes and allowed to attach for 24 h. Cells were transfected with GFP-SNCA plasmid using Lipofectamine 2000 (Life Technologies, 11668-019) and allowed to express for 24 h. Cells were treated with small molecules for 24 h and fold GFP-SNCA levels were analyzed using immuno blotting.

For the tandem RFP-GFP-LC3B assay, subconfluent cells were seeded in 60-mm dishes, transfected with tandem RFP-GFP-LC3B plasmid construct and allowed to express for 24 h. Later, cells were trypsinized, reseeded (10^5 cells) and allowed to attach on cover slips in a 12-well plate. Cells were treated with or without small molecules for 2 h and cover slips were processed for imaging.

Immunoblot analysis

Preparation of yeast lysates: Yeast strains ($A_{600}=3$) were resuspended in trichloroacetic acid (12.5%, v/v) and stored at -80°C for at least half an hour. Samples were thawed on ice, centrifuged (16000 x g, 10 min) and the pellet was washed twice with ice-cold acetone (80%, v/v). Pellets were air dried, resuspended in lysis (1% SDS and 0.1 N NaOH) solution and Laemmli buffer and boiled for 10 mins.

Preparation of mammalian cell lysates: After treatments, cells were collected in Laemmli buffer to perform the LC3B processing assay, RPS6KB1, GSK3B and EIF4EBP1 immunoblotting. To validate GFP-SNCA degradation by small molecules, treated cells were scraped and collected in growth medium. After washing with phosphate buffer, pellets were lysed in Laemmli buffer and boiled for 10 mins. Samples were electrophoresed on

SDS-PAGE (8-15%) and then transferred onto PVDF (Bio-Rad, 162-0177) membrane using Transblot turbo (Bio-Rad). Transferred blots were stained with Ponceau S, probed with appropriate primary antibodies overnight and subsequently with HRP-conjugated secondary antibody. Signals were developed using enhanced chemiluminescence substrate (Clarity, Bio-Rad), imaged using a gel documentation system (G-Box, Syngene, UK) and bands were quantified using ImageJ software (NIH).

GFP-Atg8-processing assay

A *S. cerevisiae* strain with an GFP-Atg8 plasmid was grown in SD-U (synthetic dextrose medium without uracil) under standardized conditions (30°C, 250 rpm). Using this, the secondary culture was inoculated ($A_{600} = 0.2$) and grown under the same standardized conditions until the culture absorbance reached $A_{600} = 0.7$. For assessing the effect of small molecules in inducing autophagy in growth conditions, the cells were transferred to SD-U with small molecules for 6 h. To test the effect of small molecules in enhancing starvation-induced autophagy, cells were washed twice and transferred to starvation medium with small molecules and samples were collected for 0, 2, 4 and 6 h time points⁵. Proteins were precipitated using trichloroacetic acid and resolved by SDS-PAGE (10%) followed by immunoblotting. In the blot, "GFP-Atg8 accumulation" indicates the induction of Atg8 expression and "free GFP release" indicates the degradation of Atg8 in the vacuole. The GFP-Atg8 protein is degraded in the vacuole (yeast lysosome); however, the GFP tag is relatively more resistant to vacuolar hydrolases. The levels of GFP-Atg8 (intact fusion protein) would indicate induction of Atg8 expression (which in turn is interpreted as possible autophagy induction) whereas comparison to the total GFP (summation of GFP signals from both full-length GFP-Atg8 and free GFP) indicates the autophagy flux^{6,7} (turnover of the fusion GFP-Atg8 protein to free GFP).

Microscopy

Yeast cultures after respective treatments were washed, mounted on an agarose (2%) gel pad and imaged.

For mammalian cell microscopy, after 2 h of treatment, coverslips were fixed using 4% paraformaldehyde (PFA; Sigma, 158127) and permeabilized using Triton X-100 (0.2%; HiMedia, MB031). Coverslips were mounted using antifade, Vectashield (Vector

laboratories, H-1000). For antibody staining, coverslips were blocked in 5% BSA (Sigma, RM105) for 1 h, incubated in primary antibody overnight and subsequently probed with fluorescent-conjugated antibody. Coverslips were mounted using antifade, Vectashield.

Images were acquired using DeltaVision Elite widefield microscope (API, GE, USA) with the following filters: DAPI (390/18 and 435/48), FITC (490/20 and 529/38), TRITC (542/27 and 594/45) and Cy5 (632/22 and 676/34). Images were processed using DV SoftWoRX software.

The tandem RFP-GFP-LC3B assay (sometimes referred to as traffic light assay) is one test to assess autophagic flux in mammalian cells¹. In this assay, autophagosomes appear as yellow puncta. Unlike RFP, GFP fluorescence being pH sensitive, gets quenched in the acidic pH environment of autolysosomes and thus appears red.

For the FITC-dextran uptake assay, after drug treatments, the HeLa cells were incubated with FITC-dextran (70 kDa; Sigma, 46945) for 30 mins at 2 different temperature conditions (37°C and 16°C).

Cell viability assay

SH-SY5Y cells were seeded on 96-well plates and transfected with a plasmid encoding GFP-SNCA only and/or cotransfected with *GSK3B* shRNA and GFP-SNCA. To cells, the drugs were added (24 h) after 48 h of transfection. Then, the cell viability was measured using the CellTitre-Glo® (Promega, G7570) and luminescence was measured using a Varioskan Flash reader (Thermo Scientific).

Animal studies

All procedures in this study were approved by the JNCASR Institute Animal Ethical Committee (IAEC) and conducted as per the guidelines of the Committee for the Purpose of Control and Supervision of Experiments on Animals (CPCSEA). Inbred male C57BL/6 mice (3 to 4 months old) were used for all experimental cohorts.

Studies on MPTP mouse PD model

Mice were randomly allocated to 5 different study cohorts, viz., Placebo (n = 5), small molecule-only (n = 5), MPTP (n = 5), MPTP+Pro (n = 3) and MPTP+Co (n = 5). As

described previously⁸, 23.4 mg/kg MPTP.HCl (equivalent to 20 mg/kg free base) in 10 ml/kg body weight of saline was administered intraperitoneally (i.p.) for 4 times at 2-h intervals. Further, 5 mg/kg body weight of small molecule(s) in 100 µl of saline was administered i.p. to the MPTP-injected animals by following either of the 2 different regimens; the first regimen was comprised of a prophylactic, pretreatment which was begun 2 days prior to MPTP administration (MPTP+Pro); while the second involved treatment given alongside the MPTP injection (MPTP+Co). In both the cases, small molecule(s) was administered for 7 days post-MPTP administration daily (**Fig. S5A**). The other experimental cohorts included placebo, small molecule(s) only (daily i.p.) and MPTP alone (daily vehicle) for 9 days. All mice were sacrificed 7 days post MPTP administration and brains were processed for immunohistochemistry.

Immunohistochemistry

Mice were anaesthetized using Halothane BP (Piramal Healthcare) inhalation and perfused intracardially with normal saline followed by 4% PFA in 0.1 M phosphate buffer, pH 7.4. Mice brains were removed quickly and postfixed with 4% PFA for 24 to 48 h at 4°C. Following cryoprotection in 15 and 30% sucrose (HiMedia, MB025), 40-µm-thick coronal cryosections of midbrain were collected serially on gelatinized slides. The immunoperoxidase labeling protocol was identical to that reported⁹. Briefly, endogenous peroxidase was quenched using H₂O₂ (0.1%) in methanol (70%), followed by blocking of nonspecific staining by a buffered solution (3%) of BSA for 4 h at room temperature. Sections were incubated with TH primary antibody (1:500) followed by biotin-conjugated secondary antibody (1:200 dilution; Vector Laboratories, BA-1400). Tertiary labeling was performed with avidin-biotin complex solution (1:100; Vector Laboratories, PK-6200). Staining was visualized using 3'-3'-diaminobenzidine (0.5%; Sigma, D3939) as a chromogen in a solution of 0.1 M acetate imidazole buffer (pH 7.4) and H₂O₂ (0.1%). Negative controls were processed identically, except that the primary antibody was replaced with dilution buffer.

For immunofluorescent-based double labeling, the sequential staining procedure was followed¹⁰. Brains sections were stained for TH and LC3B-APP/amyloid beta oligomer/A11 and images were acquired using a DeltaVision Elite widefield microscope (API, GE).

Stereological quantification of TH⁺ dopaminergic neurons in SNpc

As described¹¹, SNpc was delineated using the 4X objective of Olympus BX61 Microscope (Olympus, Japan) equipped with Stereo Investigator Software Version 7.2 (Micro Bright Field, USA). Stereological quantification was performed using optical fractionator probe with slight modifications¹¹. Briefly, every sixth midbrain section containing SNpc was chosen and TH⁺ cells were counted under the 100X objective, with a regular grid interval of 22,500 μm^2 ($x=150 \mu\text{m}$, $y=150 \mu\text{m}$) and counting frame with an area of 3600 μm^2 ($x=60 \mu\text{m}$, $y=60 \mu\text{m}$). Mounted thickness was determined at every fifth site, which averaged to 25 μm . A guard zone of 4 μm was applied on either side, thus providing 17 μm of z-dimension within the optical dissector. The quantification was performed starting with the first anterior appearance of TH⁺ neurons in SNpc to the caudal-most part. The SNpc volume was determined by planimetry and total number of neurons according to mean measured thickness were noted.

Densitometry-based image analysis

We used high magnification images of TH-stained nigral DAergic neurons, captured for offline assessment of expression levels. Expression intensity was measured using a Windows-based image analysis system (Q Win V3, Leica Systems, Germany). Cumulative mean was derived from the values obtained from sampling, approximately 200 DAergic neurons per animal. Intensity output measured on a grayscale of 0 to 255, where 0 equals intense staining and 255 means absence of staining. Thus, lower gray values suggest higher protein expression and vice versa.

***In vivo* blood brain barrier assay**

Animals were randomly allocated for placebo control and drug treatment cohorts. C57BL/6J mice were injected with placebo control or 6-Bio (5 mg/kg of body weight, intraperitoneally) twice with a 24-h time interval. After second injection, the brains were harvested at 15 min, 30 min, 60 min, 6 h, 12 h and 24 h by cervical dislocation. Mice brains were immediately homogenized with RIPA buffer [25 mM Tris-HCL, 150 mM sodium chloride, 1% NP-40 (v/v), 1% sodium deoxycholate (w/v) and 0.1% sodium dodecyl sulphate (w/v)] with protease inhibitor cocktail [Roche, 11836170001] for both treatment cohorts. Homogenously macerated mouse brain sample (100 μl) was mixed with

Chapter 2: *Materials and methods*

acetonitrile (ACN, 400 μ l), formic acid (0.2%, v/v) and aceclofenac (100 ng/ml, an internal standard; Sigma, A8861), vortexed for 10 min at 2000 rpm Orbital shaker (compact digital microplate shaker, 88880024, Thermo Scientific, USA). Then, samples were centrifuged and the supernatant was injected for LC MS/MS. Standard samples were prepared by spiking 6-Bio standard into a blank control brain sample. Standard spiking was performed such that resultant concentrations were 0, 10, 100, 500, 1000, 1500 and 2000 ng/ml of drug in blank brain matrix. For LC, PE 200 (Perkin Elmer, USA) HPLC with an Agilent Zorbax XDB C8 4.6X75 mm, 3.5- μ m column (Agilent Technologies, USA) was employed. The following conditions were used for LC: Mobile phases (0.1% formic acid in water (5%):methanol (95%)), isocratic flow rate (0.7 ml/min), run time (4 min), injection volume (15 μ l) and needle wash solution (1:1 methanol:water mix containing 0.1% formic acid). The mass spectrometry (API3000, AB Sciex, USA) was used with aceclofenac as an internal control and data were processed using Analyst Software V1.4.2. Drug injections of the various cohorts and preparations of the brain homogenates were performed at JNCASR. ACQUITY LABORATORIES performed the above mentioned LC-MS/MS analysis of the brain samples.

Behavioral studies

Behavioral procedures used for this study were modified from refs¹²⁻¹⁵. All the behavioral experiments were done on 3- to 4-month-old, male C57BL/6J mice. Experimenters were blind to the drug injected animals. Experimenters handled mice used for behavioral experiments for 3 consecutive days prior to the training paradigm. Behavioral experiments were designed in an order of low- to high-stress activity for mice. Therefore, the open field test was conducted in the forenoon whereas the rotarod was performed in the afternoon. Mice were habituated to the behavior room for 15 min every day before the start of experiments. The light intensity was maintained at 100 lux throughout the experiment. Mice were weighed every day before training or test to ensure their good health. Mice were randomly allocated into 3 treatment cohorts: placebo control, MPTP and MPTP+Co. Data were plotted using GraphPad prism 5 software.

Rotarod trials

The rotarod instrument was custom made at the mechanical workshop, National Centre of Biological Sciences, Bengaluru, India. The rotating rod (diameter 3.3 cm) was made of

Delrin and was textured to enhance the grip of mice. The rod was fixed at a height of 30 cm from the cushioned platform where mice fell on to during training and test. The rod was partitioned into 3 areas of 9.3-cm distance between each partition using discs (40-cm diameter) made of Teflon. Mice were trained in the rotarod for 5 consecutive days prior to drug injection. Each mouse was trained in the rotarod by gradually increasing the rotations on every day. On day 1, mice were trained at 5 to 10 rpm (accelerated at 1 rpm/5 seconds), 11 to 15 rpm (accelerated at 1 rpm/5 seconds) on second day, 16 to 20 rpm (accelerated at 1 rpm/5 seconds) on the third day and at 20 rpm (fixed) on day 4 and 5. Mice were trained at the above specific rpm thrice with 5-min interval between trials. The rod was rotated from 5 rpm to 20 rpm by manually changing the speed of the motor (nonautomated). During the test (day 13 postinjection), the rotarod was started at 20 rpm. Mice were tested in a rotating rotarod for a maximum of 60 sec and their latencies were noted down. At the end of each trial, the rotarod was wiped with 70% ethanol and left for drying before placing the next set of mice. The entire trial was video recorded using a DSLR camera (Nikon D5100) and latencies were scored manually. The average time spent on the rotating rotarod across 3 trials were plotted as mean latency to fall.

Open field test

The open field arena (50 cm X 50 cm X 45 cm) was custom-made (JNCASR) using plywood and the internal surface was coated with white polish. Mice were trained in the open field for 2 consecutive days prior to drug injection. During training or testing, one animal at a time was placed in the zone periphery in the open field arena and allowed to explore the arena for 5 min. The activity was video recorded (SONY[®] color video camera, Model no. SSC-G118, India) using software (SMART v3.0.04 from Panlab, Harvard Apparatus, USA). After 5 min, the mouse was returned to its home cage. The open field arena was then wiped using 70% ethanol and allowed to dry before placing the next mouse. Distances travelled were analyzed offline by an experimenter who was not involved in performing the experiment.

Statistical Analysis

Statistical analyses were performed using the unpaired Student t test and ANOVA (one-way or two-way) followed by the post-hoc Bonferroni test in GraphPad Prism. Error bars were expressed as mean \pm SEM.

References

1. Kimura S, Noda T, Yoshimori T. Dissection of the autophagosome maturation process by a novel reporter protein, tandem fluorescent-tagged LC3. *Autophagy* 2007; 3:452-60.
2. Furlong RA, Narain Y, Rankin J, Wytenbach A, Rubinsztein DC. Alpha-synuclein overexpression promotes aggregation of mutant huntingtin. *Biochem J* 2000; 346 Pt 3:577-81.
3. Yoeli-Lerner M, Chin YR, Hansen CK, Toker A. Akt/protein kinase b and glycogen synthase kinase-3beta signaling pathway regulates cell migration through the NFAT1 transcription factor. *Molecular cancer research : MCR* 2009; 7:425-32.
4. Sarbassov DD, Guertin DA, Ali SM, Sabatini DM. Phosphorylation and regulation of Akt/PKB by the rictor-mTOR complex. *Science* 2005; 307:1098-101.
5. Rajasekhar K, Narayanaswamy N, Mishra P, Suresh SN, Manjithaya R, Govindaraju T. Synthesis of Hybrid Cyclic Peptoids and Identification of Autophagy Enhancer. *Chempluschem* 2014; 79:25-30.
6. Graef M, Nunnari J. Mitochondria regulate autophagy by conserved signalling pathways. *The EMBO journal* 2011; 30:2101-14.
7. Silva-Alvarez C, Arrazola MS, Godoy JA, Ordenes D, Inestrosa NC. Canonical Wnt signaling protects hippocampal neurons from Abeta oligomers: role of non-canonical Wnt-5a/Ca(2+) in mitochondrial dynamics. *Frontiers in cellular neuroscience* 2013; 7:97.
8. Jackson-Lewis V, Przedborski S. Protocol for the MPTP mouse model of Parkinson's disease. *Nature protocols* 2007; 2:141-51.
9. Alladi PA, Mahadevan A, Yasha TC, Raju TR, Shankar SK, Muthane U. Absence of age-related changes in nigral dopaminergic neurons of Asian Indians: relevance to lower incidence of Parkinson's disease. *Neuroscience* 2009; 159:236-45.
10. Vidyadhara DJ, Yarreiphang H, Raju TR, Alladi PA. Admixing of MPTP-Resistant and Susceptible Mice Strains Augments Nigrostriatal Neuronal Correlates to Resist MPTP-Induced Neurodegeneration. *Mol Neurobiol* 2016.

Chapter 2: *Materials and methods*

11. Fu Y, Yuan Y, Halliday G, Rusznak Z, Watson C, Paxinos G. A cytoarchitectonic and chemoarchitectonic analysis of the dopamine cell groups in the substantia nigra, ventral tegmental area, and retrorubral field in the mouse. *Brain Struct Funct* 2012; 217:591-612.
12. Liu W, Jalewa J, Sharma M, Li G, Li L, Holscher C. Neuroprotective effects of lixisenatide and liraglutide in the 1-methyl-4-phenyl-1,2,3,6-tetrahydropyridine mouse model of Parkinson's disease. *Neuroscience* 2015; 303:42-50.
13. Patil SP, Jain PD, Ghumatkar PJ, Tambe R, Sathaye S. Neuroprotective effect of metformin in MPTP-induced Parkinson's disease in mice. *Neuroscience* 2014; 277:747-54.
14. Brooks SP, Dunnett SB. Tests to assess motor phenotype in mice: a user's guide. *Nature reviews Neuroscience* 2009; 10:519-29.
15. *Methods & new frontiers in neuroscience series*. CRC Press LLC 2001.

Chapter 3

**A novel autophagy modulator 6-Bio ameliorates
SNCA/ α -synuclein toxicity**

Note:

**This chapter is published as an original research article in
Autophagy journal (2017); Jul 3;13(7):1221-1234.**

Abstract

Parkinson disease (PD) is a life-threatening neurodegenerative movement disorder with unmet therapeutic intervention. We have identified a small molecule autophagy modulator, 6-Bio that shows clearance of toxic SNCA/α-synuclein (a protein implicated in synucleopathies) aggregates in yeast and mammalian cell lines. 6-Bio induces autophagy and dramatically enhances autolysosome formation resulting in SNCA degradation. Importantly, neuroprotective function of 6-Bio as envisaged by immunohistology and behavior analyses in a preclinical model of PD where it induces autophagy in dopaminergic neurons of mice midbrain to clear toxic protein aggregates suggesting that it could be a potential therapeutic candidate for protein conformational disorders.

Introduction

Parkinson disease is the second most common neurodegenerative disorder affecting 1% of the aging population¹. Motor abnormalities which are the major clinical clues for PD are first manifested when about 60% of the nigral dopaminergic neurons are lost², decreasing dopamine levels. Although L-DOPA has been recommended for PD patients, it does not halt neurodegeneration. Furthermore, the predominant side effect of continuous L-DOPA administration is an occurrence of L-DOPA-induced dyskinesia among PD patients³. Thus, there is an absolute need for better therapeutic agents to be made available for PD patients, aiming to stop or reduce neurodegeneration.

One of the hallmarks of PD is formation of misfolded protein aggregates (Lewy bodies) due to overexpressed SNCA or mutation in genes such as *PINK1* (PTEN induced putative kinase 1), *LRRK2* (leucine rich repeat kinase 2) that lead to death of dopaminergic neurons. The accumulation of these aggregates disrupts proteostasis machineries that process misfolded proteins such as chaperones, proteasome or macroautophagy (hereafter autophagy) leading to neuronal degeneration⁴. Misfolded SNCA aggregates are refractory to proteostasis maintaining processes and the resultant cytotoxicity is further exasperated by aging, as unlike mitotic cells non dividing neurons cannot dilute out these aggregates.⁴ In accordance, neuronal specific loss of autophagy function leads to aggregate formation and subsequent neurodegeneration suggesting a role for basal autophagy in preventing aggregate buildup⁵⁻⁷. As autophagy is dysfunctional in many neurodegenerative disorders⁴,

several studies have pointed out that restoring proteostasis by up regulating autophagy can eliminate these protein aggregates and restore cellular homeostasis⁸⁻¹⁰.

One of the main causes of this disease is the toxic build of protein aggregates leading to neuronal death. We screened for small molecule drug-like compounds that clear such protein aggregates (aggrephagy) and restore cell viability. Several model systems were employed to identify and evaluate the small molecules for aggrephagy. Towards this, rather than a conventional structure based drug designing, we sought for a phenotypic-based small molecule screening in yeast and validated the results in higher model systems. In this study, we identified a small molecule 6-Bio for its ability to clear SNCA aggregates and restore cellular homeostasis. We further show that 6-Bio induces autophagy and strongly drives autophagy flux resulting in aggregate clearance. We elucidated that 6-Bio modulates autophagy flux through inhibiting GSK3B activity. GSK3B has been associated with Alzheimer disease pathogenesis by modulating two processes namely (i) β -amyloid build up and (ii) formation of neurofibrillary tangles¹¹. It has been demonstrated at cellular level experiments that inhibiting GSK3B would ablate the expression of SNCA¹² suggesting its role in synucleopathies. Finally, in a preclinical mice model of PD, 6-Bio showed potent neuroprotective ability revealed by immunohistological and behavior analyses.

Results

Small-molecule screening reveals 6-Bio as a potent inducer of autophagy

The occurrence of protein aggregates and cytotoxicity by SNCA overexpression is also recapitulated in the budding yeast, *S. cerevisiae* (**Fig. 1, A to C**)¹³. We employed this "out-of-the-box" yeast model¹⁴ to screen for small molecules that would prevent cytotoxicity by aggregate degradation.

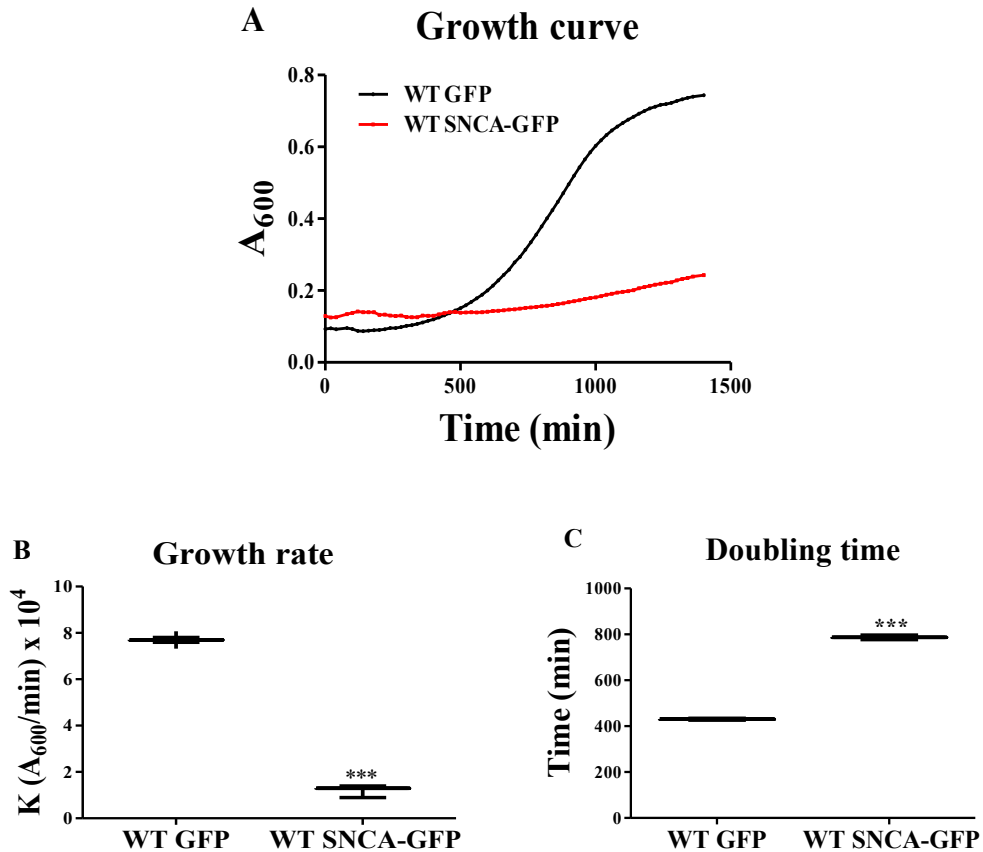


Figure 1. *S. cerevisiae* SNCA toxicity model. (A to C) Growth curve (A), growth rate (B) and doubling time (C) of WT SNCA-GFP (red curve) versus WT GFP (black curve) strains. ***- $P < 0.001$ as determined by one-way ANOVA analysis, and the post-hoc Bonferroni test. Error bar indicates, mean \pm SEM.

We screened a small molecule library containing pharmacologically active compounds (LOPAC¹²⁸⁰) using an SNCA yeast toxicity assay (Fig. 2).

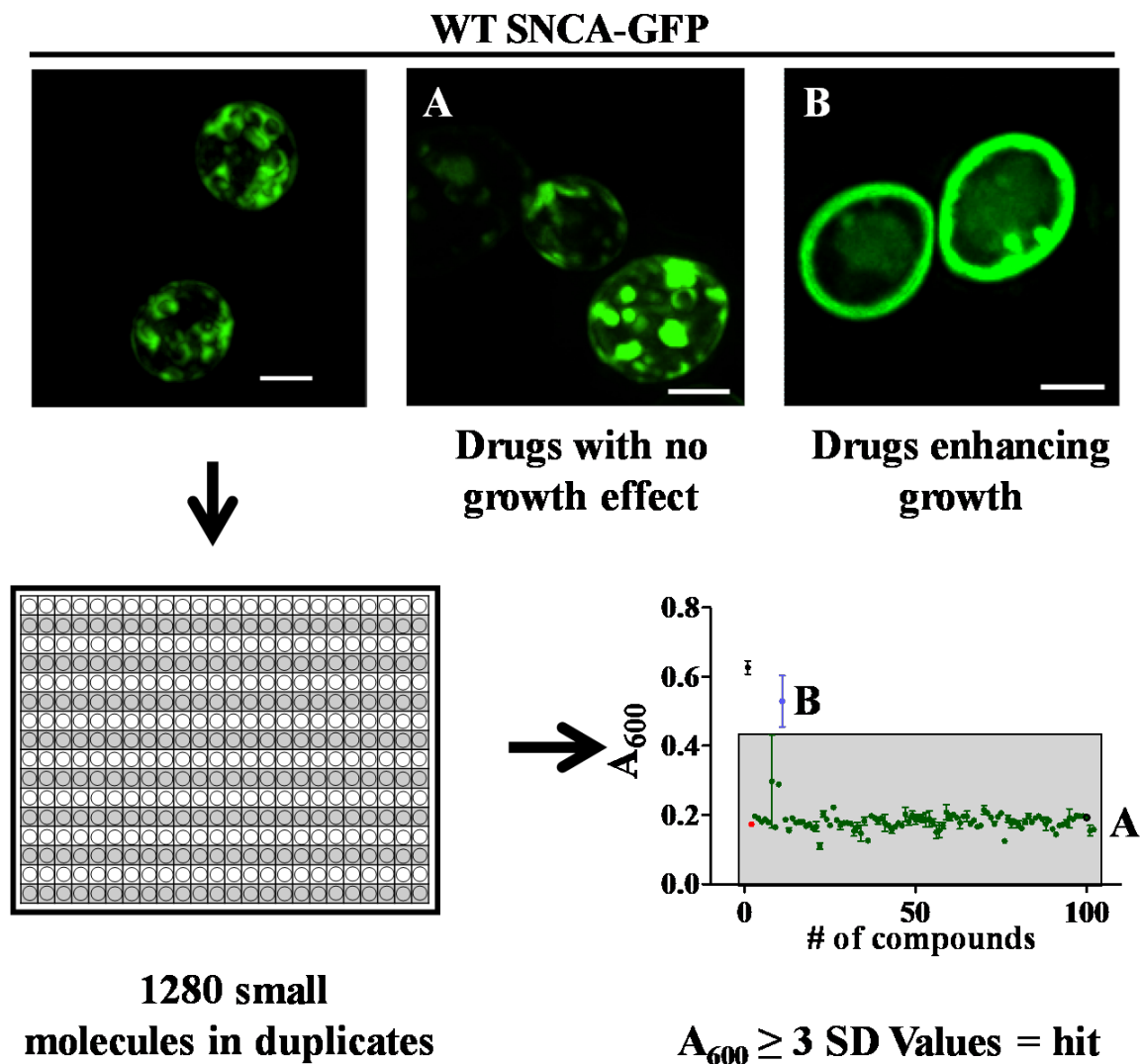


Figure 2. Schema for small-molecule screening. Schematic representation of small-molecule library screened in *S. cerevisiae* SNCA toxicity model. Induction of SNCA-GFP overexpression was carried out in presence or absence of small-molecules from the LOPAC library in duplicates. Growth was recorded as absorbance (A_{600}) and a box plot for each compound was plotted as described in methods (Small-molecule screen section). The “hits” were compounds that rescued growth (≥ 3 SD units). They also showed free GFP in the vacuole along with restoration of native localization of SNCA-GFP on the plasma membrane (B) unlike other compounds that didn’t rescue growth lag or vehicle-treated cells (A), scale bar: 2 μm .

Of the hits that rescued growth in this model was the SIRT2 inhibitor AGK2, which was shown to rescue SNCA toxicity¹⁵ affirming the reliability of the assay and the 6-Bio [(2'Z,3'E)-6-Bromoindirubin-3'-oxime]¹⁶ (Fig. 3A). Interestingly, 6-Bio did not affect the growth of yeast cells (Fig. 3B).

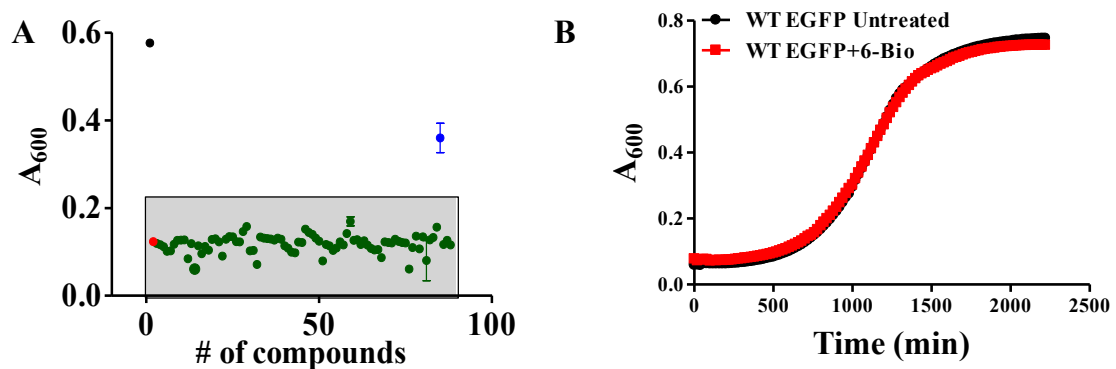


Figure 3. 6-Bio rescued SNCA toxicity. (A) Box plot demonstrating hits from a small molecule library of pharmacologically active compounds, LOPAC¹²⁸⁰, screened in *S. cerevisiae* toxicity model of SNCA. Detailed screening methodology is explained in the methods section. In the box plot, compounds that rescued the growth (denoted by absorbance, A_{600}) of WT SNCA-GFP strains ≥ 3 SD units (gray box) are considered hits (blue) and the ones that do not are in green. WT GFP (black) and untreated WT SNCA-GFP (red) represent the positive and negative controls. A representative plot for 100 compounds is shown. (B) Growth curve of WT GFP cells with or without 6-Bio (50 μ M) treatment.

In order to understand the involvement of 6-Bio in autophagy, GFP-Atg8 (GFP tagged autophagy-related 8, a yeast autophagosome marker)-processing assay under both growth and starvation conditions were employed. During growth conditions where autophagy is barely detectable, 6-Bio dramatically induced autophagy (6-h time point, $P < 0.001$ versus untreated; Fig. 4) and also the flux (6h time point, $P < 0.001$ versus untreated; Fig. 4).

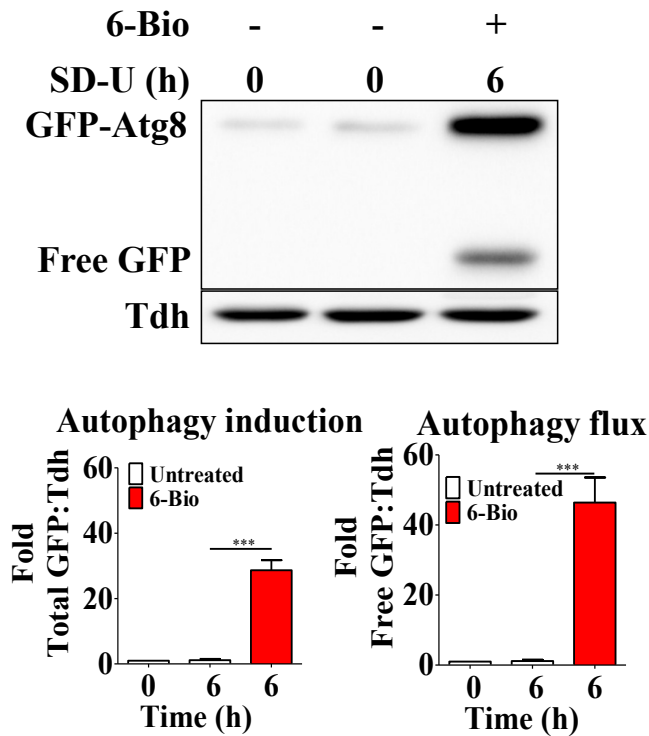


Figure 4. 6-Bio induces basal autophagy. Representative western blot of the GFP-Atg8-processing assay under growth condition. WT strain expressing GFP-Atg8 treated with or without 6-Bio (50 μ M). Fusion protein GFP-Atg8 accumulation and free GFP release was monitored across the time course (0 and 6 h). Tdh reactivity served as a loading control. Representative graph for quantification of autophagic induction and flux ($n=4$). Statistical analysis was performed using unpaired Student *t* test. Error bars, mean \pm SEM. ***- $P < 0.001$.

Similarly, 6-Bio treatment under starvation condition showed significant increase in autophagy induction (4h and 6h time points, $P < 0.001$ versus untreated; **Fig. 5**) and flux (4h and 6h time points, $P < 0.01$ and $P < 0.001$, respectively versus untreated; **Fig. 5**) by 2 fold in a time dependent manner suggesting 6-Bio augmented starvation-induced autophagy.

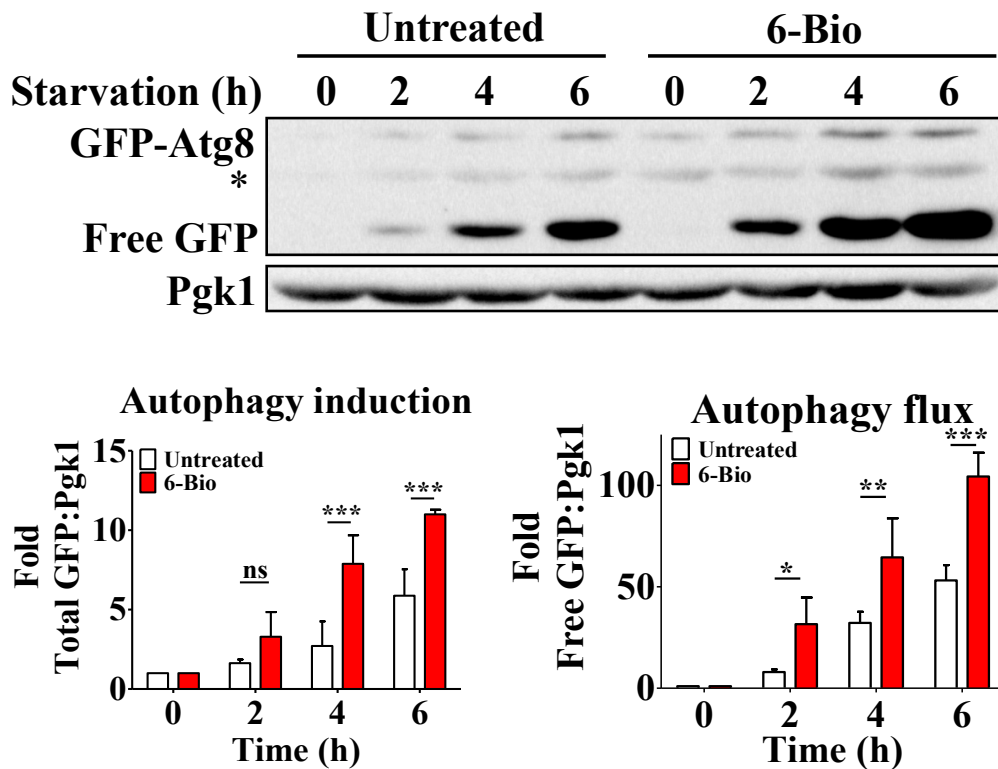
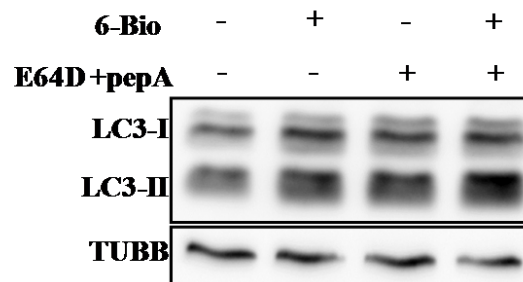


Figure 5. 6-Bio induces starvation induced autophagy. Representative western blot for the GFP-Atg8-processing assay. Fusion protein GFP-Atg8 accumulation and free GFP release monitored across the time course (0, 2, 4 and 6 h) under starvation conditions in the WT strain expressing GFP-Atg8 treated with 6-Bio (50 μ M). Representative graph for quantification of autophagic induction and flux ($n = 3$); * indicates nonspecific band. Pgk1 was assessed as loading control. Statistical analysis was performed using one-way ANOVA and the post-hoc Bonferroni test. Error bars, mean \pm SEM. ns-non significant, *- $P < 0.05$, **- $P < 0.01$, ***- $P < 0.001$.

We further tested 6-Bio for autophagy modulation in mammalian cells. Towards this, we employed MAP1LC3B/LC3B (microtubule associated protein 1 light chain 3 beta, a mammalian autophagosome marker and an ortholog of yeast Atg8) processing and tandem RFP-GFP-LC3B assays. In HeLa cells, 6-Bio increased LC3B-II (the autophagosome-associated, processed form of LC3B-I) levels in a dose-dependent manner suggesting autophagy modulation (**Fig. 14**). In the presence of lysosomal protease inhibitors, E64D and pepstatin A, LC3B-II accumulation was significantly more than that of 6-Bio only and/or

E64D and pepstatin A only (**Fig. 6, A and B**), validating that 6-Bio is indeed an autophagy enhancer.

A



B

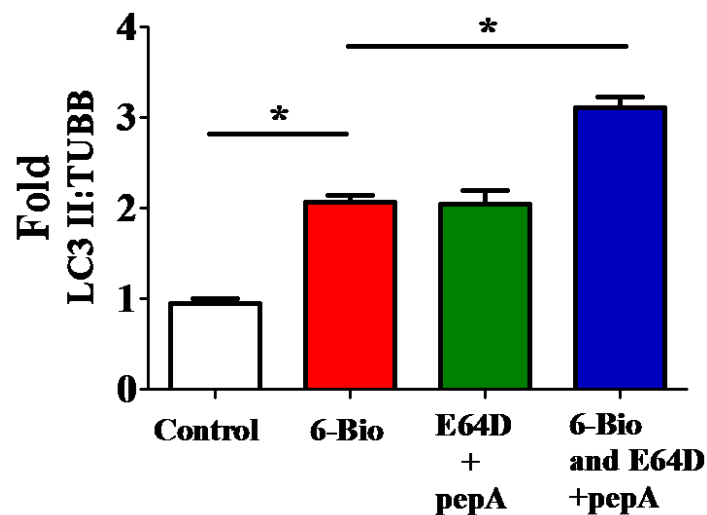


Figure 6. LC3B processing by 6-Bio in presence of protease inhibitors, E64D and pepstatin A. (A) Representative immunoblots for HeLa cells treated with 6-Bio (5 μ M), E64D (25 μ M) plus pepstatin A (50 μ M), and both (6-Bio and E64D plus pepstatin A) for 2 h. After treatments, lysates were analyzed for accumulation of LC3B-II by immunoblotting. TUBB served as a loading control. (B) Quantification indicating the fold change of LC3B-II levels normalized with TUBB for the mentioned treatments. Statistical analysis was performed using one-way ANOVA and the post-hoc Bonferroni test. Error bars, mean \pm SEM. *-P <0.05.

In the tandem RFP-GFP-LC3B assay that reveals autophagy flux, 6-Bio treatment dramatically increased autolysosome numbers (~9 fold, $P < 0.001$, compared to control; **Fig. 7**) indicating enhanced fusion of autophagosomes with lysosomes.

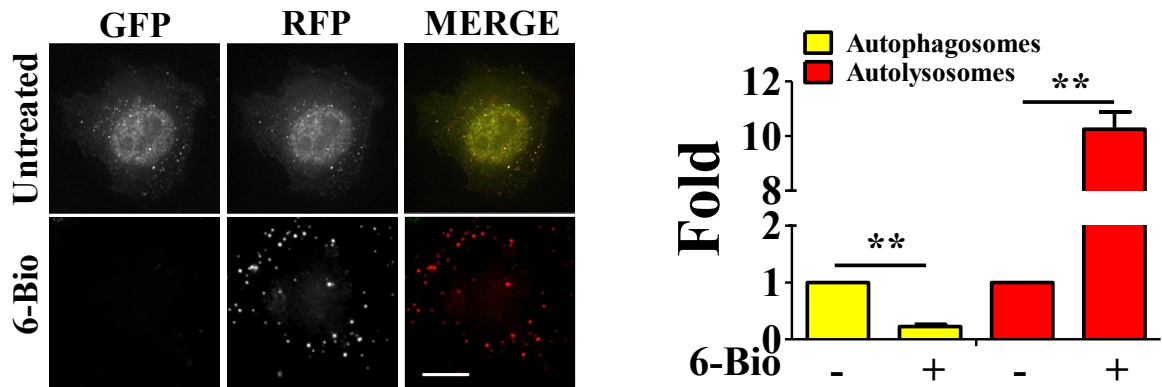


Figure 7. Tandem RFP-GFP-LC3B assay. Representative microscopy images of *ptf* LC3B transfected HeLa cells treated with 6-Bio (5 μ M) and quantification of autophagosome and autolysosome indicating fold change over its untreated counterpart ($n = 25$), scale bar: 15 μ m. Statistical analysis was performed using unpaired Student *t* test. Error bars, mean \pm SEM. **- $P < 0.01$.

Next, we checked whether the lysosomal functions are perturbed by 6-Bio since it specifically enhances autolysosomes. For this, we checked the lysosomal pH by LysoTracker Deep Red staining upon 6-Bio treatment. HeLa cells were treated with 6-Bio and/or E64D plus pepstatin A for 2 h, followed by treatment with LysoTracker Deep Red for 20 min. LysoTracker Deep Red fluorescence intensity was reduced in presence of protease inhibitors such as E64D and pepstatin A (Pep A). The fluorescence intensity of LysoTracker Deep Red was found to be comparable between untreated and 6-Bio-treated cells (**Fig. 8B**). Thus, we found no difference in both E64D + pep A only, 6-Bio and E64D + pep A treatments (**Fig. 8B**). LysoTracker Deep Red staining indicated that there was no change in lysosome acidification (**Fig. 8**). LAMP1 (lysosomal associated membrane protein 1)-positive vesicle intensities and distribution also were unaltered upon 6-Bio treatment

suggesting that perhaps lysosomal functions were not perturbed by 6-Bio (Fig. 8A).

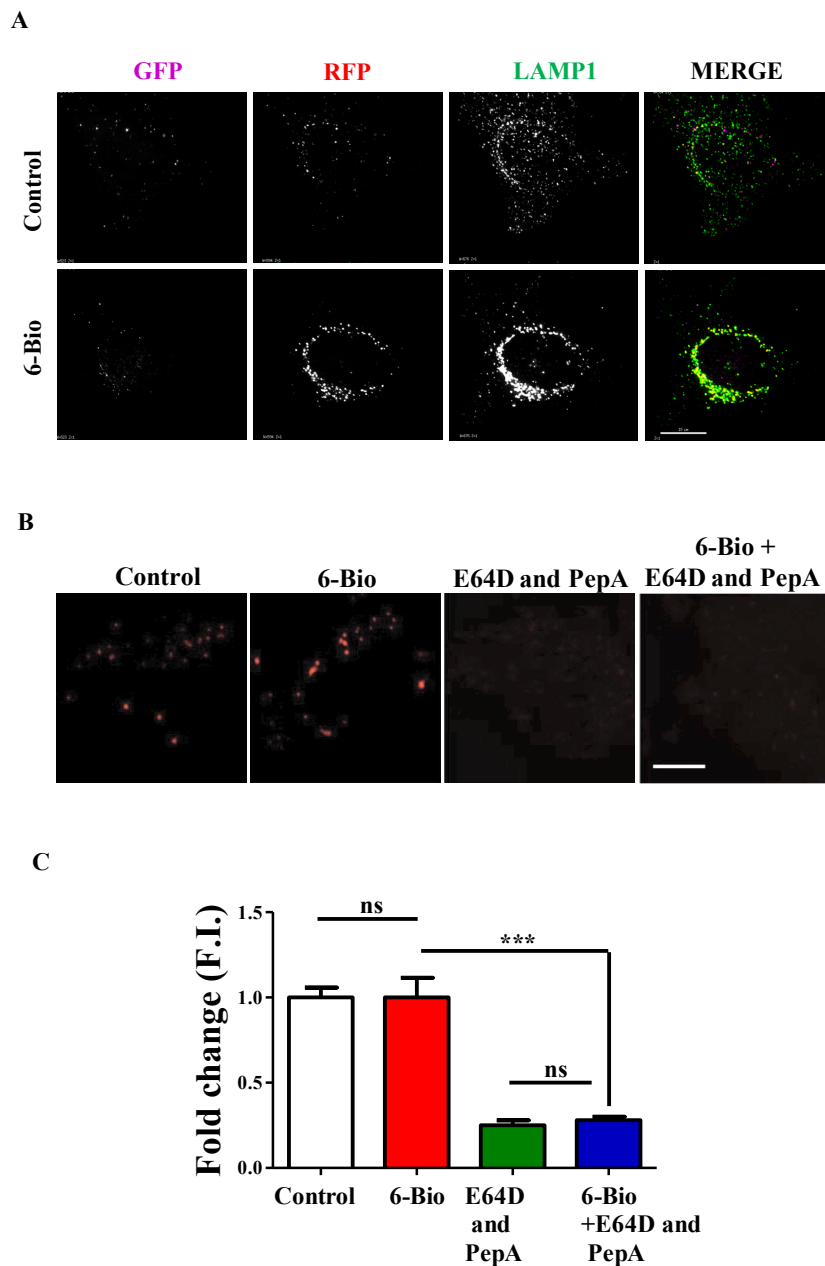
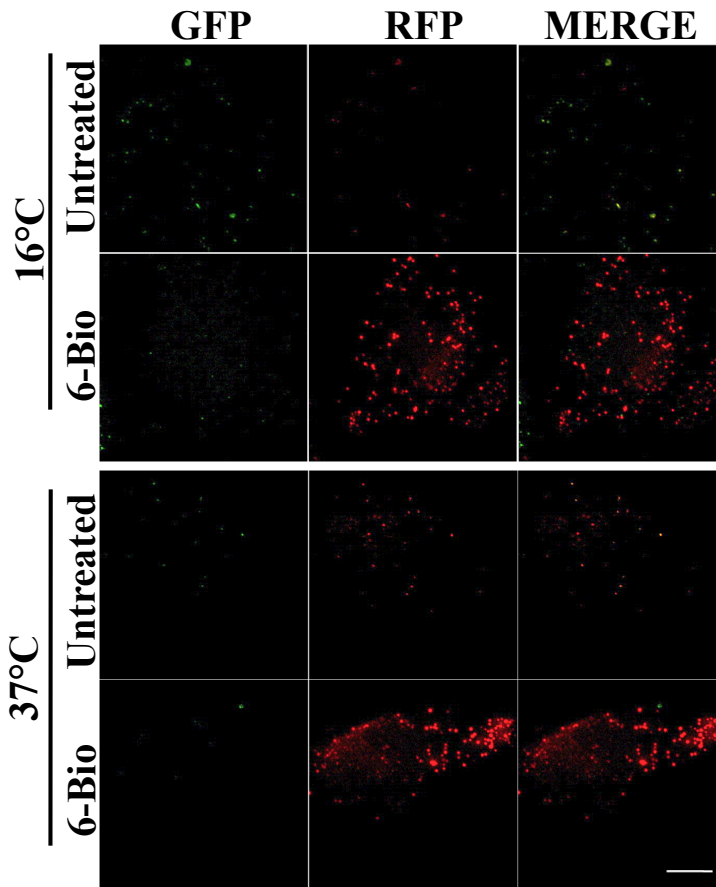


Figure 8. Immunofluorescence analysis of HeLa cells treated with 6-Bio along with lysomotropic agents. (A) Representative microscopy images of the tandem RFP-GFP-LC3B assay of HeLa cells treated with 6-Bio that were later stained for LAMP1 detection. (B) Representative microscopy images of HeLa cells stained with LysoTracker Deep Red for various treatments namely 6-Bio, [E64D (25 μ M) + pepstatin A (50 μ M)] and both. The fold changes of fluorescence intensity (F.I.) for all mentioned treatments were quantified

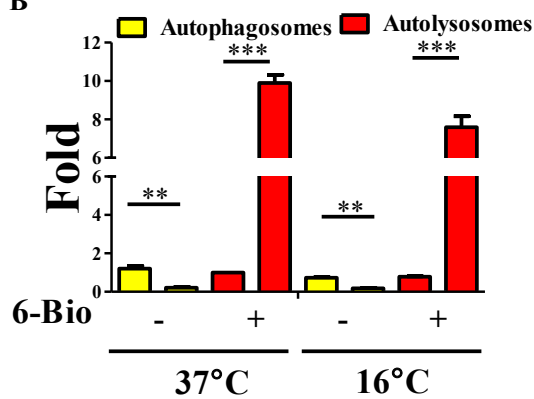
(C). Scale bar is 15 μ m. Statistical analysis was performed using one-way ANOVA and the post-hoc Bonferroni test. Error bars, mean \pm SEM. ns-non significant, ***- $P < 0.001$.

To address if the molecule enters the cell via endocytosis, we carried out the tandem RFP-GFP-LC3B assay at 16°C. At this temperature, endocytosis pathway is highly reduced as evident by the significantly decreased cellular uptake of FITC-dextran (70 kDa) as compared to 37°C (**Fig. 9C**). However, the effect of 6-Bio in increasing fusion between autophagosomes and lysosomes at 37°C (~10 fold, control vs 6-Bio-treated, $P < 0.001$, **Fig. 9, A and B**) and 16°C (~8 fold, control vs 6-Bio-treated, $P < 0.001$, **Fig. 9, A and B**) were comparable suggesting that endocytosis did not play a predominant role in the action of 6-Bio in modulating autophagy. These results suggest that 6-Bio affects autophagy independent of endocytosis perhaps by passive diffusion.

A



B



C

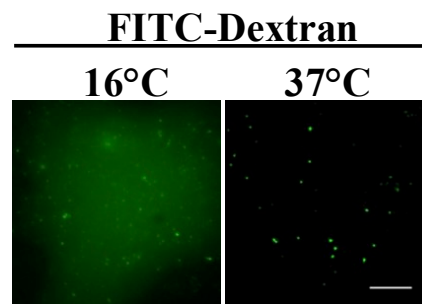


Figure 9. Autophagic modulation by 6-Bio at low temperature. (A) Representative microscopy images of HeLa cells transiently transfected with RFP-GFP-LC3B construct. 48 h post transfection, the cells were treated with 6-Bio (5 μ M) under 2 different temperature conditions (16°C and 37°C). (B) Quantification of fold change in autophagosomes and autolysosomes upon treatment with 6-Bio (5 μ M) under the mentioned

temperature conditions. (C) HeLa cells were incubated with FITC-Dextran (70 kDa) for 2 h under both low (16°C) and high (37°C) temperature conditions. Scale bar: 15 μ m. Statistical analysis was performed using one-way ANOVA and the post-hoc Bonferroni test. Error bars, mean \pm SEM. ns-non significant, **- $P < 0.01$, ***- $P < 0.001$.

From these 2 model systems, we noticed that 6-Bio not only induces autophagy but also enhances starvation-induced autophagy and strikingly promotes autolysosome formation without perturbing the lysosomal function.

6-Bio clears SNCA in an autophagy-dependent manner

Treatment of yeast cells overexpressing SNCA-GFP with 6-Bio, resulted in vacuolar degradation of SNCA-GFP cytosolic aggregates with improved normal plasma membrane localization suggesting possible involvement of autophagy-related pathways (**Fig. 10**).

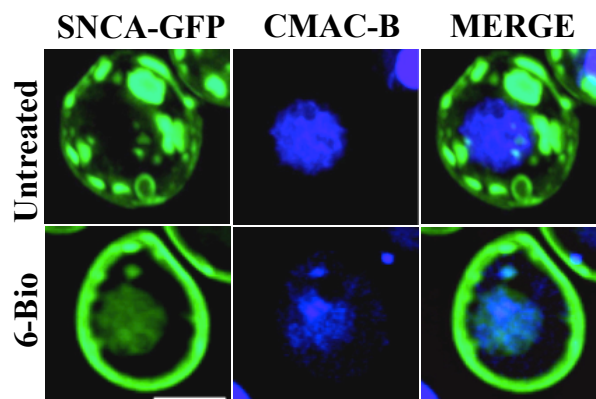


Figure 10. 6-Bio clears SNCA-GFP aggregates. Microscopy images of WT SNCA-GFP yeast cells treated with or without 6-Bio (50 μ M) for 16 h, vacuole stained with CMAC-Blue (100 nM), scale bar: 2 μ m.

In agreement with these observations, 6-Bio failed to rescue the SNCA-mediated toxicity in autophagy gene mutants (*atg1 Δ* , *atg5 Δ* , *atg8 Δ* , *atg11 Δ* and *atg15 Δ*) (Fig. 11).

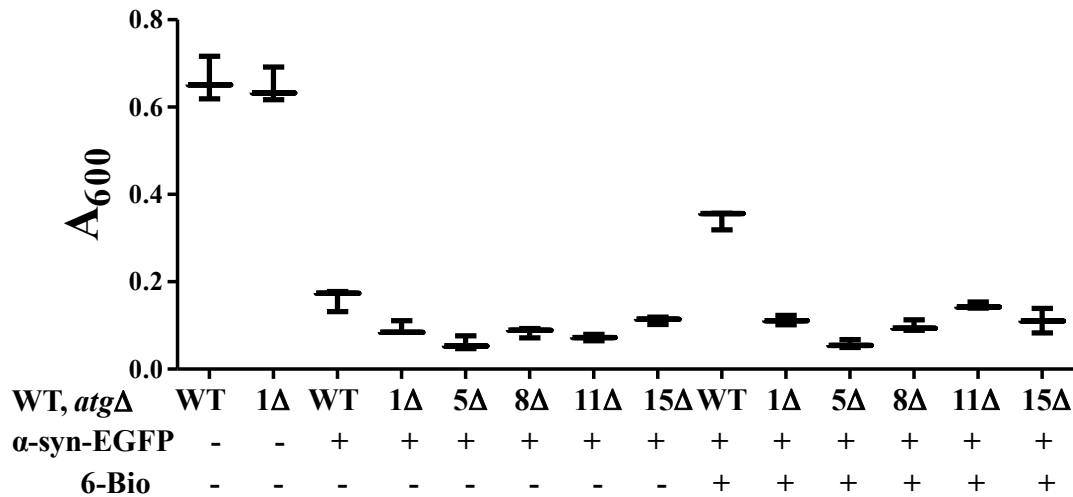


Figure 11. 6-Bio fails to rescue growth lag in autophagy mutants expressing SNCA. Growth plot of autophagy mutants (*atg1 Δ* , *atg5 Δ* , *atg8 Δ* , *atg11 Δ* and *atg15 Δ*) expressing SNCA-GFP observed with or without 6-Bio (50 μ M).

Assays carried out to monitor degradation of SNCA-GFP aggregates in presence of 6-Bio under non-starvation and starvation conditions revealed a time-dependent and significant decrease in the SNCA-GFP levels in wild-type cells (Fig. 12, A and B) but not in an autophagy mutant, *atg1 Δ* (Fig. 12, C and D). These results suggest that 6-Bio treatment was not only able to enhance starvation-induced autophagy but also resulted in a concomitant decrease of SNCA-GFP demonstrating that the prosurvival effects of 6-Bio was due to autophagy-dependent SNCA-GFP clearance.

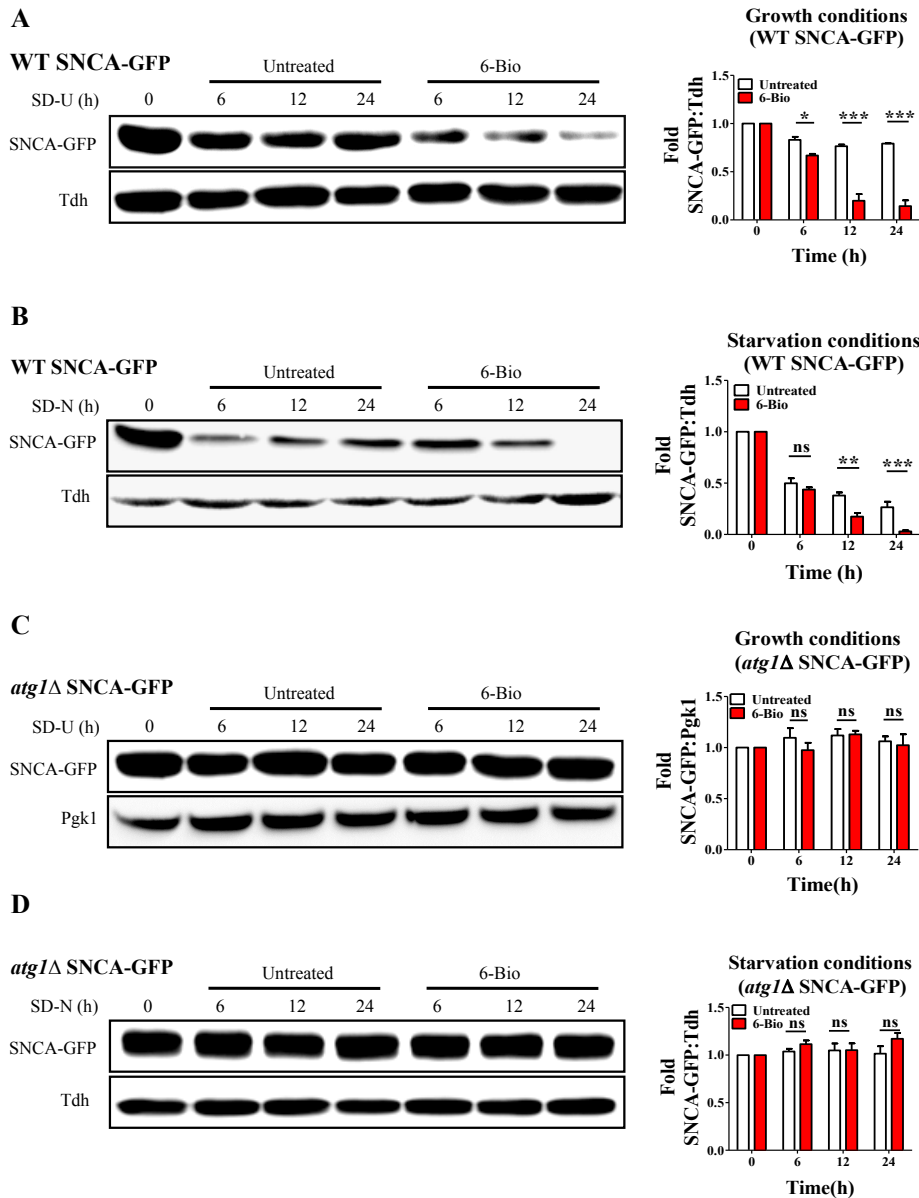


Figure 12. SNCA-GFP degradation assay. Western blots and its quantification for SNCA-GFP degradation upon 6-Bio (50 μ M) administration, in WT or autophagy mutant (*atg1Δ*) cells under growth (A and B) or starvation (C and D) conditions. Tdh reactivity or Pgk1 were assessed as loading controls. SD-U is growth medium while SD-N is nitrogen starvation medium. Statistical analysis was performed using one-way ANOVA and the post-hoc Bonferroni test. Error bars, mean \pm SEM. ns-non significant, *- $P < 0.05$, **- $P < 0.01$, ***- $P < 0.001$.

Next, using an SNCA degradation assay model in a human neuroblastoma cell line (SH-SY5Y) overexpressing GFP-SNCA, we observed that 6-Bio significantly reduced GFP-SNCA levels (~2 fold, $P < 0.001$ versus untreated). However, in the presence of the autophagy inhibitor 3-methyladenine (3-MA), the GFP-SNCA levels did not change upon 6-Bio cotreatment suggesting that autophagy was the primary mechanism for degradation (as also seen in the yeast model) (**Fig. 12 and 13**).

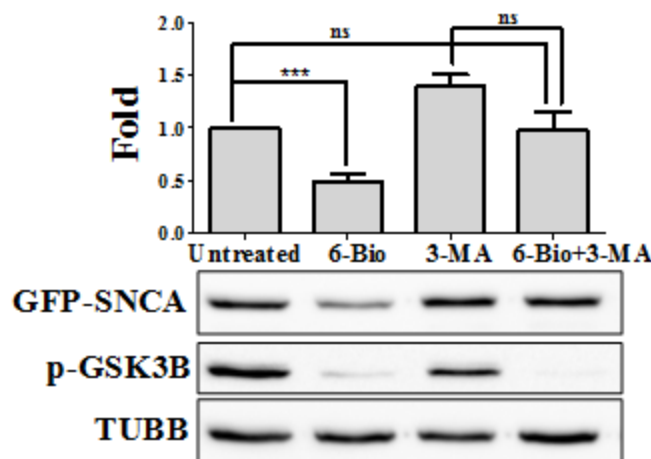


Figure 13. GFP-SNCA degradation assay in mammalian cells. GFP-SNCA transiently transfected in SH-SY5Y cells were allowed to express for 24 h, treated with 6-Bio (5 μ M), 3-MA (5 mM) or both for 24 h post-transfection and assessed for GFP-SNCA degradation. Western blot (below) and graph (above) indicating fold change in GFP-SNCA degradation over untreated. TUBB was used as a loading control. Statistical analysis was performed using one-way ANOVA and the post-hoc Bonferroni test. Error bars, mean \pm SEM. ns-non significant, ***- $P < 0.001$.

As MTOR negatively controls autophagy, we tested if 6-Bio affected MTOR (mechanistic target of rapamycin) signaling. 6-Bio decreased phosphorylation levels of RPS6KB1/p70s6K (ribosomal protein S6 kinase B1) and EIF4EBP1/4E-BP1 (eukaryotic translation initiation factor 4E binding protein 1) in a dose-dependent manner (**Fig. 3A**), indicating 6-Bio negatively regulated MTOR signaling. During normal growth conditions,

MTOR is active (and phosphorylates RPS6KB1 and EIF4EBP1) and autophagy is suppressed. Addition of 6-Bio results in autophagy induction by suppression of MTOR activity as revealed by diminished phosphorylation of its substrates RPS6KB1 and EIF4EBP1. 6-Bio is a potent GSK3B inhibitor and reduced phosphorylated (p)-GSK3B indicates its reduced activity¹⁷ (Fig. 14). These assays confirmed that 6-Bio treatment not only induced autophagy but also enhanced the autophagic flux by promoting autophagosome fusion with lysosomes in an MTOR-dependent manner.

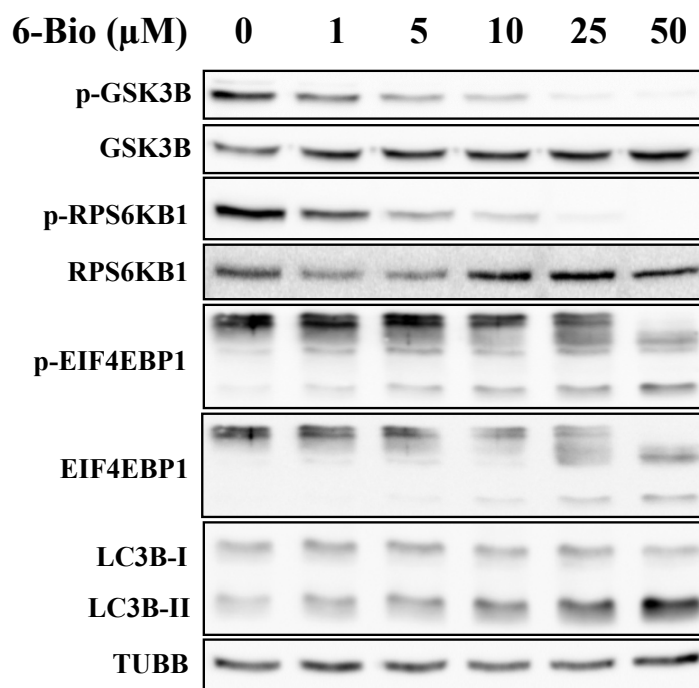


Figure 14. *6-Bio regulates autophagy in MTOR dependent manner. Representative western blots indicating dose-dependent modulation of autophagy related proteins (LC3B, RPS6KB1 and EIF4EBP1) by 6-Bio in HeLa cells. TUBB was used as a loading control.*

Autophagy-dependent GSK3B-mediated neuro(cyto)protection by 6-Bio

We observed the significant reduction of GSK3B activity upon 6-Bio treatment as revealed by the reduced p-GSK3B levels. To understand the GSK3B dependency of autophagic activity by 6-Bio, we performed the knockdown studies in SH-SY5Y cells. For this, *GSK3B* shRNA was transiently transfected into cells and after 48h the GSK3B protein levels were

reduced significantly (**Fig. 16A**). In SH-SY5Y cells, when SNCA was overexpressed for 72 h, the cell viability was significantly affected (**Fig. 16D**). When these cells were treated with 6-Bio, its viability was significantly increased and comparable to that of control (**Fig. 15**).

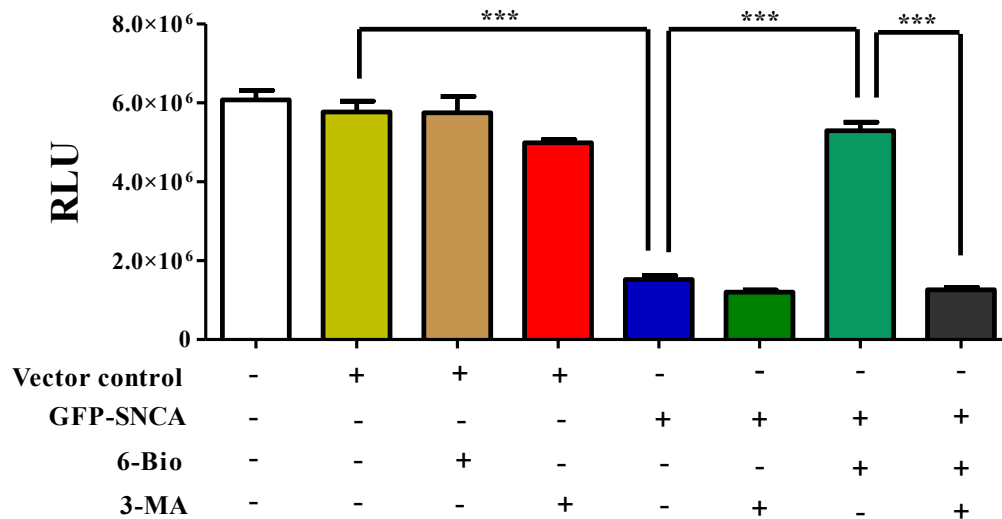


Figure 15. 6-Bio neuro (cyto) protects SH-SY5Y cells in an autophagy-dependent manner. Plot representing the cell viability of SNCA-overexpressing SH-SY5Y cells treated with 6-Bio (5 μ M) and/or 3-MA (100 nM, autophagy inhibitor). Statistical analysis was performed using one-way ANOVA and the post-hoc Bonferroni test. Error bars, mean \pm SEM. ***- $P < 0.001$.

Similar protection was noted in *GSK3B*-silenced SNCA-overexpressing cells. When *GSK3B* expression was silenced, addition of 6-Bio only showed marginal cytoprotection as compared to untreated cells with normal *GSK3B* expression (**Fig. 16D**). In fact, in silenced cells, 6-Bio was not effective in cytoprotection over and above that offered by silencing *GSK3B* but was cytotoxic (**Fig. 16D**). In addition, another *GSK3B* inhibitor, compound VIII also exerted protection against SNCA-mediated toxicity (**Fig. 16D**). Using a direct readout for autophagy (tandem RFP-GFP-LC3B assay), we employed a similar silencing strategy to address the *GSK3B* and autophagy interplay in the presence of 6-Bio. In

GSK3B-silenced cells, the autolysosomes were increased with concomitant reduction in autophagosomes than that of its scrambled shRNA control ($P < 0.001$, **Fig. 16, B and C**). Interestingly, the autophagosomes and autolysosomes formed in *GSK3B*-silenced cells were similar to that of 6-Bio treatment. Notably, the autolysosomes formed in 6-Bio-treated, *GSK3B*-silenced cells were significantly reduced than that of cells treated only with 6-Bio ($P < 0.001$, **Fig. 16, B and C**). Although 6-Bio is known to affect other signaling pathways such as PDK1 (pyruvate dehydrogenase kinase 1) and JAK-STAT3 ([Janus kinase]-[signal transducer and activator of transcription 3])¹⁸, our results suggest that 6-Bio primarily modulates autophagy in a *GSK3B*-dependent manner.

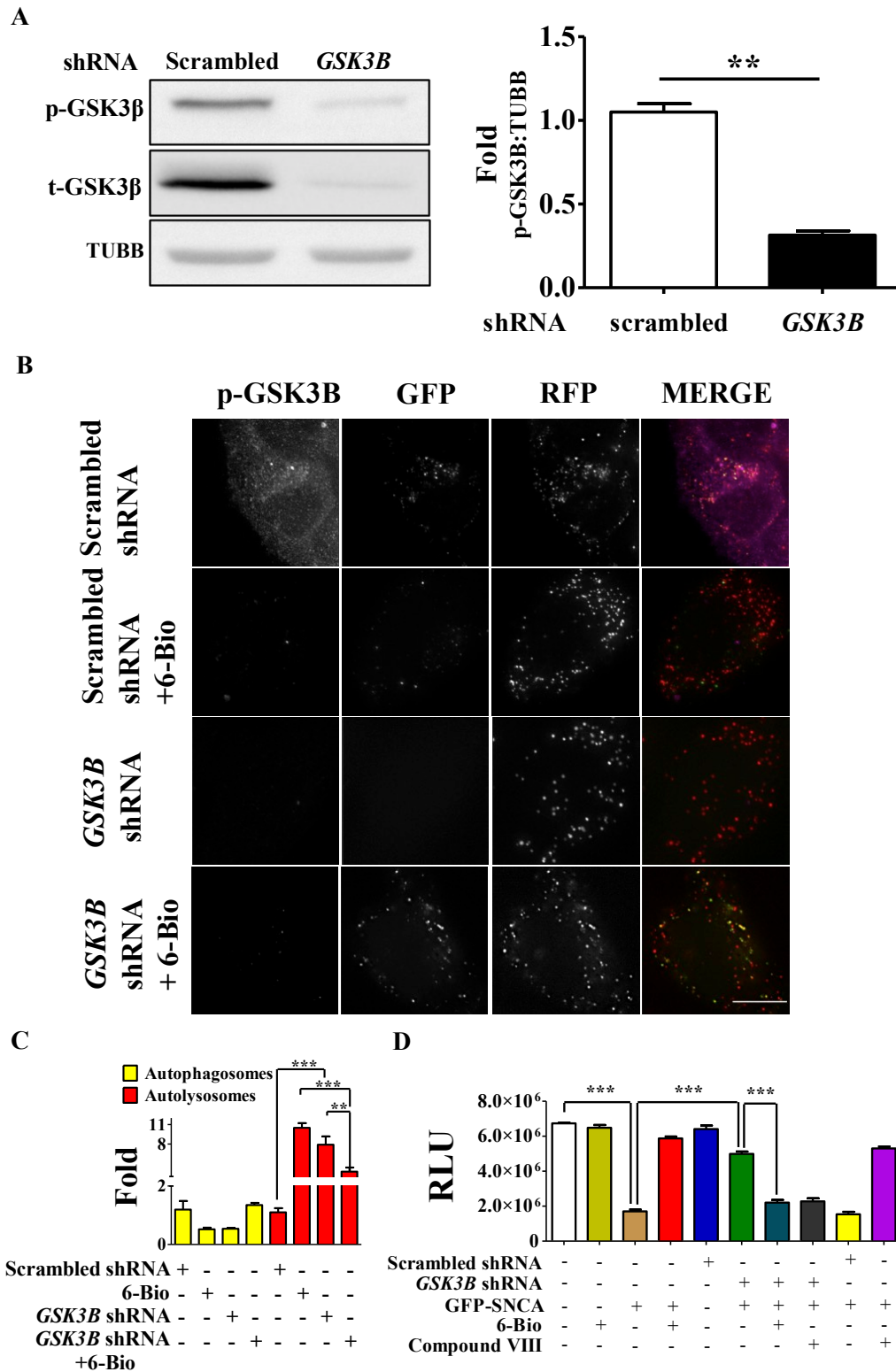


Figure 16. *GSK3B*-dependent autophagy modulation by 6-Bio. (A) SH-SY5Y cells were transiently transfected with *GSK3B* shRNA for 48 h and then protein levels were analyzed through immunoblotting (phospho-*GSK3B* and total-*GSK3B*), and then quantified. TUBB

served as a loading control. **(B)** Representative microscopy images of the GFP-RFP-LC3B assay in HeLa cells, transfected with either scrambled shRNA or GSK3B shRNA treated with or without 6-Bio (5 μ M) and then stained for p-GSK3B. **(C)** Quantification indicating the fold change of autophagosomes and autolysosomes of all the above-mentioned treatments. **(D)** Plot representing the cell viability readout of GSK3B-silenced SH-SY5Y cells overexpressing GFP-SNCA (for 48 h) and then treated with 6-Bio (5 μ M) and/or compound VIII (10 μ M) for 24 h. Cell viability was analyzed using CellTiter-Glo® (Promega) assay. Increased RLU readout was indicative of more cell viability and vice-versa. Statistical analysis was performed using unpaired Student *t* test or one-way ANOVA and the post-hoc Bonferroni test. Error bars, mean \pm SEM. **-*P* < 0.01, ***-*P* < 0.001.

6-Bio confers neuroprotection in a mouse MPTP-toxicity model

We then investigated the effect of 6-Bio in one of the widely employed preclinical model of PD, MPTP (1-methyl-4-phenyl-1,2,3,6-tetrahydropyridine) mouse model¹⁹. It was reported that 7 days post MPTP administration results in ~70% dopaminergic (DAergic) neuronal loss in the substantia nigra pars compacta (SNpc) region of brain which leads to 80 to 90% reduction in dopamine levels in the striatum¹⁹. In this model, 6-Bio was administered (5mg/kg, intraperitoneally [i.p.]) in 2 different regimen (**Fig. 18A**): on the same day of MPTP injections (coadministration, Co) or 2 days prior (prophylactic, Pro). In both cases, 6-Bio treatment was continued for 7 days post MPTP administration.

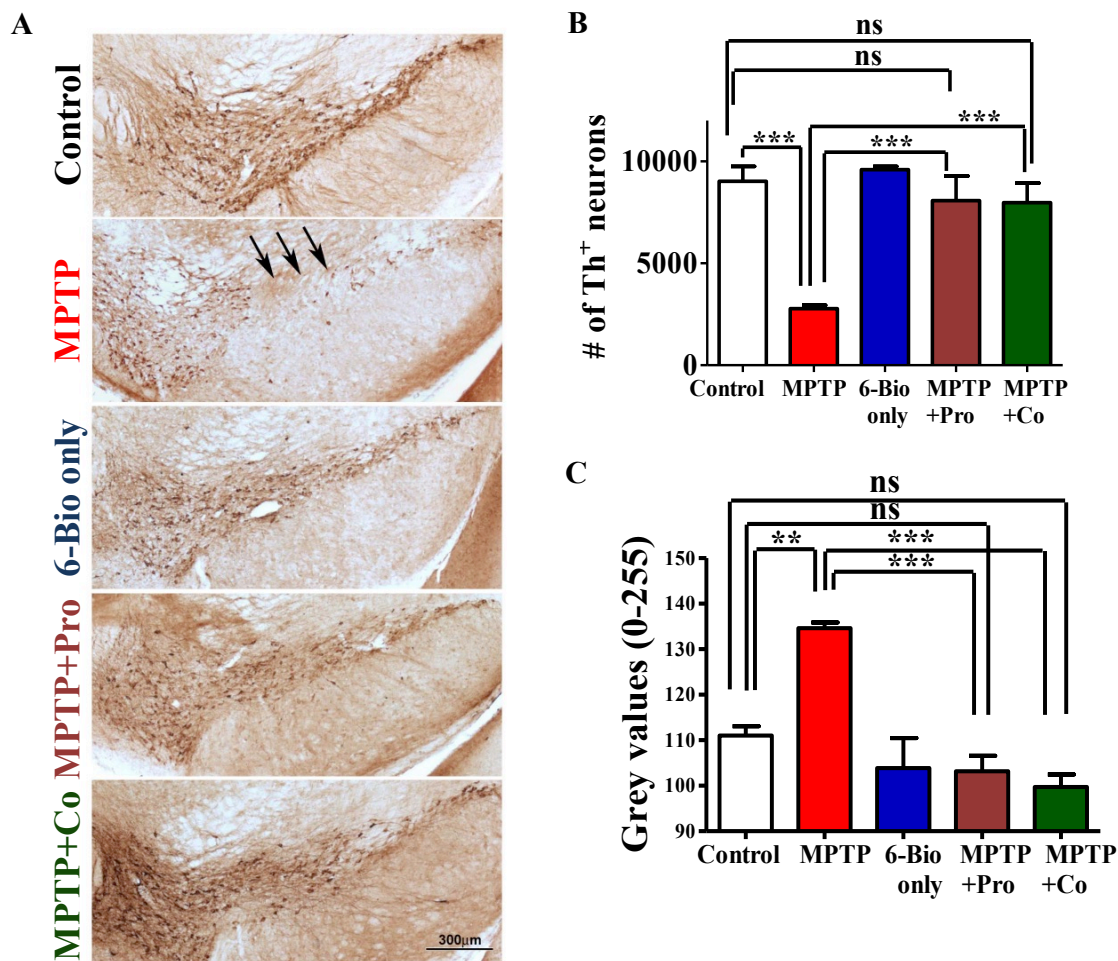


Figure 17. Stereological quantification. Representative photomicrographs of TH⁺ immunostained dopaminergic neurons (A) in SNpc (arrow) of mouse midbrain. Placebo control cohort, MPTP-treated (23 mg/kg body weight), 6-Bio (5 mg/kg body weight) or both (Prophylaxis [MPTP+Pro]/Coadministration [MPTP+Co]), scale bar: 300 μ m. Stereological (B) and densitometric quantification (C) indicating the number of TH⁺ DAergic and its intensity in SNpc neurons. Statistical analysis was performed using one-way ANOVA and the post-hoc Bonferroni test. Error bars, mean \pm SEM. ns-non significant, **- $P < 0.01$, ***- $P < 0.001$.

We then evaluated the status of DAergic neurons in SNpc. These neurons were identified by TH (tyrosine hydroxylase) immunolabeling and were quantitated by unbiased stereology and densitometry analysis. As expected, the number and health of DAergic neurons (as

revealed by TH staining intensities) were significantly reduced in MPTP-treated mice (~3 fold, $P < 0.001$ compared to placebo; **Fig. 17, A to C** and **Fig. 18B**). Strikingly, in both the 6-Bio treatment regimen, the number of DAergic neurons resembled almost that of placebo or animals injected with 6-Bio only (Co or Pro ~2.5 fold versus MPTP, $P < 0.001$; **Fig. 17, A to C** and **Fig. 18B**). In addition, the decrease in SNpc volume upon MPTP administration was not seen in 6-Bio-treated cohort ($P < 0.001$ versus Co, $P < 0.01$ versus Pro; **Fig. 18C**). These observations in mouse model of PD reassert the neuroprotective nature of 6-Bio.

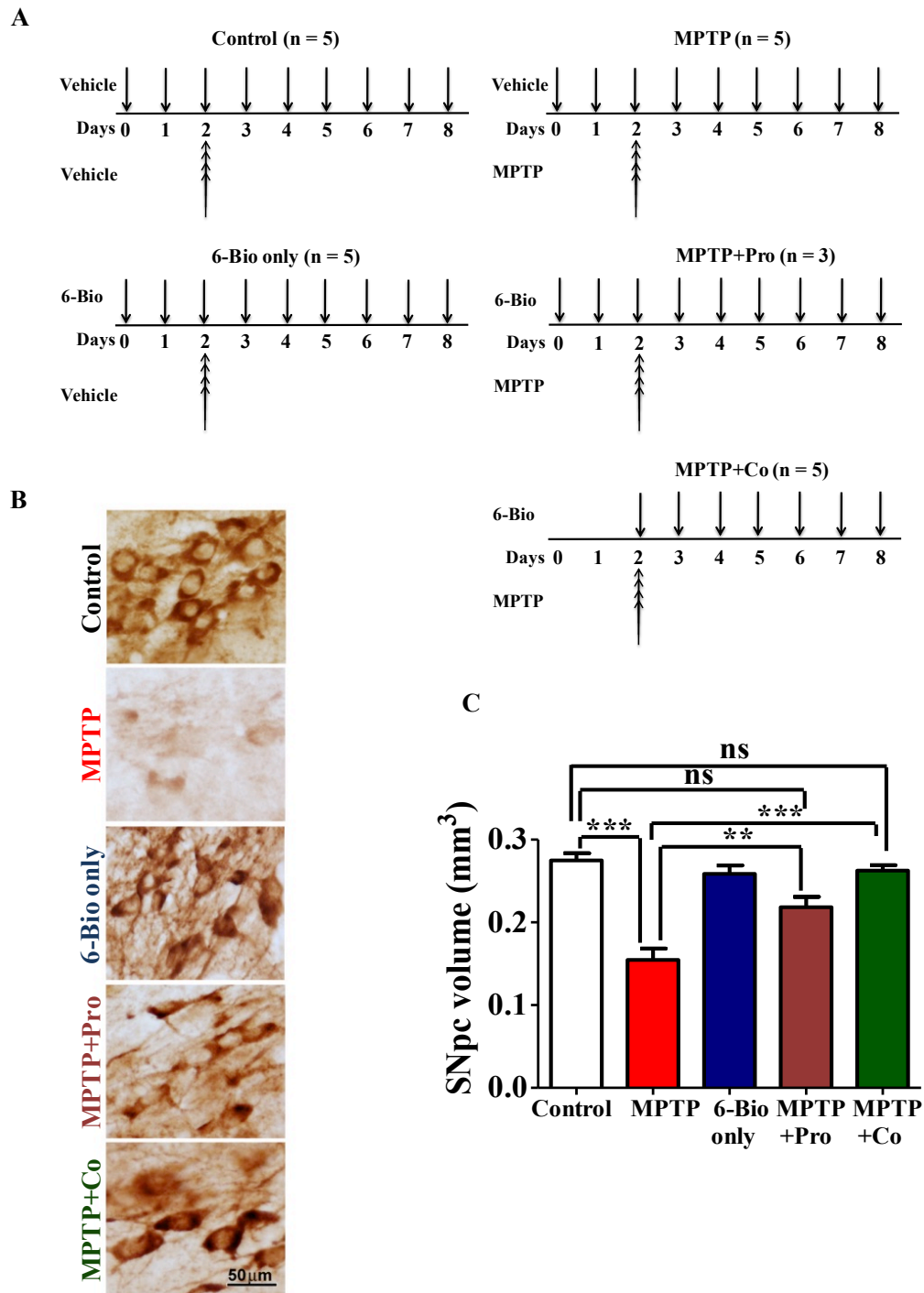


Figure 18. Densitometric quantification. 6-Bio administration in the MPTP mouse model. (A) Schema representing schedule of dosage administration of MPTP (23 mg/kg), 6-Bio (5 mg/kg) in mice groups. (B) Representative photomicrographs of TH⁺ immunostained DAergic neurons in SNpc of mouse midbrain of control, MPTP and 6-Bio or both (Prophylaxis [MPTP+Pro] or Co administration [MPTP+Co]) groups. (C) Quantitative

*plot of SNpc volume of mouse brains for all the groups. Statistical analysis was performed using one-way ANOVA and the post-hoc Bonferroni test. Error bars, mean \pm SEM. ns-non significant, **- $P < 0.01$, ***- $P < 0.001$.*

6-Bio enhances autophagy and clears toxic protein aggregates in mouse brains

We then evaluated the autophagy and toxic aggregate levels in the DAergic neurons in SNpc of midbrain. We observed the significant reduction of LC3B puncta per neuron in the MPTP-treated cohort than that of placebo (~1.8 fold, placebo vs MPTP, $P < 0.001$, **Fig. 19, A and B**). Conversely, APP/amyloid beta oligomer/A11 puncta were significantly higher (~7 fold, placebo vs MPTP, $P < 0.001$, **Fig. 19, C and D**). Along with decreased autophagy, these SNpc (TH⁺) neurons displayed toxic aggregate buildup. This reduced autophagy upon administration of MPTP is in agreement with previous observations²⁰. Furthermore, as seen in cell culture models, 6-Bio treatment alone increased LC3B puncta per neuron (~2 fold, placebo vs 6-Bio only, $P < 0.001$, **Fig. 19, A and B**) suggesting that 6-Bio could induce autophagy in mice brain by crossing the blood-brain barrier (**Table 1**). When 6-Bio was coadministered along with MPTP, LC3B puncta per neuron increased (~2.5 fold, MPTP vs MPTP+Co, $P < 0.001$, **Fig. 19, A and B**) with a significant reduction in APP/amyloid beta oligomer/A11-positive aggregates (~7 fold, MPTP vs MPTP+Co cohort, **Fig. 19, C and D**). Strikingly, the aggregate numbers in MPTP+Co were comparable to that of control suggesting that the 6-Bio treatment decreased the toxic aggregates to that of placebo neurons (placebo vs MPTP+Co, ns, $P > 0.05$, **Fig. 19, C and D**). These results imply that autophagy was drastically induced in the MPTP and 6-Bio coadministered cohort that lead to neuroprotection by clearance of the toxic aggregates. We observed reduced p-GSK3B signals in DAergic neurons of the 6-Bio-treated cohorts, namely, 6-Bio only and MPTP+Co (**Fig. 20**).

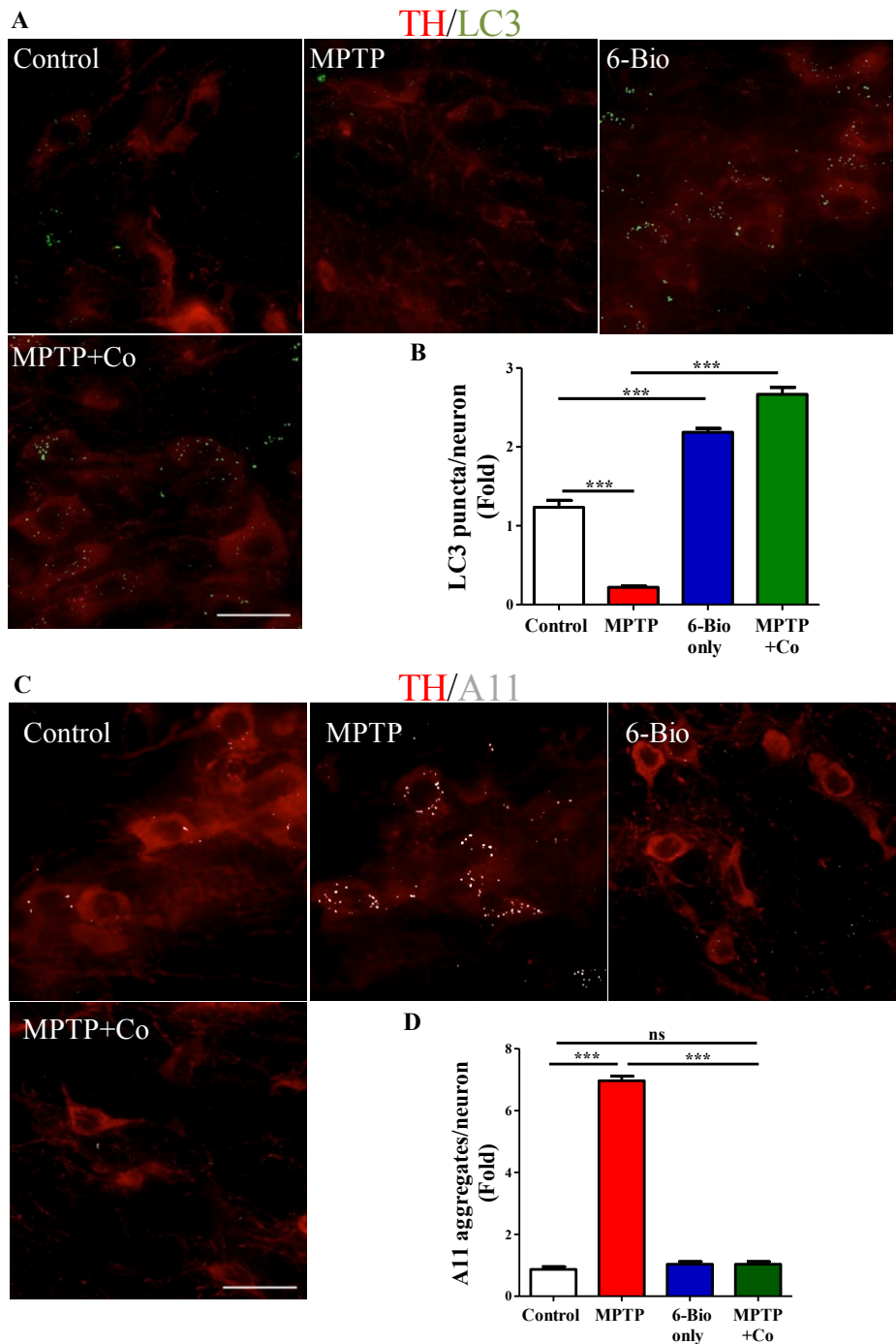


Figure 19. 6-Bio induces autophagy in mice brain to clear toxic protein aggregates. (A) Representative immuno-histofluorescent photomicrographs of various cohorts namely control, MPTP (23 mg/kg of body weight), 6-Bio (5 mg/kg of body weight) and MPTP+Co that were stained for LC3B (an autophagy marker) and TH (SNpc) in midbrain. Autophagic modulation by 6-Bio were evaluated in DAergic neurons in SNpc and the LC3B puncta fold

change per neuron was quantified (B). (C) Representative immuno-histofluorescent photomicrographs of the above mentioned cohorts were stained for APP/amyloid beta oligomer/A11 (toxic oligomers) and TH (SNpc) in midbrain. Aggregate clearance by 6-Bio were evaluated in DAergic neurons in SNpc and the APP/amyloid beta oligomer/A11 puncta fold change per neuron was quantified (D). Scale bar: 50 μ m. Statistical analysis was performed using one-way ANOVA and the post-hoc Bonferroni test. Error bars, mean \pm SEM. ns-non significant, ***- $P < 0.001$.

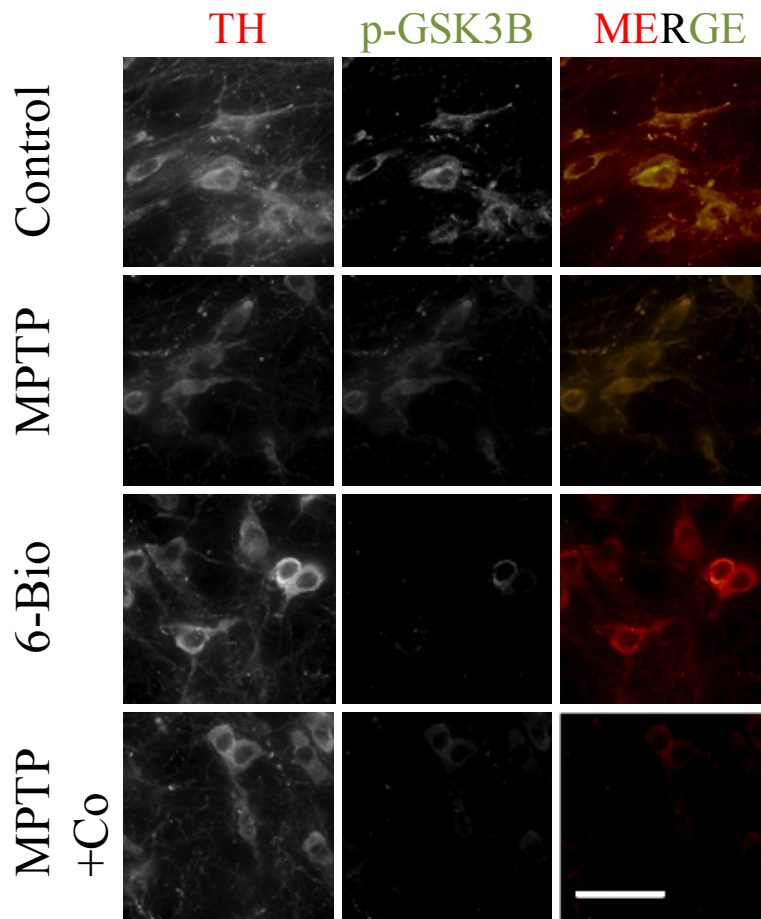


Figure 20. *p-GSK3B* levels in dopaminergic neurons of SNpc. Representative photomicrographs of double immunofluorescence with *p-GSK3B* and TH (DAergic

neurons) for various treatment cohorts, namely placebo, MPTP (23 mg/kg), 6-Bio (5 mg/kg) and MPTP+Co. Scale bar: 50 μ m.

6-Bio ameliorates MPTP-induced behavioral deficits

To study whether 6-Bio can combat the MPTP-induced behavioral impairments in motor coordination, locomotion and exploration abilities, we employed 2 widely used behavior tests namely rotarod and the open field test. Stereology were performed on day 7 post MPTP or placebo administrations, thus behavior experiments were conducted on day 13 i.e., day 7 post MPTP or placebo administrations. Behavior study scheme is illustrated in **Fig. 21**.

In rotarod test, the latency to fall for MPTP cohort reduced significantly to that of placebo cohort on day-13 post administration (MPTP versus placebo, $P < 0.001$, **Fig. 22A** and **Fig. 21, A and B**) validating the MPTP-induced motor deficits in mice. Strikingly, the latency to fall was increased in the 6-Bio-treated cohort compared to that of MPTP-treated cohort (Co versus MPTP, $P < 0.001$, **Fig. 22A** and **Fig. 21, B and C**). The latency to fall for the 6-Bio-treated cohort was comparable with the placebo cohort (Co day 7 versus placebo, $P > 0.05$, **Fig. 22A** and **Fig. 21, A and C**).

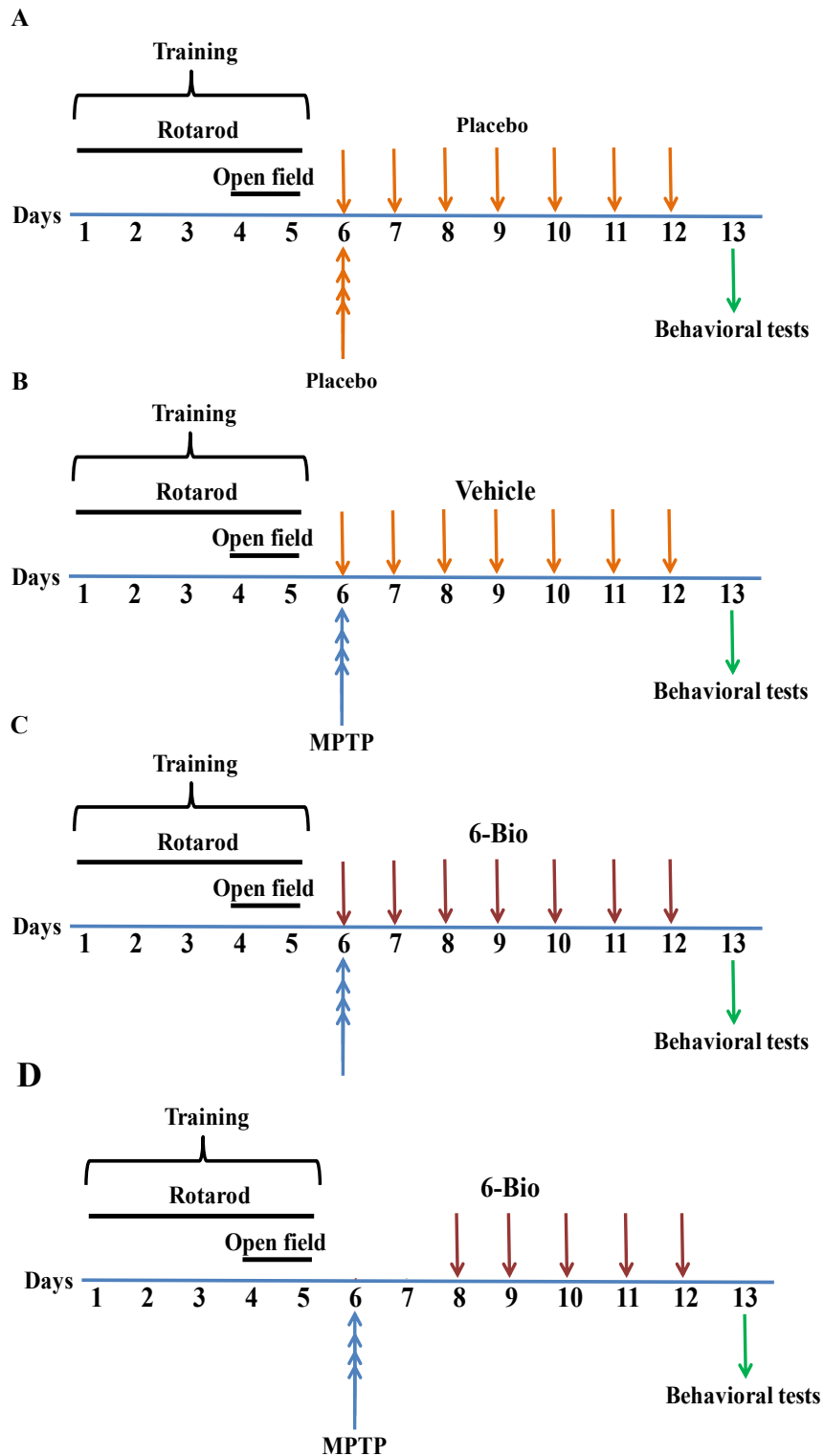


Figure 21. Behavior study design schema. Schema representing schedule of behavioral studies on cohorts, namely Placebo (**A**), MPTP (**B**), MPTP+Co (**C**) and MPTP+Post (**D**). In the MPTP+Co regimen, 6-Bio was injected 2 h before MPTP administration (**C**),

whereas in the MPTP+Post regimen, 6-Bio was injected after 48 h of MPTP administration (D). Dosage concentrations were MPTP (23 mg/kg) and 6-Bio (5 mg/kg).

Similar to the lack of motor coordination observed in rotarod, the total distance travelled by MPTP-treated cohort in the open field test arena on day13 post injection was reduced significantly compared to that of placebo (MPTP versus placebo, $P < 0.001$, **Fig. 22, B** and **C** and **Fig. 21, A** and **B**) affirming the MPTP-induced locomotion and exploratory impairments. These impairments were improved after 6-Bio administration as the distance travelled by mice increased dramatically (Co versus MPTP, $P < 0.001$, **Fig. 22, B** and **C** and **Fig. 21, B** and **C**) and matched control cohorts (Co versus placebo, $P > 0.05$, **Fig. 22, B** and **C** and **Fig. 21, A** and **C**). MPTP-induced impairments were not protected by 6-Bio when administered after 48 h of MPTP (Post versus MPTP, $P > 0.05$, **Fig. 22, D** and **E** and **Fig 21, B** and **D**).

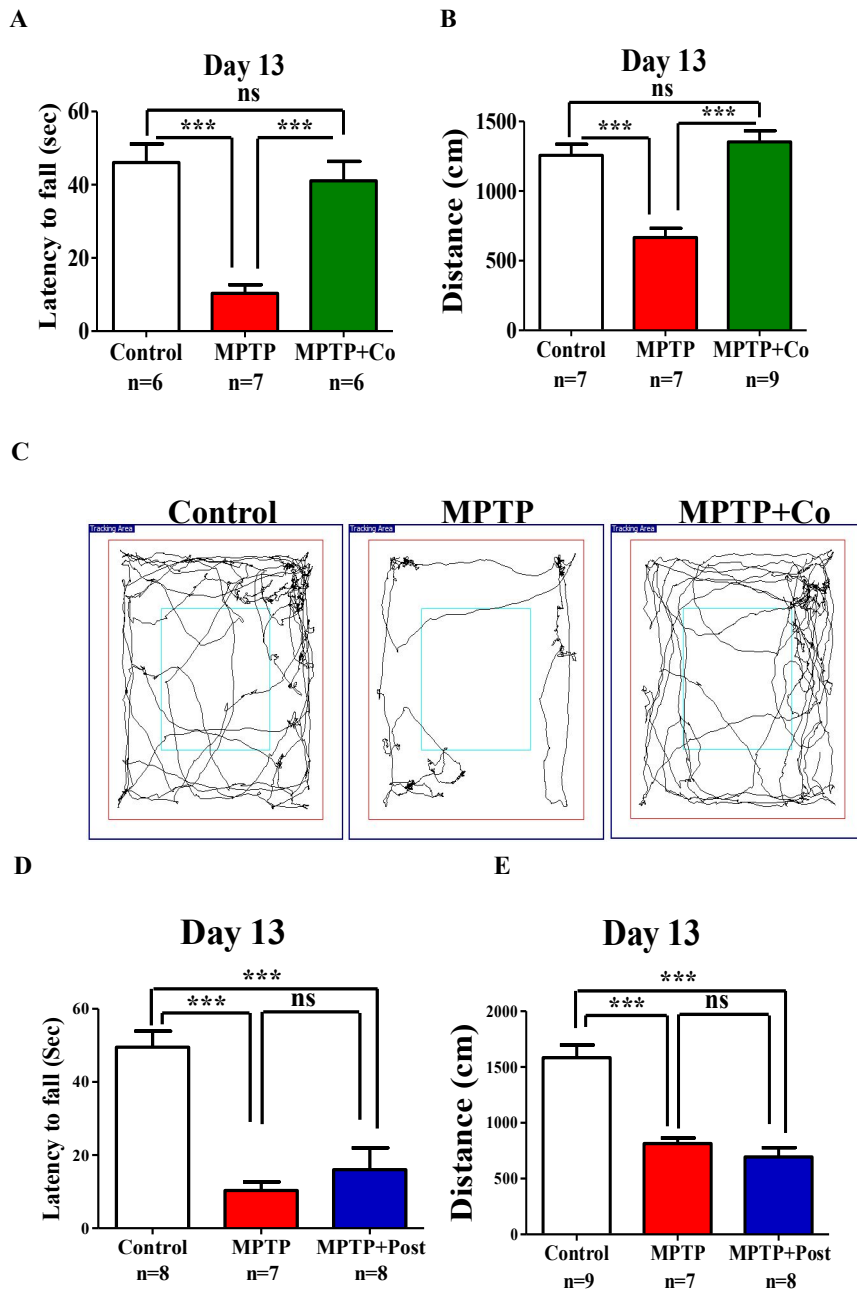


Figure 22. 6-Bio ameliorates MPTP-induced behavioral deficits. Effect of 6-Bio (5 mg/kg) on (A) latency to fall of various cohorts namely Placebo, MPTP and MPTP+Co as assessed by rotarod test (B) Representative trajectory maps of all mentioned cohorts as analyzed by open field test. (C) Periphery distance travelled by all indicated cohorts as assessed by open field test. Effect of 6-Bio (5 mg/kg) on various cohorts namely Placebo, MPTP and MPTP+Post. (D) latency to fall of various cohorts namely Placebo, MPTP and MPTP+Post as assessed by rotarod test. (E) Periphery distance travelled by all indicated cohorts as assessed by the open field test. Both the rotarod and open field behavior

*analyses were performed on day 13 or day 7 post-MPTP or vehicle administrations. Both the rotarod and open field behavior analyses were performed on day 13 or day 7 post-MPTP/vehicle administrations. 6-Bio (5 mg/kg) was administrated either along with MPTP (MPTP+Co) or post 48 h of MPTP administration (MPTP+Post). Statistical analysis was performed using one-way ANOVA and the post-hoc Bonferroni test. Error bars, mean \pm SEM. ns-non significant, ***- $P < 0.001$.*

Since the 6-Bio-treated cohort spent more time on the rotarod (as the placebo cohort) and travelled more distance in open field unlike MPTP-treated, we therefore, can infer that 6-Bio rescued the MPTP-induced motor, locomotion and exploratory impairments. We observed that 6-Bio failed to protect the MPTP-induced behavioral deficits when administered 48 h after MPTP dosage.

Discussion

Using an unbiased yeast high-throughput assay, we identified the small molecule 6-Bio that rescued SNCA cytotoxicity in an autophagy-dependent manner. 6-Bio induced autophagy even in growth conditions. Mechanistically, 6-Bio profoundly promoted autophagosome-lysosome fusion as reflected in the high autolysosome numbers with hardly any unfused autophagosomes. Increased autophagy induction and fusion resulted in degradation and clearance of aggregated proteins with a concomitant rescue of cell viability and growth. When tested in a preclinical model of PD, 6-Bio demonstrated remarkable neuroprotection revealed by both immunohistology and behavioral analyses.

Apart from toxic accumulation of SNCA aggregates as Lewy bodies, proteostasis machineries such as autophagy are also defunct in these dying neurons⁷. While autophagosome formation has been shown to be defective in PD⁴, its accumulation has been documented in the striata of human PD postmortem brains²¹. Also, recent reports suggest that apart from having a misfolding propensity, prion-like properties²² of SNCA are responsible for its spreading across neurons leading to aggravated neuronal death. Hence, enhancing SNCA clearance through modulating autophagy would be beneficial.

We show here using 2 model systems that aggregate clearance by 6-Bio is through autophagy: using yeast genetics, our studies reveal that 6-Bio is unable to rescue SNCA-mediated cytotoxicity in autophagy-defective mutants, while in mammalian cells, pharmacological inhibition of autophagy by 3-MA abolishes 6-Bio effect. In addition, although 6-Bio (50 μ M) does not affect the growth of yeast cells, it strikingly increases basal autophagy even in growth conditions, a situation where MTOR is active and is known to suppress autophagy. Interestingly, 6-Bio induction of autophagy in mammalian cells appears to be MTOR dependent. Furthermore, 6-Bio not only augments basal autophagy but also enhances the starvation induced autophagy, demonstrating its strong autophagy modulating potential. It is these properties that lead to a dramatic buildup of autolysosomes upon 6-Bio treatment. Enhanced cargo degradation thus leads to clearing up of the aggregates and preventing cytotoxicity by restoring cellular proteostasis.

The MPTP+6-Bio-treated cohort spent more time on the rotarod (as the placebo cohort) and travelled more distance in open field unlike the MPTP-treated cohort, we therefore can infer that 6-Bio rescued the MPTP-induced motor, locomotion and exploratory impairments. Importantly, 6-Bio-induced behavioral performances were indistinguishable from that of the placebo cohort. Thus, histological and behavioral analyses of the MPTP-induced preclinical mouse model of PD highlights the neuroprotective abilities of 6-Bio as demonstrated by preservation of nigral dopaminergic neurons and retention of motor coordination functions. After 48 h of MPTP administration, most of the DAergic neurons would be ablated. Thus after 48h of MPTP treatment, with highly depleted SNpc of DAergic neurons, 6 Bio was unable to rescue behavioural deficits. These results suggest that 6-Bio primarily acts through restoring autophagy function in the neurons to get rid of aggregates and perhaps does not have neuroregenerative capabilities. Strikingly, our experiment revealed that 6-bio enters the brain within 15 min after intraperitoneal administration and stayed as long as 24 h (**Table 1**). The dramatic neuroprotection could be due to abundance of 6-Bio in the mice brain that facilitates aggregate clearance through inducing autophagy.

No	Time points	Samples	Concentration (ng/ml)
1	15 min	Vehicle	0
2	30 min	Vehicle	0
3	1 hr	Vehicle	0
4	6 hr	Vehicle	0
5	12 hr	Vehicle	0
6	24 hr	Vehicle	0
7	15 min	6-Bio	1830
8	30 min	6-Bio	2020
9	1 hr	6-Bio	1190
10	6 hr	6-Bio	991
11	12 hr	6-Bio	673
12	24 hr	6-Bio	382

Table 1. *In vivo* blood barrier assay. Mass spectrometric analysis of bioavailability of 6-Bio in brain.

Our studies with other GSK3B inhibitors (with similar inhibitory potencies) reveal that none of these can bring about autophagy induction as profoundly as 6-Bio (data not shown). Though 6-Bio has been shown to modulate GSK3, PDK1 and JAK-STAT3 signaling pathways¹⁸, our results demonstrated that it modulates autophagy in GSK3B dependent manner. 6-Bio docks with GSK3B better than other inhibitors such as indirubin, hymenialdisine and meridianins²³. It also increases the accumulation of CTNNB1/ β -catenin due to the inhibition GSK3B, promotes aggression of breast cancer²⁴. 6-Bio also indirectly activates canonical WNT5A signaling in the hippocampal neurons to protect them from Ab

oligomers¹². Proof-of-principle demonstrations at the cellular level reveal that inhibiting GSK3B reduces SNCA expression²⁵ and also results in b-amyloid clearance²⁶. Thus, GSK3B would be an attractive avenue as a therapeutic target for neurodegeneration. In PD, autophagy is dysfunctional as the steps of autophagosome biogenesis⁴ and the fusion between autophagosome and lysosome are blocked²⁷. Because 6-Bio dramatically enhances autophagosome-lysosome fusion by inhibiting GSK3B through crossing the blood-brain barrier, it decreases the dramatic toxic protein aggregates in SNpc. Therefore, 6-Bio could be a promising candidate with therapeutic potential especially in case of synucleopathies including PD.

Our findings demonstrate that the neuroprotective role of 6-Bio is due to its autophagosome-lysosome fusion-enhancing function, which results in SNCA aggregate clearance, may have therapeutic potential for patients with PD and protein conformational disorders.

References

1. Mortality GBD, Causes of Death C. Global, regional, and national age-sex specific all-cause and cause-specific mortality for 240 causes of death, 1990-2013: a systematic analysis for the Global Burden of Disease Study 2013. *Lancet* 2015; 385:117-71.
2. German DC, Manaye K, Smith WK, Woodward DJ, Saper CB. Midbrain dopaminergic cell loss in Parkinson's disease: computer visualization. *Annals of neurology* 1989; 26:507-14.
3. Thanvi B, Lo N, Robinson T. Levodopa-induced dyskinesia in Parkinson's disease: clinical features, pathogenesis, prevention and treatment. *Postgraduate medical journal* 2007; 83:384-8.
4. Nixon RA. The role of autophagy in neurodegenerative disease. *Nature medicine* 2013; 19:983-97.
5. Hara T, Nakamura K, Matsui M, Yamamoto A, Nakahara Y, Suzuki-Migishima R, Yokoyama M, Mishima K, Saito I, Okano H, et al. Suppression of basal autophagy in neural cells causes neurodegenerative disease in mice. *Nature* 2006; 441:885-9.
6. Komatsu M, Waguri S, Chiba T, Murata S, Iwata J, Tanida I, Ueno T, Koike M, Uchiyama Y, Kominami E, et al. Loss of autophagy in the central nervous system causes neurodegeneration in mice. *Nature* 2006; 441:880-4.
7. Liang CC, Wang C, Peng X, Gan B, Guan JL. Neural-specific deletion of FIP200 leads to cerebellar degeneration caused by increased neuronal death and axon degeneration. *The Journal of biological chemistry* 2010; 285:3499-509.
8. Sarkar S, Perlstein EO, Imarisio S, Pineau S, Cordenier A, Maglathlin RL, Webster JA, Lewis TA, O'Kane CJ, Schreiber SL, et al. Small molecules enhance autophagy and reduce toxicity in Huntington's disease models. *Nature chemical biology* 2007; 3:331-8.
9. Anguiano J, Garner TP, Mahalingam M, Das BC, Gavathiotis E, Cuervo AM. Chemical modulation of chaperone-mediated autophagy by retinoic acid derivatives. *Nature chemical biology* 2013; 9:374-82.

10. Rajasekhar K, Suresh SN, Manjithaya R, Govindaraju T. Rationally designed peptidomimetic modulators of abeta toxicity in Alzheimer's disease. *Scientific reports* 2015; 5:8139.
11. Llorens-Martin M, Jurado J, Hernandez F, Avila J. GSK-3beta, a pivotal kinase in Alzheimer disease. *Front Mol Neurosci* 2014; 7:46.
12. Silva-Alvarez C, Arrazola MS, Godoy JA, Ordenes D, Inestrosa NC. Canonical Wnt signaling protects hippocampal neurons from Abeta oligomers: role of non-canonical Wnt-5a/Ca(2+) in mitochondrial dynamics. *Frontiers in cellular neuroscience* 2013; 7:97.
13. Outeiro TF, Lindquist S. Yeast cells provide insight into alpha-synuclein biology and pathobiology. *Science* 2003; 302:1772-5.
14. Khurana V, Lindquist S. Modelling neurodegeneration in *Saccharomyces cerevisiae*: why cook with baker's yeast? *Nature reviews Neuroscience* 2010; 11:436-49.
15. Outeiro TF, Kontopoulos E, Altmann SM, Kufareva I, Strathearn KE, Amore AM, Volk CB, Maxwell MM, Rochet JC, McLean PJ, et al. Sirtuin 2 inhibitors rescue alpha-synuclein-mediated toxicity in models of Parkinson's disease. *Science* 2007; 317:516-9.
16. Polychronopoulos P, Magiatis P, Skaltsounis AL, Myrianthopoulos V, Mikros E, Tarricone A, Musacchio A, Roe SM, Pearl L, Leost M, et al. Structural basis for the synthesis of indirubins as potent and selective inhibitors of glycogen synthase kinase-3 and cyclin-dependent kinases. *J Med Chem* 2004; 47:935-46.
17. Grassilli E, Ianzano L, Bonomo S, Missaglia C, Cerrito MG, Giovannoni R, Masiero L, Lavitrano M. GSK3A is redundant with GSK3B in modulating drug resistance and chemotherapy-induced necroptosis. *PloS one* 2014; 9:e100947.
18. Braig S, Kressirer CA, Liebl J, Bischoff F, Zahler S, Meijer L, Vollmar AM. Indirubin derivative 6BIO suppresses metastasis. *Cancer research* 2013; 73:6004-12.
19. Jackson-Lewis V, Przedborski S. Protocol for the MPTP mouse model of Parkinson's disease. *Nature protocols* 2007; 2:141-51.

20. Li XZ, Chen XP, Zhao K, Bai LM, Zhang H, Zhou XP. Therapeutic effects of valproate combined with lithium carbonate on MPTP-induced parkinsonism in mice: possible mediation through enhanced autophagy. *The International journal of neuroscience* 2013; 123:73-9.
21. Anglade P, Vyas S, Hirsch EC, Agid Y. Apoptosis in dopaminergic neurons of the human substantia nigra during normal aging. *Histology and histopathology* 1997; 12:603-10.
22. Luk KC, Kehm V, Carroll J, Zhang B, O'Brien P, Trojanowski JQ, Lee VM. Pathological alpha-synuclein transmission initiates Parkinson-like neurodegeneration in nontransgenic mice. *Science* 2012; 338:949-53.
23. Nisha CM, Kumar A, Vimal A, Bai BM, Pal D, Kumar A. Docking and ADMET prediction of few GSK-3 inhibitors divulges 6-bromoindirubin-3-oxime as a potential inhibitor. *Journal of molecular graphics & modelling* 2016; 65:100-7.
24. Yasuhara R, Irie T, Suzuki K, Sawada T, Miwa N, Sasaki A, Tsunoda Y, Nakamura S, Mishima K. The beta-catenin signaling pathway induces aggressive potential in breast cancer by up-regulating the chemokine CCL5. *Experimental cell research* 2015; 338:22-31.
25. Golpich M, Amini E, Hemmati F, Ibrahim NM, Rahmani B, Mohamed Z, Raymond AA, Dargahi L, Ghasemi R, Ahmadiani A. Glycogen synthase kinase-3 beta (GSK-3beta) signaling: Implications for Parkinson's disease. *Pharmacological research* 2015; 97:16-26.
26. Parr C, Carzaniga R, Gentleman SM, Van Leuven F, Walter J, Sastre M. Glycogen synthase kinase 3 inhibition promotes lysosomal biogenesis and autophagic degradation of the amyloid-beta precursor protein. *Molecular and cellular biology* 2012; 32:4410-8.
27. Ejlerskov P, Hultberg JG, Wang J, Carlsson R, Ambjorn M, Kuss M, Liu Y, Porcu G, Kolkova K, Friis Rundsten C, et al. Lack of Neuronal IFN-beta-IFNAR Causes Lewy Body- and Parkinson's Disease-like Dementia. *Cell* 2015; 163:324-39.

Chapter 4

**Modulation of autophagy by a small molecule
inverse agonist of ERR α is neuroprotective**

Note:

This chapter is currently *under peer review* for publication as an original research article.

Abstract

Mechanistic insights into aggrephagy, a selective basal autophagy process to clear misfolded protein aggregates, are lacking. Here, we report and describe the role of Estrogen Related Receptor α (ERR α), new molecular player of aggrephagy, in keeping autophagy flux in check by inhibiting autophagosome formation. A screen for small molecule modulators for aggrephagy identified ERR α inverse agonist XCT 790, that cleared α -synuclein aggregates in an autophagy dependent, but an MTOR independent manner. XCT 790 modulates autophagosome formation in an ERR α dependent manner as validated by siRNA mediated knockdown and over expression approaches. We show that, in a basal state, ERR α is localized on the autophagosomes and upon autophagy induction by XCT 790, this localization is lost and is accompanied with an increase in autophagosome biogenesis. In a preclinical mouse model of Parkinson's disease, XCT 790 exerted neuroprotective effects in the dopaminergic neurons of brain by inducing autophagy to clear toxic protein aggregates and in addition, ameliorated motor co-ordination deficits. Using a chemical biology approach, we unveiled the role of ERR α in regulating autophagy that can be a therapeutic target for neurodegeneration.

Introduction

Proteostasis machineries associated with the clearance of various cellular cargos including toxic proteins and damaged organelles in eukaryotic cells primarily include the chaperone, the Ubiquitin–Proteasome system (UPS) and the autophagy pathways¹. UPS predominantly degrades short-lived proteins via tagging them with Ubiquitin at specific amino acid residues¹. The bulk degradation of long-lived proteins or organelles is mediated largely by the evolutionarily conserved cellular process referred to as macroautophagy (hereafter autophagy). A selective degradation mechanism called aggrephagy can help cells to clear the toxic, long-lived, aggregate-prone proteins. Misfolded and aggregate prone proteins are substrates for autophagy². Intracellular accumulation of misfolded protein aggregates is an evident feature of several neurodegenerative diseases including Parkinson's disease (PD). Owing to their hydrophobic nature, these aggregates sequester cellular proteins thereby perturbing cellular proteostasis machineries leading to neuronal death. Neurons are non-dividing cells and can't dilute out the aggregates and thus perhaps are more sensitive to

proteotoxicity². This condition is further exasperated upon aging as efficiency of proteostasis decline. Recent studies highlight the importance of autophagy in curbing cellular cytotoxicity as a consequence of impaired clearance of aggregate prone proteins. Brain specific autophagy knockout mice (Atg5) display age related accumulation of protein aggregates, which eventually leads to neurodegenerative phenotypes, indicating that basal autophagy is vital for clearing protein aggregates³. Additionally, tissue-specific knockdown of Atg7 in CNS of mice resulted in accumulation of inclusion bodies in autophagy-deficient neurons⁴. Autophagy is shown to be dysfunctional during the neurodegenerative disease pathology². Thus, restoration of autophagy, through pharmacological approaches using small molecules have been reported to be neuroprotective⁵⁻⁷. Small molecule that induces or restores defunct autophagy could aid in toxic aggregate clearance and essential for maintaining the cellular and organismal homeostasis^{6,8}. Broadly, small molecule autophagy modulators can be classified into MTOR-dependent or -independent types, depending on their mechanism of action. Since MTOR has autophagy independent functions, targeting MTOR could have adverse side effects in patients with immunosuppression and impaired wound healing processes. Hence, this warrants for identifying new small molecules that are MTOR-independent with potent autophagy function/induction capabilities. More importantly, identifying the new molecular players that help to decipher mechanistic interplay of autophagy and basic neuroprotective mechanisms remain a challenge.

In this study, we discovered a novel autophagy inducer, XCT 790 that was identified previously in our laboratory from a high-throughput screening of library containing pharmacologically active compounds (LOPAC¹²⁸⁰) in yeast. XCT 790, a thiadiazoleacrylamide, a most selective inverse agonist of the orphan nuclear receptor, Estrogen-Related Receptor α (ERR α)⁹, was identified as a 'Hit'. Due to lack of any known natural ligand, XCT 790 has been used as a tool to delineate the lesser known functions of ERR α in different biological processes¹⁰. XCT 790, cleared α -synuclein aggregates in an autophagy-dependent manner in both yeast and human neuronal cells. It significantly induces autophagy through an mTOR-independent mechanism and ERR α -dependent manner. This neuroprotective compound uncovers the role of ERR α in an autophagy pathway. We found that ERR α inhibits autophagy in fed conditions, thus helps in regulating the basal autophagic flux. Additionally, in a preclinical mouse model of PD, XCT 790 was

found to have a neuroprotective role through clearing the toxic protein aggregates as evidenced by immunohistological and behavior analyses.

Results

XCT 790 ameliorates α -synuclein toxicity through an autophagy-dependent mechanism in yeast

As observed in neurons, overexpression of α -synuclein in *S. cerevisiae*, also causes toxic protein aggregate formation that perturbs its growth leading to cell death¹¹. To identify potential small molecules that could ameliorate α -synuclein-mediated cellular toxicity, we screened a small molecule library, LOPAC¹²⁸⁰ (Library Of Pharmacologically Active Compounds) using the established α -synuclein yeast toxicity model¹¹. Compounds were screened for their ability to rescue the growth lag caused by α -synuclein overexpression in yeast cells. α -synuclein overexpression perturbed growth related parameters in yeast. A thiadiazoleacrylamide, XCT 790 was found to be one of the ‘Hits’ that showed significant rescue of growth in yeast cells overexpressing α -synuclein (Fig. 1).

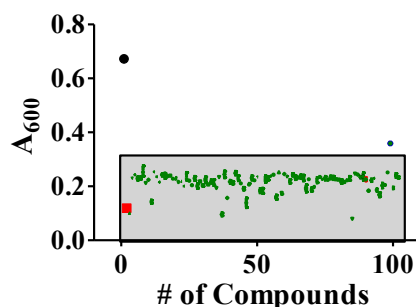


Figure 1. *XCT 790 as a hit that rescued α -synuclein-EGFP toxicity.* Representative box plot indicating chemical hits attained from small molecule library screened in α -synuclein toxicity model of *S. cerevisiae*. In the box plot, small molecules that rescued the growth (absorbance, A_{600}) of wild-type (WT) α -synuclein-EGFP strain by ≥ 3 SD units (grey box) are considered as hits (blue) and those do not rescue the growth are labeled in green. WT EGFP (black) and untreated WT α -synuclein-EGFP (red) strains represent the positive and negative controls of the screen.

Treating wild-type (WT) yeast cells overexpressing α -synuclein with XCT 790 rescued growth lag compared to that of untreated (~3.2 fold, WT α -syn cells; untreated vs XCT treated, $P < 0.001$, **Fig. 2, A to C**). Toxic protein aggregates are known to be substrates of the autophagy pathway for their effective cellular degradation². Consistently, XCT 790 failed to rescue the growth lag in core autophagy mutant cells (*atg1 Δ*) ascertaining its autophagy-mediated rescue of cells from α -synuclein toxicity (*atg1 Δ* α -syn cells; untreated vs XCT 790 treated, $P > 0.05$, **Fig. 2A**). Also, in XCT 790 treated *atg1 Δ* cells overexpressing α -synuclein, the growth related parameters like growth rate (untreated vs XCT 790 treated, $P > 0.05$, **Fig. 2D**) and doubling time (untreated vs XCT 790 treated, $P > 0.05$, **Fig. 2E**) were unaltered compared to that of untreated.

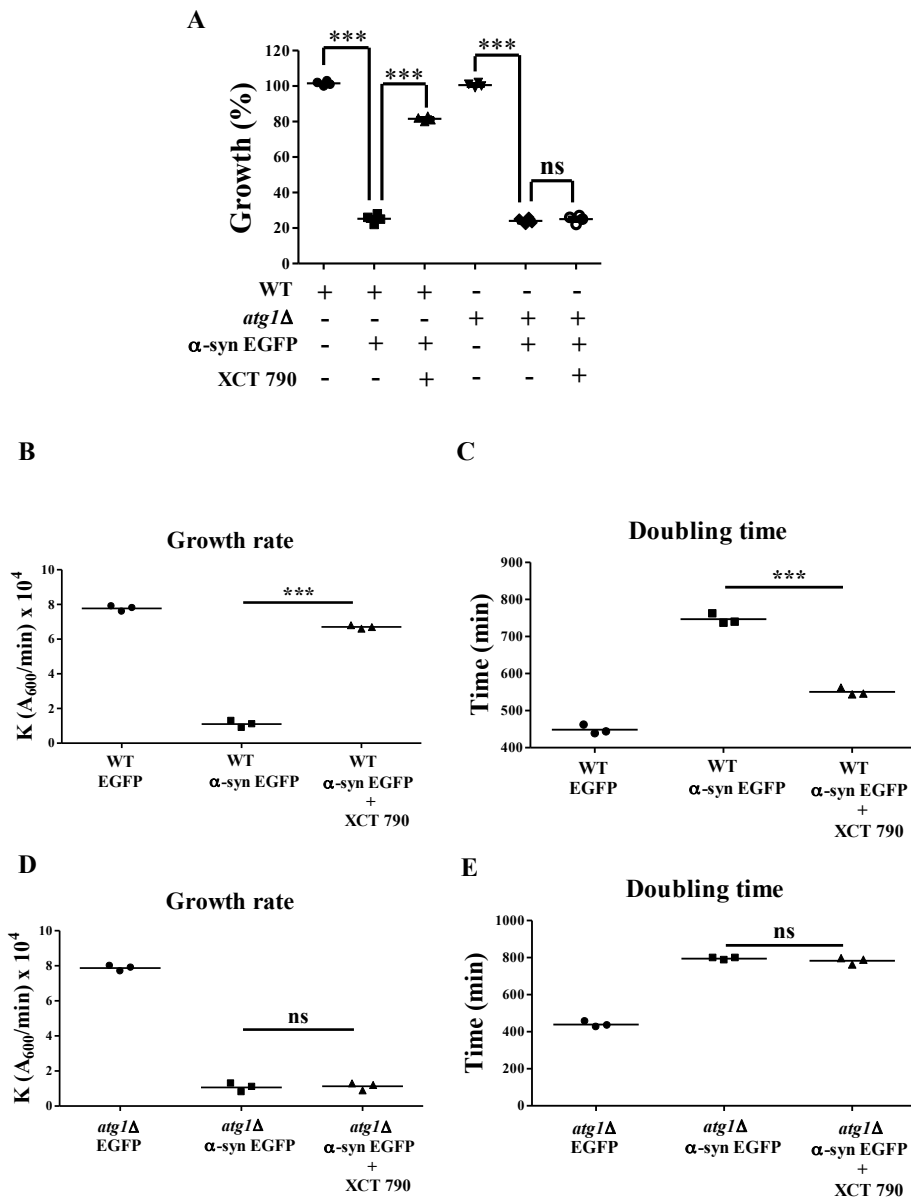


Figure 2. Growth curves. (A) Percent growth of yeast strains (WT EGFP, WT α -syn-EGFP, *atg1Δ* EGFP, *atg1Δ* α -syn-EGFP) treated with XCT 790 ($n=4$, three independent experiments). Growth rate and doubling time plots of XCT 790 treated WT α -syn-EGFP (B and C) and *atg1Δ* α -syn-EGFP (D and E) cells. Statistical analysis was performed using one-way ANOVA and the post-hoc Bonferroni test. Error bars, mean \pm SEM. ns-non significant, ***- $P < 0.001$.

XCT 790 did not affect yeast growth at 50 μ M (growth rate; untreated vs XCT 790 treated, $P > 0.05$; doubling time; untreated vs XCT 790 treated, $P > 0.05$, **Fig 3. A to C**).

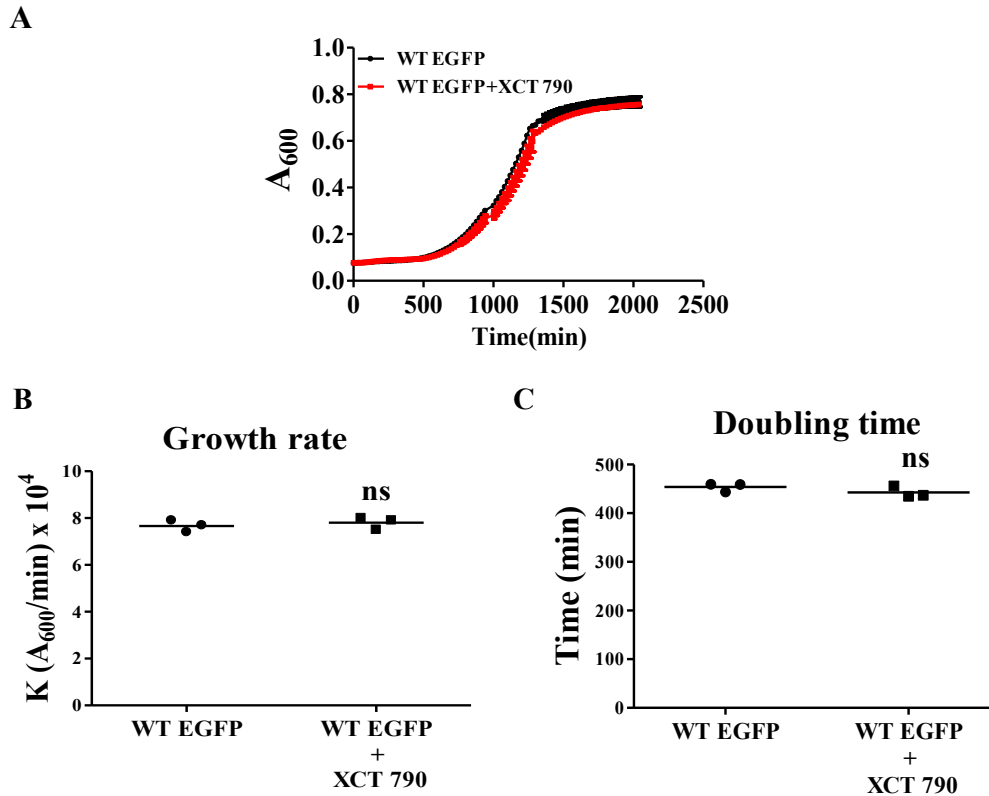


Figure 3. XCT 790 is non-toxic to yeast cells. (A) Growth curve and its related parameters like growth rate (B) and doubling time (C) of XCT 790 treated WT EGFP. Statistical analysis was performed using unpaired Student *t* test. Error bars, mean \pm SEM. ns-non significant.

To understand the autophagy modulation by XCT 790 in yeast, GFP-Atg8 (an autophagosome marker) processing assay under both growth and starvation conditions was performed. XCT 790 treatment dramatically induced autophagic flux in nutrient rich growth conditions where autophagy was barely detectable (Autophagy induction; untreated vs XCT treated, $P < 0.001$; Autophagy flux; untreated vs XCT 790 treated, $P < 0.001$, **Fig. 4**).

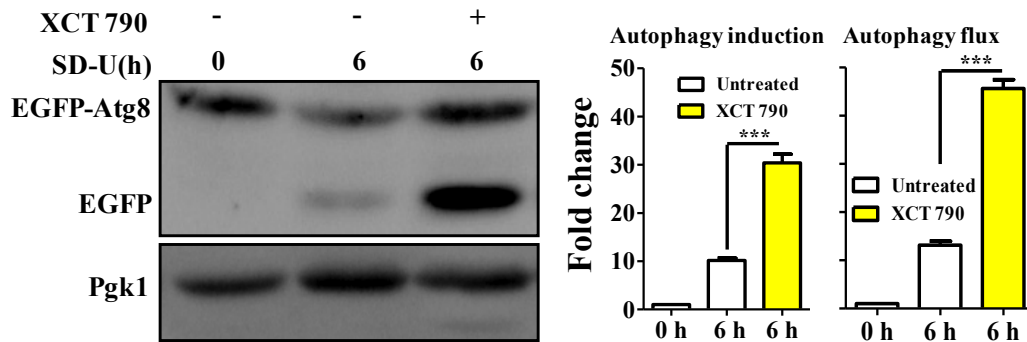


Figure 4. XCT 790 induces basal autophagy. Representative western blot of GFP Atg8 processing assay that assessed the GFP-Atg8 processing after 6h of incubation in growth conditions, in yeast cells treated with XCT 790. Fold change in autophagy induction (EGFP-Atg8 band intensity normalized by loading control) and its flux (summation of EGFP-Atg8 and free EGFP normalized by loading control) modulated by XCT 790 were quantified (three independent experiments). PGK1 served as a loading control. Statistical analysis was performed using unpaired Student *t* test. Error bars, mean \pm SEM. ***- $P < 0.001$.

Similarly, under starvation conditions XCT 790 significantly induced autophagic flux in a time-dependent manner (untreated vs XCT 790 treated: Autophagy induction: 2h, $P < 0.01$; 4h, $P < 0.001$; 6h, $P < 0.001$: Autophagy flux; 2h, $P < 0.001$; 4h, $P < 0.001$; 6h, $P < 0.001$, Fig. 5).

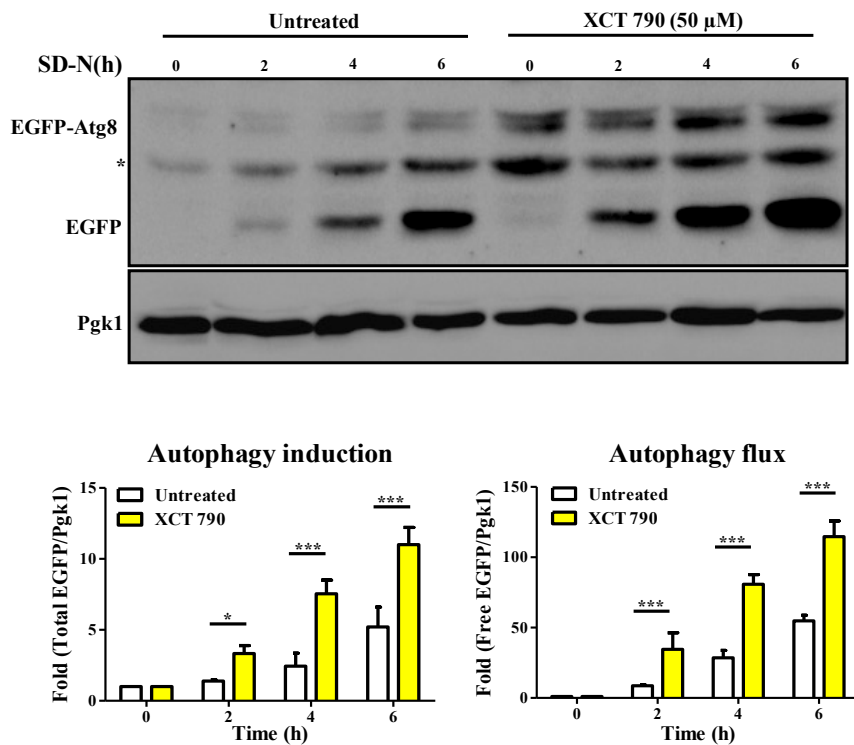


Figure 5. XCT 790 augment starvation induced autophagy. Representative blot for GFP-Atg8 processing of XCT 790 treated yeast cells monitored across time points under starvation condition (2,4 and 6 h). Modulation of autophagy induction (total EGFP/PGK1) and autophagy flux (free EGFP/PGK2) upon XCT 790 treatment, were quantified and then plotted. PGK1 served as a loading control. Statistical analysis was performed using one-way ANOVA and the post-hoc Bonferroni test. Error bars, mean \pm SEM. *- $P < 0.05$, ***- $P < 0.001$.

In yeast cells overexpressing α -synuclein-EGFP, XCT 790 treatment led to vacuolar degradation of α -synuclein-EGFP with a restoration of normal plasma membrane localization of α -synuclein-EGFP (~14 fold, untreated vs XCT 790 treated, $P < 0.001$, **Fig. 6**).

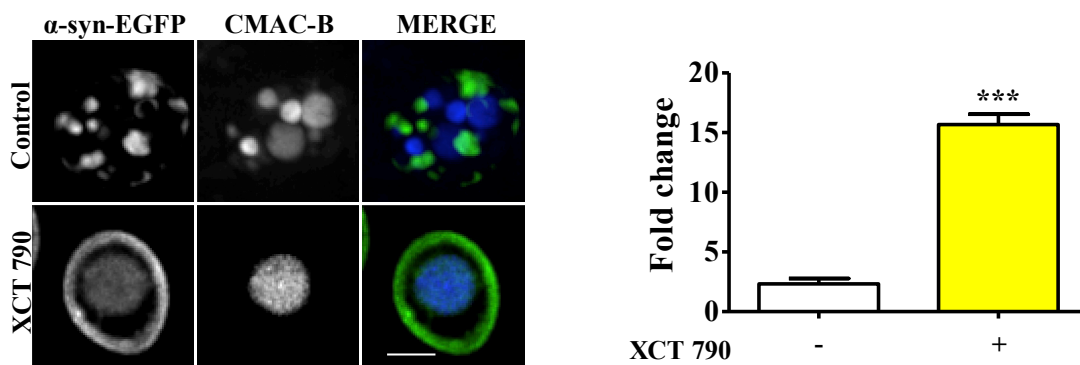


Figure 6. Microscopy based α -synuclein-EGFP degradation assay in yeast. Microscopy images of WT α -synuclein-EGFP treated with XCT 790 and then quantified for the vacuolar free EGFP in fold ($n=75$ cells). Scale bar $5 \mu\text{m}$. Statistical analysis was performed using unpaired Student t test. Error bars, mean \pm SEM. ns-non significant, ***- $P < 0.001$.



To validate this, we employed an α -synuclein-EGFP aggregate degradation assay in yeast. XCT 790 treatment significantly clears α -synuclein-EGFP in wild-type strain (~ 2.5 fold, untreated vs XCT 790 treated, $P < 0.001$, **Fig. 7A**) but not in an autophagy mutant (untreated vs XCT 790 treated, ns, $P > 0.05$, **Fig. 7B**).

The study, for the first time (to the best of our knowledge) identifies XCT 790 as an autophagy inducer with a potential to clear toxic protein aggregates.

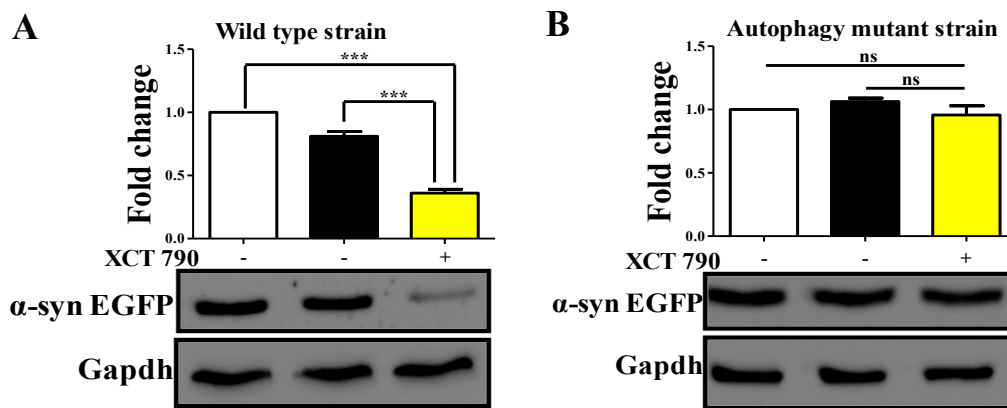


Figure 7. Immunoblotting based α -synuclein-EGFP degradation assay in yeast. (A) Representative western blot for α -synuclein-EGFP degradation in WT α -synuclein-EGFP strain analyzed after 24h of XCT 790 treatment and quantified for the levels of α -synuclein-EGFP (three independent experiments). Gapdh served as a loading control. (B) Representative western blot for α -synuclein-EGFP degradation in *atg1* Δ α -synuclein-EGFP strain analyzed after 24h of XCT 790 treatment and quantified for the levels of α -synuclein-EGFP (three independent experiments). Gapdh served as a loading control. Concentration of XCT 790 used was 50 μ M. Statistical analysis was performed using one-way ANOVA and the post-hoc Bonferroni test. Error bars, mean \pm SEM. ns-non significant, ***- $P < 0.001$.

Modulation of mammalian autophagy by XCT 790

Considering that the autophagic mechanism is highly conserved between the yeast and the mammalian systems, we validated the potential of XCT 790 to clear toxic α -synuclein protein aggregates through autophagy in mammalian cells such as human neuroblastoma SH-SY5Y and HeLa cell lines.

To test the modulation of mammalian autophagy and its flux by XCT 790, we employed western blot analysis based LC3 (autophagosome marker) and microscopy-based tandem RFP-EGFP-LC3 assays. In tandem RFP-EGFP-LC3 assay, XCT 790 treatment significantly

induced autophagosomes and autolysosome formation in both SH-SY5Y (control versus XCT 790 treated, autophagosomes, ~2 fold, $P < 0.05$; autolysosomes, ~4 fold, $P < 0.01$, **Fig. 9**) and HeLa cells (control versus XCT 790 treated, autophagosomes, ~5 fold, $P < 0.001$; autolysosomes, ~2 fold, $P < 0.001$, **Fig. 8**).

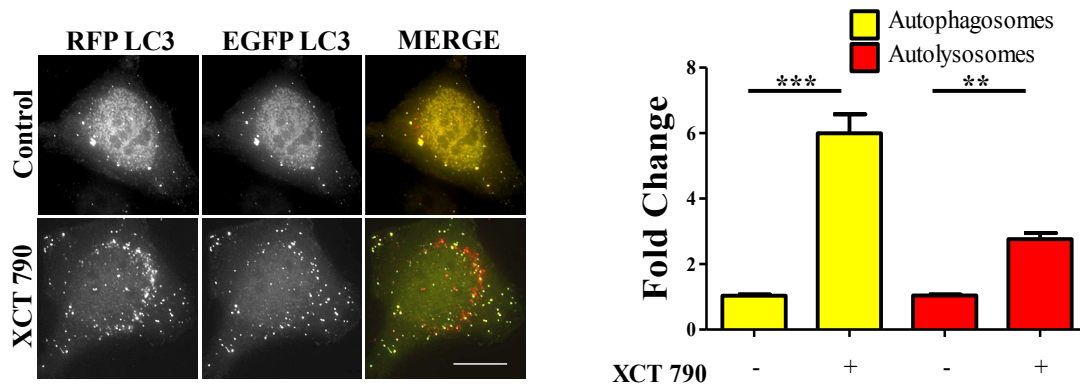


Figure 8. Tandem RFP-EGFP-LC3 assay in HeLa cells. Representative microscopy images of tandem RFP-EGFP-LC3 assay in HeLa cells treated with XCT 790 for 2h. Yellow puncta were autophagosomes and red were autolysosomes. Fold change in regulation of autophagosomes and autolysosomes by XCT 790 were quantified. Scale bar was 15 μ m. Statistical analysis was performed using unpaired Student *t* test. Error bars, mean \pm SEM. **- $P < 0.01$, ***- $P < 0.001$.

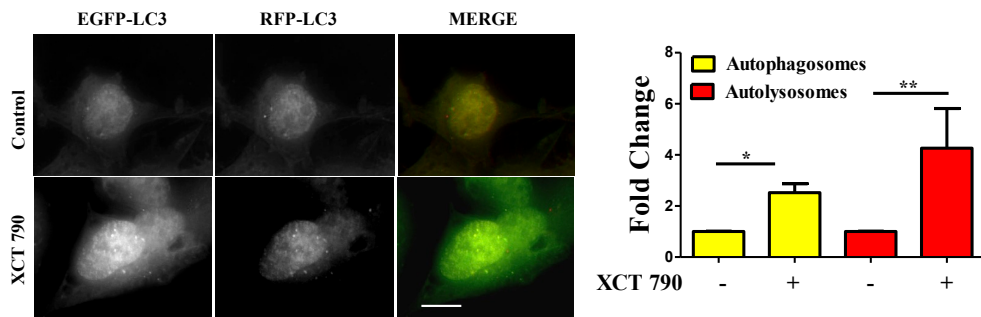


Figure 9. Tandem RFP-EGFP-LC3 assay in SH-SY5Y cells. Representative microscopy images of tandem RFP-EGFP-LC3 assay in SH-SY5Y cells treated with XCT 790 for 2h.

Yellow puncta were autophagosomes and red were autolysosomes. Fold change in autophagosomes and autolysosomes upon XCT 790 treatment were quantified. Scale bar was 15 μm . Statistical analysis was performed using unpaired Student *t* test. Error bars, mean \pm SEM. ns-non significant, *- $P < 0.05$, **- $P < 0.01$.

Additionally, XCT 790 treatment enhanced accumulation of LC3-II levels indicating the induction of autophagy (~2.5 fold, untreated versus XCT 790, $P < 0.001$, **Fig. 10**). These results clearly demonstrated that XCT 790 modulates mammalian autophagy as in yeast.

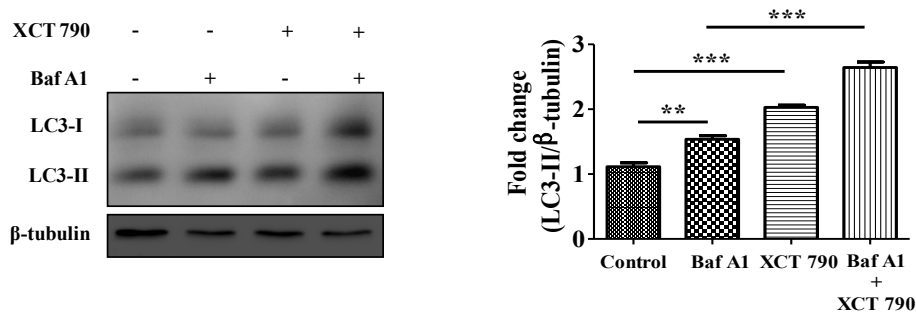


Figure 10. LC3 processing assay. Representative western blot of LC3 processing assay in SH-SY5Y cells treated with XCT 790 (2h) under growth condition and normalized LC3-II levels were quantified. β -tubulin was used as a loading control. Statistical analysis was performed using one-way ANOVA and the post-hoc Bonferroni test. Error bars, mean \pm SEM. **- $P < 0.01$, ***- $P < 0.001$.

We then addressed the question whether XCT 790 protects SH-SY5Y cells from EGFP- α -synuclein mediated toxicity. Overexpression of EGFP- α -synuclein in SH-SY5Y cells is toxic and led to significant cell death as measured by cell viability assay (~4 fold, vector control or untransfected versus α -syn transfected, **Fig. 11**). Upon administration of XCT 790 to cells overexpressing EGFP- α -synuclein, the cell viability increased significantly than that of untreated (~4 fold, α -syn over expressed cells, untreated versus XCT 790 treated, $P < 0.001$, **Fig. 11**) and was comparable to that of vector control (vector control versus α -syn over expressed cells XCT 790 treated, ns, $P > 0.05$, **Fig. 11**). We observed the potential of XCT 790 to protect from EGFP- α -synuclein toxicity is abrogated in presence of

pharmacological autophagy inhibitor, 3-MA (α -syn overexpressed cells, XCT 790 versus XCT 790+3-MA, ~4 fold, $P < 0.001$, **Fig. 11**) that is comparable to that of XCT 790 untreated (α -syn overexpressed cells, untreated versus XCT 790+3-MA, ns, $P > 0.05$, **Fig. 11**). These results clearly demonstrate that XCT 790 protects human neuroblastoma cells from EGFP- α -synuclein mediated toxicity in an autophagy dependent manner.

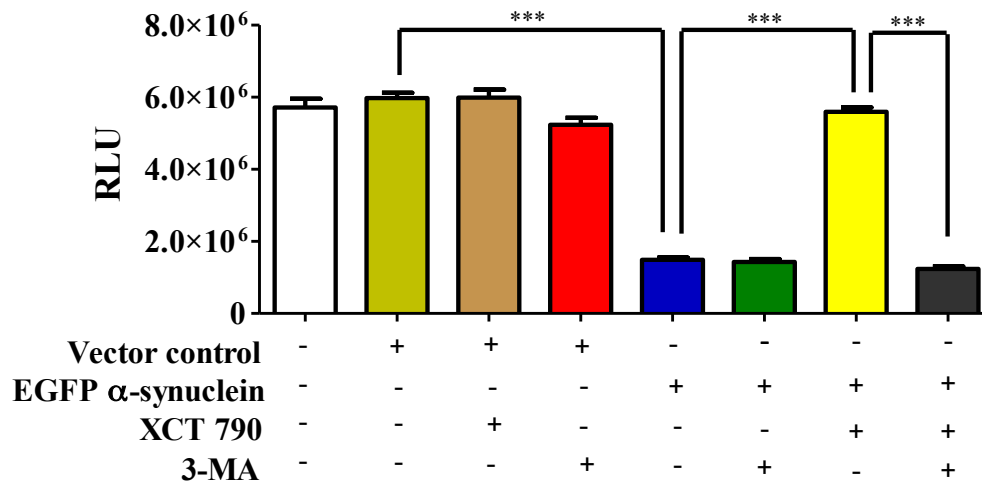


Figure 11. Neuro(cyto)protection assay in SH-SY5Y cells. Graph indicating the cell viability read out of SH-SY5Y overexpressing EGFP- α -synuclein treated with XCT 790 in presence of pharmacological autophagy inhibitor 3-MA. Cell viability was analyzed using CellTitre Glo™ (Promega) assay. More RLU readout was indicative of more cell viability and vice-versa. Statistical analysis was performed using one-way ANOVA and the post-hoc Bonferroni test. Error bars, mean \pm SEM. ns-non significant, ***- $P < 0.001$.

We demonstrate that XCT 790 exerts protection to the cells against EGFP- α -synuclein mediated toxicity by inducing autophagy which helps clear the toxic aggregates.

XCT 790 modulates autophagy through an MTOR independent pathway

Autophagy is regulated by MTOR (mechanistic target of rapamycin)-dependent and MTOR-independent pathways that are amenable to chemical perturbations¹². To delineate the mechanism of autophagy modulation by XCT 790, we examined the activity of MTOR through monitoring its substrates such as P70S6K and 4EBP1. Upon XCT 790 treatment,

MTOR activity was unaffected as revealed by protein levels of its substrates such as phospho-P70S6K and phospho-4EBP1 which were comparable to nutrient rich condition (**Fig. 12**). In contrast, the levels of phospho-P70S6K and phospho-4EBP1 were attenuated under starvation conditions where autophagy was regulated in an MTOR-dependent manner. Lithium Chloride (10mM), known to induce autophagy through an MTOR independent mechanism served as positive control¹³ (**Fig. 12**). These observations asserted that XCT 790 is an MTOR independent autophagy modulator.

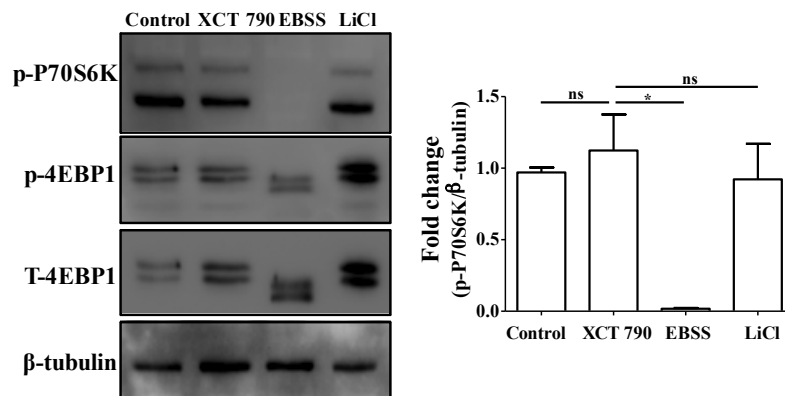


Figure 12. XCT 790 is an MTOR independent modulator. Representative western blots of MTOR substrates like P70S6K (phospho and total form) and 4EBP1 (phospho and total form) regulation by various treatments like XCT 790, EBSS and LiCl. β -tubulin was used as a loading control. Normalized p-P70S6K levels were quantified. Concentrations of XCT 790 and LiCl used were 5 μ M and 10 mM. Statistical analysis was performed using one-way ANOVA and the post-hoc Bonferroni test. Error bars, mean \pm SEM. ns-non significant, *- $P < 0.05$.

We further examined whether XCT 790 exerts its effects through AMPK pathway, one of the predominant MTOR-independent mechanisms known to regulate autophagy. It was observed that treatment of XCT 790 for 2 hours did not affect the activity of AMPK, as evident by the unchanged T172 phosphorylation of AMPK (**Fig. 13**) when compared to nutrient rich conditions. AMPK promotes autophagy in an mTOR-independent manner by directly activating Ulk1 through phosphorylation of Ser555. Whereas, under nutrient sufficiency, high MTOR activity inhibits Ulk1 activation by phosphorylating Ulk1 at Ser757 and disrupting the interaction between Ulk1 and AMPK¹². Therefore, we further

examined the regulation of levels of activating (S555) and inhibitory (S757) phosphorylation levels of ULK1 by XCT 790. Consistent with unchanged levels of phosphorylated AMPK after treatment with XCT 790 for 2 hours, the downstream phosphorylation of ULK1 at S555 was unaffected and comparable to nutrient rich conditions (Fig. 13). This suggests that XCT 790 does not exert its effects through AMPK pathway. Importantly, MTOR-dependent phosphorylation of ULK1 at S757 remained unaltered in XCT 790-treated cells unlike in starvation conditions, where a concomitant decrease in the phospho-ULK1 S757 protein levels is observed. These results further confirm that XCT 790 acts through an MTOR-independent mechanism but not through AMPK pathway.

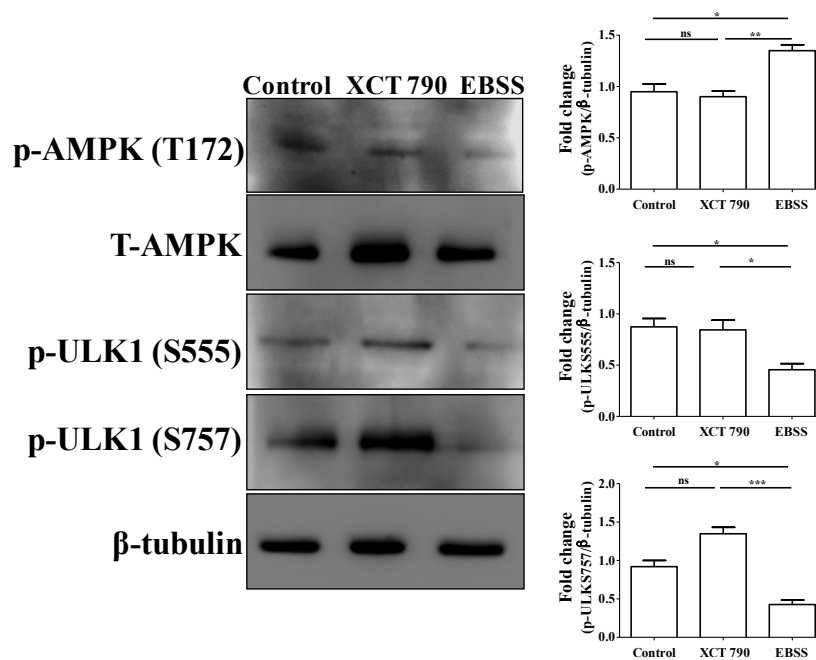


Figure 13. XCT 790 does not modulate AMPK pathway. Representative western blots of signaling pathway proteins like AMPK (phospho and total form) and ULK1 (phospho and total form) regulation by XCT 790 and EBSS. Normalized p-AMPK, p-ULK1 (S555), p-ULK1 (757) levels were quantified. β -tubulin was used as a loading control. Statistical analysis was performed using one-way ANOVA and the post-hoc Bonferroni test. Error bars, mean \pm SEM. ns-non significant, *- $P < 0.05$, **- $P < 0.01$, ***- $P < 0.001$.

XCT 790 induces autophagy through regulation of Estrogen-related receptor alpha (ERR α)

XCT 790 was found to be the first potent and selective inverse agonist of ERR α ⁹. To elucidate the role of ERR α in contributing to the function of XCT 790 as an autophagy inducer, we used the following two approaches: a) siRNA-based silencing of ERR α , b) over expression of ERR α .

To evaluate the level at which the knockdown exerted its effects, cells were transfected with siRNAs targeting ERR α . A non-targeting pool was used as a control. Post 48 hours of transfection, the effect of knockdown on regulation of autophagy by ERR α was monitored by microscopy-based tandem RFP-EGFP-LC3 assays. Knockdown efficiency was confirmed by western blotting to be around 80% (Scrambled versus ERR α siRNA, $P < 0.001$, **Fig. 14A**). Consistent with the effect of XCT 790, knockdown of ERR α also resulted in a significant induction of autophagosomes (~5 fold, Scrambled versus ERR α siRNA treated, $P < 0.001$, **Fig. 14B and C**) and autolysosomes (~3 fold, Scrambled versus ERR α siRNA treated, $P < 0.001$, **Fig. 14B and C**). Autophagosome and autolysosome numbers in XCT 790 treated and ERR α downregulated cells were found to be comparable. These results suggested that XCT 790 modulated autophagy through ERR α .

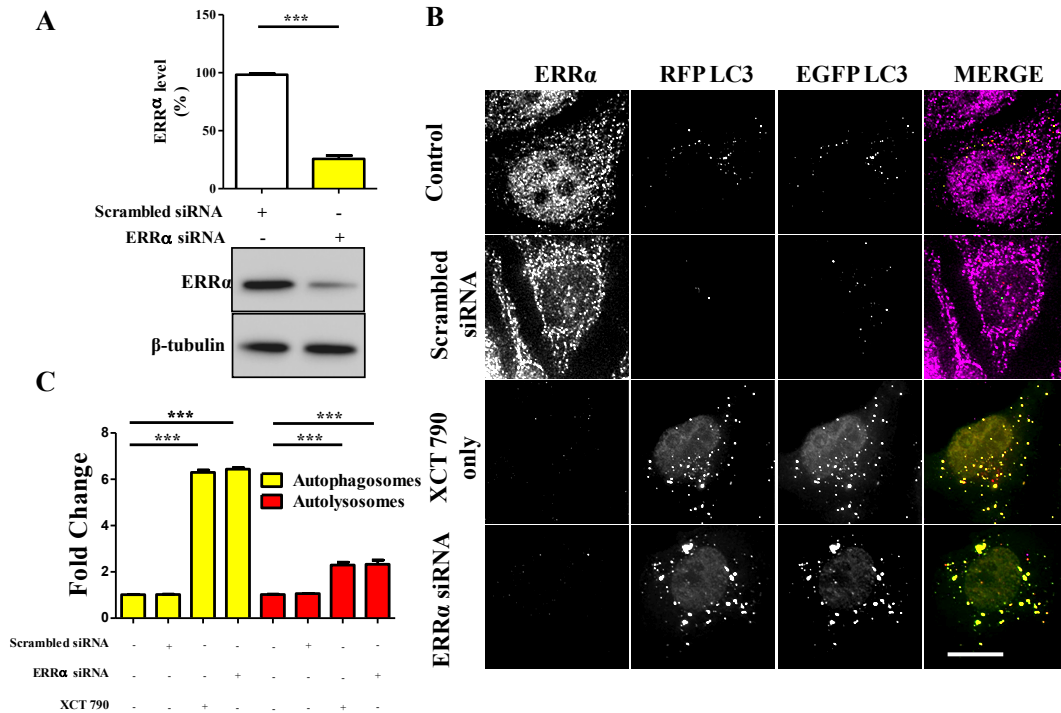


Figure 14. Inhibition of ERR α induces autophagy. (A) ERR α protein levels after transfecting either scrambled siRNA (100 picomoles) or ERR α siRNA (100 picomoles) for 48h in HeLa cells were analyzed by western blotting and then quantified. β -tubulin was used as a loading control. (B and C) Microscopy images (B) of tandem RFP-EGFP-LC3 assay in XCT 790 treated HeLa cells (2h) post ERR α siRNA transfection (48h). Cells were immunostained for ERR α in various treatments. Quantification (C) of autophagosomes (yellow puncta) and autolysosomes (red puncta) modulated by XCT 790 treatment in ERR α siRNA transfected cells. Concentration of XCT 790 used was 5 μ M. Scale bar used was 15 μ m. Statistical analysis was performed using one-way ANOVA and the post-hoc Bonferroni test. Error bars, mean \pm SEM. ***- $P < 0.001$.

We addressed this question through another approach to understand the autophagy modulation upon overexpression of ERR α . In ERR α overexpressed cells, we found more autophagosomes (~2 fold, $P < 0.01$, ERR α overexpressed versus untreated) and less autolysosomes (~2 fold, $P < 0.01$, ERR α overexpressed versus untreated) than that of control (Fig. 15, A and B). From this, we could interpret that autophagy was inhibited at its autophagosome to lysosome fusion step upon over expression of ERR α . When ERR α over

expressed cells were treated with XCT 790, more autophagosomes (~2 fold, $P < 0.01$, ERR α overexpressed versus untreated) and less autolysosomes (~2 fold, $P < 0.01$, ERR α overexpressed versus untreated) than that of untreated were found (**Fig. 15, A and B**). This autophagic scenario was similar to that of only ERR α over expressed cells (Autophagosomes; ERR α over expressed + XCT 790 versus ERR α overexpressed only, ns, $P > 0.05$ and Autolysosomes; ERR α over expressed + XCT 790 versus ERR α overexpressed only, ns, $P > 0.05$, **Fig. 15, A and B**). When ERR α was over expressed, the autophagic modulating ability of XCT 790 was indeed abrogated.

Collectively, these results suggested that XCT 790 is modulating autophagy through ERR α .

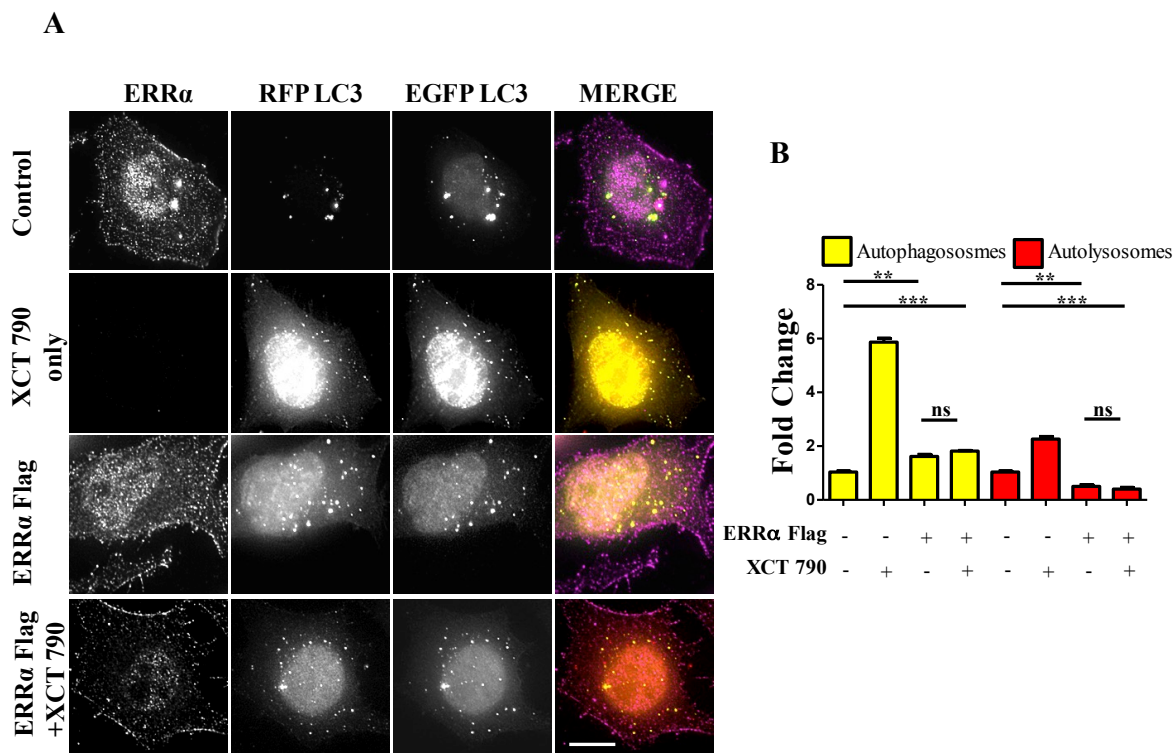


Figure 15. ERR α overexpression inhibits autophagy. Microscopy images (**A**) of tandem RFP-EGFP-LC3 assay in XCT 790 treated HeLa cells (2h) post ERR α Flag transfection (48h). Cells were immunostained for ERR α in all treatment groups. Quantification (**B**) of autophagosomes (yellow puncta) and autolysosomes (red puncta) modulated by XCT 790 treatment in ERR α Flag transfected cells. Concentration of XCT 790 used was 5 μ M. Scale

bar used was 15 μ m. Statistical analysis was performed using one-way ANOVA and the post-hoc Bonferroni test. Error bars, mean \pm SEM. ns-non significant, **- $P < 0.01$, ***- $P < 0.001$.

ERR α regulates autophagy by localizing onto autophagosomes

From knock down and over expression of ERR α studies, there was a clear indication that ERR α could modulate the autophagy pathway. Autophagy was induced when ERR α was downregulated (**Fig. 14, B and C**) but inhibited when overexpressed (**Fig. 15, A and B**). We examined whether active transcription was required for autophagic function of XCT 790. Upon XCT 790 treatment in presence of actinomycin D, the autophagosomes and autolysosomes were similar to that of only XCT 790 (XCT 790+Act D versus XCT 790 only, $P > 0.05$, **Fig. 16, A and B**). This result indicates that autophagic activity of XCT 790 remains unaffected when active transcription was inhibited.

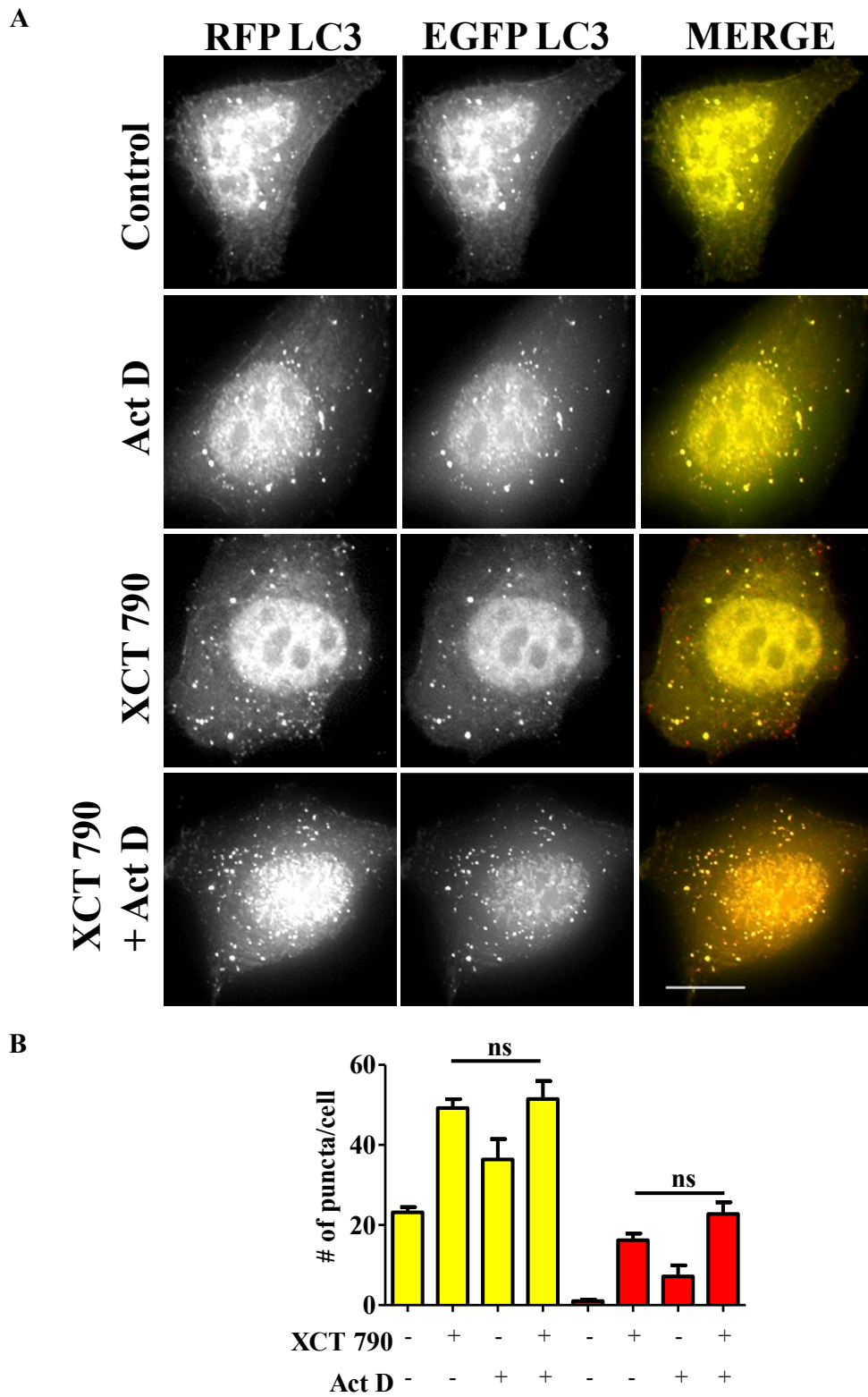


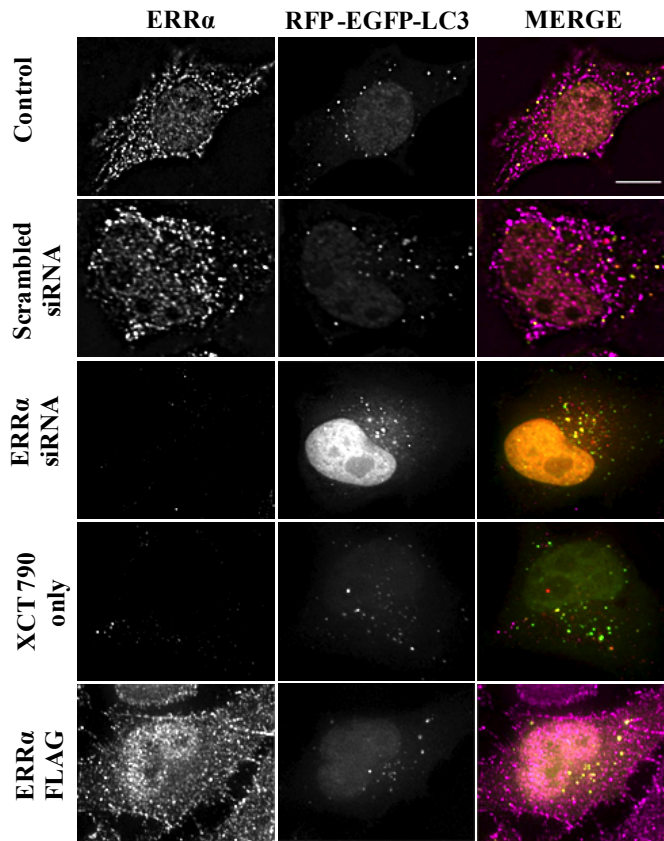
Figure 16. Autophagy modulating activity by XCT 790 is transcription independent. (A) Representative microscopy images of tandem RFP-EGFP-LC3 assay in HeLa cells co-

treated with XCT 790 and actinomycin D (act D). (B) Fold change of autophagosomes and autolysosomes across various treatments were plotted. Scale bar 15 μ m. Statistical analysis was performed using one-way ANOVA and the post-hoc Bonferroni test. Error bars, mean \pm SEM. ns-non significant.

Then, we attempted to check whether ERR α localizes to autophagic related structures such as autophagosomes and autolysosomes. PCC of ERR α with autophagosomes (\sim 0.85) were found to be significantly more than that with autolysosomes (\sim 0.3) under nutrient rich condition (\sim 2.5 fold, autophagosomes versus autolysosomes, $P > 0.001$, **Fig. 17, A and B**). In basal autophagy conditions, colocalization of ERR α with autophagosomes was significantly reduced in ERR α silenced and XCT 790 treated cells (\sim 3.5 fold, untreated or scrambled siRNA versus ERR α siRNA, $P < 0.001$, **Fig. 17, A and B**). Significantly more ERR α colocalize with autophagosomes when ERR α was overexpressed (control or scrambled siRNA versus ERR α overexpressed, $P < 0.001$, **Fig. 17, A and B**). Colocalization of ERR α with autolysosomes was not regulated when compared to that of control (control or scrambled siRNA versus ERR α siRNA or XCT 790 or ERR α overexpressed, $P > 0.05$, Fig. 4A, C) suggesting that ERR α might not interact with the autolysosomes. ERR α could most likely localized to autophagosomes than autolysosomes.

These results pointing that possibly, ERR α might regulate autophagy through its localization on the autophagosomes.

A



B

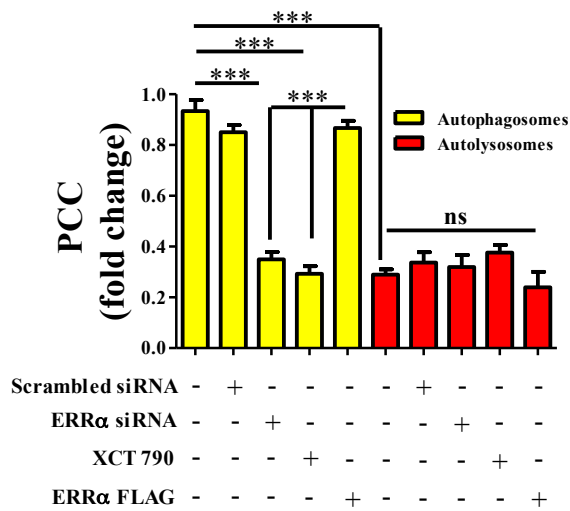


Figure 17. *ERRα* localizes onto autophagosomes to modulate autophagy. (A) Microscopy images of tandem RFP-EGFP-LC3 assay in HeLa cells transfected (48 h) with either *ERRα* siRNA or *ERRα* Flag treated with XCT 790 for 2 h. Cells were immunostained for *ERRα*. (B) PCC (Pearson's Colocalization Coefficient) analyses of *ERRα* with either autophagosome (yellow) or autolysosomes (red) in HeLa cells transfected (48 h) with either

*ERRα siRNA or ERRα Flag treated with XCT 790 for 2 h were plotted. Scale bar was 15 μm. Statistical analysis was performed using one-way ANOVA and the post-hoc Bonferroni test. Error bars, mean ± SEM. ns-non significant, *-P < 0.05, ***-P < 0.001.*

XCT 790 alleviates the MPTP induced dopaminergic neuronal loss

A significant proportion of dopaminergic neurons in Substantia Nigra pars compacta (SNpc) were lost after MPTP treatment (~68%, MPTP versus Vehicle, $P < 0.001$, **Fig. 19, A and B**) as previously described¹⁴. Co-administration of XCT 790 with MPTP, however alleviated this loss by 80% (MPTP+Co versus Vehicle, $P < 0.05$; XCT 790 versus MPTP, $P < 0.01$, **Fig. 19, A and B**). In a congruent manner, volume of SNpc reduced significantly after MPTP injection (MPTP versus Vehicle, $P < 0.01$, **Fig. 18**), whereas the shrinkage was prevented by approximately 85% when MPTP and XCT 790 were administered together (MPTP+Co versus MPTP, $P < 0.01$, **Fig. 18 and 19B**).

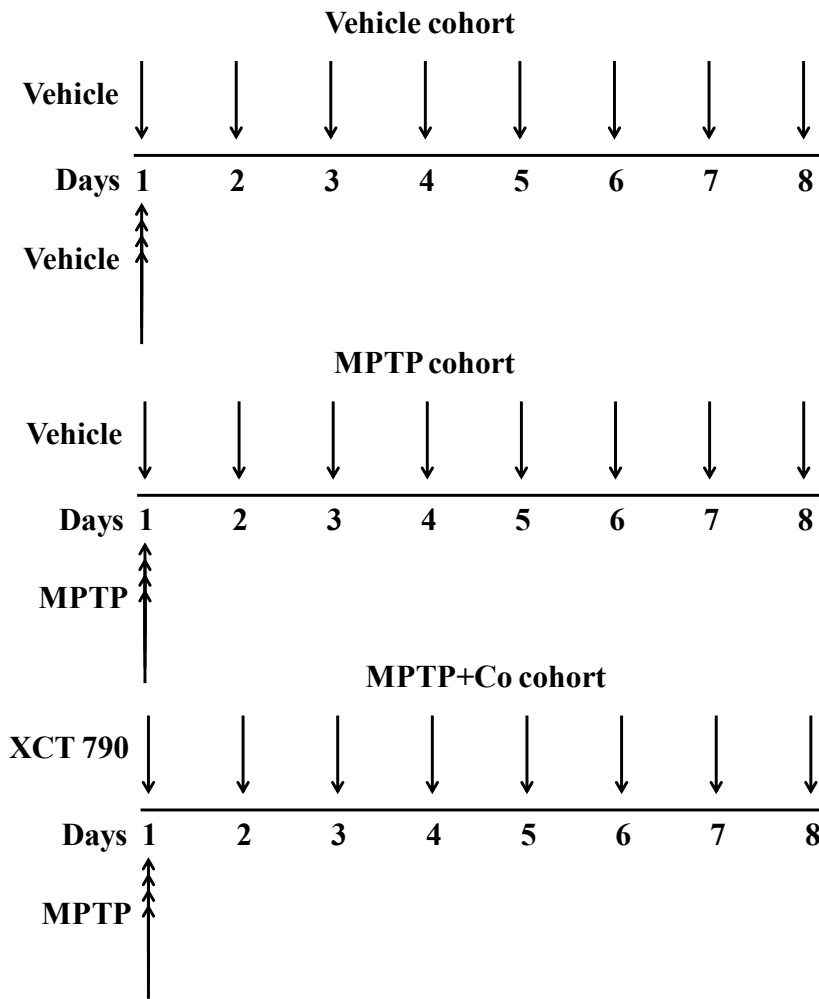


Figure 18. Scheme for injection regimen. Dosage regimen of XCT 790 in various cohorts namely vehicle, MPTP (23 mg/kg of body weight) and MPTP+Co (MPTP; 23 mg/kg of body weight and XCT 790; 5 mg/kg of body weight).

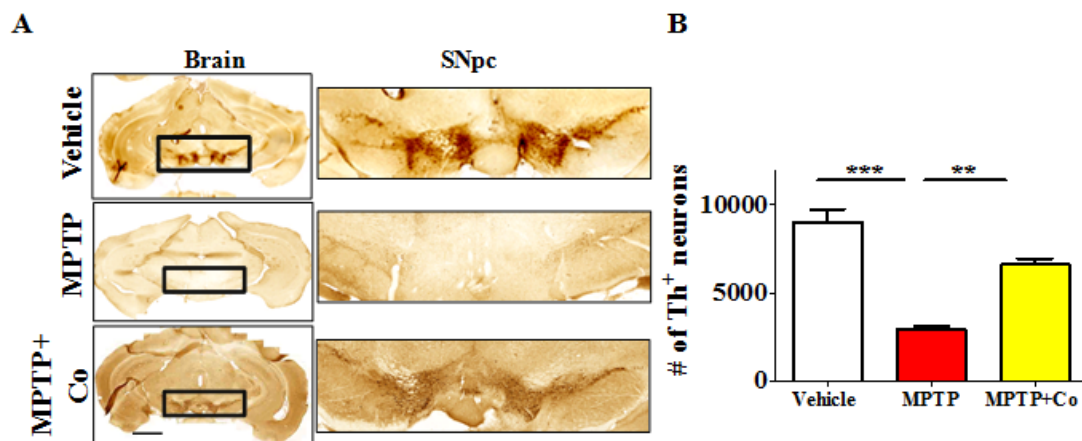


Figure 19. Stereological quantification. (A) Representative photomicrographs of whole brain and SNpc for various cohorts namely vehicle, MPTP (23 mg/kg of body weight) and MPTP+Co (Co-administration of MPTP and XCT 790: MPTP; 23 mg/kg of body weight and XCT 790; 5 mg/kg of body weight). (B) Graph representing the unbiased stereological quantification of TH-ir DA neurons in SNpc for above mentioned cohorts. Scale bar is 600 μ m. Statistical analysis was performed using one-way ANOVA and the post-hoc Bonferroni test. Error bars, mean \pm SEM. **- $P < 0.01$, ***- $P < 0.001$.

Cellular Tyrosine Hydroxylase (TH) expression was preserved in XCT 790 co-treatment group

The cellular TH expression of individual TH-immunoreactive (TH-ir) dopaminergic neurons, as measured by densitometry, was significantly reduced in surviving neurons in MPTP group (MPTP versus Vehicle, $P < 0.001$, **Fig. 20, A and B**). TH expression in the nigral neurons of MPTP and XCT 790 co-treated mice was comparable to the vehicle control group. Thus XCT 790 significantly alleviated the MPTP-induced depletion of cytoplasmic TH expression (MPTP+Co versus MPTP, $P < 0.001$, **Fig. 20, A and B**).

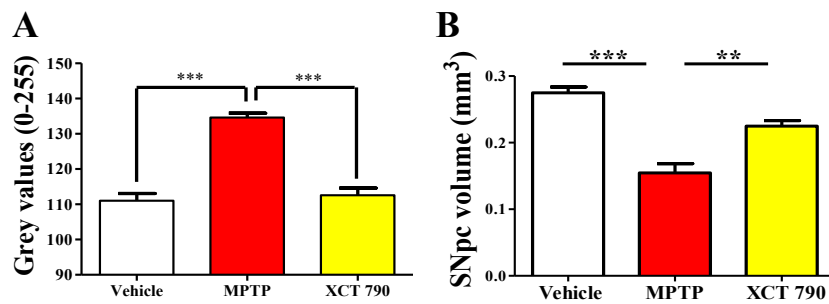


Figure 20. Densitometric quantification. (A) Plot indicating the densitometric quantification, measure of TH intensity in DAergic neurons. (B) Plot indicating the nigral volume measured for the cohorts. Statistical analysis was performed using one-way ANOVA and the post-hoc Bonferroni test. Error bars, mean \pm SEM. **- $P < 0.01$, ***- $P < 0.001$.

XCT 790 enhances autophagy and clears toxic protein aggregates in an *in vivo* mouse model of PD

In neurons, the autophagy process is indispensable for clearing the misfolded toxic protein aggregates³. During the neurodegenerative progression, autophagy is defunct and becomes incompetent to maintain cellular proteostasis². To delineate the mechanism of neuroprotective action of XCT 790, we examined the autophagy status in the various mice treatment cohorts. Our yeast and cell lines results strongly indicated that XCT 790 might exert neuroprotection through modulating autophagy. In an MPTP toxicity model, the LC3 puncta per neuron was reduced significantly than vehicle treated (~ 0.8 fold, vehicle versus MPTP treated, $P < 0.01$, **Fig. 21**) indicating dysfunctional autophagy during neurodegenerative disease progression. Interestingly, the cohort with XCT 790 only exhibits significantly increased LC3 puncta per cell compared to the vehicle treated cohort (~ 3 fold, vehicle versus XCT 790 only, $P < 0.001$, **Fig. 21**). This demonstrated that XCT 790 is a strong autophagy inducer in the dopaminergic neurons of SNpc. We observed a significantly increased LC 3 puncta per cell in the MPTP and XCT 790 co-administered cohort than the vehicle treated ones (~ 3 fold, vehicle versus MPTP+Co, $P < 0.001$, **Fig. 21**). These results demonstrated that XCT 790 could induce autophagy in the brain and strikingly surpass the autophagic deficit caused due to pathogenesis.

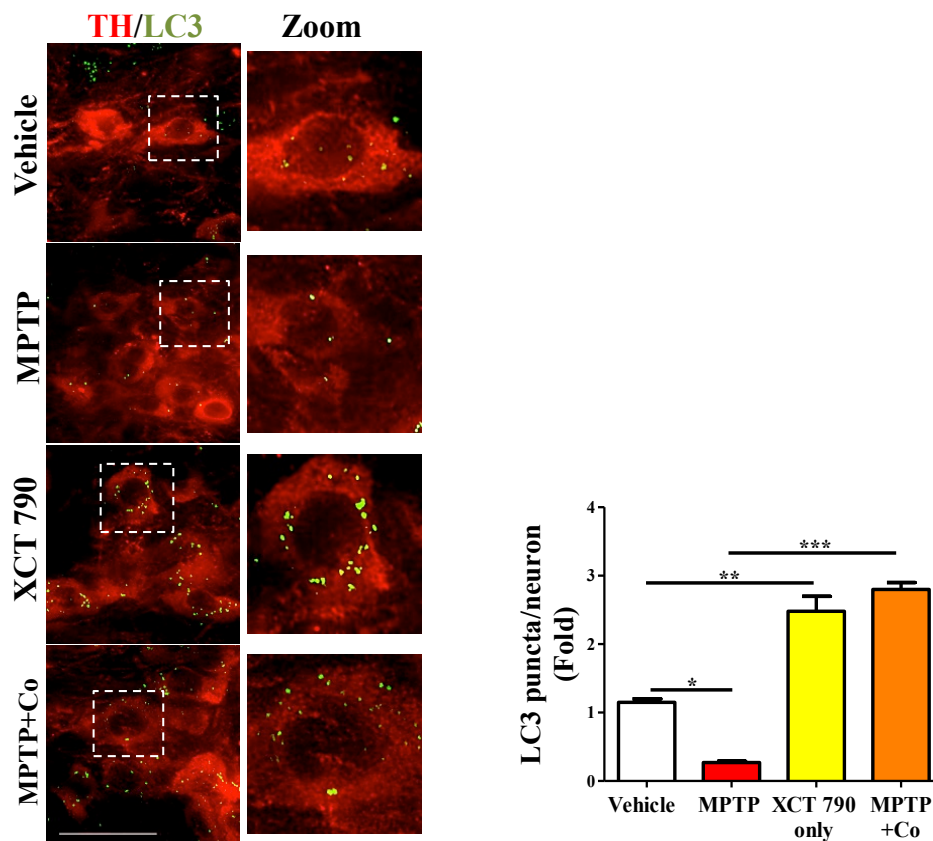


Figure 21. XCT 790 induces autophagy in dopaminergic neurons in SNpc of mice midbrain. Representative fluorescent IHC photomicrographs of DAergic neurons in SNpc double stained for LC3 (autophagy marker) and TH (SNpc marker) antibodies for various cohorts namely vehicle, MPTP, XCT only and MPTP+Co. Graph representing the LC3 puncta per neuron for various cohorts. Scale bar is 50 μ m. Statistical analysis was performed using one-way ANOVA and the post-hoc Bonferroni test. Error bars, mean \pm SEM. *- $P < 0.05$, **- $P < 0.01$, ***- $P < 0.001$.

During protein aggregation, the toxic misfolded protein oligomeric species would accumulate in the neurons¹⁵. We examined whether autophagy induction by XCT 790 could clear the toxic oligomeric intermediates in the neurons. In a vehicle treated cohort, the occurrences of aggregates were significantly less compared to that of MPTP treated cohort (~6.5 fold, vehicle versus MPTP treated, $P < 0.001$, **Fig. 22**). These observations reaffirming that toxic misfolded protein aggregates are formed during disease pathology.

Upon co-administration of MPTP along with XCT 790, we observed a significant reduction in the toxic aggregates compared to that of MPTP only treated cohort (~6 fold, MPTP versus MPTP+Co, $P < 0.001$, **Fig. 22**). We found that aggregate reduction in the MPTP+Co cohort was comparable to that of vehicle treated cohort (MPTP+Co versus vehicle, ns, $P > 0.05$, **Fig. 22**) indicating its strong potential to clear misfolded toxic protein aggregates. In addition, the presence of aggregates in a steady state level of cells in the XCT 790 only cohort was comparable to the vehicle ones (vehicle versus XCT 790 only, ns, $P > 0.05$, **Fig. 22**). This result indicated that administrated dosage regimen was not exerting any proteotoxic stress to the neurons. We demonstrated that XCT 790 could clear the pathological toxic misfolded protein aggregates upon disease progression, one of the main causatives of neurodegeneration.

Mechanistically XCT 790 exerts neuroprotection by clearing misfolded protein aggregates through inducing autophagy as demonstrated in an *in vivo* preclinical mouse model of PD.

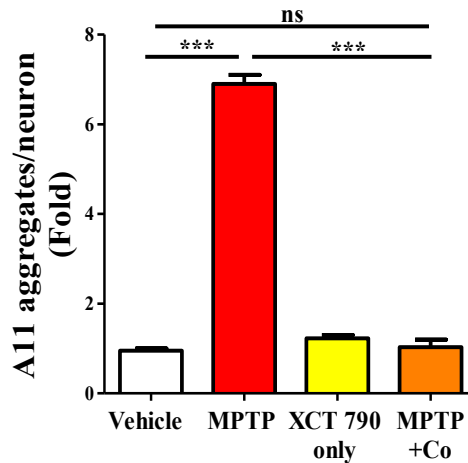
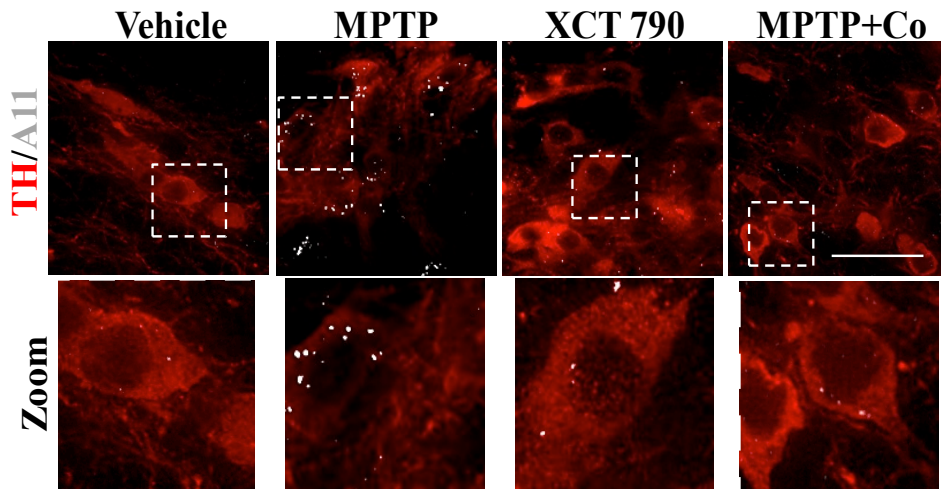


Figure 22. *XCT 790 clears toxic protein oligomers in dopaminergic neurons in SNpc of mice midbrain.* Representative IHC photomicrographs of SNpc DAergic neurons double stained for A11 (toxic oligomer marker) and TH (dopaminergic neuronal marker) antibodies for the above mentioned cohorts. Plot indicating the A11 puncta per DAergic neuron in SNpc was quantitated for all cohorts. Scale bar is 50 μ m. Statistical analysis was performed using one-way ANOVA and the post-hoc Bonferroni test. Error bars, mean \pm SEM. ns-non significant, ***- $P < 0.001$.

XCT 790 ameliorated MPTP-induced behavioral impairments

Parkinson’s disease patients exhibit movement disorder symptoms such as motor coordination and locomotion disabilities that can be recapitulated in a MPTP mouse toxicity model. As our data shows neuroprotective role of XCT 790 at both cellular and tissue level, we wished to test whether its effect can be translated to behavioral level. To address this, we performed a set of well-known behavioral experiments – Rotarod and Open Field tests – that are specific for assaying the movement disorders. The scheme followed for the behavioral paradigm is illustrated in figure 23.

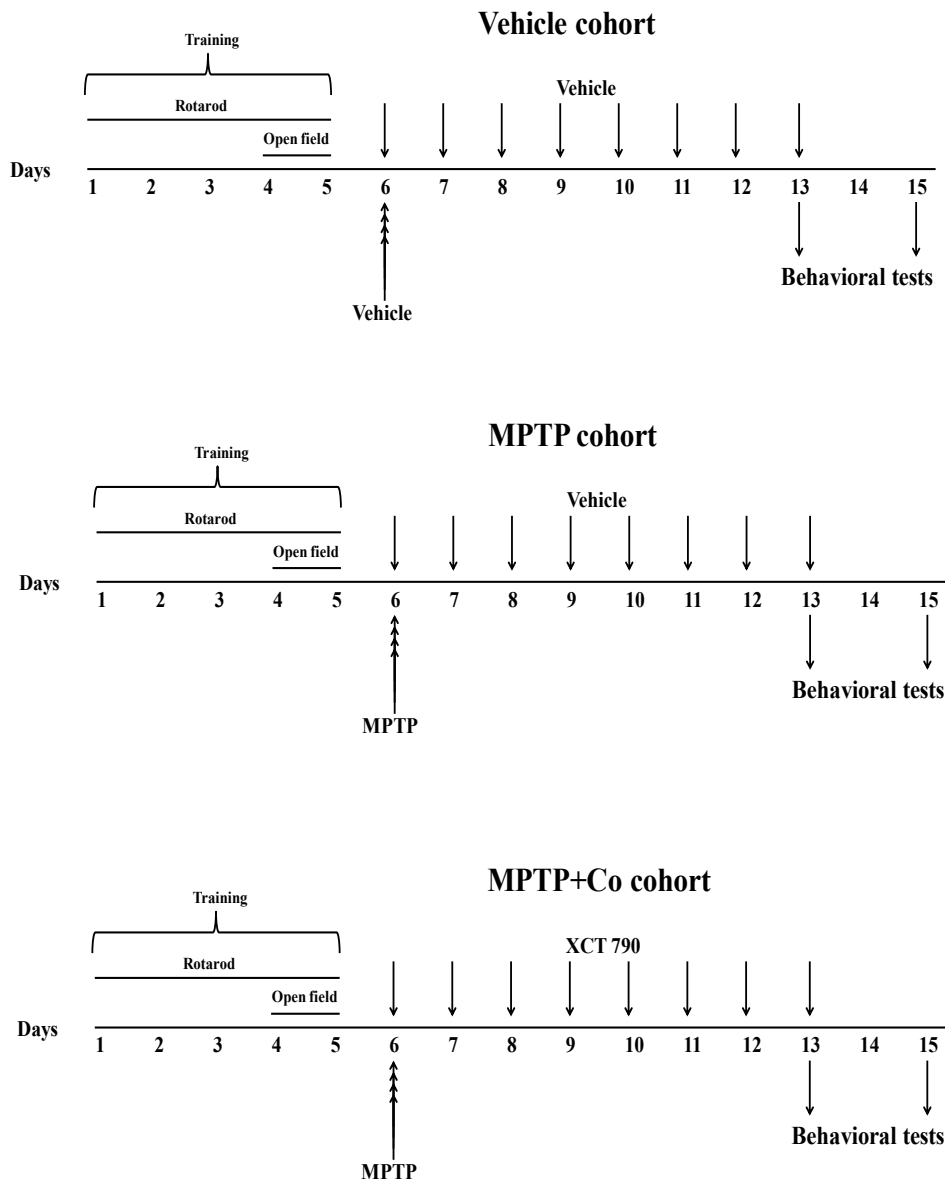


Figure 23. Scheme followed for the behavior paradigm. Scheme indicating the dosage regimen of various cohorts such as vehicle, MPTP and MPTP+Co followed for the behavioral study.

To test the exploratory ability of mice, the distance travelled in the periphery zone of open field arena was compared across different cohorts. We observed that distance travelled in the peripheral zone was drastically reduced in MPTP treated cohort compared to that of vehicle treated cohort (MPTP versus vehicle control, $P < 0.001$, **Fig. 24, D and E**) on both day 13 and day 15, validating the MPTP's effect on exploratory ability. Upon co-administration of XCT 790 along with MPTP, the distance travelled was significantly more than the MPTP cohort (Co versus MPTP cohort, $P < 0.001$, **Fig. 24, D and E**), and more importantly comparable to the vehicle treated cohort on both day 13 and day 15 (Co versus vehicle control, $P > 0.05$, **Fig. 24, D and E**). Importantly, exploratory behavior of various cohorts was evident in the represented trajectory maps (**Fig. 24C**).

Rotarod test, another standard behavioral assay to test motor co-ordination was also employed. In this test, the time spent by mice on a horizontal rotating rod (latency to fall) was used to assay the motor co-ordination ability across different cohorts. In parallel to the results observed in case of Open Field, the co-treated cohort showed improved latency to fall compared to the MPTP treated cohort (Co versus MPTP cohort, $P < 0.001$, **Fig. 24, A and B**) which showed reduced latency to fall against vehicle treated cohort on both day 13 and day 15 (MPTP versus vehicle control, $P < 0.001$, **Fig. 24, A and B**). Also the results of vehicle treated and co-treated cohorts were fairly comparable (Co versus vehicle control, $P > 0.05$, **Fig. 24, A and B**) on both days.

Therefore, these results suggest restoration of exploratory and motor coordination abilities in MPTP toxicity model, upon administration of XCT 790. Therefore, XCT 790 ameliorates the behavioral disabilities of MPTP treated mouse model.

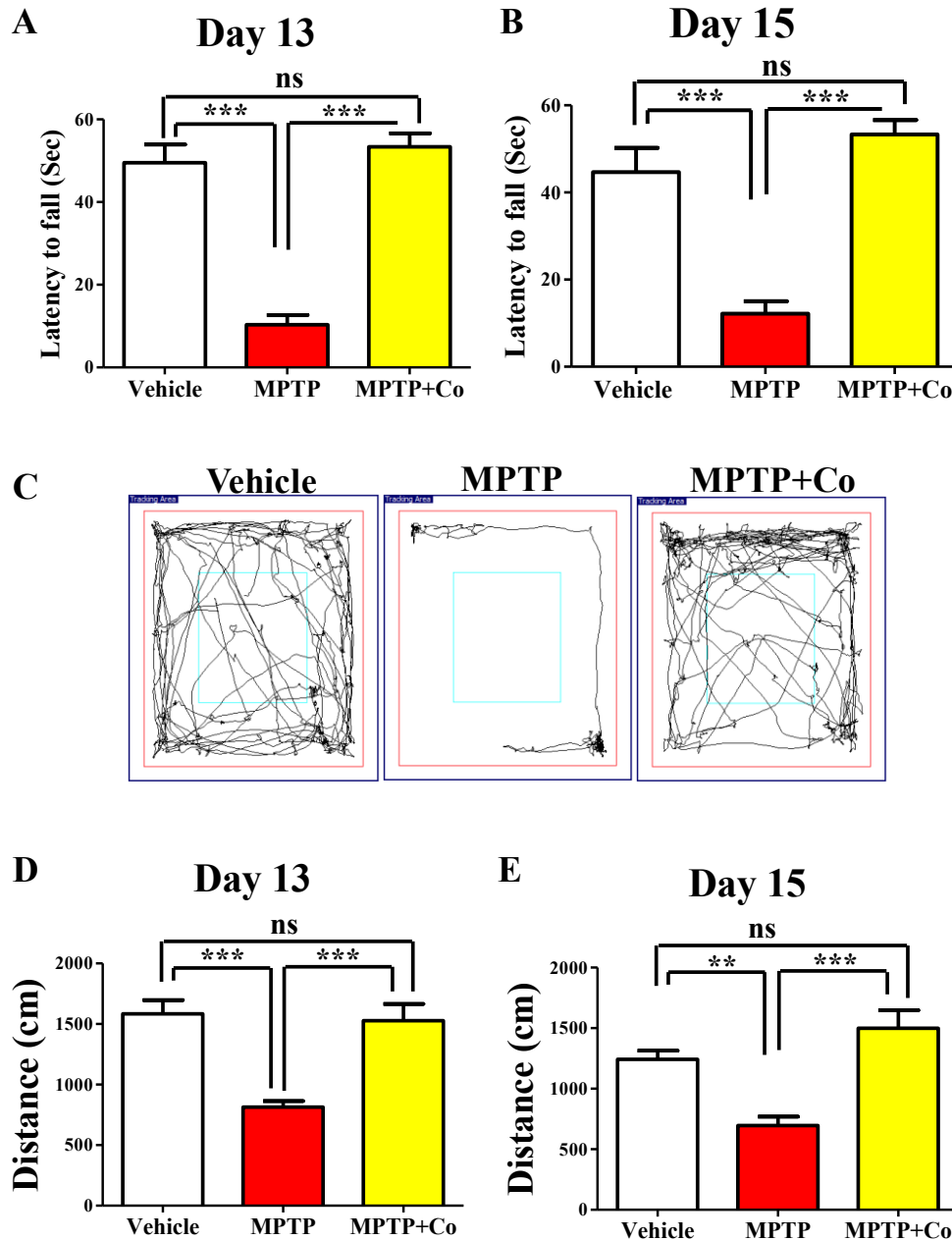


Figure 23. XCT 790 ameliorates MPTP-induced behavioral impairments. Latency to fall for various cohorts such as vehicle, MPTP and MPTP+Co on both day 13 (A) and 15 (B) were monitored using rotarod test. (C) Representative trajectory maps were indicated for all the mentioned cohorts. (D and E) Plots indicating the peripheral distance travelled by mice were assessed through open field test on both day 13 (D) and 15 (E). Statistical

*analysis was performed using one-way ANOVA and the post-hoc Bonferroni test. Error bars, mean \pm SEM. ns-non significant, ***- $P < 0.001$.*

Discussion

There are no therapeutic interventions available for neurodegeneration. New strategies to curb neurodegeneration involve identification of druggable targets and novel small molecules are necessary. In this study, we identified the small molecule XCT 790 as a novel ERR α mediated autophagy modulator that ameliorates α -synuclein toxicity and exerts neuroprotection in a preclinical mouse model of PD.

Lewy bodies are primarily due to the aggregation of misfolded proteins such as α -synuclein that exert cellular toxicity leading to neuronal death¹⁶. Such aggregates result in perturbation of cellular homeostasis due to exaggerated proteotoxicity that triggers apoptosis and eventual loss of neurons³. In addition, cellular proteostasis efficacy and also compensatory action among protein quality control machineries decline with age; as a result the relatively non-diving neuronal population are more susceptible to proteostatic insult¹⁷. Crucial protein quality control pathways like autophagy are impaired in neurodegenerative disease pathologies². Neurons with defective autophagy hamper the turnover of proteins and harbor protein aggregates such as ubiquitin positive inclusions and Lewy bodies⁴. Genetic ablation of neuronal autophagy function results in progressive accumulation of neuronal aggregates and such mice manifest neurodegenerative symptoms³. Conversely, genetically enhancing autophagy flux results in, among other things, marked clearance of autophagy adaptors (p62) that are involved in ubiquitin aggregate capture and perhaps contributing to the extended life span of such mice¹⁸. Corroborating such observations, pharmacological studies have implied that autophagy inducing small molecules have therapeutic potential as they restore autophagy flux which eventually mitigates neuronal loss and improves motor co-ordination in models of PD^{5,7,19}. In this context, our study reveals the small molecule XCT 790 as an autophagy enhancer that exerts neuroprotective action.

Autophagy a tightly regulated process; is maintained at low (basal) levels during fed condition and elevated in presence of stress such as starvation³. This low level of autophagy

is maintained by negative regulation of MTOR. We now show that in addition to MTOR pathway, ERR α too negatively regulates autophagy flux. When the ERR α inverse agonist XCT 790 relieves this regulation, the number of autophagosomes and autolysosomes increase several folds. Furthermore, it is known that MTOR activity is not perturbed in absence of ERR α ²⁰. We therefore investigated the interdependence of MTOR and ERR α in controlling autophagy and we show that XCT 790 exerts its autophagy inducing effect independent of MTOR signaling, a well-desired characteristic for further drug development to combat adverse side effects. In addition, MTOR regulates transcription of Ubiquitin Proteasome System (UPS) related genes leading to degradation of ERR α upon induction of autophagy by rapamycin²⁰. Our results suggest that autophagy inhibiting activity of ERR α in nutrient rich conditions is through an MTOR independent mechanism. In autophagy triggering conditions, where its basal inhibitory activity needs to be removed, ERR α gets ubiquitinated and degraded by UPS²⁰, that is corroborated well with our findings.

Among the MTOR independent pathways, AMPK also regulate autophagy flux. Previously, XCT 790 was reported to modulate AMPK pathway in ERR α independent fashion²¹. We observed XCT 790 modulates autophagy by not regulating the AMPK pathway, one of the reported MTOR independent pathways, but through subcellular ERR α localization dynamics.

Interestingly, this control of autophagy levels by ERR α is seemingly independent of its transcriptional role. Instead we find increased translocation of ERR α to the autophagosomes upon XCT 790 treatment.

XCT 790 is reported to be the most selective inverse agonist of ERR α . Though it is known that ERR α localizes primarily in the cytoplasm^{22, 23}, its cytoplasmic function is not yet reported. Thus, apart from its transcriptional function in nucleus²², our findings reveal a cytoplasmic role for ERR α in autophagy.

References

1. Hipp MS, Park SH, Hartl FU. Proteostasis impairment in protein-misfolding and -aggregation diseases. *Trends in cell biology* 2014; 24:506-14.
2. Nixon RA. The role of autophagy in neurodegenerative disease. *Nature medicine* 2013; 19:983-97.
3. Hara T, Nakamura K, Matsui M, Yamamoto A, Nakahara Y, Suzuki-Migishima R, Yokoyama M, Mishima K, Saito I, Okano H, et al. Suppression of basal autophagy in neural cells causes neurodegenerative disease in mice. *Nature* 2006; 441:885-9.
4. Komatsu M, Waguri S, Chiba T, Murata S, Iwata J, Tanida I, Ueno T, Koike M, Uchiyama Y, Kominami E, et al. Loss of autophagy in the central nervous system causes neurodegeneration in mice. *Nature* 2006; 441:880-4.
5. Khurana V, Lindquist S. Modelling neurodegeneration in *Saccharomyces cerevisiae*: why cook with baker's yeast? *Nature reviews Neuroscience* 2010; 11:436-49.
6. Rajasekhar K, Suresh SN, Manjithaya R, Govindaraju T. Rationally designed peptidomimetic modulators of abeta toxicity in Alzheimer's disease. *Scientific reports* 2015; 5:8139.
7. Sarkar S, Perlstein EO, Imarisio S, Pineau S, Cordenier A, Maglathlin RL, Webster JA, Lewis TA, O'Kane CJ, Schreiber SL, et al. Small molecules enhance autophagy and reduce toxicity in Huntington's disease models. *Nature chemical biology* 2007; 3:331-8.
8. Rajasekhar K, Narayanaswamy N, Mishra P, Suresh SN, Manjithaya R, Govindaraju T. Synthesis of Hybrid Cyclic Peptoids and Identification of Autophagy Enhancer. *Chempluschem* 2014; 79:25-30.
9. Busch BB, Stevens WC, Jr., Martin R, Ordentlich P, Zhou S, Sapp DW, Horlick RA, Mohan R. Identification of a selective inverse agonist for the orphan nuclear receptor estrogen-related receptor alpha. *Journal of medicinal chemistry* 2004; 47:5593-6.
10. Ariazi EA, Jordan VC. Estrogen-related receptors as emerging targets in cancer and metabolic disorders. *Current topics in medicinal chemistry* 2006; 6:203-15.

11. Outeiro TF, Lindquist S. Yeast cells provide insight into alpha-synuclein biology and pathobiology. *Science* 2003; 302:1772-5.
12. Kim J, Kundu M, Viollet B, Guan KL. AMPK and mTOR regulate autophagy through direct phosphorylation of Ulk1. *Nature cell biology* 2011; 13:132-41.
13. Sarkar S, Floto RA, Berger Z, Imarisio S, Cordenier A, Pasco M, Cook LJ, Rubinsztein DC. Lithium induces autophagy by inhibiting inositol monophosphatase. *The Journal of cell biology* 2005; 170:1101-11.
14. Jackson-Lewis V, Przedborski S. Protocol for the MPTP mouse model of Parkinson's disease. *Nature protocols* 2007; 2:141-51.
15. Luk KC, Kehm V, Carroll J, Zhang B, O'Brien P, Trojanowski JQ, Lee VM. Pathological alpha-synuclein transmission initiates Parkinson-like neurodegeneration in nontransgenic mice. *Science* 2012; 338:949-53.
16. Wakabayashi K, Tanji K, Mori F, Takahashi H. The Lewy body in Parkinson's disease: molecules implicated in the formation and degradation of alpha-synuclein aggregates. *Neuropathology : official journal of the Japanese Society of Neuropathology* 2007; 27:494-506.
17. Anglade P, Vyas S, Hirsch EC, Agid Y. Apoptosis in dopaminergic neurons of the human substantia nigra during normal aging. *Histology and histopathology* 1997; 12:603-10.
18. Pyo JO, Yoo SM, Ahn HH, Nah J, Hong SH, Kam TI, Jung S, Jung YK. Overexpression of Atg5 in mice activates autophagy and extends lifespan. *Nature communications* 2013; 4:2300.
19. Williams A, Sarkar S, Cuddon P, Ttofi EK, Saiki S, Siddiqi FH, Jahreiss L, Fleming A, Pask D, Goldsmith P, et al. Novel targets for Huntington's disease in an mTOR-independent autophagy pathway. *Nature chemical biology* 2008; 4:295-305.
20. Chaveroux C, Eichner LJ, Dufour CR, Shatnawi A, Khoutorsky A, Bourque G, Sonenberg N, Giguere V. Molecular and genetic crosstalks between mTOR and ERRA α

are key determinants of rapamycin-induced nonalcoholic fatty liver. *Cell metabolism* 2013; 17:586-98.

21. Eskiocak B, Ali A, White MA. The estrogen-related receptor alpha inverse agonist XCT 790 is a nanomolar mitochondrial uncoupler. *Biochemistry* 2014; 53:4839-46.

22. Sladek R, Bader JA, Giguere V. The orphan nuclear receptor estrogen-related receptor alpha is a transcriptional regulator of the human medium-chain acyl coenzyme A dehydrogenase gene. *Molecular and cellular biology* 1997; 17:5400-9.

23. Ju D, He J, Zheng X, Yang G. [Cloning, expression of the porcine estrogen-related receptor alpha gene and its effect on lipid accumulation in mature adipocytes]. *Sheng wu gong cheng xue bao = Chinese journal of biotechnology* 2009; 25:1627-32.

Chapter 5

Novel small molecule autophagy modulators AGK2 and PD180970 are neuroprotective

Note:

This chapter is currently *under preparation* for publication as an original research article.

Abstract

Aggrephagy-the selective autophagy pathway that is involved in clearance of protein aggregates has neuroprotective potential especially in neurodegenerative diseases. We identified and characterized two small molecule aggrephagy modulators AGK2 and PD180970 that induce autophagy and clear toxic α -synuclein aggregates in an evolutionarily conserved manner across yeast and mammalian cell lines. Both the small molecules induce autophagy in an MTOR independent manner, a desirable characteristic for therapeutic intervention. PD180970 promotes autophagosome formation whereas AGK2 enhances autophagosome-lysosome fusion. Furthermore, PD180970 exerted neuroprotective ability in a preclinical mouse model of Parkinson's Disease (PD) by inducing autophagy to degrade toxic protein aggregates.

Introduction

Parkinson's disease is a progressive movement disorder and second most commonly occurring neurodegeneration with no cure¹. Around 6.2 million people are affected with PD and 117,400 deaths occurred globally in 2015². PD symptoms include hampered motor coordination, tremor, bradykinesia, stiffness and dementia occurring mostly at the advanced stage of disease³. Other neurological problems include altered sensory perception, emotional and circadian rhythm³. The cause of PD can be sporadic and genetic. L-DOPA is the only symptomatic medication available for PD patients but does not prevent the progression of neurodegenerative pathogenesis⁴. Furthermore, long term administration of L-DOPA has profound side effects such as dyskinesia⁵. In advanced stages of the disease, surgical intervention by Deep Brain Stimulation (DBS) reduces motor symptoms but only for a period for 2-3 years⁵.

Post-mortem analyses of PD brains revealed the presence of protein aggregates known as Lewy bodies (LB) which is a hallmark of disease⁶. LB consists primarily of misfolded α -synuclein with a subset of tau aggregates⁷. These aggregates cause death of dopaminergic neurons in Substantia Nigra pars compacta (SNpc) of midbrain. Dopaminergic neurons are specifically vulnerable to α -synuclein misfolding and their aggregation leads to LB genesis⁸. α -synuclein is predominantly present in brain but smaller amounts are also present in heart and muscles⁹. In neurons, it is mainly found in presynapse and probably functions

in exocytosis by interacting with phospholipids of membranes to release neurotransmitters including dopamine⁹.

α -synuclein is an intrinsically disordered protein that has a propensity to aggregate inside cells in response to various stimuli¹⁰. The exact mechanism(s) of α -synuclein aggregation is not yet clear. In steady state equilibrium, it exists in an unstructured α -helical and β -sheets rich conformations¹⁰. Evidence suggests that it forms an intermediate conformation that is rich in β -sheets which eventually leads to aggregation⁷. Various factors such as cellular milieu, α -synuclein levels and/or mutations enhance aggregation by significantly increasing the intermediate β -sheet conformation population⁷.

Protein quality control machineries that govern aggregate clearance to maintain cellular proteostasis are chaperones, proteasome and autophagy¹¹. Over time, the aggregates overwhelm the capacity of chaperones and proteasome¹². The larger misfolded protein aggregates are also substrates for degradation by autophagy mediated lysosomal degradation-a process known as aggrephagy¹³. In PD, the aggregates also impair autophagy at specific steps making it dysfunctional¹⁴. Proof-of-principle experiments have elegantly demonstrated that clearing α -synuclein aggregates is beneficial and cytoprotective¹⁵. Genetic and pharmacological upregulation of autophagy have been shown to degrade toxic protein aggregates and exert neuroprotection^{15, 16}.

Previously, phenotypic based small molecule screen for aggrephagy conducted in our laboratory revealed several hits such as 6-Bio¹⁵, AGK2 and PD180970. AGK2 has already been reported in a fly model, to be neuroprotective by inhibiting sirtuin 2¹⁷. However, autophagic modulating ability of AGK2 is not reported. In this study, we characterized the small molecules AGK2 and PD180970 for their ability to regulate aggrephagy mechanistically in various proteotoxic model systems such as yeast, mammalian cells and a preclinical mouse model. Both small molecules abrogate α -synuclein mediated toxicity in yeast and mammalian cells in an autophagy-dependent manner. Mechanistically, they enhance autophagy without modulating the MTOR activity and so they are called MTOR independent autophagy modulators. We show that PD180970 exerts neuroprotection in preclinical mouse model of PD by inducing autophagy to clear the toxic protein oligomers. PD180970 also ameliorated the MPTP induced motor and behavioral impairments.

Results

AGK2 and PD180970 rescue α -synuclein toxicity in an autophagy dependent manner in yeast

Overexpression of α -synuclein in the budding yeast *S. cerevisiae* affects its growth and eventually causes death, replicating the cytotoxic phenotype seen in diseased neurons¹⁸. We screened a small molecule library using this α -synuclein toxicity model to identify ‘hits’ that rescue the growth lag (WT EGFP versus WT α -syn-EGFP, $P < 0.001$, **Fig. 1A**). We identified the small molecules AGK2 ($P < 0.01$, versus untreated, **Fig. 1A**) and PD180970 ($P < 0.001$, versus untreated, **Fig. 1B**) as hits that significantly enhanced the growth of wild-type α -synuclein overexpressing strain. Both AGK2 (50 μ M) and PD180970 (50 μ M) did not perturb the growth of wild-type yeast cells (**Fig. 2**).

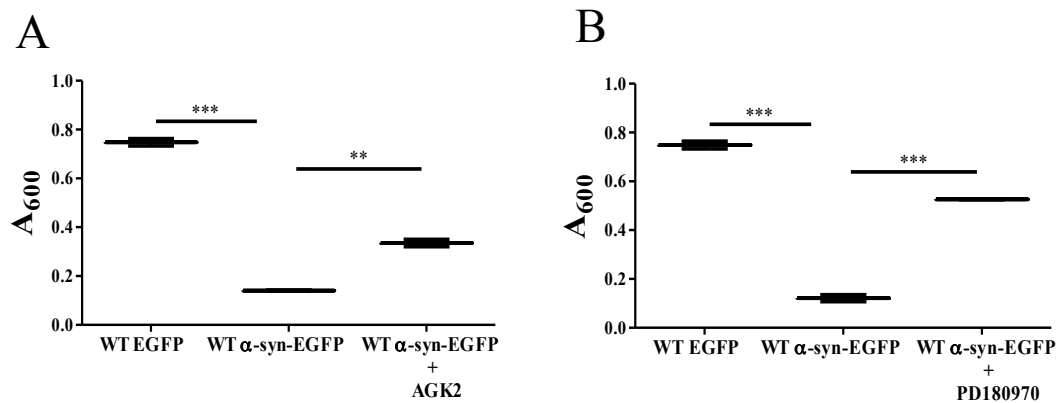


Figure 1. AGK2 and PD180970 abrogate α -synuclein toxicity in yeast. Growth curves of α -synuclein overexpressing wild-type yeast strain treated with AGK2 (A) and PD180970 treatments (B). Statistical analysis was performed using one-way ANOVA and the post-hoc Bonferroni test. Error bars, mean \pm SEM. **- $P < 0.01$, ***- $P < 0.001$.

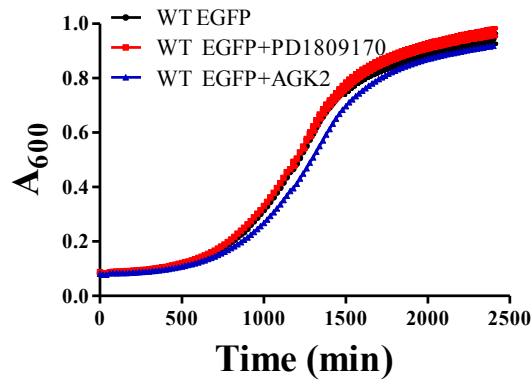


Figure 2. AGK2 and PD180970 are non-toxic to yeast cells. Growth curves of wild type cells expressing only EGFP upon AGK2 (A) and PD180970 treatments (B).

As toxic protein oligomers and aggregates are known to be substrates of autophagy pathway¹⁴, we tested the ability of these hits to rescue growth in autophagy deficient cells. In a core autophagy mutant (*atg1Δ*) strain, both AGK2 ($P > 0.05$, versus untreated, **Fig. 3A**) and PD180970 ($P > 0.05$, versus untreated, **Fig. 3B**) failed to rescue growth, suggesting that these small molecules might act through autophagy.

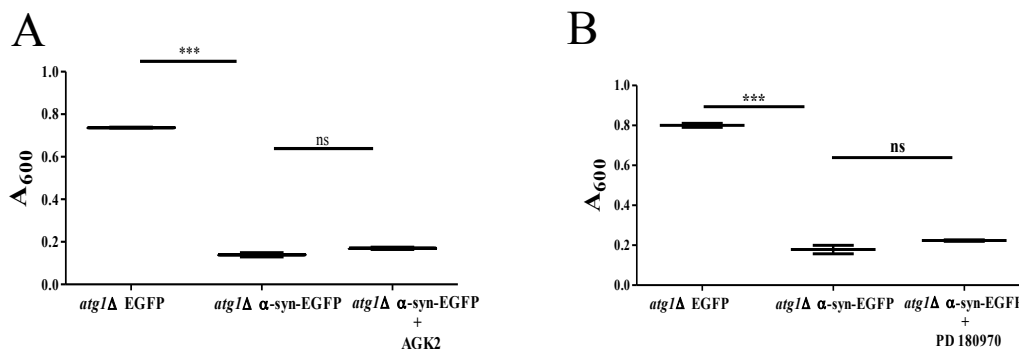


Figure 3. AGK2 and PD180970 rescued yeast cells α -synuclein toxicity is an autophagy-dependent. Growth curves of α -synuclein overexpressing autophagy mutant yeast strain upon AGK2 (A) and PD180970 treatments (B). Statistical analysis was performed using

one-way ANOVA and the post-hoc Bonferroni test. Error bars, mean \pm SEM. ns-non significant, ***- $P < 0.001$.

We then asked whether AGK2 and PD180970 could modulate autophagy temporally using the EGFP-Atg8 processing assay in starvation conditions.

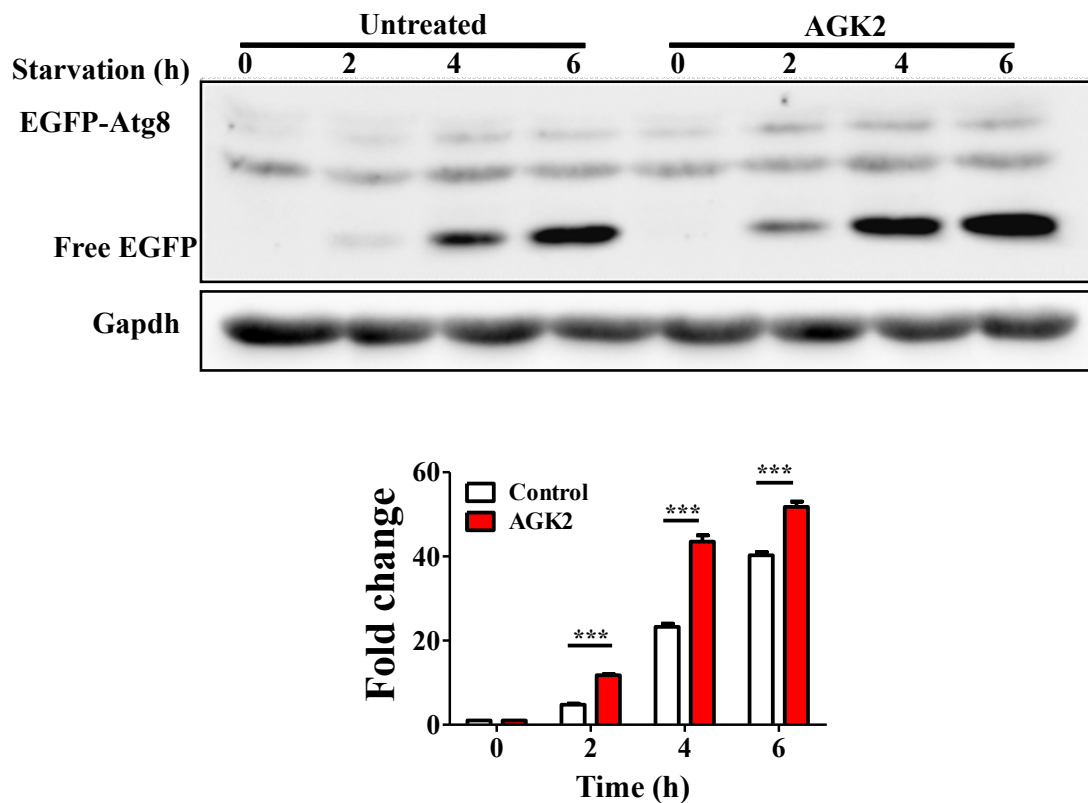


Figure 4. EGFP-Atg8 processing assay. Wild type cells expressing EGFP-Atg8 were treated with AGK2 and samples were collected at various time points (0,2,4 and 6 h) to analyse the autophagy flux. Statistical analysis was performed using one-way ANOVA and the post-hoc Bonferroni test. Error bars, mean \pm SEM. ***- $P < 0.001$.

The release of free EGFP from the EGFP-Atg8 fusion protein is a measure of ‘autophagy flux’. AGK2 (2 h, 4 h and 6 h time points, $P < 0.001$ versus untreated; **Fig. 4**) and PD180970 (2 h, 4 h and 6 h time points, $P < 0.01$ versus untreated; **Fig. 5**) treatment significantly enhanced free EGFP release across different time points than that of untreated. These results demonstrate that AGK2 and PD180970 enhance starvation-induced autophagy and help cells cope with α -synuclein induced proteotoxicity.

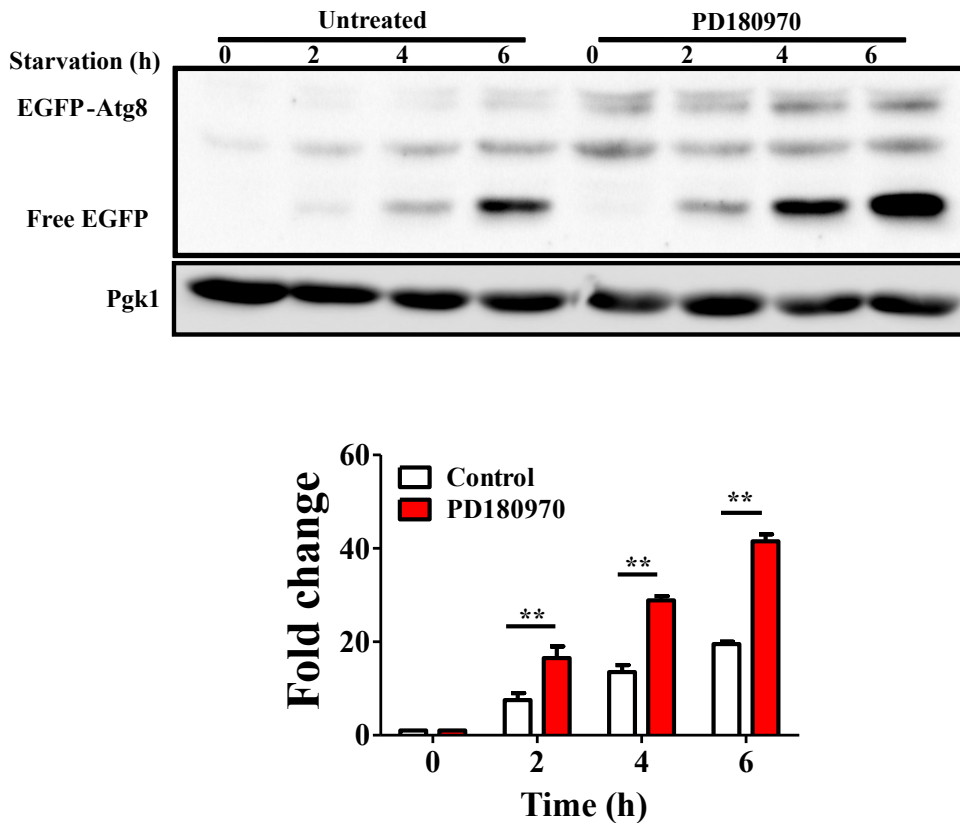


Figure 5. EGFP-Atg8 processing assay. Wild type cells expressing EGFP-Atg8 treated with PD180970 and samples were collected at various time points (0,2,4 and 6 h) to analyse the autophagy flux. Statistical analysis was performed using one-way ANOVA and the post-hoc Bonferroni test. Error bars, mean \pm SEM. ns-non significant, **- $P < 0.01$.

AGK2 and PD180970 clear α -synuclein aggregates in an autophagy dependent manner in yeast

Clearing toxic α -synuclein aggregates is one of the robust cellular defense mechanisms to combat its cytotoxicity¹⁹. Towards this, we tested the ability of AGK2 and PD180970 to clear α -synuclein aggregates in growth conditions using α -synuclein-EGFP degradation assay. Upon AGK2 ($P < 0.001$, versus untreated, **Fig. 6A**) and PD180970 ($P < 0.001$, versus untreated, **Fig. 7A**) treatment, wild-type α -synuclein-EGFP overexpressing strain displayed significantly reduced α -synuclein-EGFP levels.

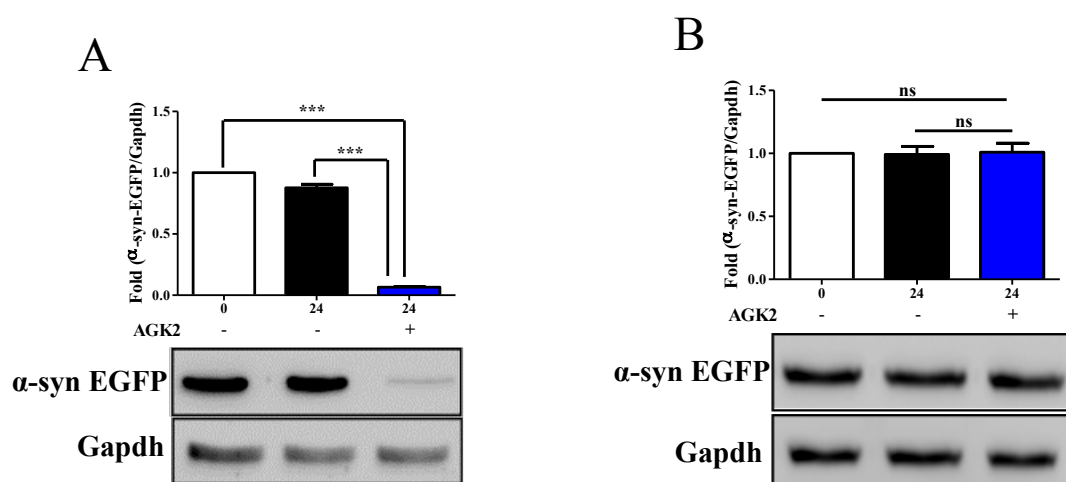


Figure 6. Immunoblotting based α -synuclein-EGFP assay. Both wild type (A) and autophagy mutant (B) strains overexpressing α -synuclein-EGFP treated with AGK2 and analysed for total α -synuclein-EGFP protein levels. Statistical analysis was performed using one-way ANOVA and the post-hoc Bonferroni test. Error bars, mean \pm SEM. ns-non significant, ***- $P < 0.001$.

Interestingly, this reduction was not seen in the core autophagy mutant (*atg1Δ*) strain for both AGK2 ($P > 0.05$, versus untreated, **Fig. 6B**) and PD 180970 ($P > 0.05$, versus untreated, **Fig. 7B**) treatments, suggesting that the clearance was through an autophagy dependent mechanism.

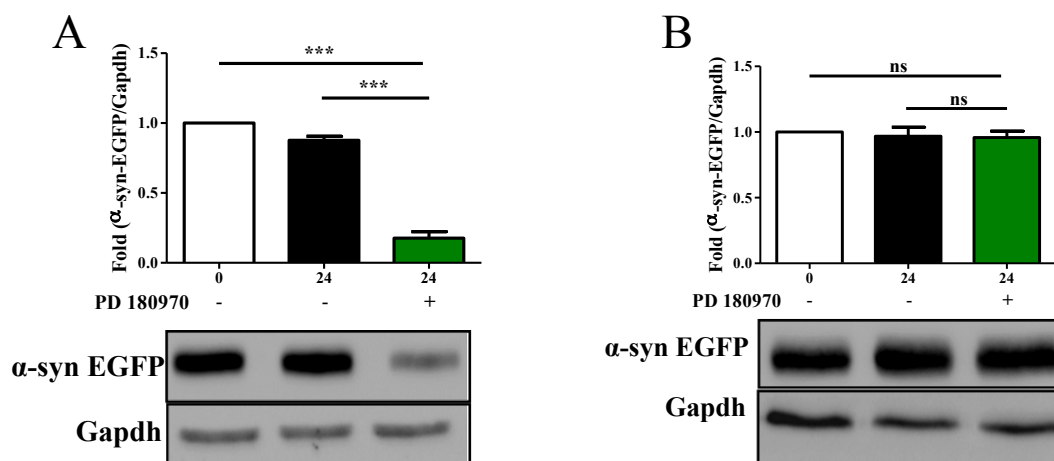


Figure 7. Immunoblotting based α -synuclein-EGFP assay. Both wild type (A) and autophagy mutant (B) strains overexpressing α -synuclein-EGFP treated with PD 180970 and analysed for total α -synuclein-EGFP protein levels. Statistical analysis was performed using one-way ANOVA and the post-hoc Bonferroni test. Error bars, mean \pm SEM. ns-non significant, ***- $P < 0.001$.

AGK2 and PD180970 induced autophagy in mammalian cells

To investigate if these hits also regulate autophagic flux in mammalian cells, we performed fluorescence microscopy based tandem RFP-GFP-LC3 assay and immunoblotting experiments. AGK2 (5 μ M) treated cells showed increased number of autophagosomes (\sim 2 fold, $P < 0.001$, compared to control; **Fig. 8**) and autolysosomes (\sim 4 fold, $P < 0.001$, compared to control; **Fig. 8**) than that of untreated cells. The high numbers of autolysosomes suggested that AGK2 promoted autophagy flux. PD180970 (1 μ M) treatment on the other hand, enhanced the autophagic flux as revealed by significant increase in both autophagosomes (\sim 4 fold, $P < 0.001$, compared to control; **Fig. 8**) and also autolysosomes (\sim 2 fold, $P < 0.001$, compared to control; **Fig. 8**). Apart from increased autophagy flux, the increase in autophagosome numbers suggested that PD180970, in addition, might enhance autophagosome biogenesis and/or maturation step.

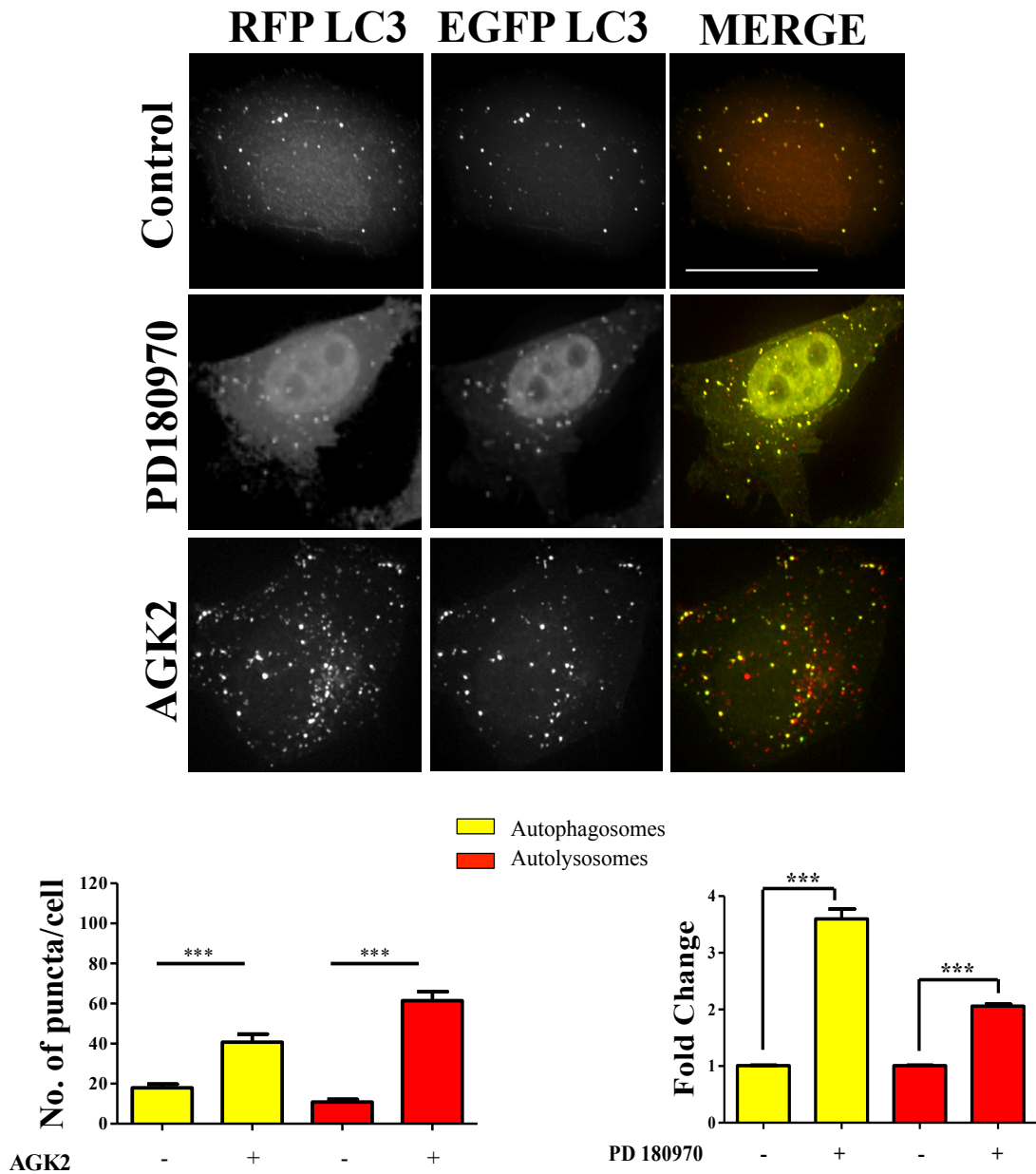
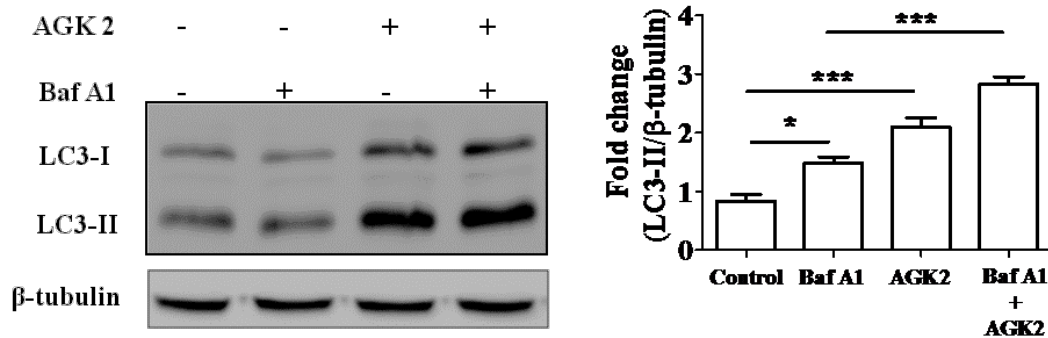


Figure 8. Microscopic tandem RFP-EGFP-LC3 assay. HeLa cells transiently expressing RFP-EGFP-LC3 were treated with AGK2 and PD180970 for 2 h. Graphs indicate the fold change or number of puncta per cell of autophagosomes and autolysosomes upon appropriate small molecule treatments. Scale bar is 15 μ m. Statistical analysis was performed using one-way ANOVA and the post-hoc Bonferroni test. Error bars, mean \pm SEM. ***- $P < 0.001$.

LC3 immunoblotting revealed that both AGK2 ($P < 0.001$, versus untreated, **Fig. 9A**) and PD180970 ($P < 0.001$, versus untreated, **Fig. 9B**) treatments enhanced the conversion of LC3-I to LC3-II as compared to untreated. In the presence of lysomotropic agent such as bafilomycin A1, LC3-II accumulation was greater than that of bafilomycin A1 only in both AGK2 ($P < 0.001$, versus Baf A1, **Fig. 9A**) and PD 180970 ($P < 0.001$, versus Baf A1, **Fig. 9B**), thus indicating that AGK2 and PD180970 are autophagy enhancers.

A



B

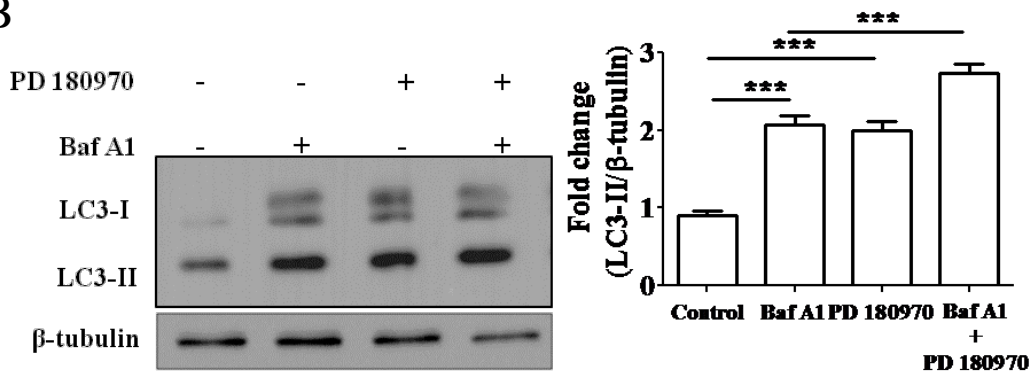


Figure 9. LC3 processing assay. Immunoblotting analyses of LC3 processing upon AGK2 (A) and PD180970 (B) treatments with or without bafilomycin A1 and LC3-II protein levels were quantified. Statistical analysis was performed using one-way ANOVA and the post-hoc Bonferroni test. Error bars, mean \pm SEM. *- $P < 0.05$, ***- $P < 0.001$.

We next investigated if the modulation of autophagy by AGK2 and PD180970 is via MTOR dependent or independent mechanisms. The phosphorylation status of MTOR substrates such as P70S6K and 4EBP1 reveals MTOR activity. The phospho-forms of these substrates are only present when MTOR is active. The phosphorylated P70S6K levels and isoforms of 4EBP1 in AGK2 and PD180970 treatments are comparable to that of nutrient rich conditions (Fig. 10, A and B) suggesting that both of them acting in an MTOR independent manner.

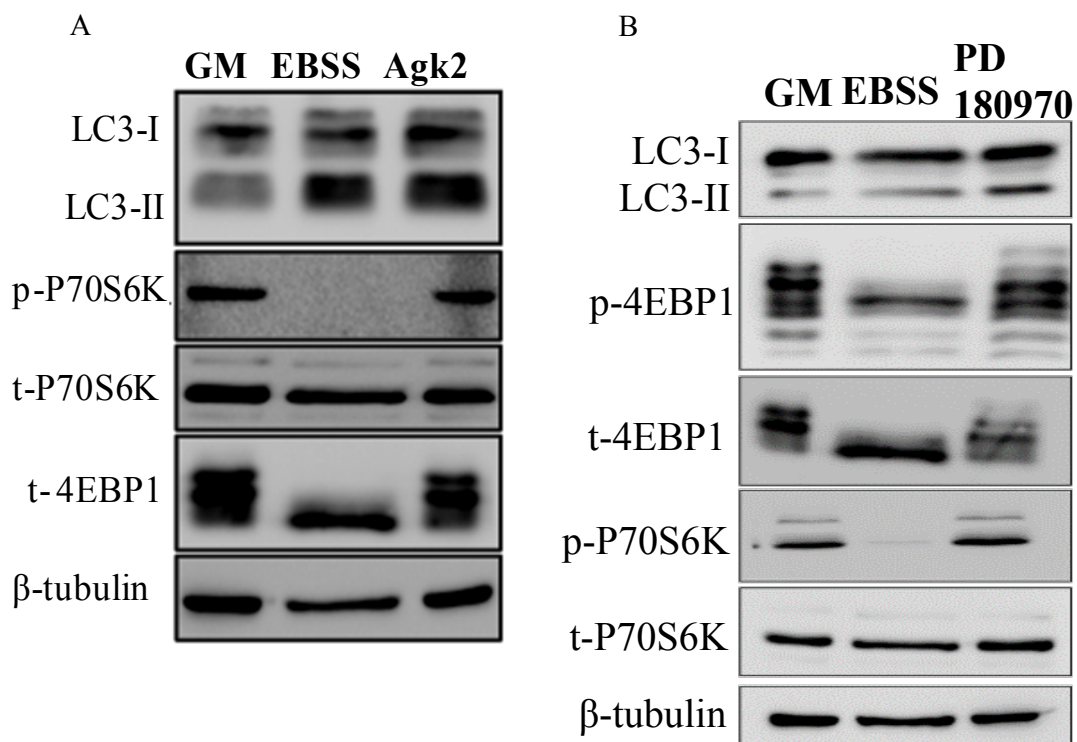


Figure 10. Signalling analyses. Investigating the modulation of mTOR signaling pathway by AGK2 (A) and PD180970 (B).

In mammalian cells, cytoprotection against α -synuclein toxicity by AGK2 and PD180970 is autophagy-dependent

We examined the cytoprotective ability of these two small molecules in a α -synuclein toxicity model of human neuroblastoma SH-SY5Y cells. When α -synuclein was overexpressed, cell viability was significantly compromised as compared to vector control or untransfected. Cell viability was significantly enhanced when treated with AGK2 ($P < 0.001$, versus untreated, **Fig. 11**) and/or PD 180970 ($P < 0.001$, versus untreated, **Fig. 11**) than that of untreated α -synuclein overexpressing cells. The cytoprotection exerted by AGK2 and PD180970 were comparable. Interestingly, this apparent cytoprotection by these hits were significantly reduced when cells along with AGK2 ($P > 0.05$, versus 3-MA, **Fig. 11**) or PD 180970 ($P > 0.05$, versus 3-MA, **Fig. 11**) were co-administered with the pharmacological autophagy inhibitor, 3-Methyl adenine (3-MA). There was no significant decrease in viability of cells treated with 3-MA only in α -synuclein overexpressing cells ruling out the possibility of its toxicity ($P > 0.05$, versus 3-MA, **Fig. 11**). Thus, both small molecules exerted cytoprotective effects in an autophagy-dependent manner.

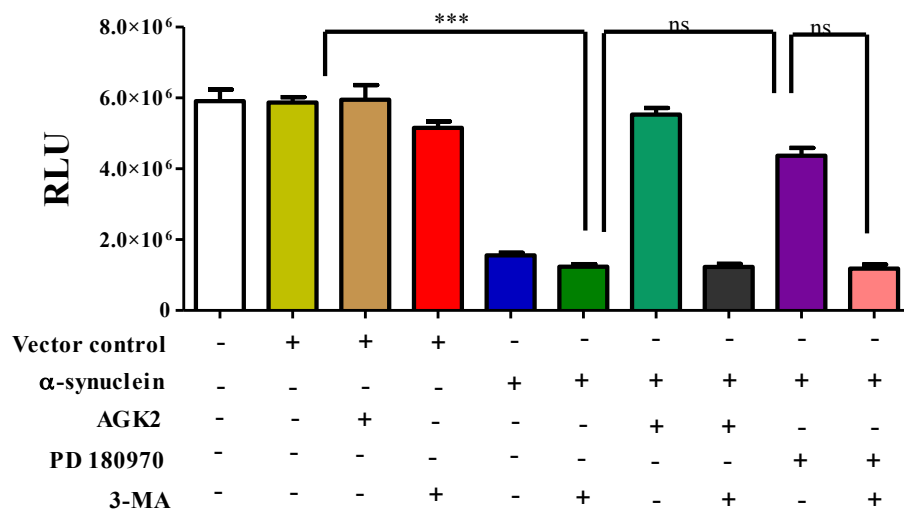


Figure 11. Cytoprotection assay. SH-SY5Y cells were transiently overexpressed with α -synuclein for 48 h. We then treated them with autophagy enhancers such as AGK2 and PD

180970 with or without autophagy inhibitor (3-MA) for 24 h. After 72 h, the cell viability was measured for all treatments and plotted. Statistical analysis was performed using one-way ANOVA and the post-hoc Bonferroni test. Error bars, mean \pm SEM. ns-non significant, ***- $P < 0.001$.

PD 180970 mitigates MPTP induced neuronal loss

In order to test if the autophagy dependent cytoprotection extends in an *in vivo* situation, we employed a preclinical mouse model of PD, MPTP (1- methyl-4-phenyl-1, 2,3,6-tetrahydropyridine) toxicity model²⁰. As AGK2 has been shown to exert *in vivo* neuroprotection, we tested only PD180970 (5 mg/kg body weight). Upon MPTP administration, around 70% dopaminergic neurons are ablated in Substantia Nigra pars compacta (SNpc) region of the brain with a concomitant reduction in the midbrain dopamine levels²⁰. In MPTP+Co regimen, MPTP was administered along with PD180970 on the same day. Tyrosine hydroxylase (TH), a dopaminergic neuronal marker, was used to quantify neuronal numbers using unbiased stereology while the TH intensity was measured by densitometry. Upon MPTP administration, there was a significant loss of dopaminergic neurons and reduced TH intensity compared to that of saline cohort ($P < 0.001$, versus saline, **Fig. 12**) confirming the MPTP induced neuronal loss. Interestingly, the neuronal numbers in MPTP+Co cohort was significantly more than that of MPTP treated cohort indicating the neuroprotective potential of PD 180970 ($P < 0.001$, MPTP versus MPTP+Co, **Fig. 12, A and B**). The TH intensity in MPTP+Co cohort animals was also significantly more than that of MPTP treated cohort ($P < 0.01$, MPTP versus MPTP+Co, **Fig. 12, A and D**). The reduction in SNpc volume due to MPTP administration was significantly alleviated upon PD180970 treatment ($P < 0.05$, MPTP versus MPTP+Co, **Fig. 12C**). These results demonstrate the neuroprotective ability of PD 180970 in a preclinical mouse model of PD.

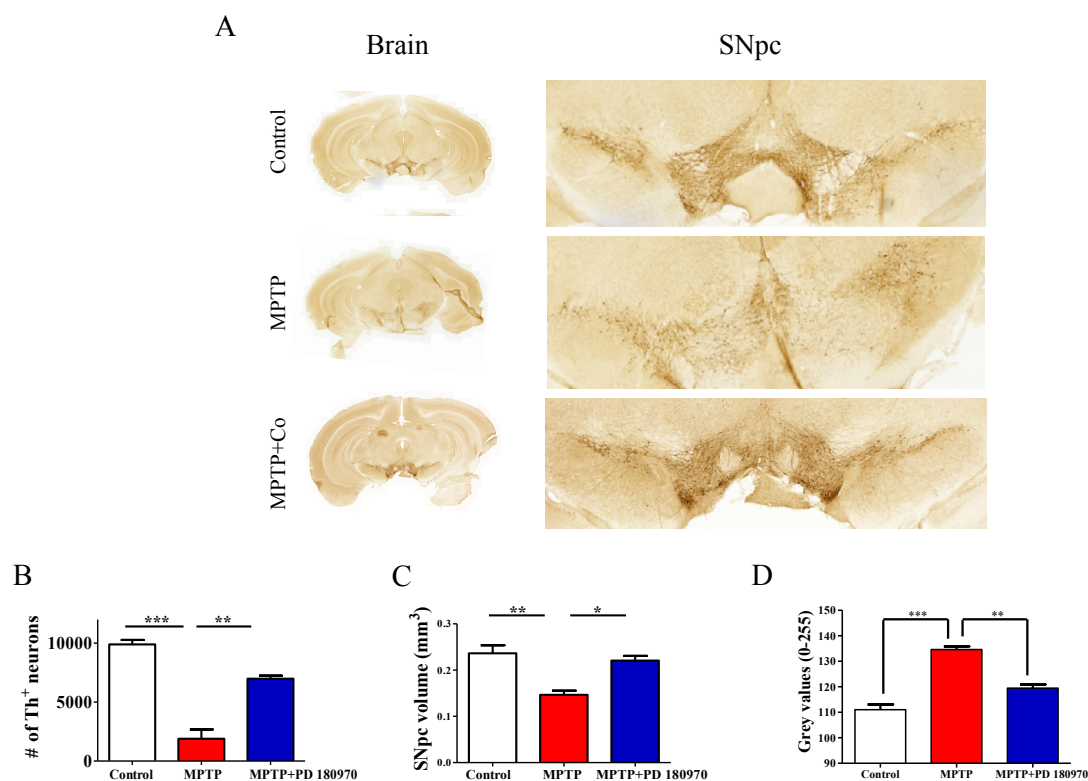


Figure 12. Stereological analyses. (A) Representative micrographs of SNpc brain sections of various cohorts namely control, MPTP and MPTP+Co. Quantitation of neuronal number (B), SNpc volume (C) and TH intensity (D) of all cohorts. Statistical analysis was performed using one-way ANOVA and the post-hoc Bonferroni test. Error bars, mean \pm SEM. *- $P < 0.05$, **- $P < 0.01$, ***- $P < 0.001$.

PD 180970 clears toxic protein oligomers by inducing autophagy in SNpc

We next examined the ability of PD180970 to induce autophagy to clear toxic protein oligomers in SNpc of midbrain. The intracellular accumulation of misfolded protein oligomers exerts cellular toxicity by promoting the sequestration of vital cellular components²¹. In MPTP-treated cohort, there was a significant down-regulation of LC3B puncta per neuron ($P < 0.05$, vehicle versus MPTP, **Fig. 13, A and B**) along with significant upregulation of toxic protein oligomers than that of saline treated ($P < 0.001$, vehicle versus MPTP, **Fig 14, A and B**). This observation is in line with the previous observations made in

this mouse model of neurodegeneration¹⁵. Thus, autophagy is perturbed in MPTP-treated animals along with concomitant build-up of toxic protein oligomers. In PD180970 treated cohort, the LC3B puncta per neuron was more ($P < 0.001$, MPTP versus MPTP+PD180970, **Fig. 13, A and B**) with significant decrease in toxic protein oligomers compared to MPTP treated cohort ($P < 0.001$, MPTP versus MPTP+PD180970, **Fig. 14, A and B**). These results show that PD180970 treatment stimulates autophagy, which results in clearance of toxic protein oligomers in the SNpc.

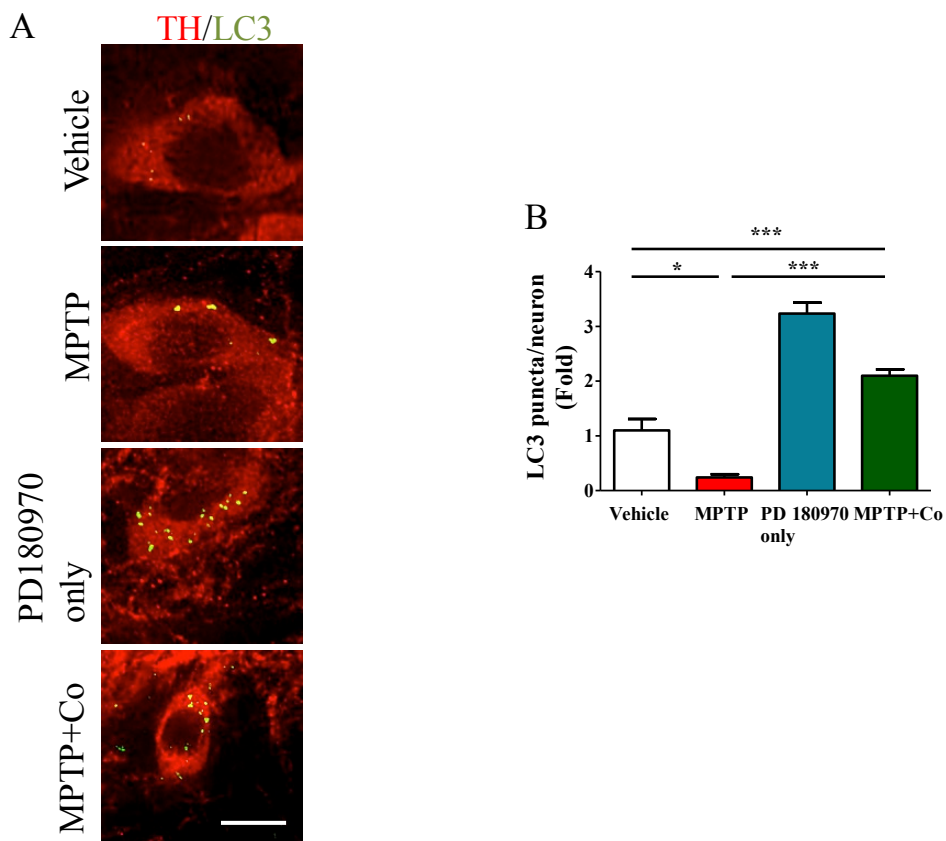


Figure 13. Immunohistochemistry of autophagy marker in SNpc. Representative fluorescent microscopy images of TH positive dopaminergic neurons co-stained with LC3 for all cohorts. (B) Quantitation of LC3 puncta per neuron for all cohorts. $n=50$ neurons/cohort and $N=3$. Scale bar is $50 \mu\text{m}$. Statistical analysis was performed using one-way ANOVA and the post-hoc Bonferroni test. Error bars, mean \pm SEM. *- $P < 0.05$, ***- $P < 0.001$.

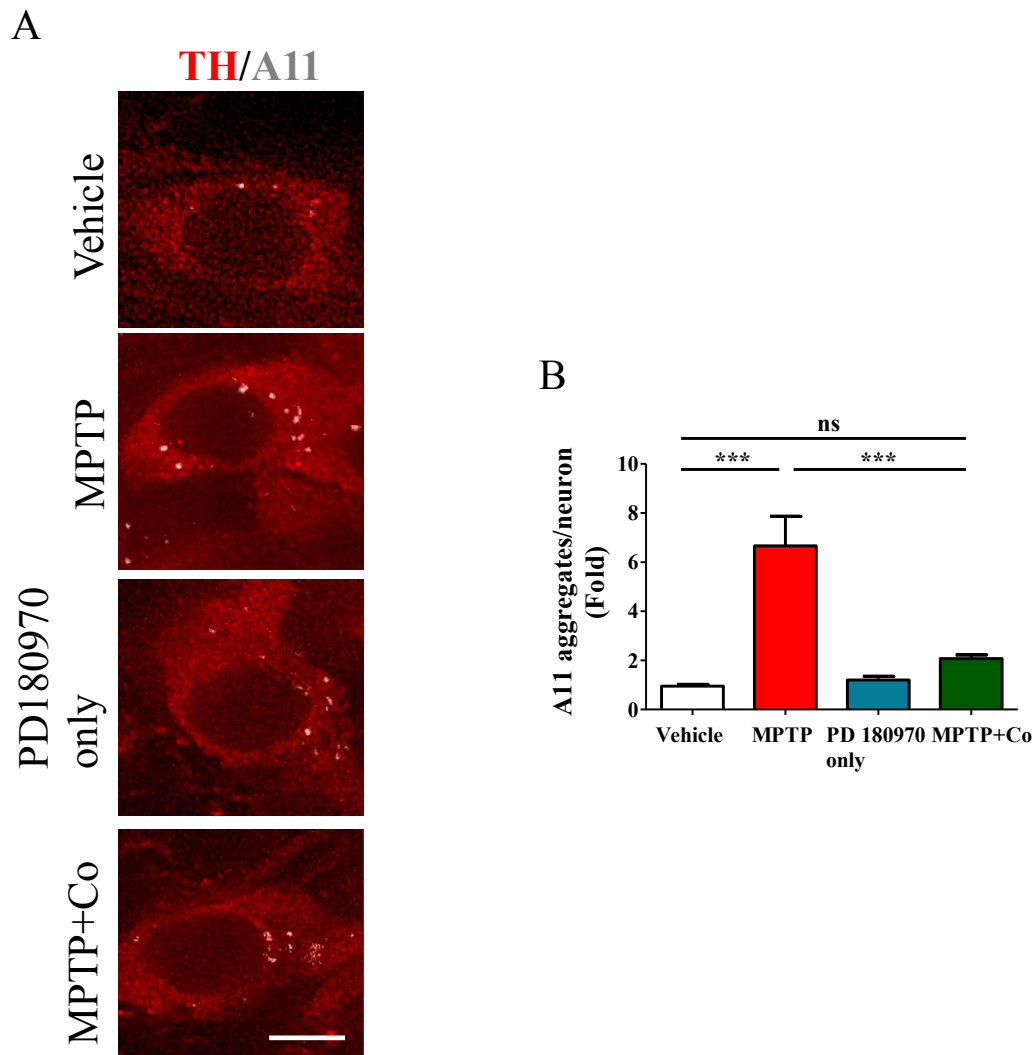


Figure 14. Immunohistochemistry of toxic protein aggregates in SNpc. Representative fluorescent microscopy images of TH positive dopaminergic neurons co-stained with toxic oligomers (A11) for all cohorts. (B) Quantitation of LC3 puncta per neuron of all cohorts. $n=50$ neurons/cohort and $N=3$. Scale bar is $50\ \mu\text{m}$. Statistical analysis was performed using one-way ANOVA and the post-hoc Bonferroni test. Error bars, mean \pm SEM. ns-non significant, ***- $P < 0.001$.

PD180970 mitigates MPTP-induced behavioral impairments

Upon MPTP administration, these mice manifest Parkinsonian-like movement disorder such as exploratory and locomotory deficits²². We used rotarod (locomotory behavior) and open

field (exploratory behavior) tests for assessing the ability of PD 180970 to ameliorate the MPTP-induced behavioral deficits. The behavior experiments were carried on day 13 and day 15 of MPTP or saline administrations.

In the rotarod test, latency to fall, was significantly reduced in the MPTP cohort as compared to that of saline cohort (day 13th and day 15th) ($P < 0.001$, vehicle versus MPTP, **Fig. 15, A and B**), confirming its motor coordination impairments. Interestingly, in PD 180970 cohort, the latency to fall, was significantly increased compared to MPTP cohort on both days ($P < 0.001$, MPTP versus MPTP+Co, **Fig. 15, A and B**), and was found to be comparable to that of saline cohort on both days ($P > 0.05$, MPTP+Co versus saline, **Fig. 15, A and B**).

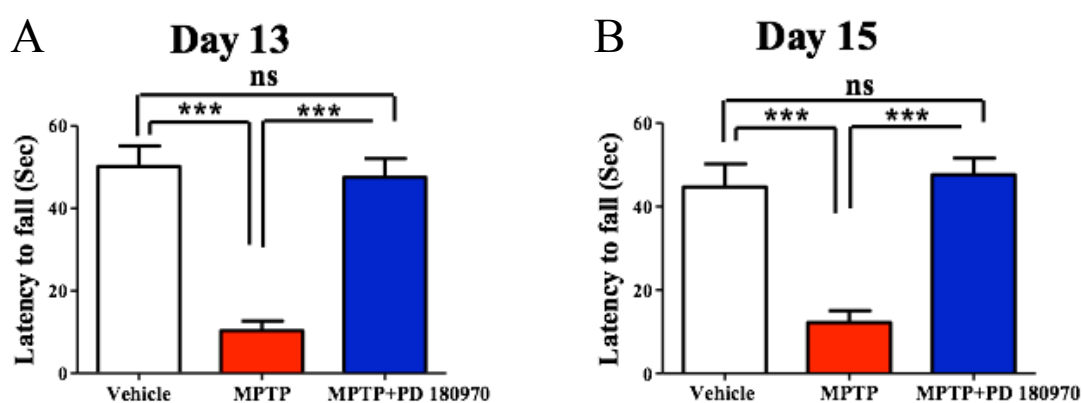


Figure 15. Rotarod analyses. Quantification of rotarod analyses as latency to fall (in sec) performed on day 13 (A) and 15 (B) for all cohorts namely vehicle or control, MPTP and MPTP+PD 180970. Statistical analysis was performed using one-way ANOVA and the post-hoc Bonferroni test. Error bars, mean \pm SEM. ns-non significant, ***- $P < 0.001$.

The MPTP cohort also exhibited exploratory deficits, as it covered significantly lesser distance in open-field arena as compared to that of saline cohort on both day 13 and day 15 ($P < 0.001$, vehicle versus MPTP, **Fig. 16, A to D**). The distance travelled by PD 180970 cohort mice was significantly improved than that of MPTP cohort on both day 13 and day

15 ($P < 0.001$, MPTP versus MPTP+Co, **Fig. 16, A to D**). Similar to our observation in rotarod test, the improvement of exploratory behavior in PD 180970 cohort mice was comparable to that of saline cohort on both days 13 and 15 ($P > 0.05$, MPTP+Co versus saline, **Fig. 16, A to D**). Thus, PD 180970 treatment improved both locomotory and exploratory abilities to alleviate MPTP induced behavioral impairments.

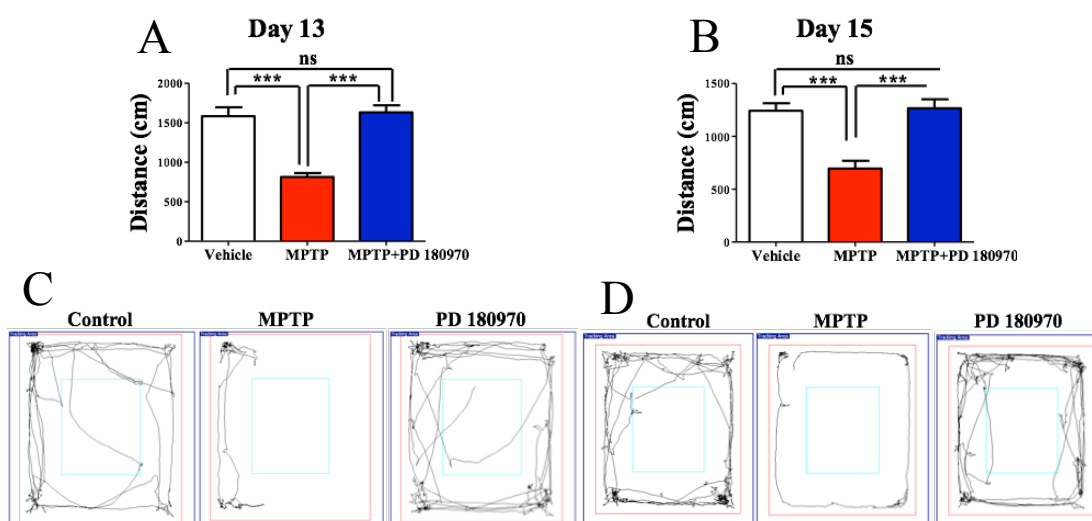


Figure 16. Open field test. Quantification of open field analyses data as distance (in cm) travelled on open field arena performed on day 13 (A) and 15 (B) with representative trajectory maps (C and D) for all cohorts. Statistical analysis was performed using one-way ANOVA and the post-hoc Bonferroni test. Error bars, mean \pm SEM. ns-non significant, ***- $P < 0.001$.

Discussion

α -synuclein protein aggregates are toxic to neuronal cells as they disrupt a plethora of cellular processes such as mRNA translation²³, endosome trafficking²⁴, redox imbalance²⁵, proteasome and autophagy²⁶. Currently, there are various evidences suggesting that α -synuclein attain prion-like conformation, which helps them to spread across cells²⁷. These efforts to understand the mechanisms of neurodegeneration reveal the complexity of pathogenesis at cellular and organismal level²⁸. Thus, clearing α -synuclein protein aggregates might be beneficial for neuronal viability and to curb neurodegeneration related pathogenesis²⁹. Multiple evidences suggest that due to several factors autophagy is dysfunctional during neurodegeneration and thus the cells fail to cope up with the increasing aggregate burden¹⁴. Interestingly, autophagy induction either by genetic or pharmacological means has been shown to clear protein aggregates to alleviate neurodegeneration^{30,31}.

We identified and characterized the two small molecules AGK2 and PD 180970 as autophagy modulators in diverse models such as yeast, mammalian cells and mouse. In yeast, both small molecules enhanced the starvation-induced autophagy and also cleared α -synuclein aggregates in an autophagy dependent manner. These hits also induced autophagy in mammalian cells. Autophagic flux assay revealed that PD 180970 enhanced the formation of autophagosomes whereas AGK2 aided the fusion of autophagosomes with lysosomes. Like in yeast, these hits, also protected neuronal cells against α -synuclein toxicity in an autophagy-dependent manner in mammalian cells. In an autophagy mutant strain of yeast, the small molecules failed to rescue growth lag due to α -synuclein toxicity. Likewise, in mammalian cells, the small molecules failed to protect the neuronal cells from α -synuclein mediated toxicity upon pharmacological inhibition of autophagy. Thus, by both genetic and pharmacological means, in two model systems, we demonstrate that these small molecules display autophagy dependent neuroprotective action. More importantly, our results reiterate that autophagy is conserved from yeast to mammalian cells.

Under cellular steady state conditions, the α -synuclein is acetylated to prevent it from attaining the toxic oligomer conformation³². Various factors such as ageing and pathological conditions upregulate the sirtuin2 activity to generate the deacetylated forms of α -synuclein. AGK2, the sirtuin2 inhibitor is shown to be neuroprotective in *Drosophila*

model of PD¹⁷. Sirtuin2, the NAD⁺ dependent deacetylase is predominantly expressed in brain whose levels enhance with ageing³³. In PD, the increased sirtuin2 activity aggravate proteotoxicity by deacetylating the α -synuclein at various lysine residues³⁴. Acetylation of α -synuclein prevents its aggregation and thus is shown to be neuroprotective in primary cortical neurons³². On the other hand, dopaminergic neuronal loss is observed when acetylation of α -synuclein is blocked. Genetic downregulation of sirtuin2 suppresses α -synuclein aggregation and its toxicity. Transgenic sirtuin2 knock out mice are protected from either α -synuclein or MPTP mediated toxicities. Also, sirtuin2 knock down cells shows increased accumulation of LC3-II with concomitant degradation of p62 that confirms the enhanced autophagic activity³². Prior evidences suggest the connection between autophagy and sirtuin2 but has not been explored much. Apart from the post-translational aspects of protein, we investigated how sirtuin2 inhibition using a small molecule (AGK2) regulates autophagy. Our results show that in mammalian cells, the AGK2 enhanced autophagosome lysosome fusion whereas PD180970 increased autophagosome biogenesis or maturation. These small molecules can now be used as tools to understand regulation of autophagy at different steps. Both AGK2 and PD180970 induce autophagy in an MTOR independent manner. This property is pharmacologically desirable as inhibiting MTOR, an important survival and growth-related pathway, leads to severe side effects such as immunosuppression and perturbed wound healing²⁹.

In a preclinical mouse model of PD, the neuroprotective ability of PD180970 is illustrated from both histological and behavioral results. PD180970 protects the dopaminergic neurons from MPTP mediated toxicity significantly. This could be possible due to the ability of PD180970 to induce autophagy and clear toxic protein oligomers in dopaminergic neurons of SNpc. Furthermore, in a preclinical mouse model of PD, PD180970 showed neuroprotective ability by increasing autophagy with concomitant degradation of toxic protein oligomers.

In conclusion, small molecule autophagy modulators such as AGK2 and PD180970 may have therapeutic implications in neurodegenerative diseases such as PD and other synucleopathies.

References

1. Mhyre TR, Boyd JT, Hamill RW, Maguire-Zeiss KA. Parkinson's disease. *Subcell Biochem* 2012; 65:389-455.
2. Disease GBD, Injury I, Prevalence C. Global, regional, and national incidence, prevalence, and years lived with disability for 310 diseases and injuries, 1990-2015: a systematic analysis for the Global Burden of Disease Study 2015. *Lancet* 2016; 388:1545-602.
3. Jankovic J. Parkinson's disease: clinical features and diagnosis. *J Neurol Neurosurg Psychiatry* 2008; 79:368-76.
4. Lundblad M, Picconi B, Lindgren H, Cenci MA. A model of L-DOPA-induced dyskinesia in 6-hydroxydopamine lesioned mice: relation to motor and cellular parameters of nigrostriatal function. *Neurobiol Dis* 2004; 16:110-23.
5. Perlmutter JS, Mink JW. Deep brain stimulation. *Annu Rev Neurosci* 2006; 29:229-57.
6. Spillantini MG, Schmidt ML, Lee VM, Trojanowski JQ, Jakes R, Goedert M. Alpha-synuclein in Lewy bodies. *Nature* 1997; 388:839-40.
7. Ma QL, Chan P, Yoshii M, Ueda K. Alpha-synuclein aggregation and neurodegenerative diseases. *J Alzheimers Dis* 2003; 5:139-48.
8. Double KL. Neuronal vulnerability in Parkinson's disease. *Parkinsonism Relat Disord* 2012; 18 Suppl 1:S52-4.
9. Lee HJ, Patel S, Lee SJ. Intravesicular localization and exocytosis of alpha-synuclein and its aggregates. *J Neurosci* 2005; 25:6016-24.
10. Uversky VN. Alpha-synuclein misfolding and neurodegenerative diseases. *Curr Protein Pept Sci* 2008; 9:507-40.
11. Balch WE, Morimoto RI, Dillin A, Kelly JW. Adapting proteostasis for disease intervention. *Science* 2008; 319:916-9.

12. Goldberg AL. Protein degradation and protection against misfolded or damaged proteins. *Nature* 2003; 426:895-9.
13. Hyttinen JM, Amadio M, Viiri J, Pascale A, Salminen A, Kaarniranta K. Clearance of misfolded and aggregated proteins by autophagy and implications for aggregation diseases. *Ageing research reviews* 2014; 18:16-28.
14. Nixon RA. The role of autophagy in neurodegenerative disease. *Nature medicine* 2013; 19:983-97.
15. Suresh SN, Chavalmane AK, Dj V, Yarreiphang H, Rai S, Paul A, Clement JP, Alladi PA, Manjithaya R. A novel autophagy modulator 6-Bio ameliorates SNCA/alpha-synuclein toxicity. *Autophagy* 2017; 13:1221-34.
16. Rajasekhar K, Suresh SN, Manjithaya R, Govindaraju T. Rationally designed peptidomimetic modulators of abeta toxicity in Alzheimer's disease. *Scientific reports* 2015; 5:8139.
17. Outeiro TF, Kontopoulos E, Altmann SM, Kufareva I, Strathearn KE, Amore AM, Volk CB, Maxwell MM, Rochet JC, McLean PJ, et al. Sirtuin 2 inhibitors rescue alpha-synuclein-mediated toxicity in models of Parkinson's disease. *Science* 2007; 317:516-9.
18. Outeiro TF, Lindquist S. Yeast cells provide insight into alpha-synuclein biology and pathobiology. *Science* 2003; 302:1772-5.
19. Sarkar S, Perlstein EO, Imarisio S, Pineau S, Cordenier A, Maglathlin RL, Webster JA, Lewis TA, O'Kane CJ, Schreiber SL, et al. Small molecules enhance autophagy and reduce toxicity in Huntington's disease models. *Nature chemical biology* 2007; 3:331-8.
20. Jackson-Lewis V, Przedborski S. Protocol for the MPTP mouse model of Parkinson's disease. *Nat Protoc* 2007; 2:141-51.
21. Ebenezer PJ, Weidner AM, LeVine H, 3rd, Markesbery WR, Murphy MP, Zhang L, Dasuri K, Fernandez-Kim SO, Bruce-Keller AJ, Gavilan E, et al. Neuron specific toxicity of oligomeric amyloid-beta: role for JUN-kinase and oxidative stress. *J Alzheimers Dis* 2010; 22:839-48.

22. Taylor JR, Elsworth JD, Sladek JR, Jr., Collier TJ, Roth RH, Redmond DE, Jr. Sham surgery does not ameliorate MPTP-induced behavioral deficits in monkeys. *Cell Transplant* 1995; 4:13-26.
23. Koukouraki P, Doxakis E. Constitutive translation of human alpha-synuclein is mediated by the 5'-untranslated region. *Open Biol* 2016; 6:160022.
24. Goncalves SA, Outeiro TF. Traffic jams and the complex role of alpha-Synuclein aggregation in Parkinson disease. *Small GTPases* 2017; 8:78-84.
25. Lashuel HA, Overk CR, Oueslati A, Masliah E. The many faces of alpha-synuclein: from structure and toxicity to therapeutic target. *Nature reviews Neuroscience* 2013; 14:38-48.
26. Colasanti T, Vomero M, Alessandri C, Barbati C, Maselli A, Camperio C, Conti F, Tinari A, Carlo-Stella C, Tuosto L, et al. Role of alpha-synuclein in autophagy modulation of primary human T lymphocytes. *Cell Death Dis* 2014; 5:e1265.
27. Chu Y, Kordower JH. The prion hypothesis of Parkinson's disease. *Curr Neurol Neurosci Rep* 2015; 15:28.
28. Wong YC, Krainc D. alpha-synuclein toxicity in neurodegeneration: mechanism and therapeutic strategies. *Nature medicine* 2017; 23:1-13.
29. Sarkar S, Davies JE, Huang Z, Tunnacliffe A, Rubinsztein DC. Trehalose, a novel mTOR-independent autophagy enhancer, accelerates the clearance of mutant huntingtin and alpha-synuclein. *The Journal of biological chemistry* 2007; 282:5641-52.
30. Williams A, Sarkar S, Cuddon P, Ttofi EK, Saiki S, Siddiqi FH, Jahreiss L, Fleming A, Pask D, Goldsmith P, et al. Novel targets for Huntington's disease in an mTOR-independent autophagy pathway. *Nature chemical biology* 2008; 4:295-305.
31. Jimenez-Sanchez M, Lam W, Hannus M, Sonnichsen B, Imarisio S, Fleming A, Tarditi A, Menzies F, Dami TE, Xu C, et al. siRNA screen identifies QPCT as a druggable target for Huntington's disease. *Nature chemical biology* 2015; 11:347-54.
32. de Oliveira RM, Vicente Miranda H, Francelle L, Pinho R, Szego EM, Martinho R, Munari F, Lazaro DF, Moniot S, Guerreiro P, et al. The mechanism of sirtuin 2-mediated

exacerbation of alpha-synuclein toxicity in models of Parkinson disease. PLoS biology 2017; 15:e2000374.

33. de Oliveira RM, Sarkander J, Kazantsev AG, Outeiro TF. SIRT2 as a Therapeutic Target for Age-Related Disorders. Front Pharmacol 2012; 3:82.

34. Singh P, Hanson PS, Morris CM. Sirtuin-2 Protects Neural Cells from Oxidative Stress and Is Elevated in Neurodegeneration. Parkinsons Dis 2017; 2017:2643587.

Chapter 6

A novel small molecule autophagy modulator TGR

63 ameliorates Parkinsonism

Note:

This chapter is currently *under preparation* for publication as an original research article.

Abstract

Aggrephagy is a selective autophagy process to clear the toxic protein aggregates. Accumulation of toxic protein aggregates is one of the main pathophysiological hallmarks of neurodegenerative diseases. We identified a small molecule TGR 63 that potently induced autophagy in model systems such as yeast, mammalian cells and mouse. Due to its autophagy inducing potential, TGR 63 also ameliorated α -synuclein toxicity. Notably, TGR 63 is neuroprotective in a mice model of Parkinson's disease and ameliorated the motor impairments. We also attempted to identify the *in vivo* target of TGR 63 using mass spectrometry.

Introduction

At the neuronal level, cytotoxicity due to accumulation of misfolded proteins is one of the main drivers of neurodegenerative diseases (ND) such as Alzheimer's (AD), Parkinson's (PD), Huntington's (HD) and Amyotrophic Lateral Sclerosis (ALS)¹. Although the occurrence of ND can be sporadic or genetic in nature, sporadic cases are strikingly more abundant than genetic cases. Protein misfolding is not an uncommon phenomenon inside a cell at steady state. For constant surveillance of protein misfolding, cells are equipped with protein quality control machineries such as chaperone, ubiquitin-proteasome system (UPS) and autophagy pathways². Owing to various factors such as ageing, genetic predisposition and so on, the misfolded proteins overwhelm the chaperone and proteasome that results in the accumulation of toxic protein aggregates³. Once such aggregates form, cells rely on autophagy machinery to clear them⁴. This selective autophagy pathway that helps in clearing the toxic protein oligomers and aggregates is known as aggrephagy⁴.

Protein aggregates exert toxicity to cells by sequestering the vital intracellular proteins and thus important cellular pathways go awry⁵. Neurons mostly do not divide further as they are terminally differentiated and thus these post-mitotic cells are unable to dilute out aggregates due to absence of cell division⁴. In addition to this limitation, owing to their specialized architecture, damaged organelles and protein aggregates accumulate in specific locations inside neurons which make them even more vulnerable for proteotoxicity such as impeding intracellular trafficking⁴. For these reasons, the neurons heavily rely on their protein quality control machineries to maintain the proteostasis by preventing or degrading the toxic protein aggregates⁶. Age related progressive decline in efficiency of these quality control

pathways further propel the cytotoxicity potential of these aggregates⁷. And perhaps, as the proverbial final nail on the coffin, the aggregates themselves sequester core proteins that maintain proteostasis including members of autophagosomes, thus further weakening the cellular ability to clear the aggregates. Genetic studies on either ablation or overexpression of autophagy pathways in the brain have profoundly indicated the prowess of this pathway to engage and clear steady state misfolded proteins⁸⁻¹⁰. In fact, the accumulation of ubiquitin aggregates and appearance of ND like phenotype in brain specific KO of autophagy function reveals the important contribution of autophagy pathways in maintaining cellular homeostasis¹¹.

Thus, such proof-of-concept studies have shown that autophagy is not only vital to prevent the occurrence of neurodegeneration but also has therapeutic potential. Therefore, it is important to understand the process of this selective autophagy pathway, autophagy in detail by identifying the critical (and potentially novel) molecular players and elaborating their functions. Towards this, we employed a chemical biology approach to identify potent small molecule modulators of autophagy.

In this study, we performed yeast based phenotypic, small molecule screen to identify the modulators that curb α -synuclein toxicity. We identified the novel, synthetic small molecule TGR 63 and used it to characterize yeast and mammalian autophagy. We tested for their neuroprotective potential in a preclinical mouse model of PD. Finally, we describe steps taken to identify the *in vivo* cellular target of TGR 63.

Results

TGR 63 protects yeast cells from α -synuclein toxicity in an autophagy dependent manner

In pursuit of a novel structural scaffold for small molecule modulators for autophagy, we screened a custom-made small molecule library against α -synuclein mediated toxicity. We employed α -synuclein toxicity model of *S. cerevisiae* as a screening assay¹². When α -synuclein is overexpressed, the growth of yeast was impeded significantly than that of wild type ($P < 0.001$ versus wild-type cells; **Fig. 1**). Small molecules that rescue the growth lag significantly were considered as 'Hits'. Upon screening custom made in house synthetic library, we observed that TGR 63 significantly alleviates α -synuclein mediated growth

deficit in yeast ($P < 0.001$ versus untreated; **Fig. 1**). TGR 63 is not toxic to yeast cells (**Fig. 2**).

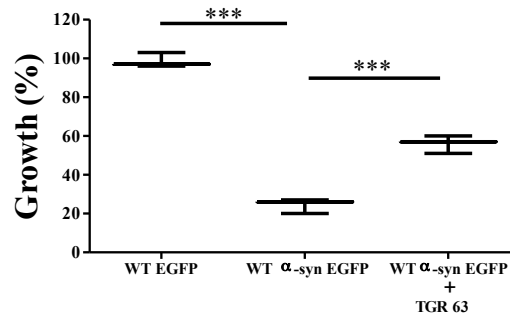


Figure 1. *Percent growth of wild-type (WT) yeast cells overexpressing α -synuclein in presence and absence of TGR 63.* Graph indicating the percent growth of WT cells treated with or without TGR 63. Statistical analysis was performed using one-way ANOVA and the post-hoc Bonferroni test. Error bars, mean \pm SEM. ***- $P < 0.001$.

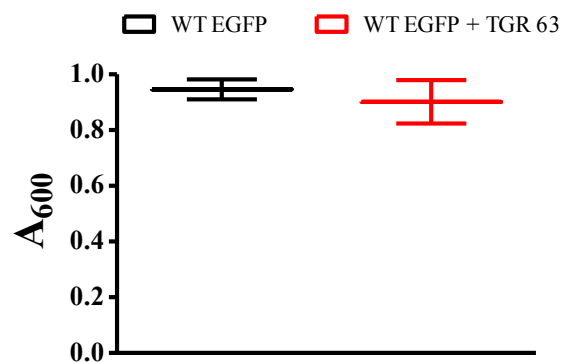


Figure 2. *Growth assay.* WT GFP cells treated with or without TGR 63 for 48 h and their absorbance was plotted.

An array of cellular pathways chaperones, UPS and autophagy can combat α -synuclein mediated proteotoxicity^{13,14}. As toxic protein oligomers and aggregates are substrates for autophagy⁴, we tested if TGR 63 rescued α -synuclein mediated toxicity in an autophagy dependent manner. TGR 63 failed to rescue the growth lag in a core autophagy mutant

strain (*atg1Δ*) overexpressing α -synuclein ($P > 0.05$ versus untreated; **Fig. 3**), indicating that TGR 63 rescued α -synuclein proteotoxicity mediated by autophagy.

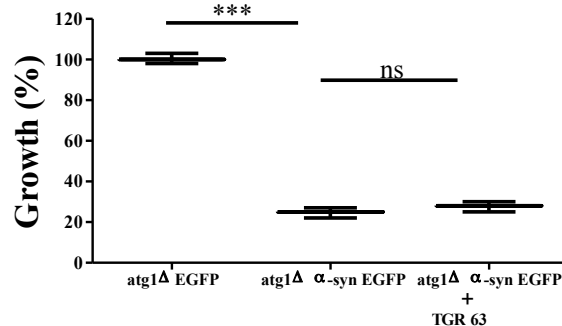


Figure 3. Percent growth of *atg1Δ* strain over expressing α -synuclein in the presence and absence of TGR 63. Graph indicating the percent growth of core autophagy mutant yeast cells treated with or without TGR 63. Statistical analysis was performed using one-way ANOVA and the post-hoc Bonferroni test. Error bars, mean \pm SEM. ns-non significant, ***- $P < 0.001$.

TGR 63 cleared α -synuclein in an autophagy dependent manner

We then tested whether TGR 63 could degrade α -synuclein-EGFP in yeast cells. Upon treating WT cells overexpressing α -synuclein-EGFP with TGR 63, we observed a significant reduction in the α -synuclein-EGFP protein level ($P < 0.001$ versus untreated; **Fig. 4A**). To reveal the autophagy dependency of TGR 63, we checked the α -synuclein-EGFP clearance in core autophagy mutant strain. In core autophagy mutant strain, we observed no significant difference in the clearance of α -synuclein-EGFP protein levels upon addition of TGR 63 ($P > 0.05$ versus untreated; **Fig. 4B**).

These results indicate that the TGR 63 clears α -synuclein-EGFP protein levels in an autophagy dependent manner that corroborates with the yeast growth assays.

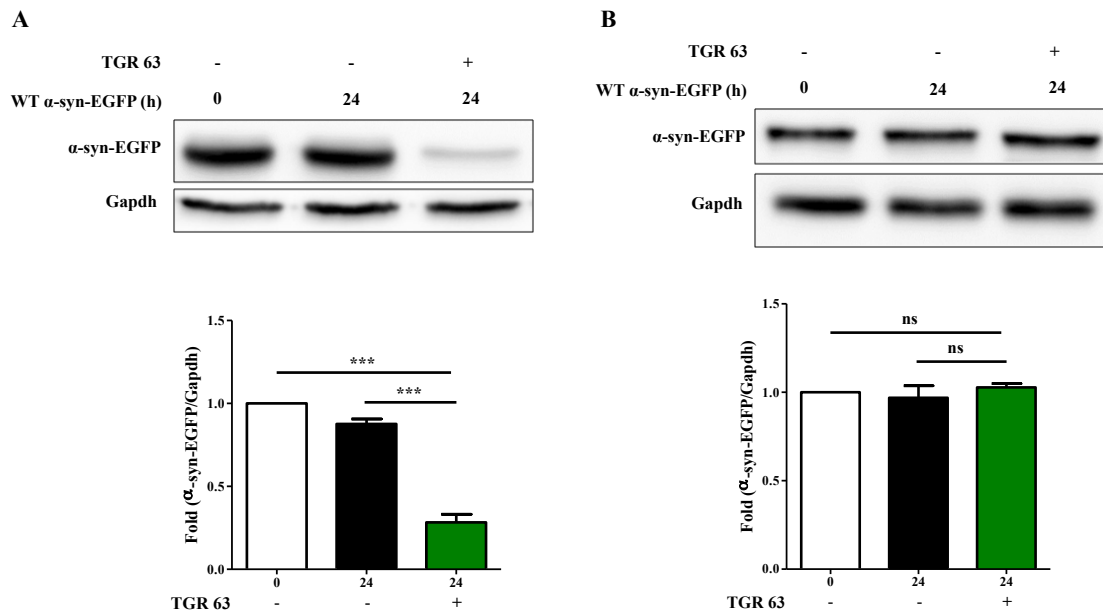


Figure 4. *α*-synuclein-EGFP clearance assay in yeast. Representative western blots and the quantification of *α*-synuclein-EGFP protein levels in WT (A) and core autophagy mutant strain (B). Statistical analysis was performed using one-way ANOVA and the post-hoc Bonferroni test. Error bars, mean \pm SEM. ns-non significant, ***- $P < 0.001$.

TGR 63 is an autophagy inducer

Next, we examined if TGR 63 could induce autophagy in yeast. Towards this, we performed a EGFP-Atg8 (N-terminally tagged EGFP to Atg8, the autophagosome marker) processing assay in presence of nutrient rich or starvation medium with and without TGR 63. Autophagy flux can be measured by the amount of free EGFP released¹⁵.

In nutrient rich condition, the free EGFP released in TGR 63 treated cells was significantly more than that of untreated ($P < 0.001$ versus untreated; **Fig. 5**).

Upon TGR 63 treatment, autophagy induction is significantly increased than that of untreated across different time points in starvation conditions (**Fig. 6**).

These results indicate that TGR 63 has the potential to induce basal autophagy and also augment starvation-induced autophagy.

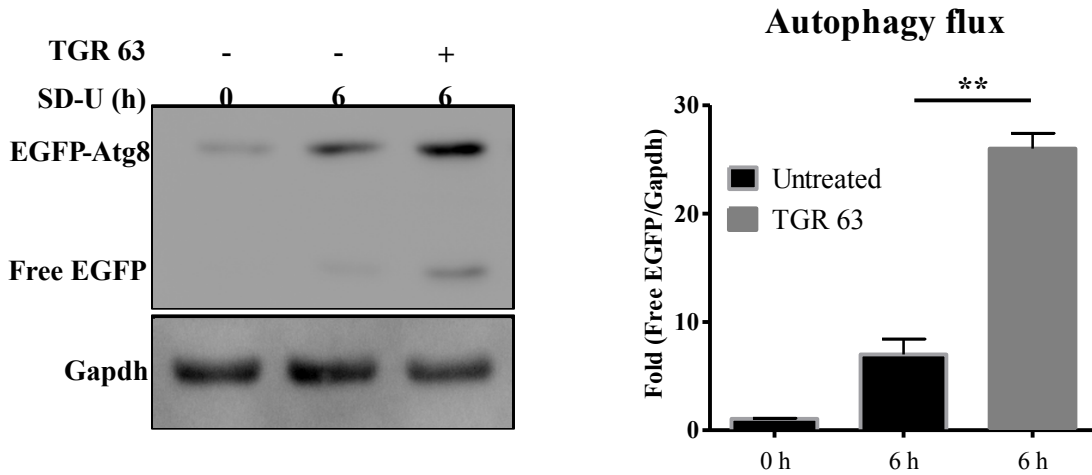


Figure 5. EGFP-Atg8 processing assay in nutrient rich conditions. WT cells expressing EGFP-Atg8 treated with or without TGR 63 for 6 h in growth or nutrient rich conditions. Statistical analysis was performed using one-way ANOVA and the post-hoc Bonferroni test. Error bars, mean \pm SEM. ns-non significant, **-P < 0.01.

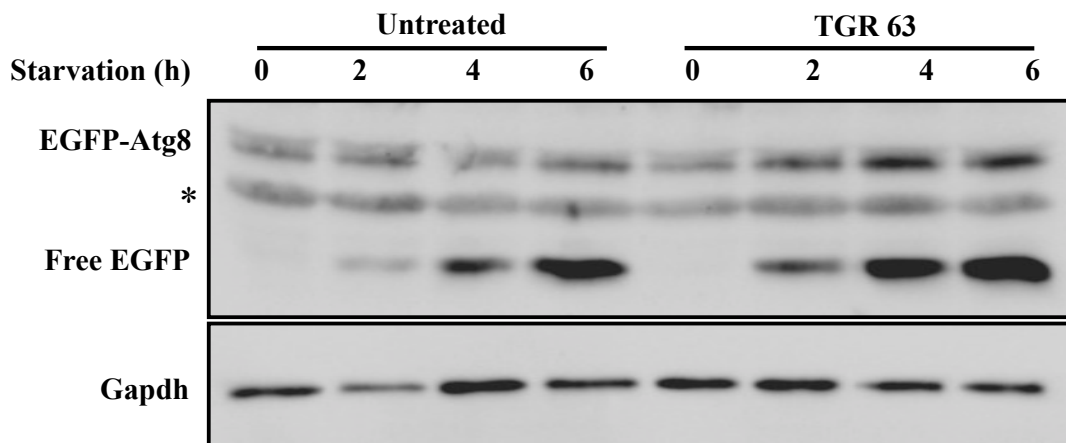


Figure 6. EGFP-Atg8 processing assay in starvation conditions. WT cells expressing EGFP-Atg8 treated with or without TGR 63 for various time points (0,2,4 and 6 h) in starvation conditions. * indicates a non-specific band.

We then tested if the autophagy inducing ability of TGR 63 is conserved in higher eukaryotes such as mammalian cells. To address this, we employed immunoblotting and fluorescence microscopy based tandem RFP-EGFP-LC3 processing assays in SH-SY5Y cells that stably expressing RFP-EGFP-LC3. Upon TGR 63 treatment, we observed significantly more number of autolysosomes ($P < 0.001$ versus untreated; **Fig. 7**) with concomitant reduction in autophagosomes ($P < 0.01$ versus untreated; **Fig. 7**) than that of untreated suggesting that TGR 63 notably increased the autophagosome lysosome fusion.

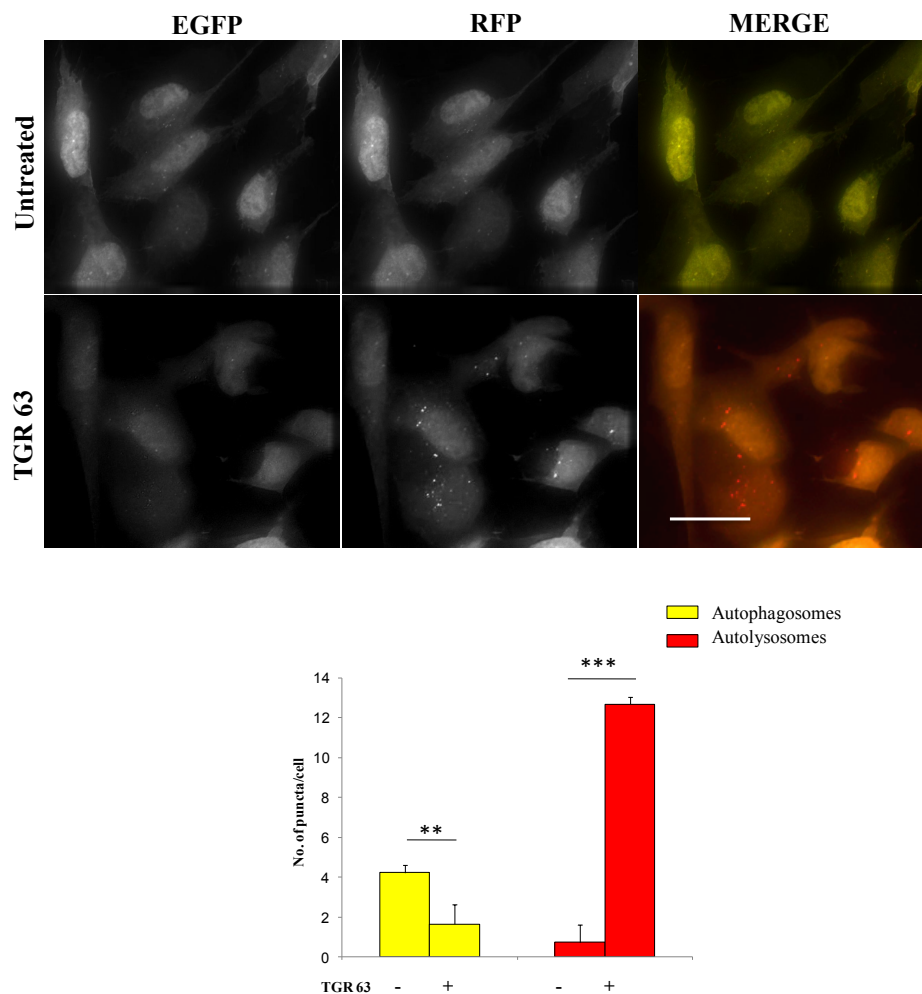


Figure 7. Tandem RFP-EGFP-LC3 assay. SH-SY5Y cells stably expressing RFP-EGFP-LC3 cells were treated with or without TGR 63 for 2 h and quantified the number of autophagosomes and autolysosomes. Scale bar: 15 μ m. Statistical analysis was performed using unpaired Student *t* test. Error bars, mean \pm SEM. **- $P < 0.01$, ***- $P < 0.001$.

Immunoblotting experiments also confirmed that in presence of TGR 63, LC3-II levels were significantly more than that of untreated ($P < 0.001$ versus untreated; **Fig. 8**). When cells were co-treated with TGR 63 and a lysomotrophic agent such as bafilomycin A1, the LC3-II levels accumulated significantly more than that of bafilomycin A1 only ($P < 0.001$ versus Baf A1; **Fig. 8**). These autophagy flux experiments revealed that TGR 63 is indeed an autophagy inducer.

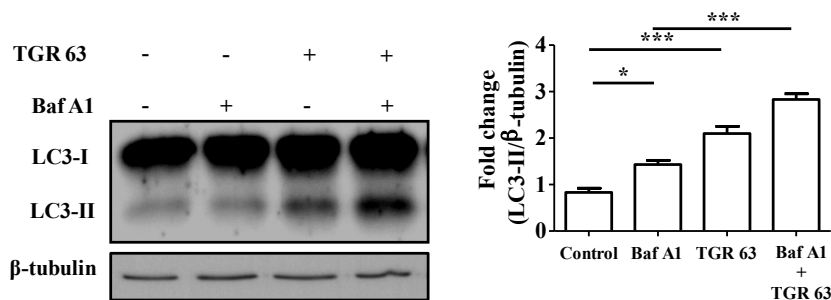


Figure 8. LC3 processing assay. Immunoblotting analysis of LC3-II conversion from LC3-I treated with or without TGR 63 for 2 h. Normalized LC3-II levels were quantified across various treatments. Statistical analysis was performed using one-way ANOVA and the post-hoc Bonferroni test. Error bars, mean \pm SEM. *- $P < 0.05$, ***- $P < 0.001$.

TGR 63 is an MTOR independent autophagy enhancer

Autophagy induction can be MTOR independent or dependent. We checked the MTOR dependency of TGR 63. MTOR activity can be revealed from the level of its substrates such as phospho P70S6K and 4EBP1. Upon TGR 63 treatment, the phospho level of P70S6K was comparable to that of untreated (**Fig. 9**). Also, the isoforms of 4EBP1 was similar to that of untreated upon addition of TGR 63 (**Fig. 9**). In TGR 63 treated condition, both phospho P70S6K and isoforms of 4EBP1 were distinctly different from that of starvation condition (**Fig. 9**).

These results clearly indicate that TGR 63 is an MTOR independent autophagy enhancer.

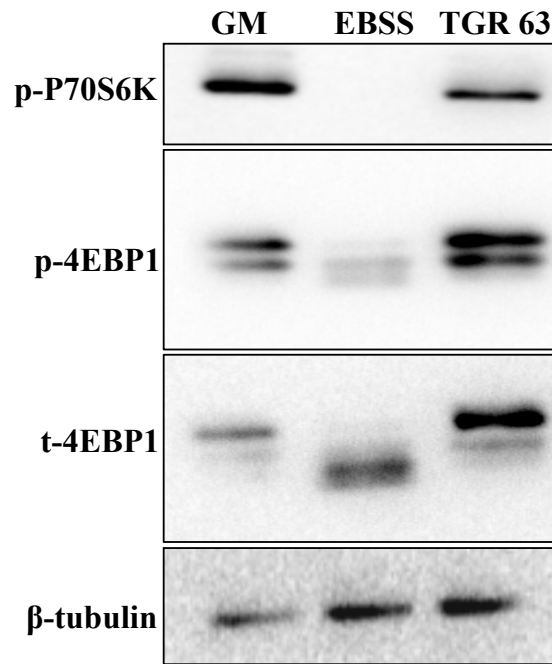


Figure 9. Immunoblotting analyses of MTOR activity. Western blotting to probe for levels of MTOR substrates such as P70S6K and 4EBP1 in SH-SY5Y cells treated with TGR 63 for 2 h.

TGR 63 protects neuronal cells from α -synuclein toxicity in an autophagy dependent manner

We further wanted to test if the autophagy inducing ability of TGR 63 was potent enough to impart cytoprotection in cell culture model of aggregate toxicity. When α -synuclein was transiently overexpressed in SH-SY5Y neuroblastoma cells for 72 h, cell viability was significantly affected ($P < 0.001$ versus vector control; **Fig. 10**) confirming α -synuclein mediated cytotoxicity. In such an experimental set up, upon TGR 63 treatment, cell viability was significantly increased than that of untreated or vector control ($P < 0.001$ versus untreated; **Fig. 10**). In α -synuclein overexpressing cells, when TGR 63 is co-administered with 3-methyl adenine (3-MA, pharmacological autophagy inhibitor), cell viability was dramatically reduced than that of TGR 63 treatment ($P < 0.001$ versus 3-MA treated; **Fig. 10**). Treatment of TGR 63 alone (5 μ M) was non-toxic to SH-SY5Y cells for a period of 72 h. These results indicate that TGR 63 is cytoprotective to cells that overexpressed α -synuclein in an autophagy-dependent manner.

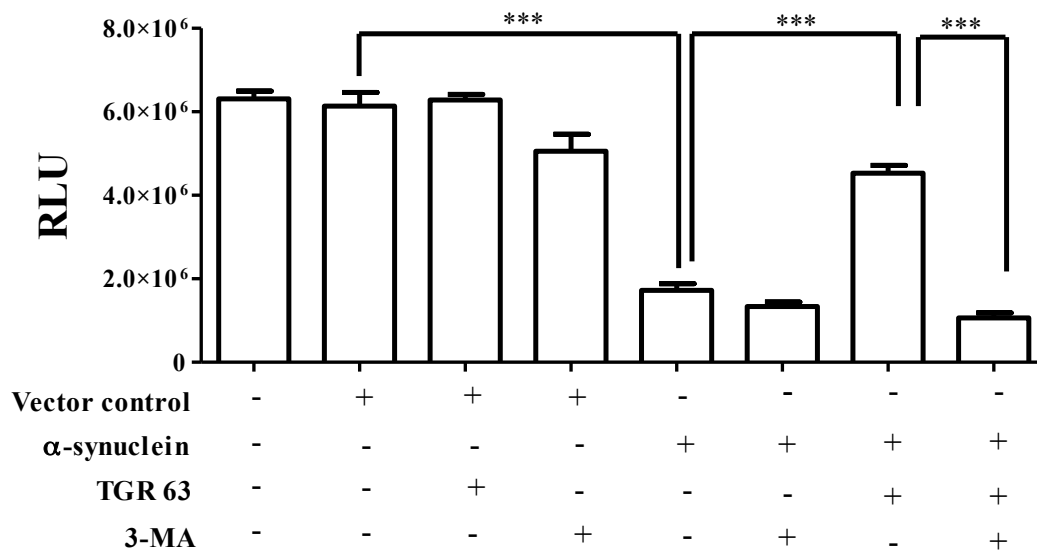


Figure 10. Cytoprotection assay in SH-SY5Y cells. SH-SY5Y cells were transiently transfected with GFP- α -synuclein for 48 h and then treated with compounds such as TGR 63 and/or 3-MA for 24 h. Cell viability was measured using Cell-Titre Glo reagent. Statistical analysis was performed using one-way ANOVA and the post-hoc Bonferroni test. Error bars, mean \pm SEM. ***- $P < 0.001$.

Target identification of TGR 63

In order to identify its cellular target, we covalently attached TGR 63 to silica beads. We incubated TGR 63 bound and control beads with SH-SY5Y lysates to pull down its *in vivo* interacting partners and the experimental scheme is illustrated (**Fig. 11A**). The bound beads (TGR 63 or control) fractions were electrophoresed and silver stained to identify the differential protein profile. We noted a significant difference in the protein profiles between TGR 63 bound and control beads lysate fractions (**Fig. 11B**). The control and TGR 63 bound fractions on gel were excised and given for mass spectrometry. Mass spectrometry analyses identified 145 unique proteins in the TGR 63 bound fraction. To ascertain true interacting partners of TGR 63, we plan to perform genetic screen by knocking down all 145 genes and analyze the autophagy response in presence or absence of TGR 63. Towards

this, 145 genes will be silenced in tandem RFP-GFP-LC3 stable cells i.e., autophagy reporter cell line and quantify the autophagy status in presence and absence of TGR 63 (Fig. 11C).

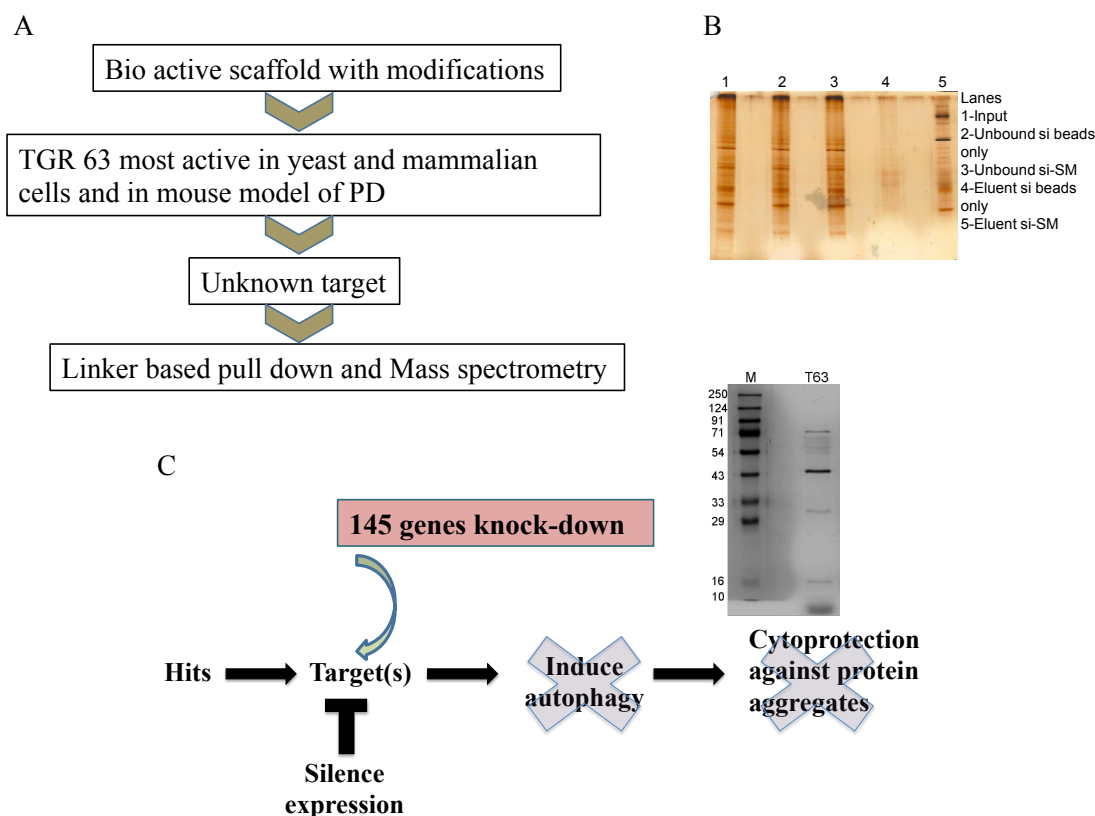


Figure 11. Target identification of TGR 63. (A) Schema representing the pull down protocol. (B) Silver stained gel of control [silica (si) beads] or silica conjugated TGR 63 (small molecule, SM) pull down lysates. (C) Schema indicating the genetic screen intended to perform in autophagy reporter or cytoprotection assays upon siRNA mediated knock down of 145 genes.

MPTP induced neuronal loss is mitigated by TGR 63

To further explore the cytoprotective abilities of TGR 63, we extended our studies in a preclinical mouse model of Parkinson’s disease, the MPTP toxicity model¹⁶. MPTP (1-methyl-4-phenyl-1,2,3,6-tetrahydropyridine) is a neurotoxin that specifically ablates the dopaminergic (DAergic) neurons (around 70%) in Substantia Nigra pars compacta (SNpc)

of midbrain with concomitant reduction of dopamine levels in striatum^{16,17}. We co-administered MPTP (23 mg/kg of bodyweight, 4 doses a day at 2 h interval) and TGR 63 (5 mg/kg of body weight) at the same day (MPTP+Co). TGR 63 dosage was continued for 7 days post MPTP administration. Using tyrosine hydroxylase (TH) staining, unbiased stereology was performed to quantitate number of neurons¹⁸. TH staining intensity was interpreted as health of DAergic neurons. Both number and health of DAergic neurons were significantly reduced in MPTP cohort than that of vehicle control, thus confirming MPTP induced impairments ($P < 0.01$ versus vehicle, **Fig. 12, A to C**). In MPTP+Co regimen, the number ($P < 0.05$ versus MPTP, **Fig. 12, A and B**) and health ($P < 0.05$ versus MPTP, **Fig. 12, A and C**) of DAergic neurons were significantly increased than that of MPTP only cohort. The protected neuronal number and health in MPTP+Co cohort was comparable to that of vehicle control. In addition, the MPTP induced reduction in SNpc volume was significantly ameliorated in MPTP+Co regimen ($P < 0.05$ versus MPTP, **Fig. 12, A and D**).

Collectively, these results suggested that TGR 63 is neuroprotective in preclinical mouse model of PD.

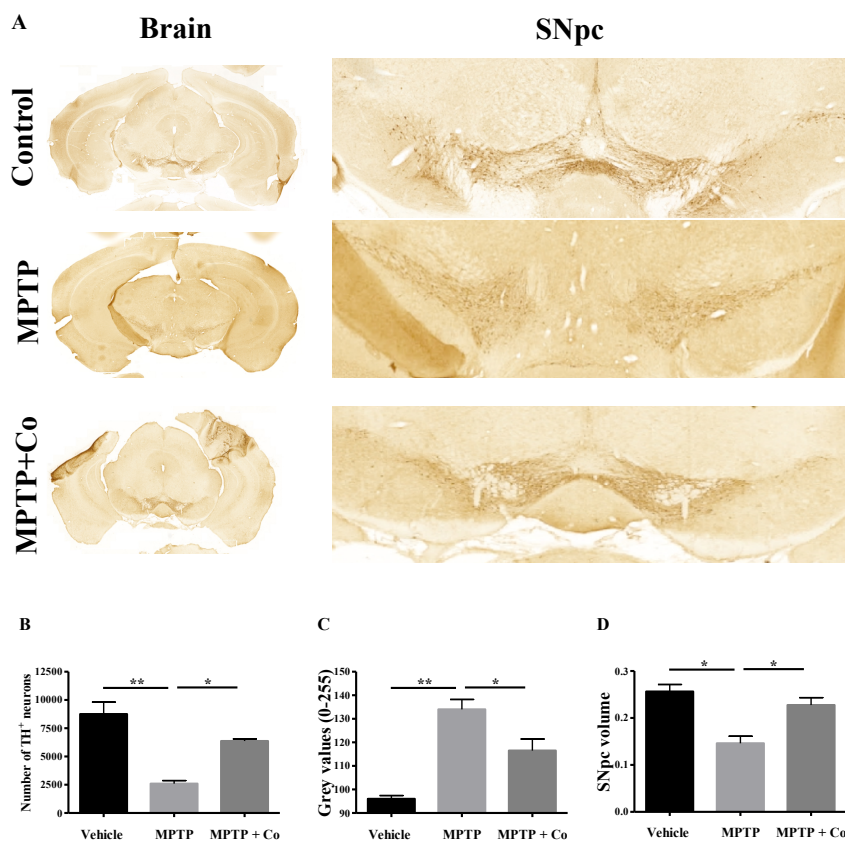


Figure 12. Stereological analyses. (A) Representative photomicrographs of whole brain

*and SNpc regions of various cohorts namely vehicle, MPTP and MPTP+Co. Quantitation of TH immunoreactive neuronal number (B), TH intensity (C) and SNpc volume (B) of above mentioned cohorts. Statistical analysis was performed using one-way ANOVA and the post-hoc Bonferroni test. Error bars, mean \pm SEM. *- $P < 0.05$, ***- $P < 0.001$.*

TGR 63 clears toxic protein oligomers by inducing autophagy in SNpc

We then investigated the mechanistic aspects underlying the neuroprotective potential of TGR 63. Using immunochemistry-based assay, we tested for the autophagy inducing ability of TGR 63 (LC3 puncta in TH⁺ cells) with toxic oligomer clearance (APP/ β amyloid/A11 oligomer specific puncta in TH⁺ cells) in mice model as it did for yeast and mammalian cells. In MPTP cohort, the LC3 puncta per dopaminergic neuron was reduced significantly than that of vehicle control ($P < 0.05$ versus vehicle; **Fig. 11, A and B**) with increased presence of toxic A11 protein oligomers ($P < 0.001$ versus vehicle; **Fig. 11, C and D**), indicating the MPTP induced impairment of autophagy.

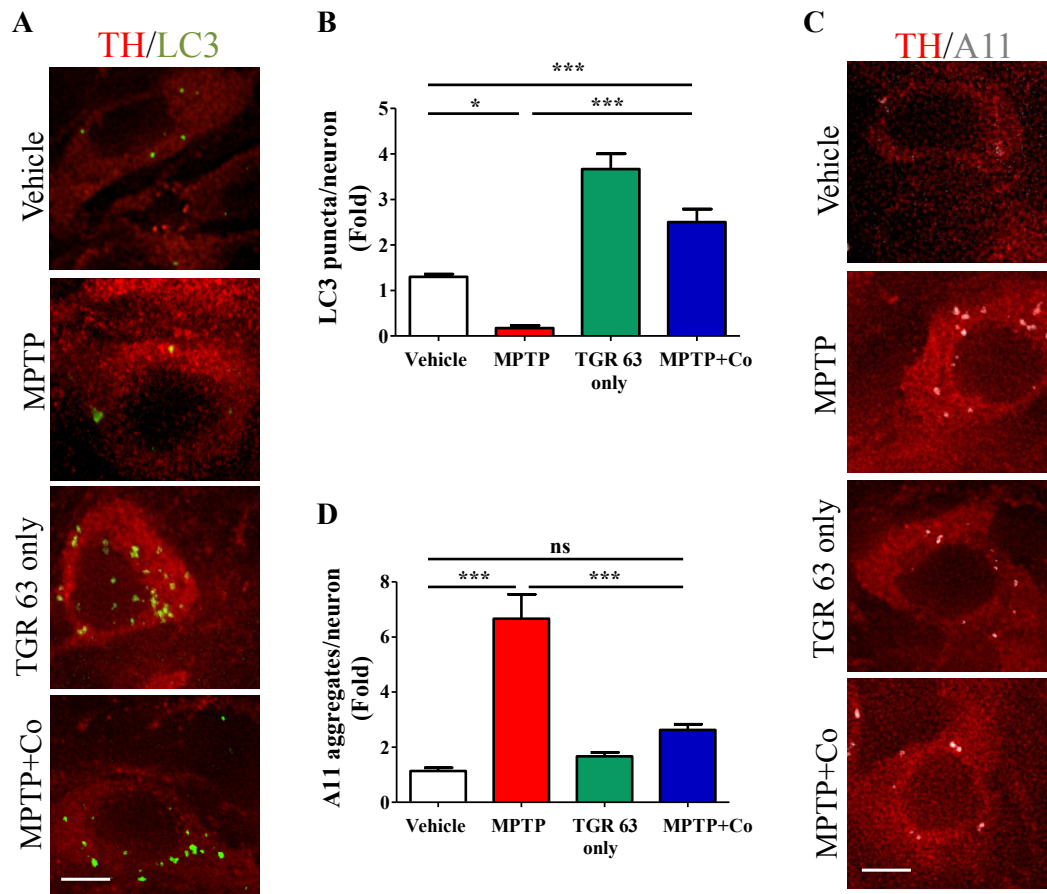


Figure 13. Immunohistological analyses. (A) Representative photographs of double staining of DAergic neurons with TH (dopaminergic neuronal marker) and LC3 (autophagy marker) of various cohorts such as vehicle, MPTP, TGR 63 only and MPTP+Co. (B) Graph representing the quantification of LC3 puncta per neuron for all cohorts. (C) Representative photographs of double staining of DAergic neurons with A11 (toxic protein oligomer marker) and TH of various cohorts such as vehicle, MPTP, TGR 63 only and MPTP+Co. (D) Graph representing the quantification of A11 puncta per neuron for all previously mentioned cohorts. Scale bar is 50 μ m. Statistical analysis was performed using one-way ANOVA and the post-hoc Bonferroni test. Error bars, mean \pm SEM. ns-non significant, *- $P < 0.05$, ***- $P < 0.001$.

In MPTP+Co regimen, the LC3 puncta was increased significantly than that of vehicle control ($P < 0.001$ versus vehicle; **Fig. 11, A and B**). This was accompanied by significant

reduction in A11 puncta per neuron suggesting the clearance of toxic protein oligomers than that of MPTP cohort ($P < 0.001$ versus MPTP; **Fig. 11, C and D**). Importantly, the administration of TGR 63 alone increased number of LC3 puncta per dopaminergic neuron confirming its autophagy inducing ability as it did in other models ($P < 0.001$ versus vehicle; **Fig. 11, A and B**). We observed no toxic A11 puncta in TGR 63 alone cohort indicating its non-toxic nature.

Thus, TGR 63 induced autophagy in DAergic neurons of SNpc to degrade the toxic protein oligomers.

MPTP induced behavioral impairments are ameliorated by TGR63

We then studied whether TGR 63 can ameliorate the MPTP-induced behavioral impairments such as exploration and locomotory deficits. We employed two popularly used behavior tests such as rotarod (to assess locomotion) and open field (to assess exploration)¹⁵. We performed behavior experiments on day 13 (day 7 post-MPTP injections) and day 15 (day 9 post-MPTP injections) with double-blinded approach.

In rotarod test, the latency to fall, of animals in MPTP cohort was reduced significantly than that of vehicle control indicating the MPTP-induced locomotory deficit on both day 13 and 15 ($P < 0.001$ versus vehicle; **Fig. 14, A and B**). In MPTP+Co cohort, latency to fall, was dramatically increased than that of MPTP cohort on both days ($P < 0.001$ versus MPTP; **Fig. 14, A and B**). We noted that latency to fall, in MPTP+Co cohort was comparable to that of vehicle control cohort.

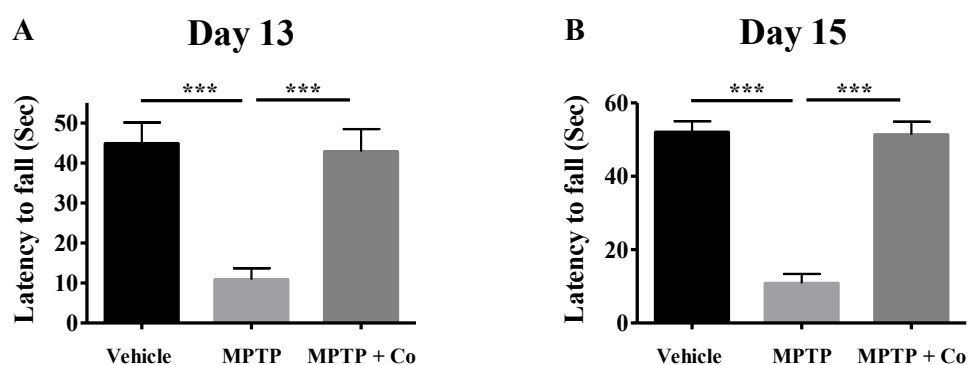


Figure 14. Rotarod test. Latency to fall of animals from various cohorts namely vehicle, MPTP and MPTP+Co observed on day 13 (A) and day 15 (B). Statistical analysis was

performed using one-way ANOVA and the post-hoc Bonferroni test. Error bars, mean \pm SEM. ***- $P < 0.001$.

The total distance travelled by animals in an open field arena suggests the exploratory ability of animals. In MPTP alone cohort, the total distance travelled by animals was significantly decreased, confirming the MPTP induced exploratory deficit ($P < 0.001$ versus vehicle; **Fig. 15, A and B**). In MPTP+Co cohort, the total distance travelled by animals was improved significantly than that of MPTP cohort on both days ($P < 0.001$ versus MPTP; **Fig. 15, A and B**). Importantly, the distance travelled by animals in MPTP+Co cohort was comparable to that of vehicle control.

These results confirm that TGR 63 can ameliorate the MPTP induced behavioral deficits such as exploration (open field test) and locomotion (rotarod).

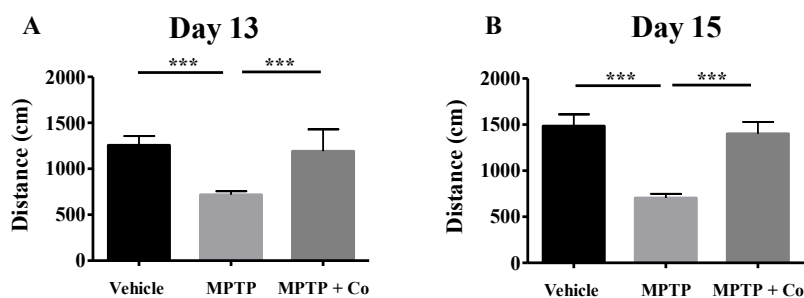


Figure 15. Open field test. Distance travelled by animals of various cohorts namely vehicle, MPTP and MPTP+Co recorded on day 13 (A) and day 15 (B). Statistical analysis was performed using one-way ANOVA and the post-hoc Bonferroni test. Error bars, mean \pm SEM. ***- $P < 0.001$.

Discussion

In this study, we identified the small molecule TGR 63 as an aggrephagy inducer that significantly curbs α -synuclein mediated proteotoxicity in model systems such as yeast and mammalian cell lines. In a preclinical mouse model of PD, TGR 63 induced autophagy, cleared toxic protein oligomers and significantly prevented motor impairments.

By screening a custom made in-house small molecule library to identify small molecules that ameliorate proteotoxicity due to overexpression of α -synuclein in yeast model, we identified a novel small molecule hit, TGR 63.

One of the profound cellular mechanisms to degrade toxic protein aggregates is the selective autophagy process, aggrephagy⁶. Due to its size and hydrophobicity, the toxic oligomers are substrates for autophagy for their effective clearance¹⁹. We observe that TGR 63 curbs proteotoxicity in an autophagy dependent manner that was revealed by both genetic and pharmacological approaches. In addition, TGR 63 had the ability to augment starvation-induced autophagy in yeast. Furthermore, in mammalian cells, it significantly enhanced autophagy flux by increasing autolysosome formation. Importantly, TGR 63 induced autophagy in dopaminergic neurons of mice midbrain that correlated with clearance of toxic protein oligomers.

The potential of TGR 63 in modulating aggrephagy in various models such as yeast, mammalian cells and mice reiterate the fact of evolutionarily conserved nature of autophagy.

TGR 63 induced autolysosome formation similar that of 6-Bio. It is important to mention that revealing the mode of action of TGR 63 might reveal the mechanistic insights on one of the bottlenecks of autophagy pathway (i.e.) autophagosome-lysosome fusion.

We attempted to identify the *in vivo* interacting partners of TGR 63 using the click chemistry and pull down based approaches. Mass spectrometry identified the set of putative 145 protein interacting partners. We aim to perform the genetic screen to identify the *in vivo* cellular target of TGR 63.

References

1. Blokhuis AM, Groen EJ, Koppers M, van den Berg LH, Pasterkamp RJ. Protein aggregation in amyotrophic lateral sclerosis. *Acta Neuropathol* 2013; 125:777-94.
2. Balch WE, Morimoto RI, Dillin A, Kelly JW. Adapting proteostasis for disease intervention. *Science* 2008; 319:916-9.
3. Ciechanover A, Kwon YT. Protein Quality Control by Molecular Chaperones in Neurodegeneration. *Front Neurosci* 2017; 11:185.
4. Nixon RA. The role of autophagy in neurodegenerative disease. *Nat Med* 2013; 19:983-97.
5. Yang H, Hu HY. Sequestration of cellular interacting partners by protein aggregates: implication in a loss-of-function pathology. *FEBS J* 2016; 283:3705-17.
6. Hyttinen JM, Amadio M, Viiri J, Pascale A, Salminen A, Kaarniranta K. Clearance of misfolded and aggregated proteins by autophagy and implications for aggregation diseases. *Ageing Res Rev* 2014; 18:16-28.
7. Andersson V, Hanzen S, Liu B, Molin M, Nystrom T. Enhancing protein disaggregation restores proteasome activity in aged cells. *Aging (Albany NY)* 2013; 5:802-12.
8. Kim M, Sandford E, Gatica D, Qiu Y, Liu X, Zheng Y, Schulman BA, Xu J, Semple I, Ro SH, et al. Mutation in ATG5 reduces autophagy and leads to ataxia with developmental delay. *Elife* 2016; 5.
9. Pyo JO, Yoo SM, Ahn HH, Nah J, Hong SH, Kam TI, Jung S, Jung YK. Overexpression of Atg5 in mice activates autophagy and extends lifespan. *Nat Commun* 2013; 4:2300.
10. Komatsu M, Waguri S, Chiba T, Murata S, Iwata J, Tanida I, Ueno T, Koike M, Uchiyama Y, Kominami E, et al. Loss of autophagy in the central nervous system causes neurodegeneration in mice. *Nature* 2006; 441:880-4.

Chapter 6: *A novel small molecule autophagy modulator TGR 63 ameliorates Parkinsonism*

11. Komatsu M, Waguri S, Ueno T, Iwata J, Murata S, Tanida I, Ezaki J, Mizushima N, Ohsumi Y, Uchiyama Y, et al. Impairment of starvation-induced and constitutive autophagy in Atg7-deficient mice. *J Cell Biol* 2005; 169:425-34.
12. Khurana V, Lindquist S. Modelling neurodegeneration in *Saccharomyces cerevisiae*: why cook with baker's yeast? *Nat Rev Neurosci* 2010; 11:436-49.
13. Alexander GE. Biology of Parkinson's disease: pathogenesis and pathophysiology of a multisystem neurodegenerative disorder. *Dialogues Clin Neurosci* 2004; 6:259-80.
14. Winslow AR, Chen CW, Corrochano S, Acevedo-Arozena A, Gordon DE, Peden AA, Lichtenberg M, Menzies FM, Ravikumar B, Imarisio S, et al. alpha-Synuclein impairs macroautophagy: implications for Parkinson's disease. *J Cell Biol* 2010; 190:1023-37.
15. Suresh SN, Chavalmane AK, Dj V, Yarreiphang H, Rai S, Paul A, Clement JP, Alladi PA, Manjithaya R. A novel autophagy modulator 6-Bio ameliorates SNCA/alpha-synuclein toxicity. *Autophagy* 2017; 13:1221-34.
16. Jackson-Lewis V, Przedborski S. Protocol for the MPTP mouse model of Parkinson's disease. *Nat Protoc* 2007; 2:141-51.
17. Jackson-Lewis V, Blesa J, Przedborski S. Animal models of Parkinson's disease. *Parkinsonism Relat Disord* 2012; 18 Suppl 1:S183-5.
18. West MJ, Slomianka L, Gundersen HJ. Unbiased stereological estimation of the total number of neurons in the subdivisions of the rat hippocampus using the optical fractionator. *The Anatomical record* 1991; 231:482-97.
19. Wong YC, Krainc D. alpha-synuclein toxicity in neurodegeneration: mechanism and therapeutic strategies. *Nat Med* 2017; 23:1-13.

Chapter 7

**Rationally designed peptidomimetic modulators of
a β toxicity in Alzheimer's disease**

Note:

**This chapter is published as an original research article in
Scientific reports (2015); Jan 30;5:8139.**

Abstract

Alzheimer's disease is one of the devastating illnesses mankind is facing in the 21st century. The main pathogenic event in Alzheimer's disease is believed to be the aggregation of the β -amyloid ($A\beta$) peptides into toxic aggregates. Molecules that interfere with this process may act as therapeutic agents for the treatment of the disease. Use of recognition unit based peptidomimetics as inhibitors are a promising approach, as they exhibit greater protease stability compared to natural peptides. Here, we present peptidomimetic inhibitors of $A\beta$ aggregation designed based on the KLVFF (**P1**) sequence that is known to bind $A\beta$ aggregates. We improved inhibition efficiency of **P1** by introducing multiple hydrogen bond donor-acceptor moieties (thymine/barbiturate) at the N-terminal (**P2** and **P3**), and blood serum stability by modifying the backbone by incorporating sarcosine (N-methylglycine) units at alternate positions (**P4** and **P5**). The activity of **P4** and **P5** were studied in a yeast cell model showing $A\beta$ toxicity. **P4** and **P5** could rescue yeast cells from $A\beta$ toxicity and $A\beta$ aggregates were cleared by the process of autophagy.

Introduction

The potential approach to clear the intracellular toxic protein aggregates is through enhancing the phenomenon of autophagy. Autophagy, a cellular mechanism of selective autophagy, involves degradation of misfolded proteins or aggregates essential for cellular homeostasis¹. Presence of $A\beta$ aggregates downregulate autophagy, which is known to play a pivotal role in clearing and neutralizing the toxic effects caused by $A\beta$ ². Designed small molecules or peptides which influence autophagy may also act as probable therapeutics³. Yeast has been popularly used as a simple model organism in literature to study $A\beta$ toxicity and screen $A\beta$ inhibitors⁴. *S. cerevisiae* is a eukaryote and, hence, shares phenomenal homology with the human genome⁴. It also recapitulates the fundamental processes of a eukaryotic cell-like transcription, translation and also its metabolism. Yeast model also provides a platform to study the autophagy-based regulation. In this report, we study the inhibition efficiency of modified core sequences of the $A\beta$ peptide (KLVFF). We prepared mimetics of this peptide by performing two types of synthetic modifications - first, by introducing a hydrogen bond donor-acceptor moiety at the N terminal of the core sequence, and, subsequently introducing unnatural amino acid units to block hydrogen bonding between $A\beta$ 42 monomers. These modifications also conferred proteolytic resistance to the

derived peptidomimetics (the parent peptide KLVFF contains natural amino acids and is not resistant to endoproteases). Further, inhibitory activity was studied in the yeast (*S. cerevisiae*) model, which expresses A β 42, to assess the ability of peptidomimetics as therapeutic agents and to understand their mechanism of action in reducing A β 42 toxicity. Thus, we report on the study of structural fine tuning and inhibitory activities of peptidomimetics towards preventing the formation of A β 42 aggregates and dissolving the preformed toxic aggregates.

Results

Peptidomimetics were non-toxic to cells

In presence of all peptidomimetics, the WT GFP culture growth curves were examined (**Fig. 1**). The concentration of peptidomimetics used was 300 μ M. In peptide treated cells, the growth curves were similar to that of untreated sample. No significant growth lag or drop in absorbance (A_{600}) in presence of peptidomimetics were observed.

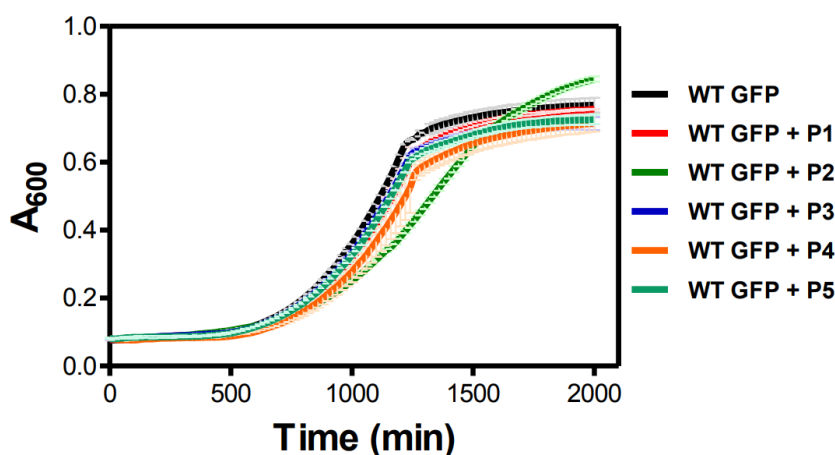


Figure 1. Analysis of peptidomimetics toxicity in yeast. Growth curves of WT GFP in presence or absence of all peptidomimetics (P1-P5) were plotted. Concentration of peptidomimetics used was 300 μ M.

Peptidomimetics (4 and 5) abrogated the β -amyloid toxicity in yeast

All peptidomimetics were screened for their ability to ameliorate the toxicity due to β -amyloid. To test this, we used the *S. cerevisiae* model of β -amyloid (β A₁₋₄₂) N-terminally

tagged GFP expressing strain. Compared to that of WT GFP strain, the growth curve of WT GFP β A exhibited severe lag which didn't enter the exponential phase due to β -amyloid toxicity. Apparent growth lag displayed by WT GFP β A strain that of WT GFP property was used for screening the peptidomimetics (**Fig. 2A**). Among five peptidomimetics, growth curves of WT GFP β A strain in P1 to P3 treated were similar to that of its untreated. However, the P4 and P5 treated curves were like WT GFP. Hence, we inferred that P4 and P5, but not others, rescued the growth lag in WT GFP β A strain (**Fig. 2, B and C**). This result indicates that P4 and P5 rescued the yeast cells from β -amyloid toxicity.

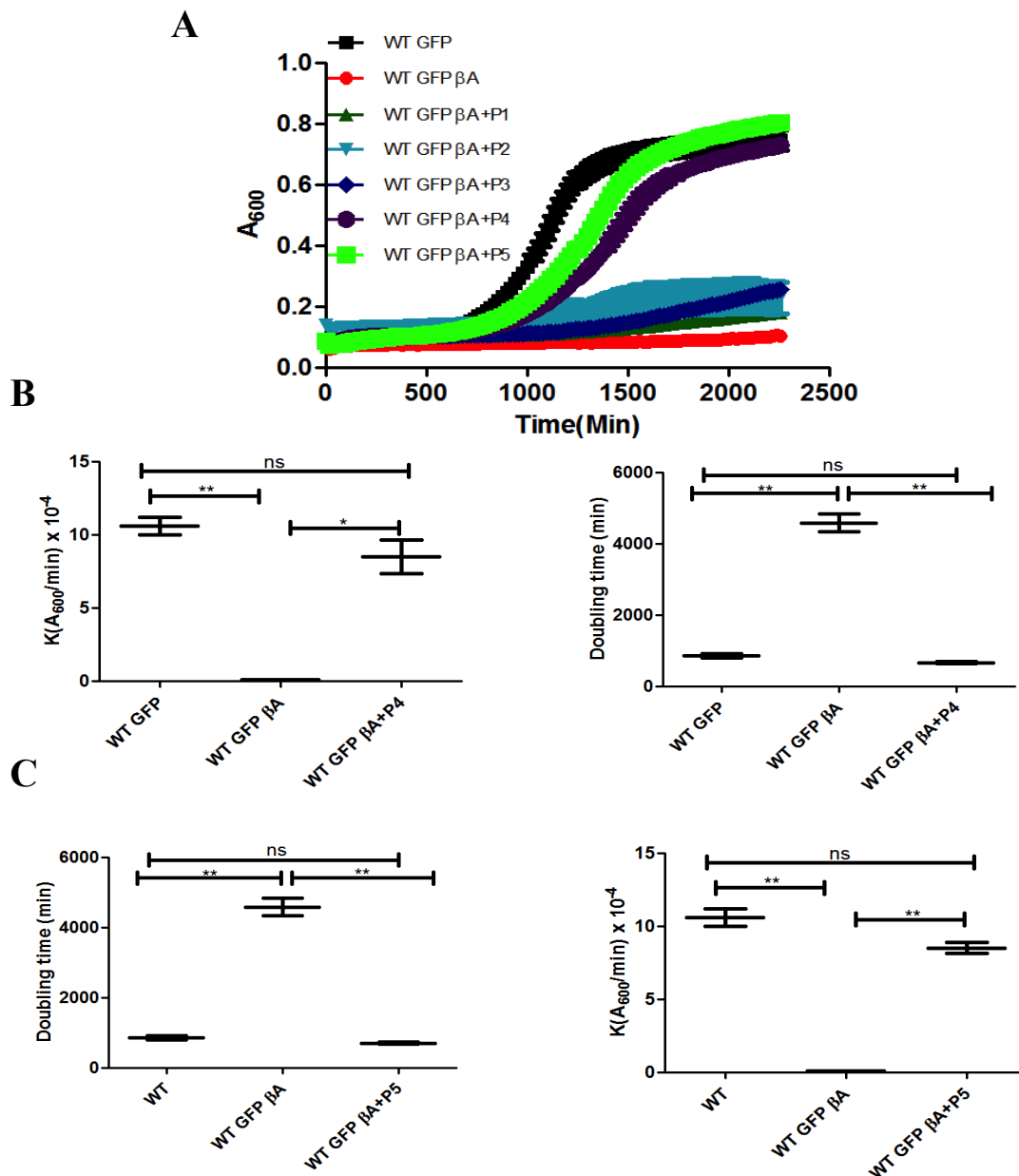


Figure 2. Screening of peptidomimetics. All peptidomimetics were screened in WT GFP β A

Chapter 7: Rationally designed peptidomimetic modulators of $a\beta$ toxicity in Alzheimer's disease

strain and concentration used was $300 \mu\text{M}$ (a). Growth parameters like growth rate and doubling time of WT GFP βA strain in presence and absence of P4 (b) and P5 (c) were analyzed. Statistical analysis was performed using one-way ANOVA and the post-hoc Bonferroni test. Error bars, mean \pm SEM. ns-non significant, $*-P < 0.05$, $** -P < 0.01$, $***-P < 0.001$.

Peptidomimetics degrade β -amyloid

β -amyloid protein (1-42) was N terminally tagged with GFP. In a cell, β -amyloid protein (tagged with GFP) aggregate clearance by peptidomimetics would be marked by presence of free GFP in the vacuole. The free GFP was observed in the vacuole in culture treated with peptides 4 and 5 but was absent in P1 and untreated (**Fig. 3**). Pertaining to P4 and P5, diffused GFP signal in the vacuole co-localized with vacuolar stained dye, CMAC-Blue, suggesting that incubating cells with these peptides resulted in GFP βA aggregates being degraded in the vacuole to release free GFP.

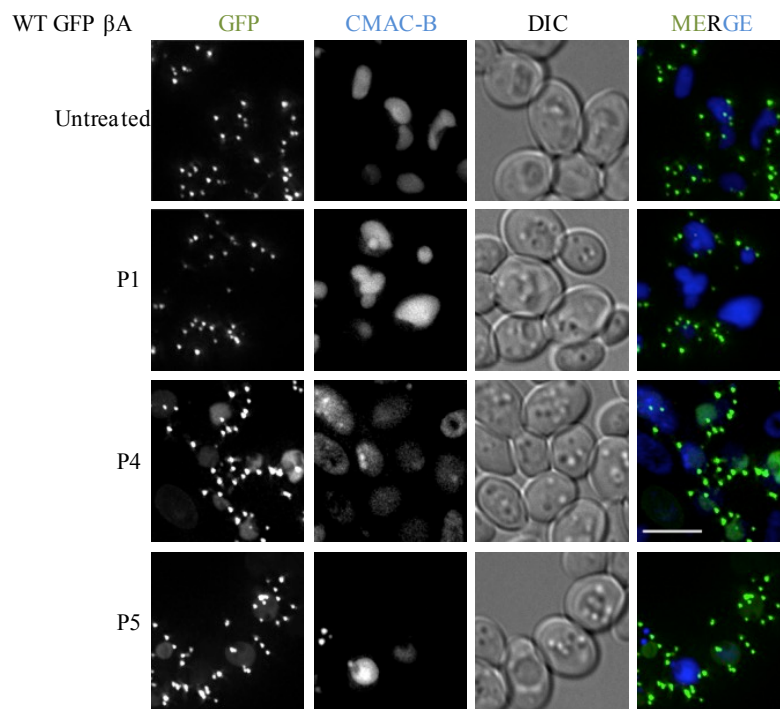


Figure 3. P4 and P5 degraded β -amyloid. Degradation of GFP β -amyloid in WT GFP β A strain in presence of P1, P4 and P5. Vacuoles stained with CMAC-Blue. Scale bar: 5 μ m. Concentration of peptides used, 300 μ M.

Peptides failed to rescue the β -amyloid toxicity in autophagy mutant

Autophagy has been shown to play a key role in degrading the β -amyloid oligomers or fibrils¹. Degradation of protein aggregates by selective autophagy mechanism is defined as aggrephagy. In a cellular context, the disaggregated fibrils are captured and released into the vacuole for degradation through autophagy. To investigate whether the appearance of free GFP in the vacuoles of cells treated with P4 and P5 was due to autophagy, we repeated the growth rescue experiment in cells defective in autophagy (*atg1 Δ* mutant). Although P4 and P5 were able to rescue the growth lag in WT GFP β A strain, they failed to do so in *atg1 Δ* GFP β A strain (**Fig. 4**).

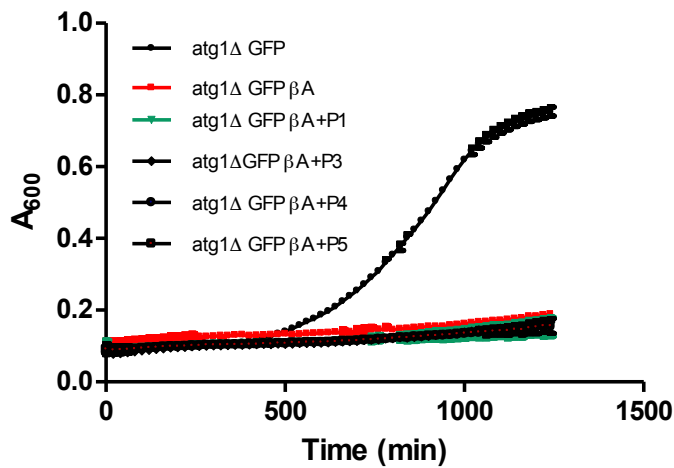


Figure 4. Growth assays of peptidomimetics in GFP β A strain. Growth curves of P1 (a), P3, P4 and P5 were examined at concentration of 300 μ M.

In addition, free vacuolar GFP was not seen in *atg1 Δ* GFP β A strain treated with P4 and P5 (Fig. 5) similar to untreated and P1 treated cells. The peptides neither reduced the A β toxicity nor degraded GFP β A in the autophagy mutant. This clearly indicated that autophagy was responsible for clearing the A β aggregates, when treated with P4/P5 in WT GFP β A cells.

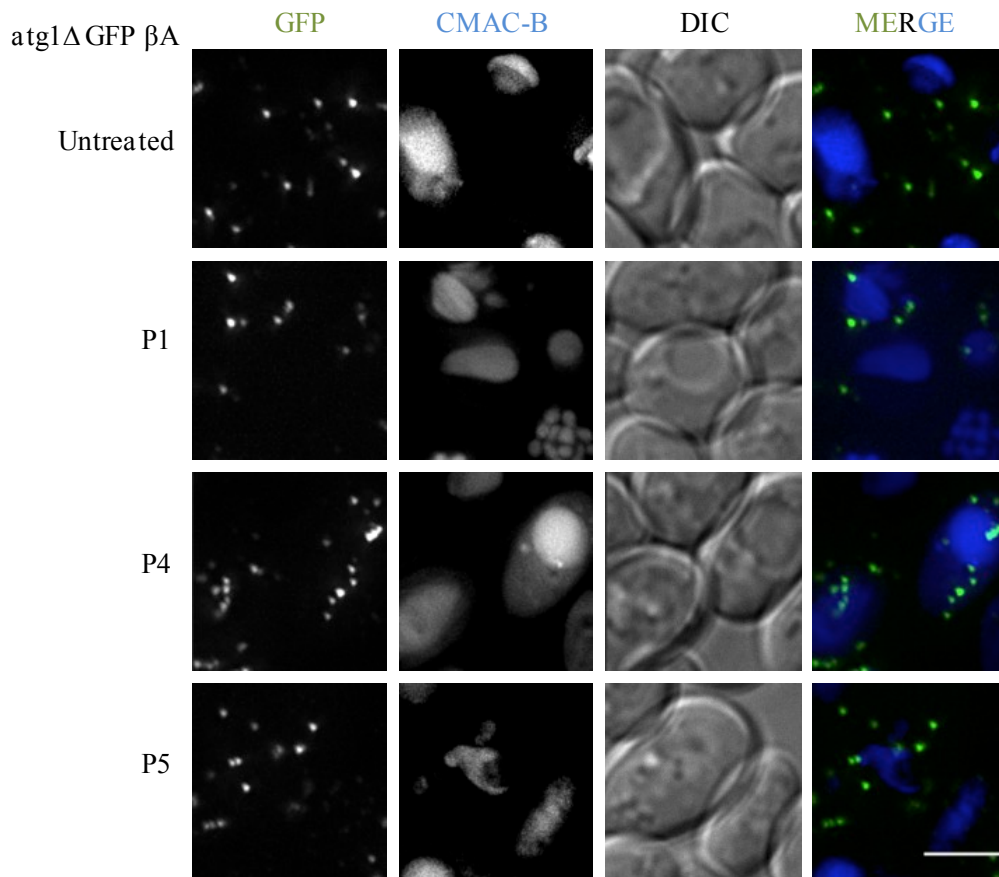


Figure 5. P4 and P5 failed to degrade β -amyloid in a core autophagy mutant strain. Degradation of GFP β -amyloid in *atg1 Δ* GFP β A strain in presence of P1, P4 and P5. Vacuoles stained with CMAC-Blue. Scale bar: 7.5 μ m. Concentration of peptides used, 300 μ M.

Discussion

Autophagy plays a key role in degrading the toxic β -amyloid oligomers or fibrils causing catastrophe inside a cell to maintain its homeostasis⁵. In this study, we have employed *S. cerevisiae* model expressing GFP tagged β -amyloid that exhibits severe growth lag as

Chapter 7: *Rationally designed peptidomimetic modulators of $a\beta$ toxicity in Alzheimer's disease*

compared to the wild type. Among all peptidomimetics, only P4 and P5 rescued this growth defect due to β -amyloid, but not others. Rescued growth was comparable to the wild type where almost entire lag was restored by P4 and P5. Toxicity analysis of peptidomimetics in cells revealed that all peptides (300 μ M) are indeed non-toxic. Growth curve of WT GFP strain in presence and absence of peptidomimetics remains similar. Subsequent analysis of these peptidomimetics in aggregate clearance revealed that P4 and P5 stimulated β -amyloid degradation which is seen by the accumulation of vacuolar free GFP. The mechanism of action of these peptidomimetics is unclear. It is possible that they either interact with the aggregates to make them accessible or recognizable to the autophagy machinery or they may directly induce autophagy flux which then results in aggregate clearance. These hypothesis forms the basis of our future work.

References

1. Ravikumar B, Vacher C, Berger Z, Davies JE, Luo S, Oroz LG, Scaravilli F, Easton DF, Duden R, O'Kane CJ, et al. Inhibition of mTOR induces autophagy and reduces toxicity of polyglutamine expansions in fly and mouse models of Huntington disease. *Nat Genet* 2004; 36:585-95.
2. Nilsson P, Saido TC. Dual roles for autophagy: degradation and secretion of Alzheimer's disease Abeta peptide. *Bioessays* 2014; 36:570-8.
3. Tsvetkov AS, Miller J, Arrasate M, Wong JS, Pleiss MA, Finkbeiner S. A small-molecule scaffold induces autophagy in primary neurons and protects against toxicity in a Huntington disease model. *Proc Natl Acad Sci U S A* 2010; 107:16982-7.
4. Khurana V, Lindquist S. Modelling neurodegeneration in *Saccharomyces cerevisiae*: why cook with baker's yeast? *Nat Rev Neurosci* 2010; 11:436-49.
5. Nixon RA. The role of autophagy in neurodegenerative disease. *Nat Med* 2013; 19:983-97.

Chapter 8

Summary and future directions

Autophagy (in this context macroautophagy) is an intracellular degradation and recycling process that is conserved from yeast to mammals¹. Not surprisingly, it is therefore a vital requirement to maintain cellular and organismal homeostasis². Apart from regular housekeeping functions, it also aids cells to cope with various stressful situations such as starvation, intracellular infection and accumulation of misfolded protein aggregates. In particular, misfolded aggregation of intrinsically disordered proteins such as α -synuclein, β -amyloid, hyper-phosphorylated tau and TDP43 are reported to be the underlying basis for neurodegenerative pathogenesis³. These protein aggregates are toxic as they sequester the key cellular proteins including transcription factors that are necessary to maintain the upkeep of essential cellular pathways. Thus, in these protein aggregation driven neurodegeneration, most of such cellular pathways become awry thereby perturbing the cellular homeostasis. Plethora of studies has highlighted the beneficial effects of clearing these disease associated protein aggregates in curbing proteotoxicity and enhancing cell viability. In the initial stages of protein aggregation, chaperones and the ubiquitin proteasome system (UPS) help in preventing their build up inside cells³. However, once the misfolded toxic aggregates overwhelm the cells with their numbers and size, the cells rely heavily on the (macro)autophagy machinery to clear them⁴. The specific pathway of macroautophagy that deals with clearing protein aggregates is called aggrephagy. Aggregates not only choke chaperone and the UPS functions, but also sequester them in aggregates themselves, thus making them unavailable for other cellular processes. Not surprisingly, autophagy is also perturbed by the presence of toxic protein aggregates. Aggregates hamper various steps of autophagy depending on the context of disease associated proteins. In addition to disrupting cellular pathways, the aggregates also damage organelles such as mitochondria and ER. Taken together, this cumulative failure of the proteostasis machinery results in compromised cellular homeostasis. As a result, the hardest hit are the post-mitotic and specialized cells like neurons that do not divide and hence cannot dilute out these lethal aggregates. Several studies have elegantly elucidated the importance of basal autophagy in maintaining cellular homeostasis by clearing the protein aggregates. Neuron specific genetic ablation of autophagy by knocking out the key autophagy genes such as Atg5 and Atg7 lead to the manifestation of neurodegenerative symptoms such as accumulation of ubiquitin positive aggregates, behavioral deficits and reduced survivability^{5, 6}. On the other hand, upregulation of autophagy by overexpressing Atg5 protein enhanced lifespan of transgenic mice⁷. Furthermore, pharmacological

upregulation of autophagy by small molecules has been shown to clear toxic protein aggregates and ameliorate neurodegeneration⁸⁻¹⁰. The latter studies have also identified novel molecular players and provided mechanistic insights into regulation of autophagy. In addition, these small molecules have also revealed their therapeutic potential in aggregate driven neurodegenerative disorders.

Although scientific literature has ample evidences to connect autophagy and neurodegeneration, there are several unanswered questions in this field. The underlying mechanism(s) behind how aggregates derail autophagy in neurons is not yet completely elucidated. Mechanistic aspects underlying the rate-limiting step(s) of autophagy is an enigma. How much autophagy can the cells do? What is the threshold of aggregate build up beyond which autophagy may not succeed in cytoprotection? Can nuclear aggregates be as efficiently cleared as their cytoplasmic counterparts? These are some questions that need to be addressed and hence, autophagy regulation turns out to be much more complex than earlier envisaged.

My study was aimed at understanding the regulation of autophagy using small molecules as a tool. Towards this, we generated yeast based models of proteotoxicity by overexpressing the disease associated proteins such as α -synuclein (PD) and β -amyloid (AD). Growth of yeast is hampered significantly upon overexpression of these toxic, disease associated proteins. This phenotypic growth defect is tapped as an assay to screen for small molecules that ameliorate the growth deficit associated with proteotoxicity. We screened numerous, structurally diverse small molecule libraries such as LOPAC¹²⁸⁰, in-house custom made compounds and peptidomimetics. Hits obtained were 6-Bio, XCT 790, AGK2, PD180970 and TGR 63. Amongst them, AGK2 has been previously reported to be neuroprotective by abrogating α -synuclein mediated toxicity in fly models¹⁴, thus validating our approach to identify autophagy inducers. In addition, we also identified peptidomimetics that clear β -amyloid mediated toxicity in yeast in an autophagy dependent manner.

All the hits that curbed proteotoxicity were mediated via autophagy. Several of them could enhance autophagy even in nutrient rich conditions (e.g., 6-Bio, XCT 790 and TGR 63) and furthermore, they augmented starvation mediated autophagy (e.g., AGK2 and PD180970).

After the initial studies in yeast, we tested if these small molecules would regulate mammalian autophagy. Autophagic flux analyses in cells surprisingly revealed that all the hits modulated autophagy. This observation that the small molecules modulate both yeast and mammalian autophagy reiterates the fact that autophagy is a conserved process from yeast to mammals.

Interestingly, the hits induced autophagy by affecting various stages of autophagy flux. For e.g., 6-Bio enhanced autophagosome and lysosome fusion dramatically and resulted in large number of autolysosomes. Like 6-Bio, TGR63 and AGK2 also enhanced autolysosome formation. In contrast, treatment of cells with XCT 790 and PD180970 increased autophagosome numbers suggesting that they induce autophagosome biogenesis. Thus, these small molecules can now be employed to investigate autophagy flux and to identify the molecular player(s) (potential targets of these hits) that act at either autophagosome biogenesis or at autophagosome-lysosome fusion steps. We also tested whether these hits also affected other trafficking pathways such as those associated with lysosomes. For e.g., 6-Bio does not perturb the lysosomal pH or endocytosis, and it appears to enter cells by passive diffusion.

MTOR is a central pathway required for cell growth and proliferation, and is also a negative regulator of autophagy. While several studies routinely induce autophagy by shutting down MTOR, therapeutically MTOR independent autophagy induction is preferred. It is not surprising that clinical trials conducted for long-term administration of MTOR dependent autophagy modulators such as rapamycin led to unwanted side effects such as immunosuppression and the complications arising therein¹¹. From a basic research point of view, mechanistic studies on such MTOR independent autophagy inducers will also provide novel insights into the diverse pathways that cells employ to control autophagy. Except 6-Bio, all our hits induced autophagy in an MTOR independent manner.

The small molecule library that we screened, LOPAC¹²⁸⁰, contains pharmacologically active compounds whose cellular target(s) are previously reported. The primary known target for our hits 6-Bio, XCT 790, AGK2 and PD 180970 is glycogen synthase kinase- β (GSK3- β)¹², estrogen related receptor α (ERR α)¹³, Sirtuin2¹⁴ and Src kinase¹⁵ respectively.

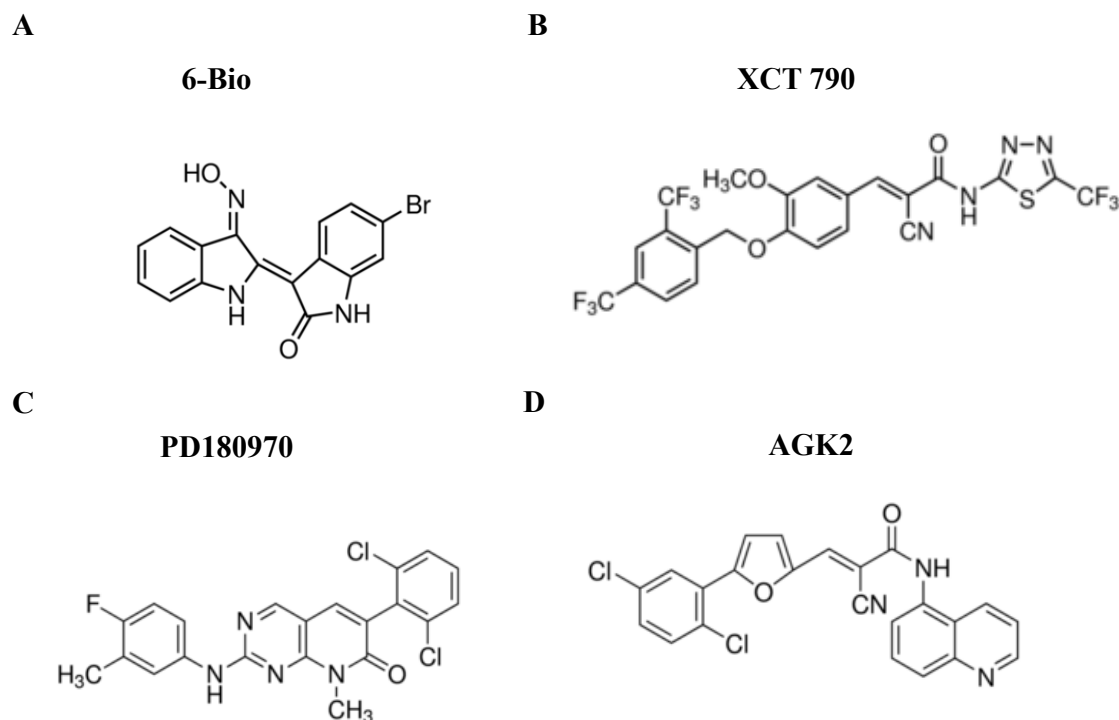


Figure 1. Structure of small molecules hits. (Source: Sigma-Aldrich website).

6-Bio enhanced autophagy in a GSK3- β dependent manner suggesting that its mode of action of autophagy induction is through its canonical reported target. Down regulating GSK3- β through RNAi also induced autophagy similar to 6-Bio. In addition, Compound VIII¹⁶, another structurally different pharmacological inhibitor of GSK3- β increased basal autophagy. Thus, apart from the reported functions of GSK3- β , we show a new role in the context of autophagy, which is to enhance autophagosome-lysosome fusion.

The known cellular target for XCT 790 is ERR α ¹³. Our studies also suggest that XCT 790 modulation of autophagy is ERR α -mediated. ERR α is a cytosolic resident orphan receptor involved in transcription of metabolism related genes such as those involved in oxidative phosphorylation. ERR α down regulation induced autophagy, whereas its overexpression inhibited autophagy. Interestingly, although a recent report suggested that ERR α induced autophagy in a transcriptional manner², our studies reveal a non-transcriptional role. We find that ERR α localizes to the autophagosomes and treatment of XCT 790 results in degradation of ERR α . The ERR α free autophagosomes appear to readily fuse with the

lysosomes thus enhancing the formation of autolysosomes. This results in efficient clearance of aggregate proteins and cytoprotection.

ERR α has a non-canonical LIR motif and further biochemical studies such as pull down and site directed mutagenesis of LIR motif might answer whether ERR α interacts with LC3 for its recruitment on autophagosomes.

The cellular target of TGR 63 is not yet known. We are attempting to identify the target by click chemistry in conjunction with affinity chromatography. Among the various strategies, TGR 63 compound was eventually functionalized with alkyne for its tethering to silica beads. TGR 63 bound silica beads were then employed to pull down bound proteins to identify its putative interacting partners using the neuronal cell (SH-SY5Y) lysates. Unconjugated beads were used as controls. Mass spectrometry revealed a dataset of putative 145 proteins as interacting partners of TGR 63. We now intend to knock down all 145 genes through siRNA approach and analyze the autophagic flux through microscopy based tandem RFP-GFP-LC3 assay with and without TGR 63 to identify the target that is responsible for its autophagy effect. In parallel, cytoprotection screen in human neuronal cells overexpressing α -synuclein will be conducted using the siRNA library of 145 genes, with and without TGR 63. Overlapping hits or genes from the two screens might identify the putative cellular target(s) of TGR 63. As none of these 145 genes have been known in literature to regulate autophagy, these screens thus hold the potential to reveal new molecular player(s) in autophagy.

Finally, we tested these small molecule hits (except AGK2) in a preclinical mouse model of Parkinson's disease (PD) to understand the regulation of neuronal aggregate clearance and evaluate their therapeutic potential. We employed an MPTP toxicity model where this toxin is known to ablate dopaminergic neurons (DA) in Substantia Nigra pars compacta (SNpc). One of the effects of this toxin on DA neurons is the production of toxic oligomers along with mitochondrial dysfunction that leads to their death. This specific loss of a vast population of DA neurons in SNpc leads to motor co-ordination and behavioral impairments.

In this model, all hits induced autophagy in DA neurons of SNpc with a concomitant clearance of toxic protein aggregates. In addition, we showed that 6-Bio crosses the blood brain barrier to induce neuronal autophagy. Also, the autophagy induction by these hits,

significantly exerted neuroprotection against MPTP induced toxicity. Furthermore, the treated mice displayed marked improvement in motor coordination. Thus, these *in vivo* experiments demonstrated not only the autophagy inducing abilities of these hits but also revealed their therapeutic potential in PD.

Among the hits obtained, the extent of neuroprotection obtained with 6-Bio is more as compared to others. But, 6-Bio is sparingly soluble in saline and this drawback gives an opportunity to design its analogues with improved solubility and potency. This is part of the ongoing and future work.

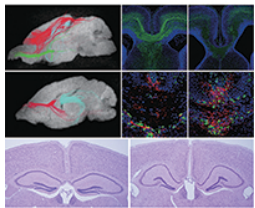
In conclusion, my thesis utilizes a chemical biology approach to identify novel molecular players for autophagy modulation. These small molecules can be further used as a tool to probe specific stages of the autophagy process such as autophagosome induction (XCT 790 and PD 180970) and autolysosome formation (6-Bio, AGK2 and TGR 63). They also exhibit promising therapeutic potential for neurodegenerative disease such as synucleopathies. The mechanism of action of these hits in terms of achieving modulation of autophagy flux through binding to their targets will be the key future direction that this study has opened up. Continued efforts towards this end will reveal specific regulatory process that govern autophagy flux.

References

1. Glick D, Barth S, Macleod KF. Autophagy: cellular and molecular mechanisms. *The Journal of pathology* 2010; 221:3-12.
2. Kim SY, Yang CS, Lee HM, Kim JK, Kim YS, Kim YR, Kim JS, Kim TS, Yuk JM, Dufour CR, et al. ESRRA (estrogen-related receptor alpha) is a key coordinator of transcriptional and post-translational activation of autophagy to promote innate host defense. *Autophagy* 2017;1-17.
3. Hyttinen JM, Amadio M, Viiri J, Pascale A, Salminen A, Kaarniranta K. Clearance of misfolded and aggregated proteins by aggrephagy and implications for aggregation diseases. *Ageing research reviews* 2014; 18:16-28.
4. Ayyadevara S, Balasubramaniam M, Gao Y, Yu LR, Alla R, Shmookler Reis R. Proteins in aggregates functionally impact multiple neurodegenerative disease models by forming proteasome-blocking complexes. *Aging cell* 2015; 14:35-48.
5. Kim M, Sandford E, Gatica D, Qiu Y, Liu X, Zheng Y, Schulman BA, Xu J, Semple I, Ro SH, et al. Mutation in ATG5 reduces autophagy and leads to ataxia with developmental delay. *Elife* 2016; 5.
6. Komatsu M, Waguri S, Chiba T, Murata S, Iwata J, Tanida I, Ueno T, Koike M, Uchiyama Y, Kominami E, et al. Loss of autophagy in the central nervous system causes neurodegeneration in mice. *Nature* 2006; 441:880-4.
7. Pyo JO, Yoo SM, Ahn HH, Nah J, Hong SH, Kam TI, Jung S, Jung YK. Overexpression of Atg5 in mice activates autophagy and extends lifespan. *Nat Commun* 2013; 4:2300.
8. Williams A, Sarkar S, Cuddon P, Ttofi EK, Saiki S, Siddiqi FH, Jahreiss L, Fleming A, Pask D, Goldsmith P, et al. Novel targets for Huntington's disease in an mTOR-independent autophagy pathway. *Nat Chem Biol* 2008; 4:295-305.
9. Sarkar S, Perlstein EO, Imarisio S, Pineau S, Cordenier A, Maglathlin RL, Webster JA, Lewis TA, O'Kane CJ, Schreiber SL, et al. Small molecules enhance autophagy and reduce toxicity in Huntington's disease models. *Nat Chem Biol* 2007; 3:331-8.

10. Sarkar S, Davies JE, Huang Z, Tunnacliffe A, Rubinsztein DC. Trehalose, a novel mTOR-independent autophagy enhancer, accelerates the clearance of mutant huntingtin and alpha-synuclein. *J Biol Chem* 2007; 282:5641-52.
11. Li J, Kim SG, Blenis J. Rapamycin: one drug, many effects. *Cell metabolism* 2014; 19:373-9.
12. Tseng AS, Engel FB, Keating MT. The GSK-3 inhibitor BIO promotes proliferation in mammalian cardiomyocytes. *Chemistry & biology* 2006; 13:957-63.
13. Eskiocak B, Ali A, White MA. The estrogen-related receptor alpha inverse agonist XCT 790 is a nanomolar mitochondrial uncoupler. *Biochemistry* 2014; 53:4839-46.
14. Outeiro TF, Kontopoulos E, Altmann SM, Kufareva I, Strathearn KE, Amore AM, Volk CB, Maxwell MM, Rochet JC, McLean PJ, et al. Sirtuin 2 inhibitors rescue alpha-synuclein-mediated toxicity in models of Parkinson's disease. *Science* 2007; 317:516-9.
15. Nimmanapalli R, O'Bryan E, Huang M, Bali P, Burnette PK, Loughran T, Tepperberg J, Jove R, Bhalla K. Molecular characterization and sensitivity of STI-571 (imatinib mesylate, Gleevec)-resistant, Bcr-Abl-positive, human acute leukemia cells to SRC kinase inhibitor PD180970 and 17-allylamino-17-demethoxygeldanamycin. *Cancer research* 2002; 62:5761-9.
16. Parr C, Carzaniga R, Gentleman SM, Van Leuven F, Walter J, Sastre M. Glycogen synthase kinase 3 inhibition promotes lysosomal biogenesis and autophagic degradation of the amyloid-beta precursor protein. *Molecular and cellular biology* 2012; 32:4410-8.

**Reprints of
publications**



A novel autophagy modulator 6-Bio ameliorates SNCA/ α -synuclein toxicity

S. N. Suresh, Aravinda K. Chavalmame, Vidyadhara DJ, Haorei Yarreiphang, Shashank Rai, Abhik Paul, James P. Clement, Phalguni Anand Alladi & Ravi Manjithaya

To cite this article: S. N. Suresh, Aravinda K. Chavalmame, Vidyadhara DJ, Haorei Yarreiphang, Shashank Rai, Abhik Paul, James P. Clement, Phalguni Anand Alladi & Ravi Manjithaya (2017) A novel autophagy modulator 6-Bio ameliorates SNCA/ α -synuclein toxicity, *Autophagy*, 13:7, 1221-1234, DOI: [10.1080/15548627.2017.1302045](https://doi.org/10.1080/15548627.2017.1302045)

To link to this article: <https://doi.org/10.1080/15548627.2017.1302045>



© Jawaharlal Nehru Centre for Advanced Scientific Research. Published with license by Taylor & Francis© Jawaharlal Nehru Centre for Advanced Scientific Research



[View supplementary material](#)



Accepted author version posted online: 28 Mar 2017.
Published online: 20 Jun 2017.



[Submit your article to this journal](#)



Article views: 1285



[View related articles](#)



[View Crossmark data](#)



Citing articles: 2 [View citing articles](#)

A novel autophagy modulator 6-Bio ameliorates SNCA/ α -synuclein toxicity

S. N. Suresh^a, Aravinda K. Chavalmane^{a,†}, Vidyadhara DJ^c, Haorei Yarreiphang^c, Shashank Rai^{a,††}, Abhik Paul^b, James P. Clement^b, Phalguni Anand Alladi^c, and Ravi Manjithaya^{a,b}

^aMolecular Biology and Genetics Unit, Jawaharlal Nehru Centre for Advanced Scientific Research, Jakkur, Bangalore, India; ^bNeuroscience Unit, Jawaharlal Nehru Centre for Advanced Scientific Research, Jakkur, Bangalore, India; ^cDepartment of Neurophysiology, National Institute of Mental Health and Neuro Sciences, Bangalore, India

ABSTRACT

Parkinson disease (PD) is a life-threatening neurodegenerative movement disorder with unmet therapeutic intervention. We have identified a small molecule autophagy modulator, 6-Bio that shows clearance of toxic SNCA/ α -synuclein (a protein implicated in synucleopathies) aggregates in yeast and mammalian cell lines. 6-Bio induces autophagy and dramatically enhances autolysosome formation resulting in SNCA degradation. Importantly, neuroprotective function of 6-Bio as envisaged by immunohistology and behavior analyses in a preclinical model of PD where it induces autophagy in dopaminergic (DAergic) neurons of mice midbrain to clear toxic protein aggregates suggesting that it could be a potential therapeutic candidate for protein conformational disorders.

ARTICLE HISTORY

Received 14 March 2016
Revised 30 January 2017
Accepted 28 February 2017

KEYWORDS

6-Bio; autolysosomes; autophagy; high-throughput screening; MPTP; neurodegeneration, SNCA; TH



Introduction


Parkinson disease is the second most common neurodegenerative disorder affecting 1% of the aging population.¹ Motor abnormalities which are the major clinical clues for PD are first manifested when about 60% of the nigral DAergic neurons are lost,² decreasing dopamine levels. Although L-DOPA has been recommended for PD patients, it does not halt neurodegeneration. Furthermore, the predominant side effect of continuous L-DOPA administration is an occurrence of L-DOPA-induced dyskinesia among PD patients.³ Thus, there is an absolute need for better therapeutic agents to be made available for PD patients, aiming to stop or reduce neurodegeneration.

One of the hallmarks of PD is formation of misfolded protein aggregates (Lewy bodies) due to overexpressed SNCA or mutation in genes such as *PINK1* (PTEN induced putative kinase 1), *LRRK2* (leucine rich repeat kinase 2) that leads to death of DAergic neurons. The accumulation of these aggregates disrupts proteostasis machineries such as chaperones, proteasome or macroautophagy (hereafter autophagy) leading to neuronal degeneration.⁴ Misfolded SNCA aggregates are refractory to proteostasis maintaining processes and the resultant cytotoxicity is further exasperated by aging, as unlike mitotic cells, nondividing neurons cannot dilute out these aggregates.⁴ In accordance, neuronal specific loss of autophagy function leads to aggregate formation and subsequent neurodegeneration suggesting a role for basal autophagy in preventing aggregate

buildup.^{5–7} As autophagy is dysfunctional in many neurodegenerative disorders,⁴ several studies have pointed out that restoring proteostasis by upregulating autophagy can eliminate these protein aggregates and restore cellular homeostasis.^{8–10}

One of the main causes of this disease is the toxic buildup of protein aggregates leading to neuronal death. We screened for small molecule drug-like compounds that clear such protein aggregates (aggrephagy) and restore cell viability. Several model systems were used to identify and evaluate the small molecules for aggrephagy. Toward this, rather than a conventional structure based drug designing, we sought for a phenotypic-based small molecule screening in yeast and validated the results in higher model systems. In this study, we identified a small molecule 6-Bio for its ability to clear SNCA aggregates and restore cellular homeostasis. We further show that 6-Bio induces autophagy and strongly drives autophagy flux resulting in aggregate clearance. We elucidated that 6-Bio modulates autophagy flux through inhibiting GSK3B activity. GSK3B has been associated with Alzheimer disease pathogenesis by modulating 2 processes namely (i) β -amyloid buildup and (ii) formation of neurofibrillary tangles.¹¹ It has been demonstrated at cellular level experiments that inhibiting GSK3B would ablate the expression of SNCA¹² suggesting its role in synucleopathies. Finally, in a preclinical mouse model of PD, 6-Bio showed potent neuroprotective ability revealed by immunohistological and behavior analyses.

CONTACT Ravi Manjithaya  ravim@jncsar.ac.in  Assistant Professor (Faculty Fellow), Molecular Biology and Genetics Unit, Associate Faculty, Neuroscience Unit, Jawaharlal Nehru Centre for Advanced Scientific Research, Jakkur, Bangalore 560 064, India.

 Supplemental data for this article can be accessed on the [publisher's website](#).

[†]Present address - School of Biological Sciences, Nanyang Technological University, Singapore.

^{††}Present address - Bio-Medical Research Centre, Faculty of Medicine and Health, University of East Anglia, United Kingdom.

© Jawaharlal Nehru Centre for Advanced Scientific Research. Published with license by Taylor & Francis.

This is an Open Access article distributed under the terms of the Creative Commons Attribution-Non-Commercial License (<http://creativecommons.org/licenses/by-nc/3.0/>), which permits unrestricted non-commercial use, distribution, and reproduction in any medium, provided the original work is properly cited. The moral rights of the named author(s) have been asserted.

Results

Small-molecule screening reveals 6-Bio as a potent inducer of autophagy

The occurrence of protein aggregates and cytotoxicity by SNCA overexpression is also recapitulated in the budding yeast, *Saccharomyces cerevisiae* (Fig. S1, A to C).¹³ We used this “out-of-the-box” yeast model¹⁴ to screen for small molecules that would prevent cytotoxicity by aggregate degradation. We screened a small molecule library containing pharmacologically active compounds (LOPAC¹²⁸⁰) using an SNCA yeast toxicity assay (Fig. 1A, Fig. S2). Of the hits that rescued growth in this model was the SIRT2 inhibitor AGK2, which was shown to rescue SNCA toxicity¹⁵ affirming the reliability of the assay, and the compound 6-Bio [(2′Z,3′E)-6-Bromoindirubin-3′-oxime]¹⁶ (Fig. S3A). Interestingly, 6-Bio did not affect the growth of yeast cells (Fig. 1B). To understand the involvement of 6-Bio in autophagy, GFP-Atg8 (GFP tagged autophagy-related 8, a yeast autophagosome marker)-processing assay under both growth and starvation conditions were used. During growth conditions where autophagy is barely detectable, 6-Bio dramatically induced autophagy (6 h time point, $P < 0.001$ vs untreated; Fig. 1C) and also the flux (6 h time point, $P < 0.001$ vs untreated; Fig. 1C). Similarly, 6-Bio treatment under starvation condition showed significant increase in autophagy induction (4 h and 6 h time points, $P < 0.001$ vs untreated; Fig. 1D) and flux (4 h and 6 h time points, $P < 0.01$ and $P < 0.001$, respectively vs untreated; Fig. 1D) by 2-fold in a time-dependent manner suggesting 6-Bio augmented starvation-induced autophagy.

We further tested 6-Bio for autophagy modulation in mammalian cells. Toward this, we used MAP1LC3B/LC3B (microtubule associated protein 1 light chain 3 β , a mammalian autophagosome marker and an ortholog of yeast Atg8) processing and tandem RFP-GFP-LC3B assays. In HeLa cells, 6-Bio increased LC3B-II (the autophagosome-associated, processed form of LC3B-I) levels in a dose-dependent manner suggesting autophagy modulation (Fig. 3A). In the presence of lysosomal protease inhibitors, E64D and pepstatin A, LC3B-II accumulation was significantly more than that of 6-Bio only and/or E64D and pepstatin A only (Fig. S9, A and B), validating that 6-Bio is indeed an autophagy enhancer. In the tandem RFP-GFP-LC3B assay that reveals autophagy flux, 6-Bio treatment dramatically increased autolysosome numbers (~9-fold, $P < 0.001$, compared with control; Fig. 1E) indicating enhanced fusion of autophagosomes with lysosomes.

Next, we checked whether the lysosomal functions are perturbed by 6-Bio since it specifically enhances autolysosomes. For this, we checked the lysosomal pH by LysoTracker Deep Red staining upon 6-Bio treatment. HeLa cells were treated with 6-Bio and/or E64D plus pepstatin A for 2 h, followed by treatment with LysoTracker Deep Red for 20 min. LysoTracker Deep Red fluorescence intensity was reduced in presence of protease inhibitors such as E64D and pepstatin A (Pep A). The fluorescence intensity of LysoTracker Deep Red was found to be comparable between untreated and 6-Bio-treated cells (Fig. S10B). Thus, we found no difference in both E64D + pep A only, 6-Bio and E64D + pep A treatments (Fig. S10B).

LysoTracker Deep Red staining indicated that there was no change in lysosome acidification (Fig. S10). LAMP1 (lysosomal associated membrane protein 1)-positive vesicle intensities and distribution also were unaltered upon 6-Bio treatment suggesting that perhaps lysosomal functions were not perturbed by 6-Bio (Fig. S10A).

To address whether the molecule enters the cell via endocytosis, we performed the tandem RFP-GFP-LC3B assay at 16°C. At this temperature, endocytosis pathway is highly reduced as evident by the significantly decreased cellular uptake of FITC-dextran (70 kDa) as compared with 37°C (Fig. S11C). However, the effect of 6-Bio in increasing fusion between autophagosomes and lysosomes at 37°C (~10-fold, control vs 6-Bio-treated, $P < 0.001$, Fig. S11, A and B) and 16°C (~8-fold, control vs 6-Bio-treated, $P < 0.001$, Fig. S11, A and B) were comparable suggesting that endocytosis did not play a predominant role in the action of 6-Bio in modulating autophagy. These results suggest that 6-Bio affects autophagy independent of endocytosis perhaps by passive diffusion.

From these 2 model systems, we noticed that 6-Bio not only induces autophagy but also enhances starvation-induced autophagy and strikingly promotes autolysosome formation without perturbing the lysosomal function.

6-Bio clears SNCA in an autophagy-dependent manner

Treatment of yeast cells overexpressing SNCA-GFP with 6-Bio, resulted in vacuolar degradation of SNCA-GFP cytosolic aggregates with improved normal plasma membrane localization suggesting possible involvement of autophagy-related pathways (Fig. 2A). In agreement with these observations, 6-Bio failed to rescue the SNCA-mediated toxicity in autophagy gene mutants (*atg1 Δ* , *atg5 Δ* , *atg8 Δ* , *atg11 Δ* and *atg15 Δ*) (Fig. S3B).

Assays performed to monitor degradation of SNCA-GFP aggregates in presence of 6-Bio under nonstarvation and starvation conditions revealed a time-dependent and significant decrease in the SNCA-GFP levels in wild-type cells (Fig. 2, B and D and Fig. S4, B and C) but not in an autophagy mutant, *atg1 Δ* (Fig. 2, C and E and Fig. S4, D and E). These results suggest that 6-Bio treatment was not only able to enhance starvation-induced autophagy but also resulted in a concomitant decrease of SNCA-GFP demonstrating that the prosurvival effects of 6-Bio was due to autophagy-dependent SNCA-GFP clearance.

Next, using an SNCA degradation assay model in a human neuroblastoma cell line (SH-SY5Y) overexpressing GFP-SNCA, we observed that 6-Bio significantly reduced GFP-SNCA levels (~2-fold, $P < 0.001$ vs untreated). However, in the presence of the autophagy inhibitor 3-methyladenine (3-MA), the GFP-SNCA levels did not change upon 6-Bio cotreatment suggesting that autophagy was the primary mechanism for degradation (as also seen in the yeast model) (Fig. 2, C and E; Fig. 2F and Fig. S4, D and E). As MTOR (mechanistic target of rapamycin) negatively controls autophagy, we tested if 6-Bio affected MTOR signaling. 6-Bio decreased phosphorylation levels of RPS6KB1/p70s6K (ribosomal protein S6 kinase B1) and EIF4EBP1/4E-BP1 (eukaryotic translation initiation factor 4E binding protein 1) in a dose-dependent manner (Fig. 3A),

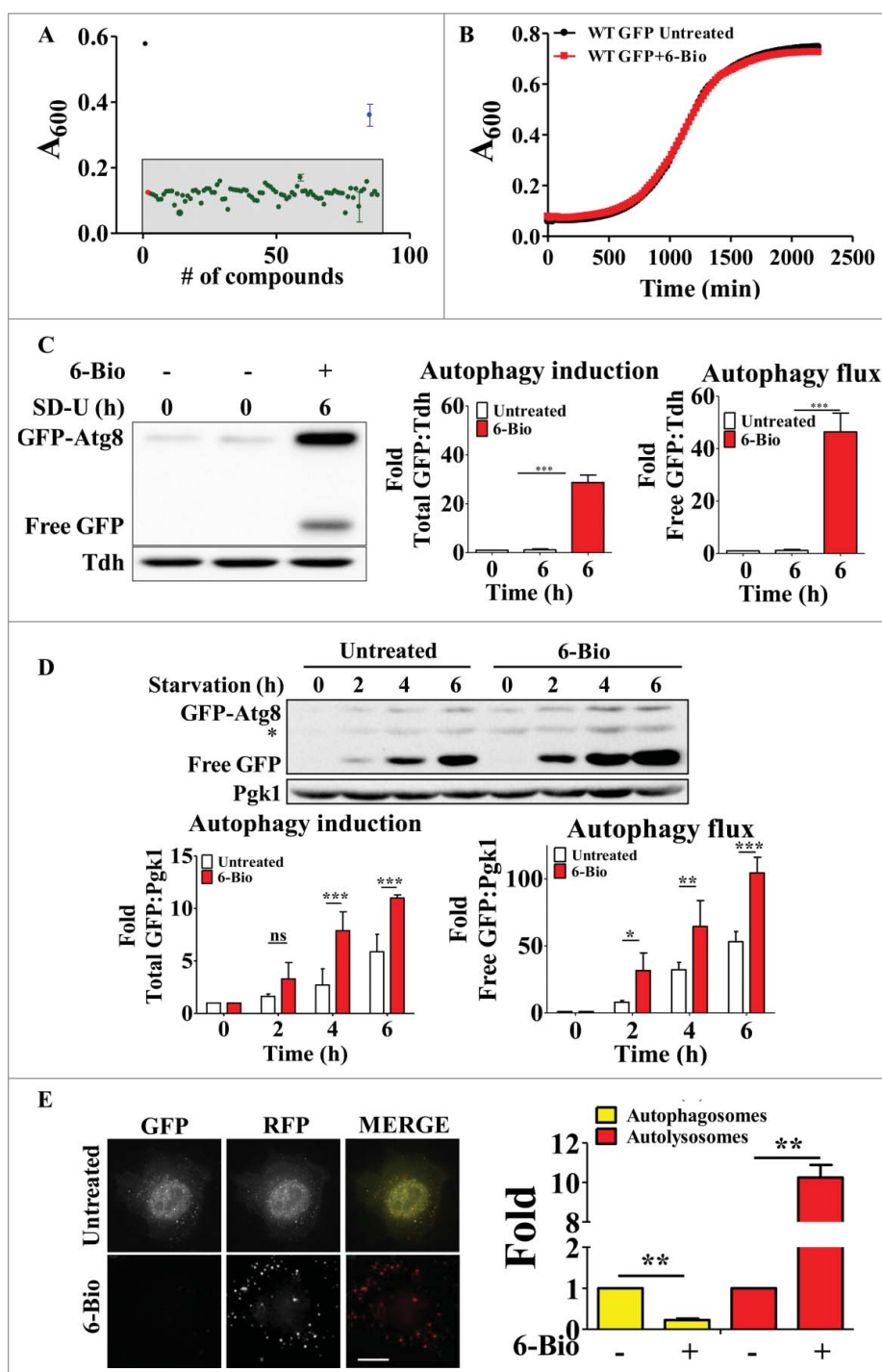


Figure 1. 6-Bio induces autophagy. (A) Box plot demonstrating hits from a small molecule library of pharmacologically active compounds, LOPAC¹²⁸⁰, screened in *S. cerevisiae* toxicity model of SNCA. Detailed screening methodology is explained in the methods section. In the box plot, compounds that rescued the growth (denoted by absorbance, A_{600}) of WT SNCA-GFP strains ≥ 3 SD units (gray box) are considered hits (blue) and the ones that do not are in green. WT GFP (black) and untreated WT SNCA-GFP (red) represent the positive and negative controls. A representative plot for 100 compounds is shown. (B) Growth curve of WT GFP cells with or without 6-Bio (50 μ M) treatment. (C) Representative western blot of the GFP-Atg8-processing assay under growth condition. WT strain expressing GFP-Atg8 treated with or without 6-Bio (50 μ M). Fusion protein GFP-Atg8 accumulation and free GFP release was monitored across the time course (0 and 6 h). Tdh reactivity served as a loading control. Representative graph for quantification of autophagic induction and flux ($n = 4$). (D) Representative western blot for the GFP-Atg8-processing assay. Fusion protein GFP-Atg8 accumulation and free GFP release monitored across the time course (0, 2, 4 and 6 h) under starvation conditions in the WT strain expressing GFP-Atg8 treated with 6-Bio (50 μ M). Representative graph for quantification of autophagic induction and flux ($n = 3$); * indicates nonspecific band. Pgk1 was assessed as loading control. (E) Representative microscopy images of ptf LC3B transfected HeLa cells treated with 6-Bio (5 μ M) and quantification of autophagosome and autolysosome indicating fold change over its untreated counterpart ($n = 25$), scale bar: 15 μ m. Statistical analysis was performed using the Student unpaired t test, 2-way ANOVA and the post-hoc Bonferroni test. Error bars, mean \pm SEM ns-nonsignificant, * $P < 0.05$, ** $P < 0.01$, *** $P < 0.001$.

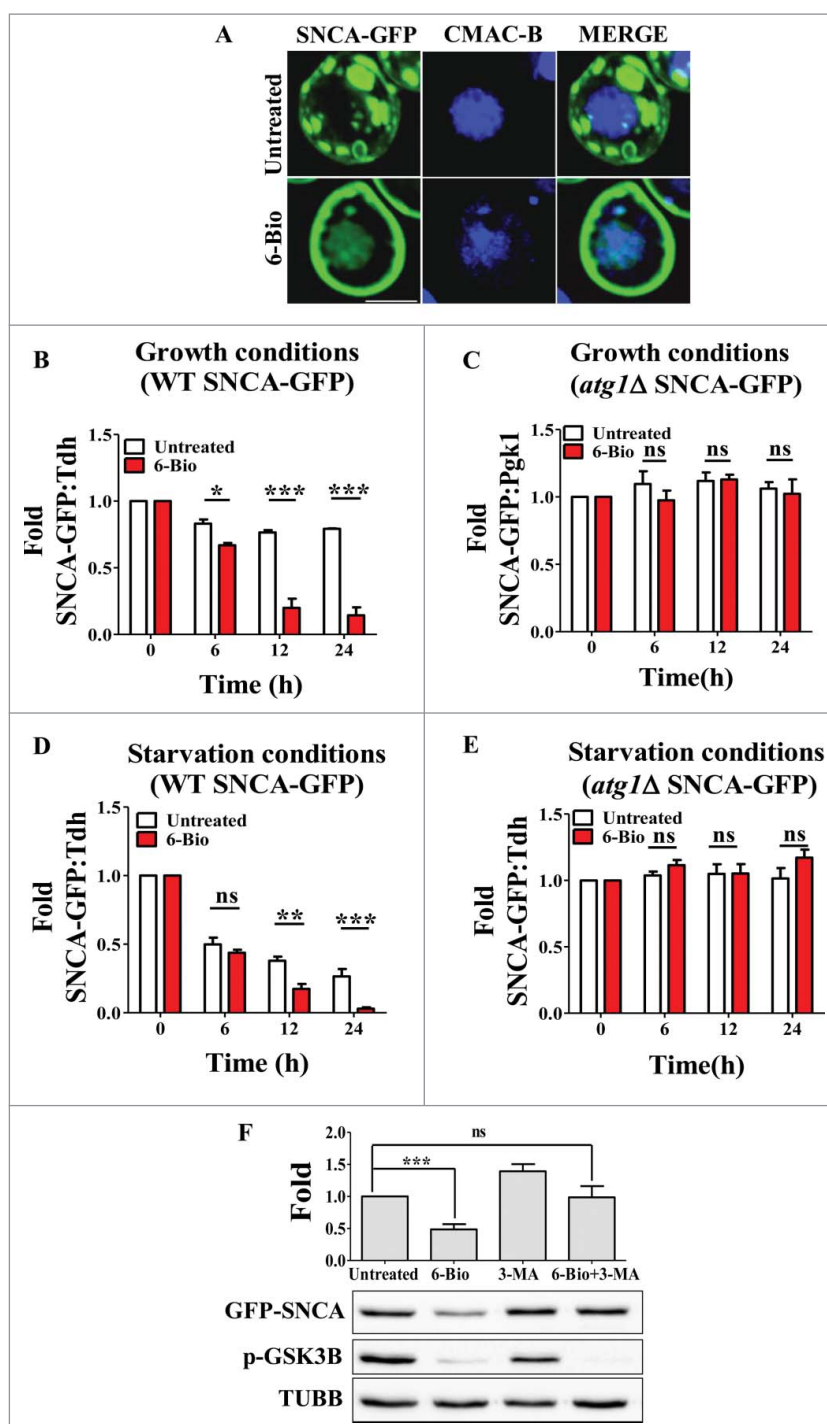


Figure 2. 6-Bio clears SNCA in an autophagy-dependent manner. (A) Microscopy images of WT SNCA-GFP yeast cells treated with or without 6-Bio (50 μ M) for 16 h, vacuole stained with CMAC-Blue (100 nM), scale bar: 2 μ m. (B) to (E) Quantification plots for SNCA-GFP degradation assay in wild-type (WT) yeast strain for growth (B) and starvation (D) conditions. SNCA-GFP degradation assay in the autophagy mutant (*atg1Δ*) strain under the given growth (C) and starvation (E) conditions (assay details are explained in Fig. S4A). SNCA-GFP protein levels after 6-Bio (50 μ M) treatment are analyzed for different time points (0, 6, 12 and 24 h). Tdh reactivity was used as loading control. (F) GFP-SNCA transiently transfected in SH-SY5Y cells were allowed to express for 24 h, treated with 6-Bio (5 μ M), 3-MA (5 mM) or both for 24 h post-transfection and assessed for GFP-SNCA degradation. Western blot (below) and graph (above) indicating fold change in GFP-SNCA degradation over untreated. TUBB was used as a loading control. Statistical analysis was performed using 2-way ANOVA and the post-hoc Bonferroni test. Error bars, mean \pm SEM ns-nonsignificant, * P < 0.05, ** P < 0.01, *** P < 0.001.

indicating 6-Bio negatively regulated MTOR signaling. During normal growth conditions, MTOR is active (and phosphorylates RPS6KB1 and EIF4EBP1) and autophagy is suppressed. Addition of 6-Bio results in autophagy induction by suppression of MTOR activity as revealed by diminished phosphorylation of its substrates RPS6KB1 and EIF4EBP1. 6-Bio is a potent

GSK3B inhibitor and reduced phosphorylated (p)-GSK3B indicates its reduced activity¹⁷ (Fig. 3A and Fig. 2F). These assays confirmed that 6-Bio treatment not only induced autophagy but also enhanced the autophagic flux by promoting autophagosome fusion with lysosomes in an MTOR-dependent manner.

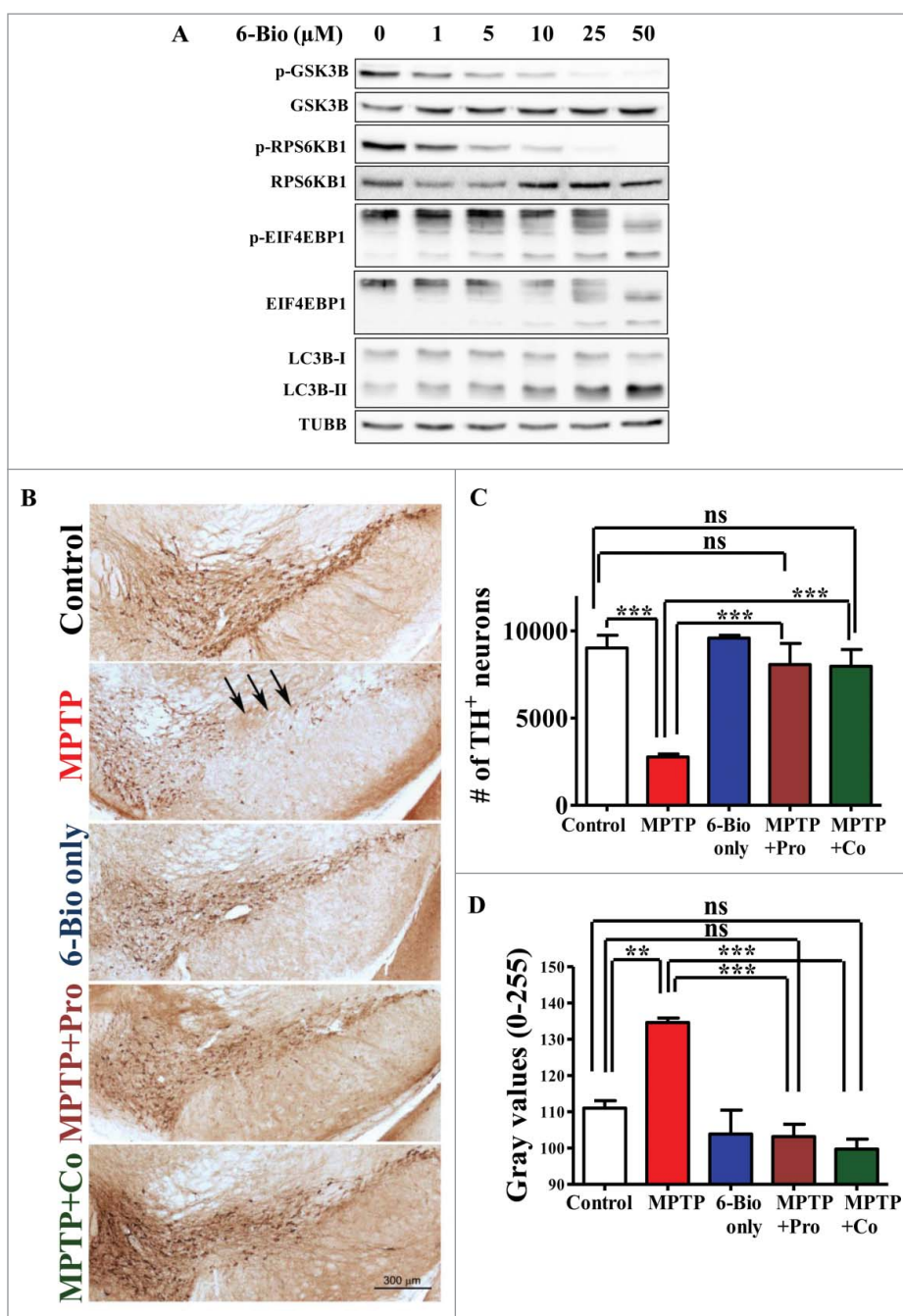


Figure 3. 6-Bio enhances MTOR-dependent autophagy and confers neuroprotection in a mouse MPTP toxicity model. (A) Representative western blots indicating dose-dependent modulation of autophagy related proteins (LC3B, RPS6KB1 and EIF4EBP1) by 6-Bio in HeLa cells. TUBB was used as a loading control. (B) to (D) Representative photomicrographs of TH⁺ immunostained DAergic neurons (B) in SNpc (arrow) of mouse midbrain. Placebo control cohort, MPTP-treated (23.4 mg/kg body weight), 6-Bio (5 mg/kg body weight) or both [Prophylaxis (MPTP+Pro)/Coadministration (MPTP+Co)], scale bar: 300 μm. Stereological (C) and densitometric quantification (D) indicating the number of TH⁺ DAergic neurons and their intensity in SNpc neurons. Statistical analysis was performed using the Student unpaired *t* test, one-way ANOVA and the post-hoc Bonferroni test. Scale bar: 50 μm. Error bars, mean ± SEM ns-nonsignificant, ***P* < 0.01, ****P* < 0.001.

Autophagy-dependent GSK3B-mediated neuro(cyto) protection by 6-Bio

We observed the significant reduction of GSK3B activity upon 6-Bio treatment as revealed by the reduced p-GSK3B levels (Fig. 2F and Fig. 3A). To understand the GSK3B dependency of autophagic activity by 6-Bio, we performed the knockdown studies in SH-SY5Y cells. For this, GSK3B shRNA was transiently transfected into cells and after 48 h the GSK3B protein levels were reduced significantly (Fig. S8A). In SH-SY5Y cells,

when SNCA was overexpressed for 72 h, the cell viability was significantly affected (Fig. S8D). When these cells were treated with 6-Bio, its viability was significantly increased and comparable to that of control (Fig. S7). Similar protection was noted in GSK3B-silenced SNCA-overexpressing cells. When GSK3B expression was silenced, addition of 6-Bio only showed marginal cytoprotection as compared with untreated cells with normal GSK3B expression (Fig. S8D). In fact, in silenced cells, 6-Bio was not effective in cytoprotection over and above that offered by silencing GSK3B but was cytotoxic (Fig. S8D). In

addition, another GSK3B inhibitor, compound VIII also exerted protection against SNCA-mediated toxicity (Fig. S8D). Using a direct readout for autophagy (tandem RFP-GFP-LC3B assay), we used a similar silencing strategy to address the GSK3B and autophagy interplay in the presence of 6-Bio. In GSK3B-silenced cells, the autolysosomes were increased with concomitant reduction in autophagosomes than that of its scrambled shRNA control ($P < 0.001$, Fig. S8, B and C). Interestingly, the autophagosomes and autolysosomes formed in GSK3B-silenced cells were similar to that of 6-Bio treatment. Notably, the autolysosomes formed in 6-Bio-treated, GSK3B-silenced cells were significantly reduced than that of cells treated only with 6-Bio ($P < 0.001$, Fig. S8, B and C). Although 6-Bio is known to affect other signaling pathways such as PDK1 (pyruvate dehydrogenase kinase 1) and JAK-STAT3 [(Janus kinase)-(signal transducer and activator of transcription 3)],¹⁸ our results suggest that 6-Bio primarily modulates autophagy in a GSK3B-dependent manner.

6-Bio confers neuroprotection in a mouse MPTP-toxicity model

We then investigated the effect of 6-Bio in one of the widely used preclinical models of PD, MPTP (1-methyl-4-phenyl-1,2,3,6-tetrahydropyridine) mouse model.¹⁹ It was reported that 7 d post MPTP administration results in ~70% DAergic neuronal loss in the substantia nigra pars compacta (SNpc) region of brain which leads to 80% to 90% reduction in dopamine levels in the striatum.¹⁹ In this model, 6-Bio was administered [5mg/kg, intraperitoneally (i.p.)] in 2 different regimen (Fig. S5A): on the same day of MPTP injections (coadministration, Co) or 2 d prior (prophylactic, Pro). In both cases, 6-Bio treatment was continued for 7 d post- MPTP administration. We then evaluated the status of DAergic neurons in SNpc. These neurons were identified by TH (tyrosine hydroxylase) immunolabeling and were quantitated by unbiased stereology and densitometry analysis. As expected, the number and health of DAergic neurons (as revealed by TH staining intensities) were significantly reduced in MPTP-treated mice (~3-fold, $P < 0.001$ compared with placebo; Fig. 3, B to D and Fig. S5B). Strikingly, in both the 6-Bio treatment regimen, the number of DAergic neurons resembled almost that of placebo or animals injected with 6-Bio only (Co or Pro ~2.5-fold vs MPTP, $P < 0.001$; Fig. 3, B to D and Fig. S5B). In addition, the decrease in SNpc volume upon MPTP administration was not seen in 6-Bio-treated cohort ($P < 0.001$ vs Co, $P < 0.01$ vs Pro; Fig. S5C). These observations in mouse model of PD reassert the neuroprotective nature of 6-Bio.

6-Bio enhances autophagy and clears toxic protein aggregates in mouse brains

We then evaluated the autophagy and toxic aggregate levels in the DAergic neurons in SNpc of midbrain. We observed the significant reduction of LC3B puncta per neuron in the MPTP-treated cohort than that of placebo (~1.8-fold, placebo vs MPTP, $P < 0.001$, Fig. 4, A and B). Conversely, APP/amyloid β oligomer/A11 puncta were significantly higher (~7-fold, placebo vs MPTP, $P < 0.001$, Fig. 4, C and D). Along with

decreased autophagy, these SNpc (TH⁺) neurons displayed toxic aggregate buildup. This reduced autophagy upon administration of MPTP is in agreement with previous observations.²⁰ Furthermore, as seen in cell culture models, 6-Bio treatment alone increased LC3B puncta per neuron (~2-fold, placebo vs 6-Bio only, $P < 0.001$, Fig. 4, A and B) suggesting that 6-Bio could induce autophagy in mice brain by crossing the blood-brain barrier (Fig. S13). When 6-Bio was coadministered along with MPTP, LC3B puncta per neuron increased (~2.5-fold, MPTP vs MPTP+Co, $P < 0.001$, Fig. 4, A and B) with a significant reduction in APP/amyloid β oligomer/A11-positive aggregates (~7-fold, MPTP vs MPTP+Co cohort, Fig. 4, C and D). Strikingly, the aggregate numbers in MPTP+Co were comparable to that of control suggesting that the 6-Bio treatment decreased the toxic aggregates to that of placebo neurons (placebo vs MPTP+Co, ns, $P > 0.05$, Fig. 4, C and D). These results imply that autophagy was drastically induced in the MPTP and 6-Bio coadministered cohort that lead to neuroprotection by clearance of the toxic aggregates. We observed reduced p-GSK3B signals in DAergic neurons of the 6-Bio-treated cohorts, namely, 6-Bio only and MPTP+Co (Fig. S13).

6-Bio ameliorates MPTP-induced behavioral deficits

To study whether 6-Bio can combat the MPTP-induced behavioral impairments in motor coordination, locomotion and exploration abilities, we used 2 widely used behavior tests namely rotarod and the open field test. Stereology were performed on d 7 post MPTP or placebo administrations, thus behavior experiments were conducted on d 13 i.e., d 7 post MPTP or placebo administrations. Behavior study scheme is illustrated in Fig. S6.

In rotarod test, the latency to fall for MPTP cohort reduced significantly to that of placebo cohort on d 13 postadministration (MPTP vs placebo, $P < 0.001$, Fig. 5A and Fig. S6, A and B) validating the MPTP-induced motor deficits in mice. Strikingly, the latency to fall was increased in the 6-Bio-treated cohort compared with that of MPTP-treated cohort (Co vs MPTP, $P < 0.001$, Fig. 5A and Fig. S6, B and C). The latency to fall for the 6-Bio-treated cohort was comparable with the placebo cohort (Co d 7 vs placebo, $P > 0.05$, Fig. 5A and Fig. S6, A and C).

Similar to the lack of motor coordination observed in rotarod, the total distance traveled by MPTP-treated cohort in the open field test arena on d 13 postinjection was reduced significantly compared with that of placebo (MPTP vs placebo, $P < 0.001$, Fig. 5B, C and Fig. S6, A and B) affirming the MPTP-induced locomotion and exploratory impairments. These impairments were reduced after 6-Bio administration as the distance traveled by mice increased dramatically (Co vs MPTP, $P < 0.001$, Fig. 5, B and C and Fig. S6, B and C) and matched control cohorts (Co vs placebo, $P > 0.05$, Fig. 5, B and C and Fig. S6, A and C). MPTP-induced impairments were not protected by 6-Bio when administered after 48 h of MPTP (Post vs MPTP, $P > 0.05$, Fig. 5, D and E and Fig. S6, B and D).

Since the 6-Bio-treated cohort spent more time on the rotarod (as the placebo cohort) and traveled more distance in open field unlike MPTP-treated, we therefore, can infer that 6-Bio rescued the MPTP-induced motor, locomotion and

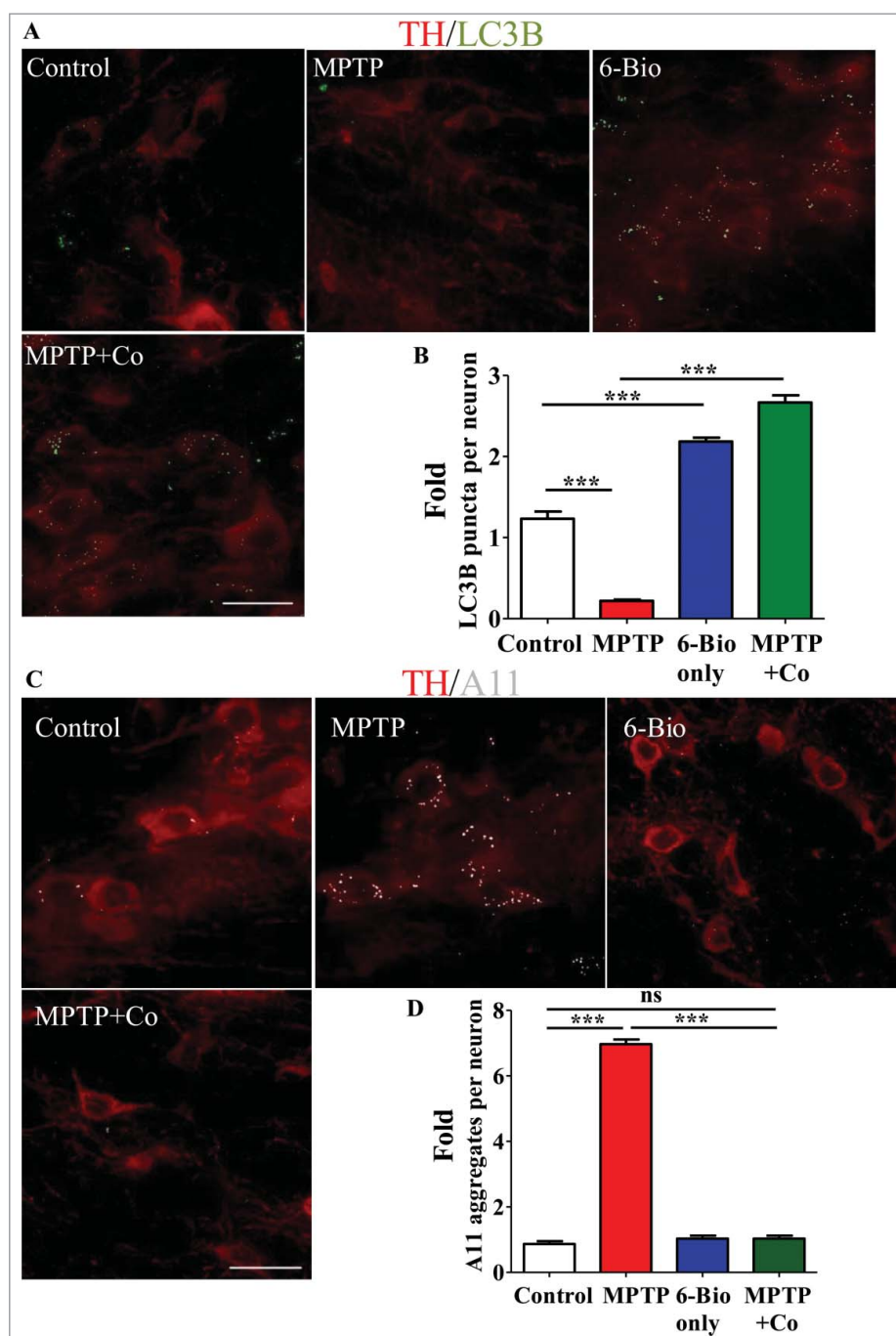


Figure 4. 6-Bio induces autophagy in mice brain to clear toxic protein aggregates. (A) Representative immuno-histofluorescent photomicrographs of various cohorts namely control, MPTP (23.4 mg/kg of body weight), 6-Bio (5 mg/kg of body weight) and MPTP+Co that were stained for LC3B (an autophagy marker) and TH (SNpc) in midbrain. Autophagic modulation by 6-Bio were evaluated in DAergic neurons in SNpc and the LC3B puncta fold change per neuron was quantified (B). (C) Representative immuno-histofluorescent photomicrographs of the above mentioned cohorts were stained for APP/amyloid β oligomer/A11 (toxic oligomers) and TH (SNpc) in midbrain. Aggregate clearance by 6-Bio were evaluated in DAergic neurons in SNpc and the APP/amyloid β oligomer/A11 puncta fold change per neuron was quantified (D). Statistical analysis was performed using one-way ANOVA and the post-hoc Bonferroni test. Scale bar: 50 μ m. Error bars, mean \pm SEM ns-nonsignificant, ***- $P < 0.001$.

exploratory impairments. We observed that 6-Bio failed to protect the MPTP-induced behavioral deficits when administered 48 h after MPTP dosage.

Discussion

Using an unbiased yeast high-throughput assay, we identified the small molecule 6-Bio that rescued SNCA cytotoxicity in an autophagy-dependent manner. 6-Bio induced autophagy even

in growth conditions. Mechanistically, 6-Bio profoundly promoted autophagosome-lysosome fusion as reflected in the high autolysosome numbers with hardly any unfused autophagosomes. Increased autophagy induction and fusion resulted in degradation and clearance of aggregated proteins with a concomitant rescue of cell viability and growth. When tested in a preclinical model of PD, 6-Bio demonstrated remarkable neuroprotection revealed by both immunohistology and behavioral analyses.

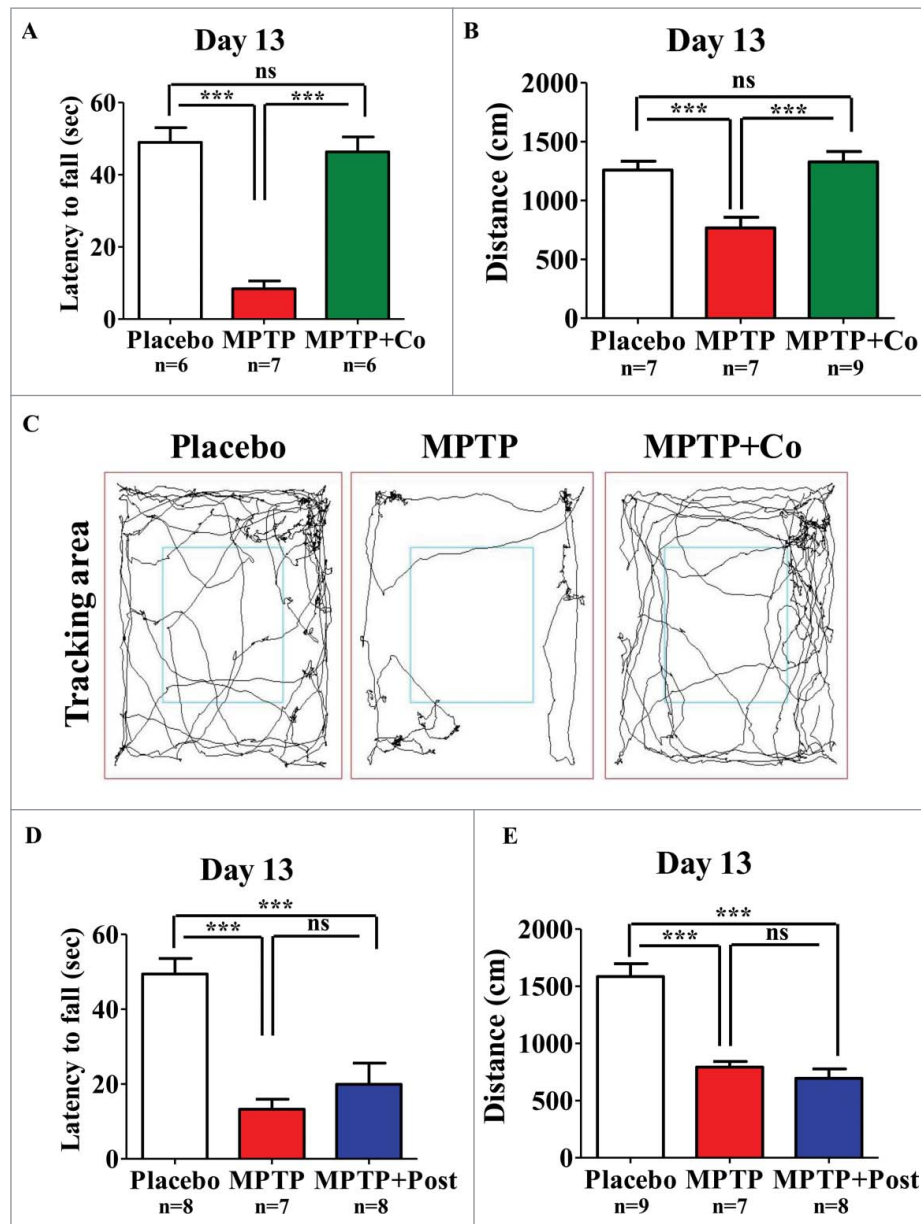


Figure 5. 6-Bio ameliorates MPTP-induced behavioral deficits. Effect of 6-Bio (5 mg/kg) on (A) latency to fall of various cohorts namely Placebo, MPTP and MPTP+Co as assessed by rotarod test (B) Representative trajectory maps of all mentioned cohorts as analyzed by open field test. (C) Periphery distance traveled by all indicated cohorts as assessed by open field test. Effect of 6-Bio (5 mg/kg) on various cohorts namely Placebo, MPTP and MPTP+Post. (D) latency to fall of various cohorts namely Placebo, MPTP and MPTP+Post as assessed by rotarod test. (E) Periphery distance traveled by all indicated cohorts as assessed by the open field test. Both the rotarod and open field behavior analyses were performed on d 13 or d 7 post MPTP or vehicle administrations. 6-Bio (5 mg/kg) was administered either along with MPTP (MPTP+Co) or post 48 h of MPTP administration (MPTP+Post). Dosage regimens are illustrated in Fig. S4. Statistical analysis was performed using one-way ANOVA and the post-hoc Bonferroni test. Scale bar: 50 μ m. Error bars, mean \pm SEM ns-nonsignificant, ***- $P < 0.001$.

Apart from toxic accumulation of SNCA aggregates as Lewy bodies, proteostasis machineries such as autophagy are also defunct in these dying neurons.⁷ While autophagosome formation has been shown to be defective in PD,⁴ its accumulation has been documented in the striata of human PD postmortem brains.²¹ Also, recent reports suggest that apart from having a misfolding propensity, prion-like properties²² of SNCA are responsible for its spreading across neurons leading to aggravated neuronal death. Hence, enhancing SNCA clearance through modulating autophagy would be beneficial.

We show here using 2 model systems that aggregate clearance by 6-Bio is through autophagy: using yeast genetics, our

studies reveal that 6-Bio is unable to rescue SNCA-mediated cytotoxicity in autophagy-defective mutants, while in mammalian cells, pharmacological inhibition of autophagy by 3-MA abolishes 6-Bio effect. In addition, although 6-Bio (50 μ M) does not affect the growth of yeast cells, it strikingly increases basal autophagy even in growth conditions, a situation where MTOR is active and is known to suppress autophagy. Interestingly, 6-Bio induction of autophagy in mammalian cells appears to be MTOR dependent. Furthermore, 6-Bio not only augments basal autophagy but also enhances the starvation induced autophagy, demonstrating its strong autophagy modulating potential. It is these properties that lead to a dramatic

buildup of autolysosomes upon 6-Bio treatment. Enhanced cargo degradation thus leads to clearing up of the aggregates and preventing cytotoxicity by restoring cellular proteostasis.

The MPTP+6-Bio-treated cohort spent more time on the rotarod (as the placebo cohort) and traveled more distance in open field unlike the MPTP-treated cohort, we therefore can infer that 6-Bio rescued the MPTP-induced motor, locomotion and exploratory impairments. Importantly, 6-Bio-induced behavioral performances were indistinguishable from that of the placebo cohort. Thus, histological and behavioral analyses of the MPTP-induced preclinical mouse model of PD highlights the neuroprotective abilities of 6-Bio as demonstrated by preservation of nigral DAergic neurons and retention of motor coordination functions. After 48 h of MPTP administration, most of the DAergic neurons would be ablated. Thus after 48 h of MPTP treatment, with highly depleted SNpc of DAergic neurons, 6 Bio was unable to rescue behavioral deficits. These results suggest that 6-Bio primarily acts through restoring autophagy function in the neurons to get rid of aggregates and perhaps does not have neuroregenerative capabilities. Strikingly, our experiment revealed that 6-bio enters the brain within 15 min after intraperitoneal administration and stayed as long as 24 h (Table S2). The dramatic neuroprotection could be due to abundance of 6-Bio in the mice brain that facilitates aggregate clearance through inducing autophagy.

Our studies with other GSK3B inhibitors (with similar inhibitory potencies) reveal that none of these can bring about autophagy induction as profoundly as 6-Bio (data not shown). Though 6-Bio has been shown to modulate GSK3, PDK1 and JAK-STAT3 signaling pathways,¹⁸ our results demonstrated that it modulates autophagy in GSK3B dependent manner. 6-Bio docks with GSK3B better than other inhibitors such as indirubin, hymenialdisine and meridianins.²³ It also increases the accumulation of CTNNB1/ β -catenin due to the inhibition GSK3B, thus promoting aggression of breast cancer cells.²⁴ 6-Bio also indirectly activates canonical WNT5A signaling in the hippocampal neurons to protect them from A β oligomers.¹² Proof-of-principle demonstrations at the cellular level reveal that inhibiting GSK3B reduces SNCA expression²⁵ and also results in β -amyloid clearance.²⁶ Thus, GSK3B would be an attractive avenue as a therapeutic target for neurodegeneration. In PD, autophagy is dysfunctional as the steps of autophagosome biogenesis⁴ and the fusion between autophagosome and lysosome are blocked.²⁷ Because 6-Bio dramatically enhances autophagosome-lysosome fusion by inhibiting GSK3B through crossing the blood-brain barrier, it decreases the dramatic toxic protein aggregates in SNpc. Therefore, 6-Bio could be a promising candidate with therapeutic potential especially in case of synucleopathies including PD.

Our findings demonstrate that the neuroprotective role of 6-Bio is due to its autophagosome-lysosome fusion-enhancing function, which results in SNCA aggregate clearance, and thus may have therapeutic potential for patients with PD and protein conformational disorders.

Methods

Chemicals and antibodies

Yeast extract (RM027), peptone (RM667), dextrose (GRM077), galactose (RM101) and amino acids [leucine (GRM054),

methionine (GRM200), histidine (RM051) and uracil (RM264)] were purchased from HiMedia. 3-MA (M9281), 6-Bio (B1686), LOPAC (LO1280), anti-LC3B antibody (L7543), MPTP (methyl-4-phenyl-1,2,3,6-tetrahydropyridine, M0896), DMEM (D5648), DMEM F-12 (D8900), penicillin and streptomycin (P4333), DAB (3,3'-Diaminobenzidine, D3939), Atto 663 (41176), lysine (L5501) and trypsin EDTA (59418C) were purchased from Sigma-Aldrich. Anti-p-RPS6KB1 T389 antibody (9862) and total RPS6KB1 antibody (9202), anti-p-GSK3B S9 antibody (5558) and total GSK3B antibody (9315), anti-p-EIF4EBP1 T37/46 antibody (2855) and total EIF4EBP1 antibody (9452), anti-LAMP1 antibody (9091) and anti-rabbit IgG, horseradish peroxidase (HRP; 7074) antibody were purchased from Cell Signaling Technology. Anti TUBB/ β -Tubulin (MA5-16308) and anti Tdh (MA5-15738) antibodies were purchased from Thermo Scientific. Yeast does not express GAPDH but instead expresses 3 orthologs (Tdh1/2/3) of the mammalian protein, and that the antibody was raised against recombinant GAPDH (Thermo Scientific). While the antibody has been used in yeast studies, publication cannot be interpreted as validation unless there is supporting experimental data that the antibody indeed detects yeast Tdh. Anti-APP/amyloid β oligomer/A11 (AB9234) was purchased from Merck Millipore. Anti-Pgk1 (ab 38007) antibody was purchased from Abcam. Anti-GFP (11 814 460 001) antibody was purchased from Roche. Anti TH/tyrosine hydroxylase (N196) antibody was purchased from Santa Cruz Biotechnology. Anti-mouse IgG, HRP (172-1011) antibody was purchased from Bio-Rad. CMAC-Blue (C2110) was purchased from Life Technologies. Bafilomycin A₁ (11038) was purchased from Cayman chemical. VECTASTAIN Elite ABC Kit (PK-6200) was purchased from VECTOR laboratories.

Plasmid constructs, shRNA and yeast strains

Plasmids used were GFP-Atg8 (pRS316) [gift from Y. Oshumi (Tokyo Institute of Technology)], SNCA-GFP (pRS 306) under the galactose promoter (gift from Paulo Ludovico) and GFP- β A₁₋₄₂ (pRS306). ptfLC3B²⁸ (gift from Tamotsu Yoshimori; Addgene, 21074), GFP-SNCA²⁹ (gift from David Rubinzstein; Addgene, 40822). pLKO.1-GSK3B-#1 was a gift from Alex Toker³⁰ (Addgene, 32496). Scrambled shRNA was a gift from David Sabatini³¹ (Addgene, 1864). All yeast strains in this study are listed in Table S1.

Yeast media, culture conditions, growth assays and SNCA-GFP aggregate induction

Yeast media used for culturing were YPD (yeast extract, peptone and dextrose) for wild-type (WT) GFP and autophagy mutant strains, SD-Ura [synthetic dextrose (2%) medium without uracil] for culturing the SNCA-GFP strain and the GFP-Atg8-processing assay, SG-Ura [synthetic galactose (2%) medium without uracil] to induce SNCA-GFP expression. All strains were cultured at 30°C and 250 rpm.

Growth assays: In a 384-well plate, appropriate yeast strains were seeded ($A_{600} \sim 0.07$) with or without drugs and incubated (80 μ l, 30°C and 420 rpm) in a multiplate reader (Varioskan Flash, Thermo Scientific, USA) for 48 h with automatic

absorbance (A_{600}) recording every 20 min. Growth curves were plotted and analyzed using GraphPad Prism.

Induction of SNCA-GFP aggregates: To induce SNCA-GFP aggregates, the corresponding strains were inoculated in SD-Ura medium. Secondary culture was inoculated from primary inoculum until the absorbance at A_{600} reached 0.8/ml. Cells were washed twice with sterile water and adding SG-Ura for 12 to 16 h induced aggregates.

Small molecule screen

To screen small molecule library LOPAC¹²⁸⁰ in the *S. cerevisiae* SNCA toxicity model, working plates containing 50 μ M drugs in 1.5% DMSO (190 compounds/plate) were prepared in a 384-well format. WT SNCA-GFP with or without small molecules and untreated WT GFP were grown under optimized conditions (80 μ l, 30°C and 420 rpm) for 36 h in a plate reader (Varioskan Flash, Thermo Scientific) in duplicates with automatic absorbance (A_{600}) recording every 20 min. Growth curves of untreated WT GFP and WT SNCA-GFP strains were plotted and mid to late exponential phase time point of untreated WT GFP strain was chosen as reference for data analysis. Its corresponding time point of untreated and drug-treated WT SNCA-GFP strains were plotted separately in a box plot. Small molecules that rescued the growth lag by ≥ 3 SD units of untreated WT SNCA-GFP strain were considered as ‘hits’.

SNCA-GFP degradation assays

To assess SNCA-GFP degradation efficacy by 6-Bio, after inducing SNCA-GFP aggregate, the galactose promoter was turned off by adding dextrose. Cells were treated with 6-Bio (50 μ M) for 0, 6, 12 and 24 h. Subsequent degradation of SNCA-GFP levels were analyzed using immunoblotting (Fig. S4A).

Mammalian cell culture

HeLa cells were maintained in DMEM containing 10% fetal bovine serum (Pan-Biotech, P03–6510). Undifferentiated SH-SY5Y cells were maintained in DMEM-F12 containing 10% fetal bovine serum (Life Technologies, 12500062). Cell lines were cultured in the presence of 5% CO₂ at 37°C. To perform autophagy assays, equal numbers of subconfluent HeLa cells were seeded in 6-well dishes, allowed to attach for 24 h, treated with 6-Bio (5 μ M) and/or 3-MA (5 mM) in growth medium for 2 h. For the GFP-SNCA degradation assay, equal numbers of subconfluent SH-SY5Y cells were seeded in 6-well dishes and allowed to attach for 24 h. Cells were transfected with GFP-SNCA plasmid using Lipofectamine 2000 (Life Technologies, 11668–019) and allowed to express for 24 h. Cells were treated with 6-Bio (5 μ M) for 24 h and fold GFP-SNCA levels were analyzed using immunoblotting.

For the tandem RFP-GFP-LC3B assay, subconfluent cells were seeded in 60-mm dishes, transfected with tandem RFP-GFP-LC3B plasmid construct and allowed to express for 24 h. Later, cells were trypsinized, reseeded (10^5 cells) and allowed to attach on coverslips in a 12-well plate. Cells were treated with or without 6-Bio (5 μ M) for 2 h and coverslips were processed for imaging.

Immunoblot analysis

Preparation of yeast lysates: Yeast strains ($A_{600} = 3$) were resuspended in trichloroacetic acid (12.5%) and stored at -80°C for at least half an hour. Samples were thawed on ice, centrifuged (16000 \times g, 10 min) and the pellet was washed twice with ice-cold acetone (80%). Pellets were air-dried, resuspended in lysis (1% SDS and 0.1 N NaOH) solution and Laemmli buffer and boiled for 10 min.

Preparation of mammalian cell lysates: After treatments, cells were collected in Laemmli buffer to perform the LC3B processing assay, RPS6KB1, GSK3B and EIF4EBP1 immunoblotting. To validate GFP-SNCA degradation by 6-Bio, treated cells were scraped and collected in growth medium. After washing with phosphate buffer, pellets were lysed in Laemmli buffer and boiled for 10 min. Samples were electrophoresed on SDS-PAGE (8–15%) and then transferred onto PVDF (Bio-Rad, 162–0177) membrane using Transblot turbo (Bio-Rad). Transferred blots were stained with Ponceau S, probed with appropriate primary antibodies overnight and subsequently HRP-conjugated secondary antibody. Signals were developed using enhanced chemiluminescence substrate (Clarity, Bio-Rad), imaged using a gel documentation system (G-Box, Syngene, UK) and bands were quantified using ImageJ software (NIH).

GFP-Atg8-processing assay

An *S. cerevisiae* strain with an GFP-Atg8 plasmid was grown in SD-U (synthetic dextrose medium without uracil) under standardized conditions (30°C, 250 rpm). Using this, the secondary culture was inoculated ($A_{600} = 0.2$) and grown under the same standardized conditions until the culture absorbance reached $A_{600} = 0.7$. For assessing the effect of 6-Bio (50 μ M) in inducing autophagy in growth conditions, the cells were transferred to SD-U with 6-Bio for 6 h. To test the effect of 6-Bio in enhancing starvation-induced autophagy, cells were washed twice and transferred to starvation medium with 6-Bio and samples were collected for 0, 2, 4 and 6 h time points.³² Proteins were precipitated using trichloroacetic acid and resolved by SDS-PAGE (10%) followed by immunoblotting. In the blot, “GFP-Atg8 accumulation” indicates the induction of Atg8 expression and “free GFP release” indicates the degradation of GFP-Atg8 in the vacuole. The GFP-Atg8 protein is degraded in the vacuole (yeast lysosome); however, the GFP tag is relatively more resistant to vacuolar hydrolases. The levels of GFP-Atg8 (intact fusion protein) would indicate induction of Atg8 expression (which in turn is interpreted as possible autophagy induction) whereas comparison to the total GFP (summation of GFP signals from both full-length GFP-Atg8 and free GFP) indicates the autophagy flux^{12,33} (turnover of the fusion GFP-Atg8 protein to free GFP).

Microscopy

Yeast cultures after respective treatments were washed, mounted on an agarose (2%) pad and imaged.

For mammalian cell microscopy, after 2 h of treatment, coverslips were fixed using 4% paraformaldehyde (PFA; Sigma, 158127) and permeabilized using Triton X-100 (0.2%;

HiMedia, MB031). Coverslips were mounted using antifade, Vectashield (Vector laboratories, H-1000). For antibody staining, coverslips were blocked in 5% BSA (Sigma, RM105) for 1 h, incubated in primary antibody overnight and subsequently probed with fluorescent-conjugated antibody. Coverslips were mounted using antifade, Vectashield.

Images were acquired using DeltaVision Elite widefield microscope (API, GE, USA) with following filters: DAPI (390/18 and 435/48), FITC (490/20 and 529/38), TRITC (542/27 and 594/45) and Cy5 (632/22 and 676/34). Images were processed using DV SoftWoRX software.

The tandem RFP-GFP-LC3B assay (sometimes referred to as traffic light assay) is one test to assess autophagic flux in mammalian cells.²⁸ In this assay, autophagosomes appear as yellow puncta. Unlike RFP, GFP fluorescence being pH sensitive, gets quenched in the acidic pH environment of autolysosomes and thus appears red.

For the FITC-dextran uptake assay, after drug treatments, the HeLa cells were incubated with FITC-dextran (70 kDa; Sigma, 46945) for 30 min at 2 different temperature conditions (37°C and 16°C).

Cell viability assay

SH-SY5Y cells were seeded on 96-well plates and transfected with a plasmid encoding GFP-SNCA only and/or cotransfected with GSK3B shRNA and GFP-SNCA. To cells, the drugs were added (24 h) after 48 h of transfection. Then, the cell viability was measured using the CellTitre-Glo[®] (Promega, G7570) and luminescence was measured using a Varioskan Flash reader (Thermo Scientific).

Animal studies

All procedures in this study were approved by the JNCASR Institute Animal Ethical Committee (IAEC) and conducted as per the guidelines of the Committee for the Purpose of Control and Supervision of Experiments on Animals (CPCSEA). Inbred male C57BL/6J mice (3 to 4 mo old) were used for all experimental cohorts.

Studies on MPTP mouse PD model

Mice were randomly allocated to 5 different study cohorts, viz., Placebo (n = 5), 6-Bio-only (n = 5), MPTP (n = 5), MPTP+Pro (n = 3) and MPTP+Co (n = 5). As described previously,¹⁹ 23.4 mg/kg MPTP.HCl (equivalent to 20 mg/kg free base) in 10 ml/kg body weight of saline was administered i.p. for 4 times at 2 h intervals. Further, 5 mg/kg body weight of 6-Bio in 100 μ l of saline was administered i.p. to the MPTP-injected animals by following either of the 2 different regimens; the first regimen comprised a prophylactic, pretreatment which was begun 2 d before MPTP administration (MPTP+Pro); while the second involved treatment given alongside the MPTP injection (MPTP+Co). In both the cases, 6-Bio was administered for 7 d post MPTP administration daily (Fig. S5A). The other experimental cohorts included placebo, 6-Bio only (daily i.p.) and MPTP alone (daily vehicle) for 9 d. All mice were

killed 9 d post MPTP administration and brains were processed for immunohistochemistry.

Immunohistochemistry

Mice were anaesthetized using Halothane BP (Piramal Healthcare, India) inhalation and perfused intracardially with normal saline followed by 4% PFA in 0.1 M phosphate buffer, pH 7.4. Mice brains were removed quickly and postfixed with 4% PFA for 24 to 48 h at 4°C. Following cryoprotection in 15 and 30% sucrose (HiMedia, MB025), 40- μ m-thick coronal cryosections of midbrain were collected serially on gelatinized slides. The immunoperoxidase labeling protocol was identical to that reported.³⁴ Briefly, endogenous peroxidase was quenched using H₂O₂ (0.1%) in methanol (70%), followed by blocking of non-specific staining by a buffered solution (3%) of BSA for 4 h at room temperature. Sections were incubated with TH primary antibody (1:500) followed by biotin-conjugated secondary antibody (1:200 dilution; Vector Laboratories, BA-1400). Tertiary labeling was performed with avidin-biotin complex solution (1:100; Vector Laboratories, PK-6200). Staining was visualized using 3'-3'-diaminobenzidine (0.05%; Sigma, D3939) as a chromogen in a solution of 0.1 M acetate imidazole buffer (pH 7.4) and H₂O₂ (0.1%). Negative controls were processed identically, except that the primary antibody was replaced with dilution buffer.

For immunofluorescent-based double labeling, the sequential staining procedure was followed.³⁵ Brain sections were stained for TH and LC3B-APP/amyloid β oligomer/A11 and images were acquired using a DeltaVision Elite widefield microscope (API, GE).

Stereological quantification of TH⁺ DAergic neurons in SNpc

As described,³⁶ SNpc was delineated using the 4X objective of Olympus BX61 Microscope (Olympus, Japan) equipped with Stereo Investigator Software Version 7.2 (Micro Bright Field, USA). Stereological quantification was performed using optical fractionator probe with slight modifications.³⁶ Briefly, every sixth midbrain section containing SNpc was chosen and TH⁺ cells were counted under the 100X objective, with a regular grid interval of 22,500 μ m² (x = 150 μ m, y = 150 μ m) and counting frame with an area of 3600 μ m² (x = 60 μ m, y = 60 μ m). Mounted thickness was determined at every fifth site, which averaged to 25 μ m. A guard zone of 4 μ m was applied on either side, thus providing 17 μ m of z-dimension within the optical disector. The quantification was performed starting with the first anterior appearance of TH⁺ neurons in SNpc to the caudal-most part. The SNpc volume was determined by planimetry and total numbers of neurons according to mean measured thickness were noted.

Densitometry-based image analysis

We used high magnification images of TH-stained nigral DAergic neurons, captured for offline assessment of expression levels. Expression intensity was measured using a Windows-based image analysis system (Q Win V3, Leica Systems,

Germany). Cumulative mean was derived from the values obtained from sampling, approximately 200 DAergic neurons per animal. Intensity output measured on a grayscale of 0 to 255, where 0 equals intense staining and 255 means absence of staining. Thus, lower gray values suggest higher protein expression and vice versa.

In vivo blood brain barrier assay

Animals were randomly allocated for placebo control and drug treatment cohorts. C57BL/6J mice were injected with placebo control or 6-Bio (5 mg/kg of body weight, intraperitoneally) twice with a 24 h time interval. After second injection, the brains were harvested at 15 min, 30 min, 60 min, 6 h, 12 h and 24 h by cervical dislocation. Mice brains were immediately homogenized with RIPA buffer [25 mM Tris-HCL, 150 mM sodium chloride, 1% NP-40 (Roche, 11332473001), 1% sodium deoxycholate (Sigma-Aldrich, D6750) and 0.1% sodium dodecyl sulfate with protease inhibitor cocktail (Roche, 11836170001)] for both treatment cohorts. Homogenously macerated mouse brain sample (100 μ l) was mixed with acetonitrile (ACN, 400 μ l), formic acid (0.2%) and aceclofenac (100 ng/ml, an internal standard; Sigma, A8861), vortexed for 10 min at 2000 rpm Orbital shaker (compact digital microplate shaker, 88880024, Thermo Scientific, USA). Then, samples were centrifuged and the supernatant was injected for LC MS/MS. Standard samples were prepared by spiking 6-Bio standard into a blank control brain sample. Standard spiking was performed such that resultant concentrations were 0, 10, 100, 500, 1000, 1500 and 2000 ng/ml of drug in blank brain matrix. For LC, PE 200 (Perkin Elmer, USA) HPLC with an Agilent Zorbax XDB C8 4.6 \times 75 mm, 3.5- μ m column (Agilent Technologies, USA) was used. The following conditions were used for LC: Mobile phases (0.1% formic acid in water (5%):methanol (95%)), isocratic flow rate (0.7 ml/min), run time (4 min), injection volume (15 μ l) and needle wash solution (1:1 methanol:water mix containing 0.1% formic acid). The mass spectrometry (API3000, AB Sciex, USA) was used with aceclofenac as an internal control and data were processed using Analyst Software V1.4.2. Drug injections of the various cohorts and preparations of the brain homogenates were performed at JNCASR. Acquity laboratories, India performed the above mentioned LC-MS/MS analysis of the brain samples.

Behavioral studies

Behavioral procedures used for this study were modified from.³⁷⁻⁴⁰ All the behavioral experiments were done on 3- to 4-mo-old male C57BL/6J mice. Experimenters were blind to the drug injected animals. Experimenters handled mice used for behavioral experiments for 3 consecutive d before the training paradigm. Behavioral experiments were designed in an order of low- to high-stress activity for mice. Therefore, the open field test was conducted in the forenoon whereas the rotarod was performed in the afternoon. Mice were habituated to the behavior room for 15 min every day before the start of experiments. The light

intensity was maintained at 100 lx throughout the experiment. Mice were weighed every day before training or test to ensure their good health. Mice were randomly allocated into 3 treatment cohorts: placebo control, MPTP and 6-Bio. Data were plotted using GraphPad prism 5 software.

Rotarod trials

The rotarod instrument was custom made at the mechanical workshop, National Center for Biological Sciences, Bengaluru, India. The rotating rod (diameter 3.3 cm) was made of Delrin and was textured to enhance the grip of mice. The rod was fixed at a height of 30 cm from the cushioned platform where mice fell on to during training and test. The rod was partitioned into 3 areas of 9.3-cm distance between each partition using discs (40-cm diameter) made of Teflon. Mice were trained in the rotarod for 5 consecutive d before drug injection. Each mouse was trained in the rotarod by gradually increasing the rotation on every day. On d 1, mice were trained on 5 to 10 rpm (accelerated at 1 rpm/5 seconds), 11 to 15 rpm (accelerated at 1 rpm/5 seconds) on second day, 16 to 20 rpm (accelerated at 1 rpm/5 seconds) on the third d and at 20 rpm (fixed) for d 4 and 5. Mice were trained at the above specific rpm for 3 times with 5-min interval between trials. The rod was rotated from 5 rpm to 20 rpm by manually changing the speed of the motor (nonautomated). During the test (d 13 postinjection), the rotarod was started at 20 rpm. Mice were tested in a rotating rotarod for a maximum of 60 seconds and their latencies were noted down. At the end of each trial, the rotarod was wiped with 70% ethanol and left for drying before placing the next set of mice. The entire trial was video recorded using a DSLR camera (Nikon D5100, India) and latencies were scored manually. The average time spent on the rotating rotarod across 3 trials were plotted as mean latency to fall.

Open field test

The open field arena (50 cm \times 50 cm \times 45 cm) was custom-made (JNCASR) using plywood and the internal surface was coated with white polish. Mice were trained in the open field for 2 consecutive days before drug injection. During training or testing, one animal at a time was placed in the zone periphery in the open field arena and allowed to explore the arena for 5 min. The activity was video recorded (SONY[®] color video camera, Model no. SSC-G118, India) using software (SMART v3.0.04 from Panlab, Harvard Apparatus, USA). After 5 min, the mouse was returned to its home cage. The open field arena was then wiped using 70% ethanol and allowed to dry before placing the next mouse. Distances traveled were analyzed offline by an experimenter who was not involved in performing the experiment.

Statistical analysis

Statistical analyses were performed using the unpaired Student *t* test and ANOVA (one-way or 2-way) followed by the post-hoc Bonferroni test in GraphPad Prism. Error bars were expressed as mean \pm SEM.

Abbreviations

A ₆₀₀ ,	absorbance at 600 nm;
6-Bio,	6-Bromindirubin-3'-oxime;
DA,	dopamine;
GFP,	green fluorescent protein;
GSK3B,	glycogen synthase kinase 3.
HRP,	horseradish peroxidase;
i.p.,	intraperitoneally;
LOPAC,	Library of Pharmacologically Active Compounds;
3-MA,	3-methyladenine;
MAP1LC3B/LC3B,	microtubule associated protein 1 light chain 3 β ;
MPTP,	1-methyl-4-phenyl-1,2,3,6-tetrahydropyridine;
PD,	Parkinson disease;
Pep A,	pepstatin A;
Pgk1,	phosphoglycerate kinase 1;
RFP,	red fluorescent protein;
SD,	standard deviation;
SEM,	standard error mean;
SNpc,	substantia nigra pars compacta;
TH,	tyrosine hydroxylase;

Disclosure of potential conflicts of interest

No potential conflicts of interest were disclosed.

Acknowledgments

We thank Y. Ohsumi, Paulo Ludovico, Tamotsu Yoshimori and David Rubinzstein for the kind gift of plasmids and Prof. MRS Rao, Dr. Subba Rao, Dr. K. Vijayachandra, Dr. Prathibha Ranganathan, Dr. Tej Kumar Pareek, Aparna Hebbar and members of the autophagy laboratory (JNCASR) for critical reading of the manuscript. Dr. Prakash and Muthumenakshi Bhaskaran's help in animal facility at JNCASR is acknowledged. We thank Dr. Alicia Brantley, Director, Behavior Core and Dr. Thomas Creson, Staff Scientist, Scripps Research Institute, Florida for their valuable suggestions on behavioral experiments.

Funding

This work was supported by the Wellcome Trust/DBT India Alliance Intermediate Fellowship awarded to RM (500159-Z-09-Z), JNCASR intramural funds to RM, DST-SERB (SR/SO/HS/0121/2012) to PAA and DST-SERB (SB/YS/LS-215/2013) to JPC. Application of 6-Bio in autophagy modulation and neurodegeneration is patent pending.

References

- [1] Mortality GBD, Causes of Death C. Global, regional, and national age-sex specific all-cause and cause-specific mortality for 240 causes of death, 1990-2013: a systematic analysis for the Global Burden of Disease Study 2013. *Lancet* 2015; 385:117-71; PMID:25530442; [https://doi.org/10.1016/S0140-6736\(14\)61682-2](https://doi.org/10.1016/S0140-6736(14)61682-2)
- [2] German DC, Manaye K, Smith WK, Woodward DJ, Saper CB. Midbrain dopaminergic cell loss in Parkinson's disease: computer visualization. *Ann Neurol* 1989; 26:507-14; PMID:2817827; <https://doi.org/10.1002/ana.410260403>
- [3] Thanvi B, Lo N, Robinson T. Levodopa-induced dyskinesia in Parkinson's disease: clinical features, pathogenesis, prevention and treatment. *Postgraduate Med J* 2007; 83:384-8; PMID:17551069; <https://doi.org/10.1136/pgmj.2006.054759>
- [4] Nixon RA. The role of autophagy in neurodegenerative disease. *Nat Med* 2013; 19:983-97
- [5] Hara T, Nakamura K, Matsui M, Yamamoto A, Nakahara Y, Suzuki-Migishima R, Yokoyama M, Mishima K, Saito I, Okano H, et al. Suppression of basal autophagy in neural cells causes neurodegenerative disease in mice. *Nature* 2006; 441:885-9; PMID:16625204; <https://doi.org/10.1038/nature04724>
- [6] Komatsu M, Waguri S, Chiba T, Murata S, Iwata J, Tanida I, Ueno T, Koike M, Uchiyama Y, Kominami E, et al. Loss of autophagy in the central nervous system causes neurodegeneration in mice. *Nature* 2006; 441:880-4; PMID:16625205; <https://doi.org/10.1038/nature04723>
- [7] Liang CC, Wang C, Peng X, Gan B, Guan JL. Neural-specific deletion of FIP200 leads to cerebellar degeneration caused by increased neuronal death and axon degeneration. *J Biol Chem* 2010; 285:3499-509; PMID:19940130; <https://doi.org/10.1074/jbc.M109.072389>
- [8] Sarkar S, Perlstein EO, Imarisio S, Pineau S, Cordenier A, Maglathlin RL, Webster JA, Lewis TA, O'Kane CJ, Schreiber SL, et al. Small molecules enhance autophagy and reduce toxicity in Huntington's disease models. *Nat Chem Biol* 2007; 3:331-8; PMID:17486044; <https://doi.org/10.1038/nchembio883>
- [9] Anguiano J, Garner TP, Mahalingam M, Das BC, Gavathiotis E, Cuervo AM. Chemical modulation of chaperone-mediated autophagy by retinoic acid derivatives. *Nat Chem Biol* 2013; 9:374-82; PMID:23584676; <https://doi.org/10.1038/nchembio.1230>
- [10] Rajasekhar K, Suresh SN, Manjithaya R, Govindaraju T. Rationally designed peptidomimetic modulators of abeta toxicity in Alzheimer's disease. *Scientific Reports* 2015; 5:8139; PMID:25633824; <https://doi.org/10.1038/srep08139>
- [11] Llorens-Martin M, Jurado J, Hernandez F, Avila J. GSK-3beta, a pivotal kinase in Alzheimer disease. *Front Mol Neurosci* 2014; 7:46; PMID:24904272; <https://doi.org/10.3389/fnmol.2014.00046>
- [12] Silva-Alvarez C, Arrazola MS, Godoy JA, Ordenes D, Inestrosa NC. Canonical Wnt signaling protects hippocampal neurons from Abeta oligomers: role of non-canonical Wnt-5a/Ca(2+) in mitochondrial dynamics. *Frontiers Cell Neurosci* 2013; 7:97; PMID:23805073; <https://doi.org/10.3389/fncel.2013.00097>
- [13] Outeiro TF, Lindquist S. Yeast cells provide insight into alpha-synuclein biology and pathobiology. *Science* 2003; 302:1772-5; PMID:14657500; <https://doi.org/10.1126/science.1090439>
- [14] Khurana V, Lindquist S. Modelling neurodegeneration in *Saccharomyces cerevisiae*: why cook with baker's yeast? *Nat Rev Neurosci* 2010; 11:436-49; PMID:20424620; <https://doi.org/10.1038/nrn2809>
- [15] Outeiro TF, Kontopoulos E, Altmann SM, Kufareva I, Strathearn KE, Amore AM, Volk CB, Maxwell MM, Rochet JC, McLean PJ, et al. Sirtuin 2 inhibitors rescue alpha-synuclein-mediated toxicity in models of Parkinson's disease. *Science* 2007; 317:516-9; PMID:17588900; <https://doi.org/10.1126/science.1143780>
- [16] Polychronopoulos P, Magiatis P, Skaltsounis AL, Myrianthopoulos V, Mikros E, Tarricone A, Musacchio A, Roe SM, Pearl L, Leost M, et al. Structural basis for the synthesis of indirubins as potent and selective inhibitors of glycogen synthase kinase-3 and cyclin-dependent kinases. *J Med Chem* 2004; 47:935-46; PMID:14761195; <https://doi.org/10.1021/jm031016d>
- [17] Grassilli E, Ianzano L, Bonomo S, Missaglia C, Cerrito MG, Giovannoni R, Masiero L, Lavitrano M. GSK3A is redundant with GSK3B in modulating drug resistance and chemotherapy-induced necroptosis. *PloS One* 2014; 9:e100947; PMID:24984063; <https://doi.org/10.1371/journal.pone.0100947>
- [18] Braig S, Kressirer CA, Liebl J, Bischoff F, Zahler S, Meijer L, Vollmar AM. Indirubin derivative 6BIO suppresses metastasis. *Cancer Res* 2013; 73:6004-12; PMID:23946383; <https://doi.org/10.1158/0008-5472.CAN-12-4358>
- [19] Jackson-Lewis V, Przedborski S. Protocol for the MPTP mouse model of Parkinson's disease. *Nat Protocols* 2007; 2:141-51; PMID:17401348; <https://doi.org/10.1038/nprot.2006.342>
- [20] Li XZ, Chen XP, Zhao K, Bai LM, Zhang H, Zhou XP. Therapeutic effects of valproate combined with lithium carbonate on MPTP-induced parkinsonism in mice: possible mediation through enhanced autophagy. *Int J Neurosci* 2013; 123:73-9; PMID:22978383; <https://doi.org/10.3109/00207454.2012.729234>

- [21] Anglade P, Vyas S, Hirsch EC, Agid Y. Apoptosis in dopaminergic neurons of the human substantia nigra during normal aging. *Histol Histopathol* 1997; 12:603-10; PMID:9225140
- [22] Luk KC, Kehm V, Carroll J, Zhang B, O'Brien P, Trojanowski JQ, Lee VM. Pathological alpha-synuclein transmission initiates Parkinson-like neurodegeneration in nontransgenic mice. *Science* 2012; 338:949-53; PMID:23161999; <https://doi.org/10.1126/science.1227157>
- [23] Nisha CM, Kumar A, Vimal A, Bai BM, Pal D, Kumar A. Docking and ADMET prediction of few GSK-3 inhibitors divulges 6-bromoindirubin-3-oxime as a potential inhibitor. *J Mol Graphics Modelling* 2016; 65:100-7; PMID:26967552; <https://doi.org/10.1016/j.jmngm.2016.03.001>
- [24] Yasuhara R, Irie T, Suzuki K, Sawada T, Miwa N, Sasaki A, Tsunoda Y, Nakamura S, Mishima K. The beta-catenin signaling pathway induces aggressive potential in breast cancer by up-regulating the chemokine CCL5. *Exp Cell Res* 2015; 338:22-31; PMID:26363360; <https://doi.org/10.1016/j.yexcr.2015.09.003>
- [25] Golpich M, Amini E, Hemmati F, Ibrahim NM, Rahmani B, Mohamed Z, Raymond AA, Dargahi L, Ghasemi R, Ahmadiani A. Glycogen synthase kinase-3 beta (GSK-3beta) signaling: Implications for Parkinson's disease. *Pharmacological Res* 2015; 97:16-26; PMID:25829335; <https://doi.org/10.1016/j.phrs.2015.03.010>
- [26] Parr C, Carzaniga R, Gentleman SM, Van Leuven F, Walter J, Sastre M. Glycogen synthase kinase 3 inhibition promotes lysosomal biogenesis and autophagic degradation of the amyloid-beta precursor protein. *Mol Cell Biol* 2012; 32:4410-8; PMID:22927642; <https://doi.org/10.1128/MCB.00930-12>
- [27] Ejlerskov P, Hultberg JG, Wang J, Carlsson R, Ambjorn M, Kuss M, Liu Y, Porcu G, Kolkova K, Friis Rundsten C, et al. Lack of Neuronal IFN-beta-IFNAR Causes Lewy Body- and Parkinson's Disease-like Dementia. *Cell* 2015; 163:324-39; PMID:26451483; <https://doi.org/10.1016/j.cell.2015.08.069>
- [28] Kimura S, Noda T, Yoshimori T. Dissection of the autophagosome maturation process by a novel reporter protein, tandem fluorescently-tagged LC3. *Autophagy* 2007; 3:452-60; PMID:17534139
- [29] Furlong RA, Narain Y, Rankin J, Wyttenbach A, Rubinsztein DC. Alpha-synuclein overexpression promotes aggregation of mutant huntingtin. *Biochem J* 2000; 346 Pt 3:577-81; PMID:10698681
- [30] Yoeli-Lerner M, Chin YR, Hansen CK, Toker A. Akt/protein kinase b and glycogen synthase kinase-3beta signaling pathway regulates cell migration through the NFAT1 transcription factor. *Mol Cancer Res* 2009; 7:425-32; PMID:19258413; <https://doi.org/10.1158/1541-7786.MCR-08-0342>
- [31] Sarbassov DD, Guertin DA, Ali SM, Sabatini DM. Phosphorylation and regulation of Akt/PKB by the rictor-mTOR complex. *Science* 2005; 307:1098-101; PMID:15718470; <https://doi.org/10.1126/science.1106148>
- [32] Rajasekhar K, Narayanaswamy N, Mishra P, Suresh SN, Manjithaya R, Govindaraju T. Synthesis of Hybrid Cyclic Peptoids and identification of autophagy enhancer. *Chempluschem* 2014; 79:25-30
- [33] Graef M, Nunnari J. Mitochondria regulate autophagy by conserved signalling pathways. *EMBO J* 2011; 30:2101-14; PMID:21468027; <https://doi.org/10.1038/emboj.2011.104>
- [34] Alladi PA, Mahadevan A, Yasha TC, Raju TR, Shankar SK, Muthane U. Absence of age-related changes in nigral dopaminergic neurons of Asian Indians: relevance to lower incidence of Parkinson's disease. *Neuroscience* 2009; 159:236-45; PMID:19135503; <https://doi.org/10.1016/j.neuroscience.2008.11.051>
- [35] Vidyadhara DJ, Yarreiphang H, Raju TR, Alladi PA. Admixing of MPTP-resistant and susceptible mice strains augments Nigrostriatal Neuronal Correlates to Resist MPTP-Induced Neurodegeneration. *Mol Neurobiol* 2016; PMID:27704331; <https://doi.org/10.1007/s12035-016-0158-y>
- [36] Fu Y, Yuan Y, Halliday G, Rusznak Z, Watson C, Paxinos G. A cytoarchitectonic and chemoarchitectonic analysis of the dopamine cell groups in the substantia nigra, ventral tegmental area, and retrorubral field in the mouse. *Brain Struct Funct* 2012; 217:591-612; PMID:21935672; <https://doi.org/10.1007/s00429-011-0349-2>
- [37] Liu W, Jalewa J, Sharma M, Li G, Li L, Holscher C. Neuroprotective effects of lixisenatide and liraglutide in the 1-methyl-4-phenyl-1,2,3,6-tetrahydropyridine mouse model of Parkinson's disease. *Neuroscience* 2015; 303:42-50; PMID:26141845; <https://doi.org/10.1016/j.neuroscience.2015.06.054>
- [38] Patil SP, Jain PD, Ghumatkar PJ, Tambe R, Sathaye S. Neuroprotective effect of metformin in MPTP-induced Parkinson's disease in mice. *Neuroscience* 2014; 277:747-54; PMID:25108167; <https://doi.org/10.1016/j.neuroscience.2014.07.046>
- [39] Brooks SP, Dunnett SB. Tests to assess motor phenotype in mice: a user's guide. *Nat Rev Neurosci* 2009; 10:519-29; PMID:19513088; <https://doi.org/10.1038/nrn2652>
- [40] Buccafusco JJ. The revival of scopolamine reversal for the assessment of cognition-enhancing drugs. In: Buccafusco JJ, ed. *Methods of behavior analysis in neuroscience*. Boca Raton (FL): CRC Press; 2009.



OPEN

Rationally Designed Peptidomimetic Modulators of A β Toxicity in Alzheimer's Disease

SUBJECT AREAS:
STRUCTURE-BASED DRUG
DESIGN
CHEMISTRYK. Rajasekhar¹, S. N. Suresh², Ravi Manjithaya² & T. Govindaraju¹Received
12 September 2014Accepted
8 January 2015Published
30 January 2015Correspondence and
requests for materials
should be addressed to
R.M. (ravim@jncasr.
ac.in) or T.G. (tgraju@
jncasr.ac.in)

¹Bioorganic Chemistry Laboratory, New Chemistry Unit, Jawaharlal Nehru Centre for Advanced Scientific Research, Jakkur P.O., Bengaluru 560064, Karnataka, India, ²Molecular Biology and Genetics Unit, Jawaharlal Nehru Centre for Advanced Scientific Research, Jakkur P.O., Bengaluru 560064, Karnataka, India.

Alzheimer's disease is one of the devastating illnesses mankind is facing in the 21st century. The main pathogenic event in Alzheimer's disease is believed to be the aggregation of the β -amyloid (A β) peptides into toxic aggregates. Molecules that interfere with this process may act as therapeutic agents for the treatment of the disease. Use of recognition unit based peptidomimetics as inhibitors are a promising approach, as they exhibit greater protease stability compared to natural peptides. Here, we present peptidomimetic inhibitors of A β aggregation designed based on the KLVFF (P1) sequence that is known to bind A β aggregates. We improved inhibition efficiency of P1 by introducing multiple hydrogen bond donor-acceptor moieties (thymine/barbiturate) at the N-terminal (P2 and P3), and blood serum stability by modifying the backbone by incorporating sarcosine (N-methylglycine) units at alternate positions (P4 and P5). The peptidomimetics showed moderate to good activity in both inhibition and dissolution of A β aggregates as depicted by thioflavin assay, circular dichroism (CD) measurements and microscopy (TEM). The activity of P4 and P5 were studied in a yeast cell model showing A β toxicity. P4 and P5 could rescue yeast cells from A β toxicity and A β aggregates were cleared by the process of autophagy.

Alzheimer's disease (AD) is a major contributor of dementia with no clinically accepted treatment to cure or halt its progression¹. Over the past two decades, tremendous efforts have been devoted to understanding the pathogenesis of AD². Although the detailed mechanism of neurodegeneration encountered in AD is not entirely understood yet, several reports indicate that the fibrillar aggregation of β -amyloid (A β) 36–42 peptides and, in particular, highly toxic A β 42 play a key role in the pathogenesis of AD^{3–6}. The A β 36–42 peptides are derived from a transmembrane protein called amyloid precursor protein (APP). Amyloidogenic pathway for processing of APP by enzymes β - and γ -secretases lead to the release of A β 36–42 peptides and their deposition in the brain as plaques⁷. Hence, the development of molecular agents that are capable of inhibiting the A β fibril formation or dissolution of the preformed toxic A β fibrillar aggregates are key concepts for AD treatment^{8,9}.

Elucidation of the structural properties of A β fibrils in the recent years has enabled the design of inhibitors for fibril formation^{10–16}. The hydrophobic core residues from 11 to 25 in A β 40/42 is very crucial for their assembly into fibrils, and these short peptide sequences have a recognition ability towards A β polypeptides. The pentapeptide sequences KLVFF or LVFFA can recognize A β polypeptides and, therefore be used as recognition units in the design of inhibitors for A β fibrillization. For example, Tjernberg *et al.*¹⁷ demonstrated that A β _{16–20} binds residues 25 to 35 of A β and prevents fibril formation. Soto and co-workers¹⁸ rationally designed a proline-containing residue (LPFFD), which is known to be a β -sheet breaker and was found to inhibit the fibrillization of A β aggregation. KLVFF-conjugated oligolysine or oligoglutamic acid units were useful means of generating binders to A β , which resulted in the formation of large aggregates that might lead to reduced cell toxicity^{19–21}. A tetramer of KLVFF was designed and was found to inhibit the transformation of A β 42 soluble oligomers into fibrils and also promoted the dissolution of preformed A β 42 aggregates²². Conjugation of hydrophobic moieties with A β recognition unit was also attempted to construct inhibitors of A β aggregation. Cholic acid as a hydrophobic moiety at the N-terminal of LVFFA and its D-analog sequence strongly inhibited the A β fibrillization²³. Ferrocene attached at the N-terminal of KLVFF showed inhibitory action towards A β 42 aggregates²⁴. Methylation of amide groups in short recognition peptides is also an effective means of designing A β inhibitors. These N-methylated peptides were able to cap growing β -sheets, blocking one face of the A β polypeptide from participating in hydrogen bond driven fibrillar aggregation due to lack of amide proton and sterically hindered N-methyl groups.



Furthermore, the chemical modifications at the N-terminal and amide N-methylated designed peptides also provided extra stability towards proteases^{25–27}. Several N-methylated peptides based on recognition sequence (KLVFF) have been systematically synthesized and analysed for their ability to function as fibrillar inhibitors and their effect on the A β toxicity. Digit *et al.*²⁸ synthesized an analog peptide D-[chGly-Tyr-chGly-chGly-mLeu]-NH₂ (ch = cyclohexyl, male = N-methyl lysine) to demonstrate its striking inhibitory activity. Introducing N-methyl analogs of natural amino acids at alternating positions of recognition peptide have also shown promising activity in both inhibition and dissolution of A β aggregates²⁹. A completely synthetic analog of the recognition peptide with N-substituted amino acids (peptides) have been shown to have prominent inhibition activity towards A β aggregates³⁰. Designing hybrid peptide-peptoid based modulators targeting hydrogen bonding involved in β -sheet formation and subsequent elongation leading to fibrillar aggregates has not been addressed adequately in the literature. Therefore, developing hybrid peptide-peptoid based modulators aiming to target multiple phases of A β 42 aggregation would provide highly efficient inhibitors.

Another potential approach is through enhancing the phenomenon of aggrephagy. Aggrephagy, a cellular mechanism of selective autophagy, involves degradation of misfolded proteins or aggregates essential for cell homeostasis³¹. Presence of A β aggregates down-regulates autophagy, which is known to play a pivotal role in the clearance and neutralizing the toxic effects caused by A β . Designed small molecules or peptides which influence autophagy may also act as probable therapeutics³². Yeast has been popularly used as a simple model organism in literature to study A β toxicity and screen A β inhibitors³³. *Saccharomyces cerevisiae* is a eukaryote and, hence, shares phenomenal homology with the human genome³⁴. It also recapitulates the fundamental processes of a human-like transcription, translation and also its metabolism³⁵. Yeast model also provides a platform to study the autophagy-based regulation³⁶.

In this report, we present effective inhibition of A β 42 aggregation using hybrid peptide-peptoid modulators based on the core sequences of A β peptide (KLVFF). The hybrid peptide-peptoids modulators were designed to act on multiple phases of A β 42 aggregation by introducing a non-amino acid moiety with multiple hydrogen bond donor-acceptor sites, at the N-terminal to target A β 42 β -sheet formation. The introduction of peptoid monomers (sarcosine) at alternative positions of the recognition motif (KLVFF) prevents the oligomerization of A β 42 monomers upon its binding through the face of amino acids. Furthermore, the hybrid peptide-peptoid modulators were anticipated to confer proteolysis resistance to the derived peptidomimetics, thus increasing their biostability and bioavailability (the parent peptide KLVFF contains natural amino acids and is not resistant to endoproteases). Thioflavin T (ThT) binding, assayed by fluorescence spectroscopy, was used to probe A β 42 fibril formation and effect of peptidomimetic inhibitors on their growth. Circular dichroism (CD) was used to study the effect of inhibitors on the secondary structure of A β 42 aggregates. The morphological analysis of A β 42 in the absence and presence of peptidomimetic inhibitors was investigated using transmission electron microscopy (TEM). The structural integrity and stability of inhibitory peptides and peptidomimetics was analyzed in the presence of proteases. Further, inhibitory activity was studied in the yeast (*Saccharomyces cerevisiae*) model, which expresses A β 42, to assess the ability of peptidomimetics as therapeutic agents and to understand their mechanism of action in reducing A β 42 toxicity. Thus, we report on the study of structural fine tuning and inhibitory activities of peptidomimetics towards preventing the formation of A β 42 aggregates and dissolving the preformed toxic aggregates (Fig. 1).

Results and Discussion

Design strategy for Peptidomimetics. The principle of the design was to rationally introduce a minimum number of simple chemical

modifications into a small recognition peptide sequence extracted from A β 42, which is considered crucial for β -sheet conformation and fibrillogenesis. These peptidomimetics bind and stabilize the amyloidogenic conformational population of A β 42 and inhibit its aggregation into toxic amyloid aggregates. The chemical modifications are aimed at interfering with hydrogen bonding found in the β -sheet conformations of A β 42³⁷. Inhibition of β -sheet formation in A β 42 affects its self-assembly to fibrillar aggregates. We considered KLVFF (A β 16–20) as the recognition sequence, which has been reported in the literature to interact with A β 42 and its aggregates¹⁶. Although KLVFF (P1) has the ability to interfere with fibrillization, the extent of inhibition is very marginal due to higher stabilization of A β 42 β -sheet conformations than the A β 42/KLVFF complex³⁸. To enhance the stabilization of A β 42/KLVFF complex we introduced small organic moieties with multiple hydrogen bond donors and acceptors at the N-terminal of KLVFF (Fig. 1). This specially chosen organic moiety could participate in hydrogen bonding to form much stronger A β 42/inhibitor complex. We selected two organic moieties, thymine and barbiturate, as N-terminal pendent functionalities to obtain peptides P2 and P3, respectively as shown in Fig. 1. These organic moieties contain multiple hydrogen bond donor and acceptor centers, which are capable of forming additional hydrogen bonds with β -sheet forming A β 42 monomer or A β 42 aggregates³⁹. Subsequently, we performed inhibition studies and concluded that the extent of inhibition was moderate, and moreover, the blood serum or protease stability of P2 and P3 was not encouraging. The next level of modification was then considered on P2 as it displayed better inhibition activity over P3. Meredith *et al.* used N-substituted amino acids at alternate positions of KLVFFAE, where α -substituents of Leu, Phe and Ala were attached to amide nitrogen atom. These modifications were presumed to help retain the recognition ability and inhibition of A β 40 fibrillogenesis or dissolution of A β 40 fibrils. In this case, the inhibitor was anticipated to work by blocking the hydrogen bonding interactions. However, involvement of other noncovalent interactions from the α -substituents either in the inhibitor or A β 40 were not considered in the design²⁹. It should be noted that the fibrillogenesis of A β 40/42 is guided by both hydrogen bonding and other noncovalent interactions²⁹. Thus, we intend to target the key role of hydrogen bonding in A β 42 aggregation as well as minimizing other noncovalent interactions among A β 42 and modulators, in our design strategy. Keeping this in mind, we introduced sarcosine (Sr) in alternate positions of P2 to obtain P4 (Thymine-Sr-Leu-Sr-Phe-Sr-Ala) and P5 [Thymine-Lys-Sr-Val-Sr-Phe-Sr] (Fig. 1). We hypothesized that the peptidomimetics P4 and P5 would interact with A β 42 through the face containing normal amino acids (blocking hydrogen bonding) while minimizing other noncovalent interactions to prevent the fibrillogenesis of A β 42⁴⁰.

Studying inhibition and dissolution efficiency by thioflavin assay and CD measurements.

ThT assay has been widely used to monitor the transformation of A β 42 monomers to fibrillar aggregates. We employed ThT assay to evaluate the ability of our peptidomimetic candidates to either prevent fibril assembly (inhibition) or to break down preformed fibrils of A β 42 (dissolution). For the inhibition assay all the peptidomimetics (P2, P3, P4 and P5) along with control peptide P1 were added at 0 h of the experiment, whereas for the aggregates reversal (dissolution) assay they were added to A β 42 fibrillar aggregates grown for 2 days. Once they had been incubated together, A β 42/inhibitors were analyzed using ThT by measuring the fluorescence changes. First, we performed concentration-dependent experiments where different ratios of P1, P2, P3, P4 and P5 were incubated with fixed concentrations of A β 42 (20 μ M) and its aggregates to study their effect on both inhibition and reversal assay, respectively. Experiments were performed at stoichiometric ratios (A β 42/inhibitor) of 1:0.2, 1:1, and 1:2 with

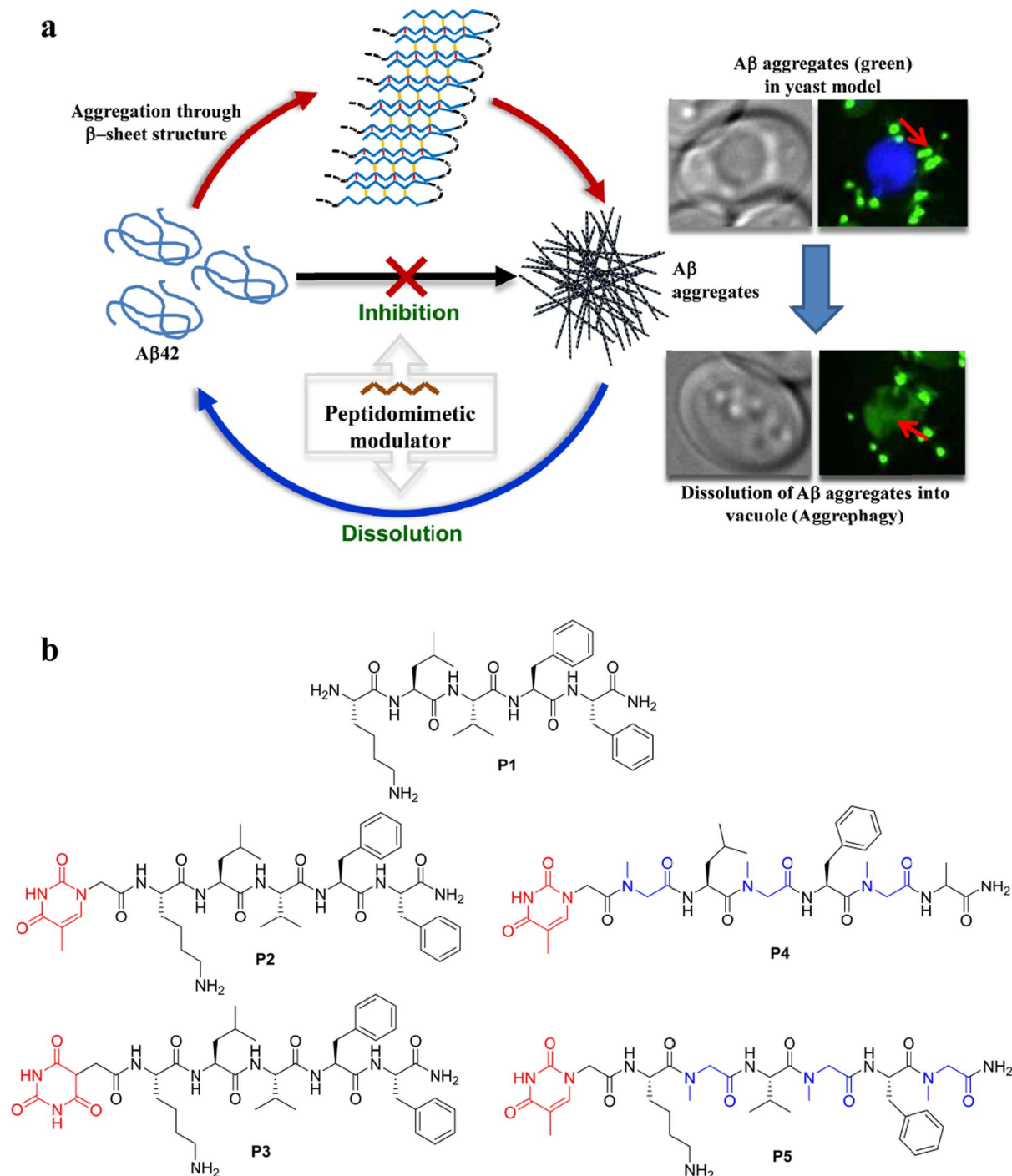


Figure 1 | Peptidomimetic inhibitors. (a), Inhibition and dissolution of A β 42 aggregates, and their evaluation in yeast model for Alzheimers disease. (b), Structures of peptide and peptidomimetic inhibitors.

the fixed concentration of A β 42 of 20 μ M. Inhibition experiments demonstrated that P4 and P5 were able to prevent A β 42 aggregation as indicated by a reduction in the fluorescence intensity of ThT up to 95% in case of 1:2 stoichiometric ratio after four days of incubation at 37°C (Fig. 2). Conversely, P1, P2 and P3 showed low to moderate inhibition efficiencies of 20%, 55% and 40%, respectively for 1:2 stoichiometry. Similar trends were observed in the case of fibril reversal assay with dissolution efficiencies of 20% (P1), 45% (P2), 34% (P3), 80% (P4) and 80% (P5), for 1:2 stoichiometric ratios (Fig. 2). Thus, P4 and P5 were found to be promising as they displayed a pronounced effect on both inhibition and reversal assay. However, the efficiencies of P4 and P5 were only marginally

better in inhibition assay compared to reversal assay with a difference of about 15%. Increasing the molar ratio of peptides (> 2 fold) did not lead to improvements in inhibition or reversal assay and, therefore, we performed all our further experiments with 1:2 stoichiometry of A β 42:inhibitor (20 μ M:40 μ M).

Next, we performed time-dependent assays to monitor the effect of inhibitors on the growth kinetics of A β 42 monomers to fibrillar aggregates and dissolution of toxic aggregates. A sigmoid growth curve was obtained for A β 42 fibrillization, which has been well-reported in the literature⁶. P1 showed a slight variation in the growth curve, indicating least effect on the A β 42 aggregation, whereas P2 and P3 showed decreased growth phase to < 60%, signifying mod-

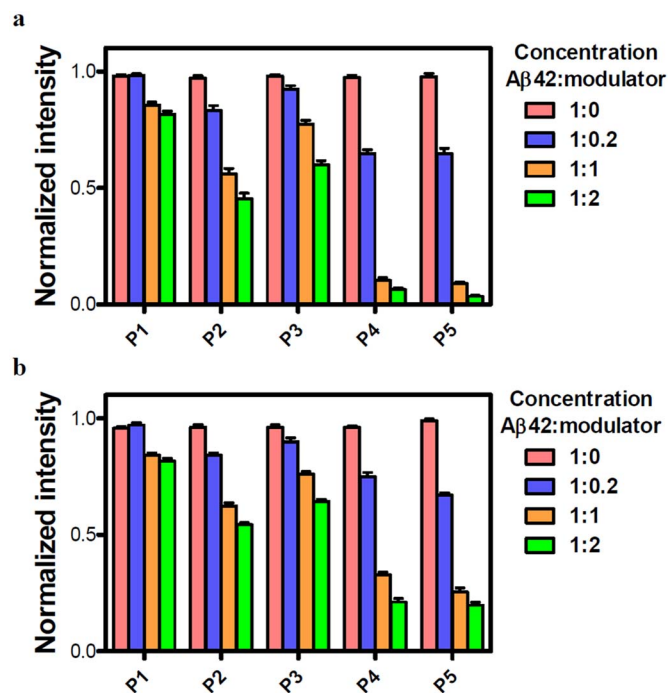


Figure 2 | Inhibition and reversal data of A β 42 aggregates studied by ThT assay. The data in (a) and (b) show the effects of different stoichiometries of P1, P2, P3, P4 and P5 on the aggregation of 20 μ M A β 42 (on day 4 for the inhibition assay and day 6 for the reversal assay). Molar ratios (A β 42:peptide) of 1:0, 1:0.2, 1:1 and 1:2 were used for each peptide. Values are the normalized maximal fluorescence intensity at 485 nm compared to that of the control (A β 42 with no inhibitor). P4 and P5 showed most prominent effect in both the experiments compared to other three peptides (P1–P3). Each experiment was repeated three times ($n = 3$). Error bars represent the standard deviation (SD) of the fluorescence measurement.

erate inhibition efficiency. P4 and P5 were most competent among all the candidates with an inhibition efficiency of $> 90\%$ as shown in Fig. 3. During the growth phase, A β 42:P4/P5 complex showed a slight enhancement in fluorescence (9 h), which decreased at further time points indicating that A β 42 aggregates formed at a faster rate during the growth phase, but at further time points inhibitors managed to dissolve the aggregates and showed a decrease in fluorescence²⁰. In time-dependent reversal assays, a similar order of efficiency was observed where P1/A β 42 complex showed a slight decrement in fluorescence and P2 and P3 were moderately active in dissolving the A β 42 aggregates with efficiencies of 35% and 25%, respectively. P4 and P5 again exhibited best dissolution efficiencies of 68% and 75% on the A β 42 aggregates. To further validate the inhibition efficiency of our most efficient inhibitor P5, we performed dot blot analysis in a time dependent manner using specific antibody for A β 42 aggregates³⁰. A β 42 (20 μ M) aggregates were incubated with P5 in 1:2 stoichiometry and their influence on the dissolution is quantified at different time points (6, 12, 24 and 48 h) by measuring chemiluminescence intensity (supplementary Fig. S1). The dot blot analysis data clearly supported our ThT dissolution assay of A β 42 aggregates with P5 as shown in Fig. 3b.

To further validate our results, we performed CD studies. A β 42 aggregates are predominantly made of β -sheet assembly, which can be assessed by CD measurements. Hence, a decrease in β -sheet content and corresponding characteristic CD signal intensity directly correlate with the inhibition efficiencies of inhibitors. In this assay, we monitored the intensity of negative CD band centered at 218 nm, characteristic of a β -sheet structure and a decrease in its intensity was correlated with a reduction in the toxic A β 42 aggregates (supple-

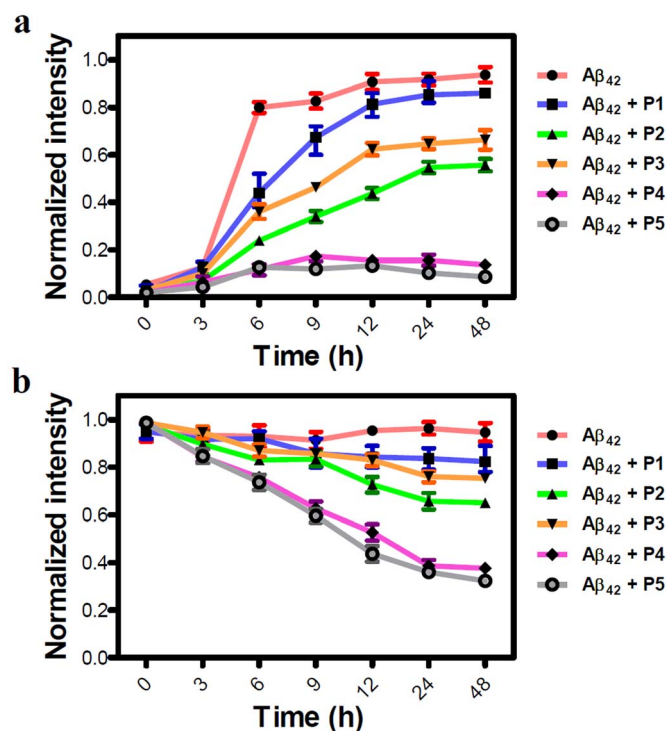


Figure 3 | Kinetics of P1–P5 on inhibition and reversal of A β 42 fibril using ThT assay. A 20 μ M of A β 42 monomers (a) or their aggregates (b) were incubated with inhibitors (P1, P2, P3, P4 and P5) at 37°C in 1:2 stoichiometry and their influence on fibrillization or dissolution is quantified by measuring ThT fluorescence intensity, which is represented as normalized fluorescence intensity at 485 nm for a given time point. Each experiment was repeated three times ($n = 3$). Error bars represent the standard deviation (SD) of the fluorescence measurement.

mentary Fig. S2). In these CD measurements, samples similar to ThT fluorescence assays were used to allow for direct comparison between the two experiments. In the case of inhibition assay, A β 42 monomers were incubated with inhibitor candidates for 4 days at 37°C and then CD measurements were performed to evaluate the inhibition efficiency. A β 42/P1 mixture showed a slight decrease in β -sheet content (deduced by a decrease in negative band at 218 nm). A β 42/P2 showed a slight blue shift and $> 50\%$ reduction in CD intensity (a decrease in intensity at 218 nm compared to the A β 42 control, P1) as compared to untreated A β 42 while P3 showed only $\sim 30\%$ decrease in β -sheet content. Supporting our results obtained in the ThT assay, P4 and P5 emerged as efficient inhibitors as they exhibited $> 80\%$ inhibition (corresponding to a decrease in CD band intensity at 218 nm) of the formation of A β 42 aggregates (Fig. 4). In the reversal assay, A β 42 aggregates were incubated with the inhibitor candidates for six days at 37°C and then, CD measurements were performed. CD data was in excellent agreement with the dissolution efficiency obtained in reversal assay experiments monitored by the ThT assay (Fig. 2). P2 and P3 showed moderate dissolution efficiencies of 40% and 25%, respectively towards the A β 42 aggregates. P4 and P5 showed appreciable dissolution efficiencies of $> 75\%$ (Fig. 4). Overall, inhibition and dissolution efficiencies obtained in the ThT fluorescence assay and CD measurements were in good agreement.

To prove that the above results were purely due to changes in A β 42 and had not been altered by the self-aggregation of inhibitory peptides, we performed a time-dependent assay over a period of 10 days where all the inhibitor candidates (P1–P5) were incubated at 37°C and their effect on the fluorescence of ThT was monitored. Fluorescence enhancement shown by inhibitor (P1–P5) alone was almost negligible, which was further confirmed by CD measurement,

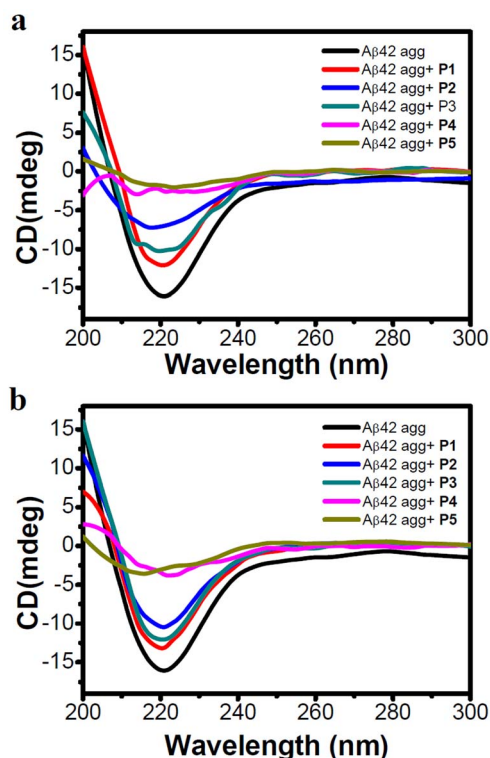


Figure 4 | Studying Inhibition and reversal assay of A β 42 aggregates by CD measurements. The data in (a) and (b) show the effects of **P1**, **P2**, **P3**, **P4** and **P5** (40 μ M) on the aggregation of 20 μ M A β 42 (on day 4 for the inhibition assay and day 6 for the reversal assay). Insets in (a) and (b) shows the intensity of negative signal at 218 nm (represents β -sheet content) observed in corresponding experiments. **P4** and **P5** effectively decreased the β -sheet content corresponding to A β 42 aggregates compared to **P1**-**P3**.

even on the tenth day of incubation modulator peptides did not adopt any secondary conformations (supplementary Fig. S3)³⁰.

TEM Analysis. To further consolidate our conclusions drawn from the ThT assay and CD measurements, we performed TEM to analyze the effect of **P4** and **P5** on the process of fibrillization and preformed toxic aggregates of A β 42 (Fig. 5). All the experiments were performed with 20 μ M of A β 42 in PBS buffer (10 mM, pH 7.4). For inhibition experiments, A β 42 monomers were incubated with **P4** or **P5** for 6 days at 37°C while for reversal experiments preformed A β 42 aggregates were incubated with **P4** or **P5** for 12 days at 37°C. A β 42, when incubated in PBS buffer at 37°C for two days, showed the presence of long fibrillar aggregates (Fig. 5a). **P1** was used as a negative control as it did not show any significant changes in the inhibition or dissolution experiments as monitored in the ThT assay and CD measurements. **P1** incubated with A β 42 showed the presence of fibrillar aggregates in both inhibition and reversal experiments as shown in Figures 5b and 5e, respectively. In contrast, **P4** showed complete absence of fibrils in the inhibition experiment confirming the prevention of fibrillar growth of A β 42 (Fig. 5c). In the case of reversal experiment, there were no signs of fibrils in **P4** (Fig. 5f). Similarly, **P5** showed the absence of fibrillar aggregates in inhibition (Fig. 5d) and reversal (Fig. 5g) experiments. Further, the observed globular morphology of **P4** treated A β 42 fibrillar aggregates as shown in Fig. 5f could be misunderstood as toxic oligomeric species. To investigate this, we performed a dot blot analysis where A β 42 (20 μ M) aggregates were incubated with **P4** and **P5** in 1:2 (A β 42: inhibitor) stoichiometry for 12 days at 37°C and then treated with A11 antibody (which specifically binds to toxic A β 42 oligomeric species) followed by treatment with secondary

antibody and finally chemiluminescence intensity was measured. Positive control, A β 42 oligomers showed a signal, whereas A β 42 + **P4** and A β 42 + **P5** did not show any signal indicating absence of toxic oligomeric species. To further verify the findings, toxicity assay was performed where yeast cells (*Saccharomyces cerevisiae*) were incubated with A β 42 oligomers (50 μ M) and A β 42 (50 μ M) aggregates which were treated with **P4** in 1:2 (A β 42: **P4**) stoichiometry, at 37°C and their effect on the growth curve was monitored. A β 42 oligomers showed high toxicity (Fig. S5), whereas A β 42 + **P4** sample showed least effect on the growth curve of yeast cells. Therefore, the dot blot analysis and toxicity assay confirms that globular structures seen in Fig. 5f are not toxic A β 42 oligomeric species (supplementary Fig. S4 and Fig. S5)⁴¹. Therefore, TEM data confirmed that **P4** and **P5** were involved in the inhibition and dissolution of toxic aggregates, which is in agreement with the conclusions drawn from other experiments.

Blood plasma and proteolytic stability for peptidomimetics. The impact of N-terminal modification (**P2** and **P3**) and Sr (N-methylglycine) substitution (**P4** and **P5**) in **P1** were investigated for their proteolytic stability towards blood plasma proteases³⁷. The assay involved the incubation of peptides (50 μ M) with blood serum at 37°C for a period of 24 h and assessing the amount of intact peptides at different time points (0, 3, 6, 12 and 24 h) using RP-HPLC. **P1** exhibited greatest susceptibility towards the serum proteases with a serum half-life of \sim 3 h, and 80% of the **P1** was degraded at 24 h (Fig. 6). In contrast to that, **P2** and **P3** with modified N-terminal of **P1** (thymine and barbiturate, respectively) showed a better protease stability towards blood plasma. Both **P2** and **P3** followed almost a similar path of degradation with time, where they showed a half-life of \sim 10 h. This was 3 times higher compared to **P1** indicating that the N-terminal modification with a non-amino acid moiety had enhanced the blood protease stability by interfering with the degradation ability of proteases. At 24 h, both **P2** and **P3** were degraded to 70%, which was comparable to **P1** suggesting that stability of both **P2** and **P3** decreased with time. Remarkably, **P4** and **P5** were very stable towards blood plasma proteases in comparison to the other peptides (**P1**, **P2** and **P3**). After 24 h, more than 90% of **P4** and **P5** were intact with **P5** exhibiting relatively higher stability than **P4** (Fig. 6). Proteolytic enzymes generally recognize the specific amide bond between the natural amino acids and cleave them. In the case of **P1**, **P2** and **P3** all the amino acids were natural (except N-terminal modifications in **P2** and **P3**, which showed marginally higher stability) and could be easily recognized by proteases; these peptides thus, degraded with time. On the other hand, **P4** and **P5** with an unnatural amino acid (Sr: N-methylglycine) in alternate positions were not recognized by the blood plasma proteases, resulting in their high blood plasma protease stability.

To further validate these results, we performed a stability assay for **P1**-**P5** (50 μ M) in the presence of proteolytic enzymes trypsin and pepsin. Enzymes trypsin and pepsin are well-known to cleave the C-terminal of lysine and amide bond involving aromatic amino acids, respectively³⁹. Peptides were incubated with both the enzymes at 37°C for 24 h, and the amount of the residual intact peptide was monitored in each case at different time points (0, 3, 6, 12 and 24 h) using RP-HPLC. **P1**, **P2** and **P3** were less stable, of which **P1** degradation was fastest followed by **P2** and **P3**. However, **P4** and **P5** were highly stable under similar conditions and > 90% of the peptidomimetics was intact after 24 h of incubation in the presence of both the enzymes suggesting their poor recognition by the two proteases (supplementary Fig. S6). Overall, the stability assays with blood plasma and proteolytic enzymes led to similar conclusions and confirmed the stability, order **P5**>**P4**>>**P3**≈**P2**>**P1**.

Designed Peptidomimetics Nullify A β Toxicity in an Autophagy-Dependent Manner. All the peptides and their analogs (**P1**-**P5**) were screened for their ability to ameliorate the toxicity caused by A β 42 in

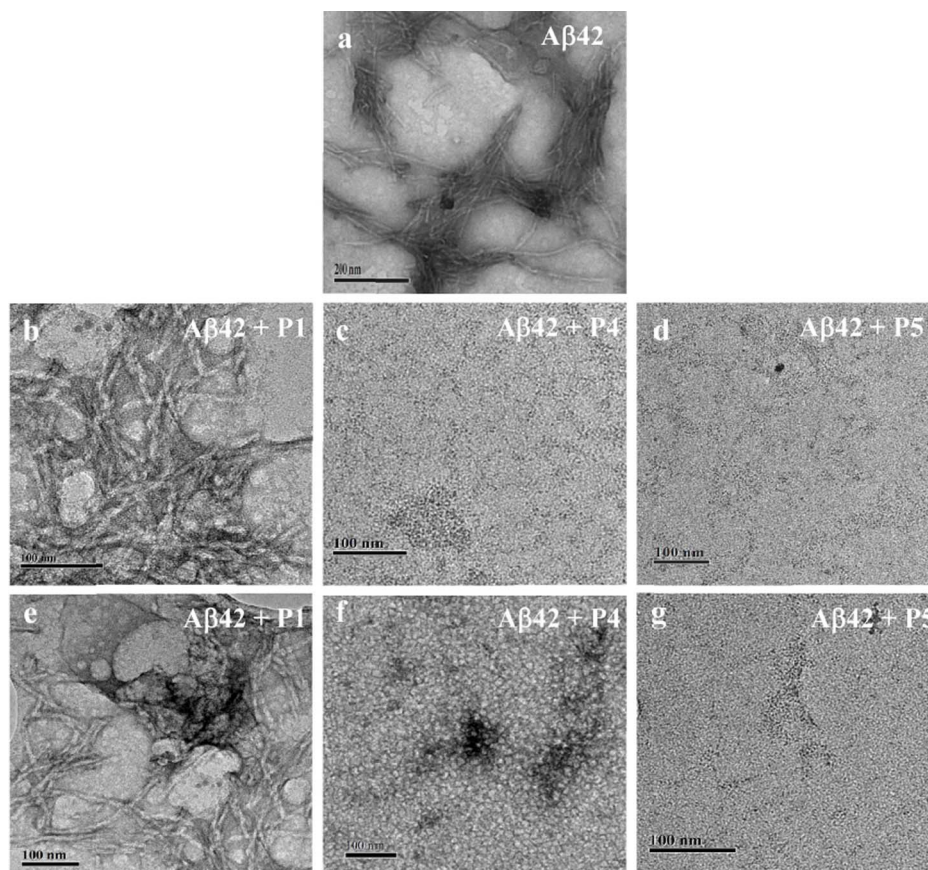


Figure 5 | Electron microscopy examination to study the effect of P1, P4 and P5 on A β 42 fibrillization and dissolution of aggregates. P1, P4 and P5 were incubated with 20 μ M of A β 42 monomers or their aggregates at 37°C in 1:2 (A β 42:inhibitor) stoichiometry and analyzed on day 6 for the inhibition assay and day 12 for the reversal assay experiments. Inhibition assay: A β 42 a, A β 42 + P1 b, A β 42 + P4 c, and A β 42 + P5 d. Reversal assay: A β 42 + P1 e, A β 42 + P4 f, and A β 42 + P5 g. P1 showed least effect on morphology of A β 42 fibrils, whereas P4 and P5 showed prevention of A β 42 fibrils formation in inhibition assay and dissolution of A β 42 aggregates in reversal assay. Scale bar: 100 nm.

a *Saccharomyces cerevisiae* model. N-terminal of A β 42 was tagged with GFP (WT GFP β A) while the WT GFP strain was used as a control. To study the non-toxic nature of inhibitor candidates, their influence on culture growth curves of WT GFP were analyzed

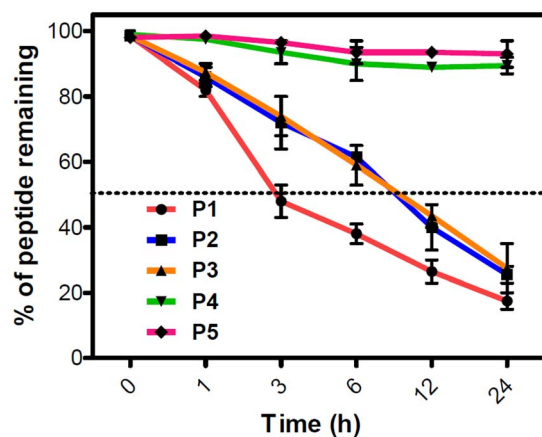


Figure 6 | Serum stability of inhibitors. Inhibitors (50 μ M) (P1-P5) were incubated in human blood serum (HBS) and were analyzed at different time points over a duration of 24 h to determine the percentage of intact inhibitor. P1, P2 and P3 degraded with time, whereas P4 and P5 showed high stability towards the serum proteases. Each experiment was repeated three times ($n = 3$). Error bars represent the standard deviation (SD) of the fluorescence measurement.

(supplementary Fig. S7). In P1-P5 (300 μ M) treated cells, the growth curves were similar to that of the untreated sample. No significant growth lag or drop in absorbance (A_{600}) was observed in the presence of peptides. On the other hand, the growth curve of WT GFP β A exhibited a severe lag with the culture not entering the exponential phase due apparently to A β toxicity³⁶. The apparent growth lag displayed by WT GFP β A strain compared to WT GFP was used for screening the inhibitors (Fig. 7a). Among five inhibitors, growth curves of WT GFP β A strain in the presence of peptides P1, P2 and P3 appeared similar to that of untreated cells. However, the cells treated with peptides P4 and P5 displayed a growth pattern similar to that of WT GFP. Hence, it is inferred that peptides P4 and P5, but not the others, successfully rescued the growth lag in WT GFP β A strain. Upon P4 and P5 treatments, various growth parameters like growth rate and doubling time in WT GFP β A strain showed significant rescue comparable to that of WT GFP where the growth rate was increased whereas doubling time was reduced evidently (supplementary Fig. S8).

Next, we probed if the inhibitors were able to clear the A β aggregates (tagged with GFP) *in vivo*. For this, we performed a microscopy assay wherein the GFP β A appear as punctate dots when present as aggregates while its clearance in the vacuole is marked by the presence of free GFP. GFP β A-expressing cells, when either untreated or treated with peptide P1, displayed characteristic punctate formation inside the cells and no free GFP was present in the vacuole (Fig. 8a). The free GFP was observed in vacuoles in culture treated with P4 and P5, but was absent in P1 (control) and untreated cells (Fig. 8a) of WT GFP β A strain. Pertaining to P4 and P5, diffused GFP signal in the

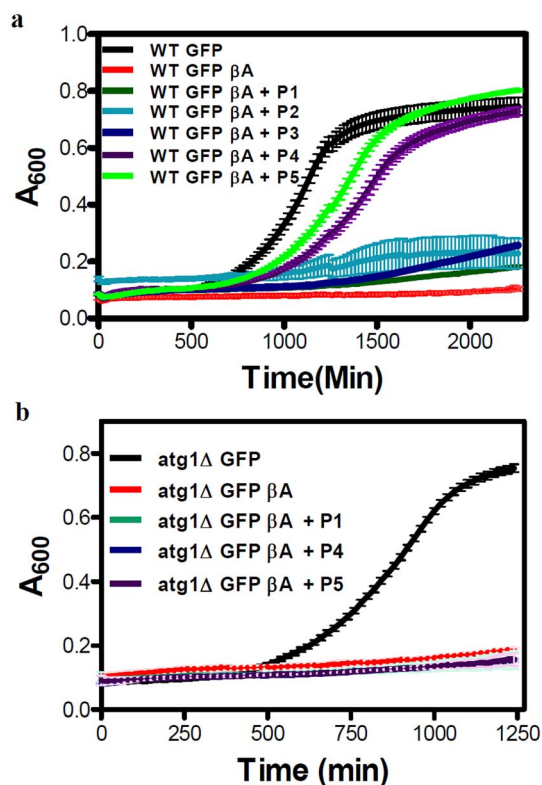


Figure 7 | Screening of inhibitors in a yeast model of A β toxicity. (a), All inhibitor candidates were screened in WT GFP β A strain at the concentration of 300 μ M. (b), Investigation of P1, P4 and P5 in the *atg1 Δ* GFP β A strain by monitoring growth curves at peptide concentrations of 300 μ M. Each experiment was repeated three times ($n = 3$). Error bars represent the standard deviation (SD) of the measurement.

vacuole co-localized with the vacuolar lumen staining dye CMAC-Blue, suggesting that incubating cells with these peptides resulted in GFP β A aggregates being degraded in the vacuole to release free GFP. Autophagy has been shown to play a key role in degrading the β -amyloid oligomers or fibrils⁴². Degradation of protein aggregates by selective autophagy mechanism is defined as aggrephagy⁴³. In cellular context, the disaggregated fibrils are captured and released into the vacuole for degradation through autophagy. To investigate whether the appearance of free GFP in the vacuoles of cells treated with P4 and P5 was due to autophagy, we repeated the growth rescue experiment in cells defective in autophagy (Δ atg1 mutant). Although P4 and P5 were able to rescue the growth lag in WT GFP β A strain, they failed to do so in *atg1 Δ* GFP β A strain (Fig. 7b). In addition, vacuolar free GFP was not seen in *atg1 Δ* GFP β A strain treated with P4 and P5 (Fig. 8b) similar to untreated and P1 treated cells. The peptides neither reduced the A β toxicity nor degraded GFP β A in the autophagy mutant. This clearly indicated that autophagy was responsible for clearing the A β aggregates, by P4/P5 treatments in WT GFP β A cells.

Conclusion

In conclusion, we rationally designed recognition unit based peptidomimetic inhibitors, which target hydrogen bonding and other noncovalent interactions necessary for A β aggregation to form toxic aggregates in Alzheimer's disease progression. ThT fluorescence assay and CD data confirmed that peptides with N-terminal thymine-modification (P2) and peptidomimetics containing N-terminal thymine and sarcosine (N-methylglycine) in alternate positions of KLVFFA (P4 and P5) exhibited both inhibition and dissolution ability towards A β 42 aggregates with the latter two being considerably

more efficient. TEM analysis demonstrated that P4/P5 treated A β 42 monomers or its aggregates showed no signs of fibrillar aggregates compared aggregates found in control study, which further strengthen our hypothesis that P4 and P5 are involved in inhibition and dissolution of A β 42 aggregates. Furthermore, peptidomimetics P4 and P5 showed high stability towards blood serum and proteolytic enzymes like trypsin and pepsin compared to P1-P3. Therapeutic contenders P4 and P5 were tested in a *Saccharomyces cerevisiae* model of A β 42, where they could rescue the yeast cells from A β 42 toxicity by clearing them through the autophagy pathway. Although down-regulation of autophagy is implicated in Alzheimer's disease, for the first time we validated the role of active autophagy in clearance of toxic A β aggregates using peptidomimetics. These results on rationally designing peptidomimetic inhibitors for tackling A β 42 toxicity in Alzheimer's disease will strongly impact the identification of novel drug candidates for this hitherto incurable disease.

Methods

Synthesis of Peptide and its Mimetics, Purification, and Analysis. The control peptide P1 (KLVFF), N-terminal modified peptides P2 (Thymine-Lys-Leu-Val-Phe-Phe) and P3 (Barbiturate-Lys-Leu-Val-Phe-Phe), and the N-methyl glycine (sarcosine: Sr) substituted peptidomimetics P4 (Thymine-Sr-Leu-Sr-Phe-Sr-Ala) and P5 (Thymine-Lys-Sr-Val-Sr-Phe-Sr) were synthesized following standard 9-fluorenylmethoxycarbonyl (Fmoc) chemistry on an automated peptide synthesizer Syro II from MultiSynTech. Rink amide resin (Novabiochem) was used as a solid support in the synthesis with an amide at the C-terminal. Fmoc-protected sarcosine (Sr) was prepared using standard protection procedure and directly used for the synthesis of P4 and P5 using the peptide synthesizer. Amino acids were coupled using HBTU as the activating reagent, DIPEA as the base and DMF as solvent; for deprotection of Fmoc 40% piperidine in DMF was used. P1, P2 and P3 were synthesized with a coupling time of 1 h per amino acid, whereas for P4 and P5 coupling time was increased to 2 h to obtain higher coupling yields. All the peptides and peptidomimetics were purified using a reverse-phase (RP) preparative HPLC on C18 column at 40°C. Product purity was greater than 99% as ascertained by analytical HPLC. The molecular masses of the peptides and their mimetics were verified with HRMS (Q-TOF) analysis.

Preparation of A β 42 fibrillar aggregates and oligomers. A β 42 peptide (0.25 mg) (Calbiochem, Merck) was dissolved in hexafluoro-2-propanol (HFIP, 0.2 mL) and incubated at room temperature for 1 h. HFIP was then removed by the flow of nitrogen and further dried under vacuum. HFIP-treated A β 42 was then dissolved in 10 mM PBS buffer to a concentration of 200 μ M at pH 7.4. The solution was incubated at 37°C for 48 h with constant shaking for fibril formation. The formation of A β 42 fibrillar aggregates was confirmed by ThT fluorescence, CD measurements and electron microscopy. For oligomers, HFIP-treated A β 42 dissolved in 10 mM PBS buffer and incubated at 4°C for 24 h⁴⁴.

Fluorescence Spectroscopy. Fluorescence spectral measurements were carried out using Perkin Elmer Model LS 55 fluorescence spectrophotometer. Maximum fluorescence of ThT was observed with the excitation and emission wavelengths set to 450 and 483 nm, respectively. A ThT concentration of 5–10 μ M was used for amyloid fibrillization and dissolution assay based on the A β 42 fibrillar concentration.

Circular Dichroism. The circular dichroic (CD) spectra were recorded using a Jasco J-815 spectrometer under nitrogen atmosphere. Peptides were dissolved in 10 mM PBS buffer at pH 7.4 at concentrations of 20 μ M. A 10 mm path length was used for the measurements. Four to five scans were acquired from 200 to 300 nm.

Fibrillogenesis and Fibril Dissolution Assays. Prior to the experiment, P1, P2, P3, P4 and P5 were dissolved in HFIP and were evaporated under a stream of dry nitrogen. The dried samples were re-suspended in 10 mM PBS buffer at pH 7.4. An aliquot of A β 42 peptide was then added to the solution with or without one of the inhibitor P1, P2, P3, P4 and P5. The mixtures were vortexed for approximately 30 s and then incubated at 37°C for 2–3 days without shaking. The final concentration of A β 42 in the mixture was 20 μ M. For a dissolution experiment, A β 42 was incubated alone for 2 days to allow fibrils to form. An aliquot of the formed fibrils in 10 mM PBS buffer was then added to the inhibitor peptidomimetics. The amount of fibrils remaining intact was assayed using that fluorescence, CD measurements and transmission electron microscopy as described below.

Transmission Electron Microscopy (TEM). An aliquot of appropriately formed samples of A β 42 aggregates, A β 42-inhibitor and A β 42 aggregate-inhibitor (5 μ L) were adsorbed onto 200-mesh carbon and formavar-coated grids for 2 min and washed for 1 min with distilled water. The samples were negatively stained with 2% uranyl acetate for 5 min and washed for 1 min with distilled water⁴⁴. The samples

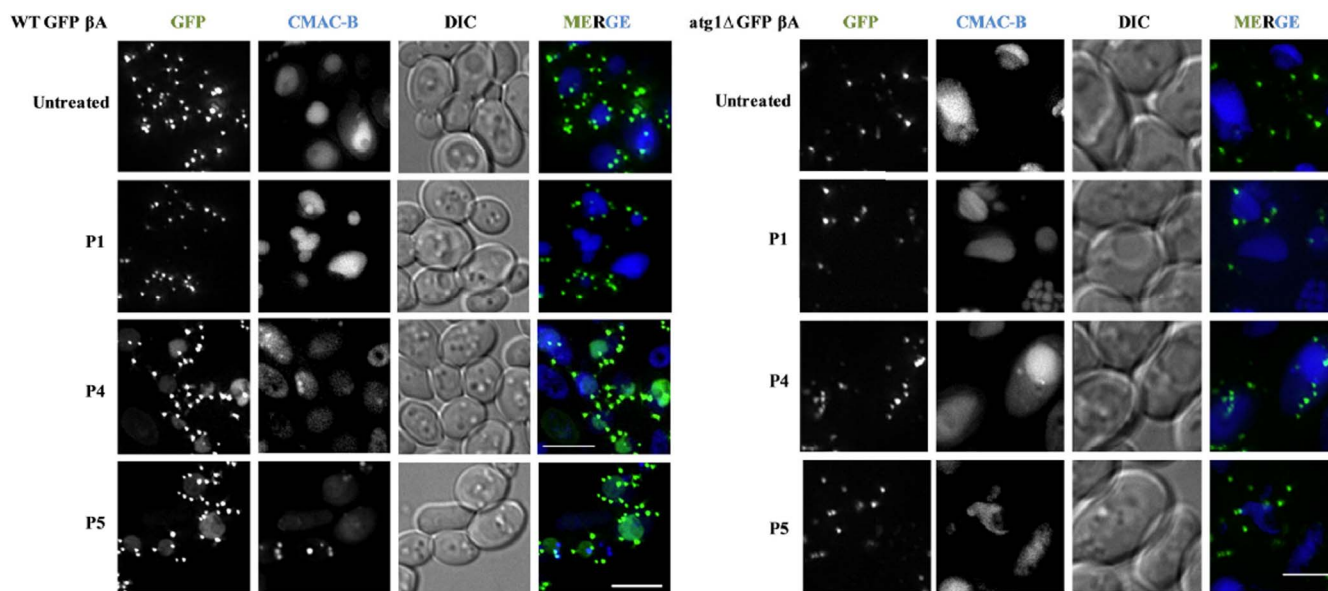


Figure 8 | Degradation of GFP A β in monitored by fluorescence microscope. (a), WT GFP β A and (b), atg1 β A strains were treated with P1 (control), P4 and P5 and vacuoles stained with CMAC-Blue Scale bars: 7.5 μ m (a) and 5 μ m (b). Concentration of P1/P4/P5: 300 μ M.

were air-dried overnight and viewed with a JEOL, JEM 3010 instrument operating at 300 kV.

Dot Blot Analysis. PVDF membranes (Sigma aldrich) were activated by incubating them in methanol solution for 5 min followed by washing with 10 mM PBS buffer (3X). Samples were spotted on the membranes (in triplicate) and non-specific sites were blocked by soaking in 5% BSA in PBS buffer, and skim milk (0.5–1 hour, RT). Then membranes were incubated with either primary antibody A11 (1:3000) for oligomer or Anti-beta-amyloid 1-42 antibody (Merck millipore) for A β 42 fibrillar aggregates at 4°C for overnight and then washed with PBS buffer (3 \times 5 min). These membranes were further incubated with anti-mouse secondary antibody (1:10000) conjugated with horseradish peroxidase (HRP) for 30 min at RT. These membranes were washed with PBS buffer (3 \times 5 min), incubated with enhanced chemiluminescence (ECL) reagent for 1 min and recorded the chemiluminescence in SYNGENE G-box. The signals from the unknown samples were compared to that of standard and concentration was estimated³⁰.

Serum Stability Assay. Human blood serum (HBS) was used to determine serum stability of the inhibitors. The HBS was centrifuged to remove the lipid component, and the supernatant was incubated at 37°C. 50 Mm of each inhibitor (P1, P2, P3, P4 and P5) was incubated in HBS and then 40 μ L triplicate aliquots were removed at 0, 1, 3, 6, 10, 16, and 24 h. Each serum sample was quenched with 40 μ L of 6 M urea and incubated at 4°C for 10 min. Then, each serum sample was quenched with 40 μ L of trichloroacetic acid (20%) and incubated for another 10 min at 4°C to precipitate the serum proteins. The samples were centrifuged for 10 min, and 200 μ L of the supernatant was analyzed on RP-HPLC using a linear gradient of solvent B (0.3 mL/min flow rate). The control samples containing equivalent amounts of inhibitors in PBS buffer were subjected to the same treatment procedure. The percentage recovery of inhibitors was detected by integration at 254 nm⁴⁵.

Protease Stability Assay. Preliminary stability assays were performed using the enzymes pepsin and trypsin. For all assays, peptides were incubated with the enzyme at 37°C for 24 h. All digestion assay data were analyzed by RP-HPLC. Trypsin and pepsin stocks were prepared in 100 mM ammonium bicarbonate (NH₄HCO₃) buffer (pH 8) and 100 mM formic acid buffer (pH 2), respectively. All the peptides/peptidomimetics (P1, P2, P3, P4 and P5) were incubated with trypsin and pepsin enzymes in 100 mM NH₄HCO₃ buffer (pH 8) and formic acid buffer (pH 2), respectively, at 37°C. The trypsin reactions were halted with 0.05% formic acid, and the pepsin reactions were halted with 100 mM NH₄HCO₃. Then the samples were analyzed by RP-HPLC using a linear gradient of solvent B (0.3 mL/min flow rate); similar data points were collected at various time points between 0 and 24 h (1 h, 3 h, 6 h, 12 h and 24 h) during incubation and analyzed in triplicates. The percentages of recovered peptide/peptidomimetics were detected by integration at 254 nm⁴⁶.

Yeast Media, Plasmids and Media Used. Wild type (BY4741; Mat α ; his3 Δ 1; leu2 Δ 0; met15 Δ 0; ura3 Δ 0) and autophagy mutant (atg1 Δ ; BY4741; Mat α ; his3 Δ 1; leu2 Δ 0; met15 Δ 0; ura3 Δ 0; atg1: KanMX4) strains of yeast were employed. Plasmids pRS 416 GFP, pRS 416 β A were gifted by Ian Macreadie (CSIRO, Australia)^{47,48}. The plasmid pRS 306 Gal β A was generated by sticky end ligation of vector pRS 306 Gal (Spe I/Xho I) and insert GFP- β A (Spe I/Xho I) obtained from the plasmid under pRS 416 vector backbone. These plasmids were used to generate sSNS1, sSNS50 and sSNS51 strains

expressing GFP only, GFP-tagged β -amyloid (β A) protein in wild type and autophagy mutant, respectively. These strains expressed genomically integrated GFP tagged A β or GFP only under an inducible galactose promoter. SD-Ura (Synthetic Dextrose without uracil) media and galactose (2%) were used for protein induction.

Yeast Culturing and Growth Assay. Strains were inoculated into SD-Ura growth medium and incubated overnight (250 rpm, 30°C). Secondary culture was inoculated (absorbance = A₆₀₀ around 0.2 OD) from the primary inoculum and incubated as above till A₆₀₀ reached 0.8 OD. High throughput growth curve analysis (using Varioskan Flash, Thermo Scientific) in the presence and absence of peptides (300 μ M) was performed by automatically recording A₆₀₀ every 20 min in a 384-well plate.

β -Amyloid Degradation Assay. The cells were inoculated in SD-Ura medium under appropriate conditions (250 rpm, 30°C). Secondary culture was inoculated from this primary inoculum and incubated till A₆₀₀ reached 0.8. Then, cells were washed twice with sterile water. Subsequently, the A β proteins were induced in yeast cells by incubating them in 2% galactose. During the induction, these cells were incubated in the presence or absence of peptidomimetics (300 μ M). After 12 h, 7-amino-4-chloromethylcoumarin-Blue (CMAC-Blue) was added and incubated further for 2 h after which cultures were imaged on a fluorescent widefield microscope (DV Elite, Deltavision).

Vacuole Staining by CMAC-Blue. CMAC Blue dye (Life technologies) was used to stain the yeast vacuole. Excitation and emission peaks for CMAC-Blue were 350 nm and 450 nm, respectively. Dye was added to the culture at a final working concentration of 100 nM, incubated for 30 min (250 rpm, 30 μ C) and then imaged.

Fluorescence Microscopy. Cells were washed and mounted on agarose pad (2%) and imaged using Delta Vision Elite widefield microscope with FITC and DAPI filters. The collected images were processed using Axiovision or DV SoftWoRX software. The excitation CWL/BP and emission CWL/BP for filters used were 490/20 and 529/38 (FITC), 390/18 and 435/48 (DAPI).

1. Prince, M. *et al.* The global prevalence of dementia: A systematic review and metaanalysis. *Alzheimer's & Dementia* **9**, 63–75 (2013).
2. Selkoe, D. J. Folding proteins in fatal ways. *Nature* **426**, 900–904 (2003).
3. Ross, C. A. & Poirier, M. A. Protein aggregation and neurodegenerative disease. *Nat. Med.* **10**, S10–S17 (2004).
4. Hamley, I. W. The amyloid beta peptide: a chemist's perspective. Role in Alzheimer's and fibrillization. *Chem. Rev.* **112**, 5147–5192 (2012).
5. DeToma, A. S., Salamekh, S., Ramamoorthy, A. & Lim, M. H. Misfolded proteins in Alzheimer's disease and type II diabetes. *Chem. Soc. Rev.* **41**, 608–621 (2012).
6. Savellieff, M. G., Lee, S., Liu, Y. & Lim, M. H. Untangling Amyloid- β , Tau, and Metals in Alzheimer's Disease. *ACS Chem. Biol.* **8**, 856–865 (2013).
7. Rauk, A. The chemistry of Alzheimer's disease. *Chem. Soc. Rev.* **38**, 2698–2715 (2009).
8. Nie, Q., Du, X. G. & Geng, M. Y. Small molecule inhibitors of amyloid β peptide aggregation as a potential therapeutic strategy for Alzheimer's disease. *Acta Pharmacol. Sin.* **32**, 545–551 (2011).



9. Takahashi, T. & Mihara, H. Peptide and protein mimetics inhibiting amyloid β peptide aggregation. *Acc. Chem. Res.* **41**, 1309–1318 (2008).
10. Acerra, N. *et al.* Retro-inversion of intracellular selected β -amyloid-interacting peptides: implications for a novel Alzheimer's disease treatment. *Biochemistry* **53**, 2101–2111 (2014).
11. Castelletto, V., Hamley, I. W., Lim, T., De Tullio, M. B. & Castano, E. M. β -amino acid modified heptapeptide containing a designed recognition element disrupts fibrillization of the amyloid β -peptide. *J. Pept. Sci.* **16**, 443–450 (2010).
12. Ouberai, M., Dumy, P., Chierici, S. & Garcia, J. Synthesis and biological evaluation of clicked curcumin and clicked KLVFFA conjugates as inhibitors of β amyloid fibril formation. *Bioconjugate Chem.* **20**, 2123–2132 (2009).
13. Soto, C., Kindy, M. S., Baumann, M. & Frangione, B. Inhibition of Alzheimer's amyloidosis by peptides that prevent β -sheet conformation. *Biochem. Biophys. Res. Commun.* **226**, 672–680 (1996).
14. Ghanta, J., Shen, C. L., Kiessling, L. L. & Murphy, R. M. A strategy for designing inhibitors of β -amyloid toxicity. *J. Biol. Chem.* **271**, 29525–29528 (1996).
15. Mishra, R. *et al.* Small-molecule inhibitors of islet amyloid polypeptide fibril formation. *Angew. Chem. Int. Ed.* **47**, 4679–4682 (2008).
16. Serpell, C. L. Alzheimer's amyloid fibrils: Structure and assembly. *Biochim. Biophys. Acta.* **1502**, 16–30 (2000).
17. Tjernberg, L. O. *et al.* Arrest of amyloid fibril formation by a pentapeptide ligand. *J. Biol. Chem.* **271**, 8545–8548 (1996).
18. Soto, C. *et al.* β -Sheet breaker peptide inhibits fibrogenesis in a rat brain model of amyloidosis: Implications in Alzheimer's therapy. *Nat. Med.* **4**, 822–826 (1998).
19. Pallitto, M. M., Ghanta, J., Heinzelman, P., Kiessling, L. L. & Murphy, R. M. Recognition sequence design for peptidyl modulators of β -amyloid aggregation and toxicity. *Biochemistry* **38**, 3570–3578 (1999).
20. Lowe, T. L., Strzelec, A., Kiessling, L. L. & Murphy, R. M. Structure-function relationships for inhibitors of β -amyloid toxicity containing the recognition sequence KLVFF. *Biochemistry* **40**, 7882–7889 (2001).
21. Gibson, T. J. & Murphy, R. M. Design of peptidyl compounds that affect β -amyloid aggregation: importance of surface tension and context. *Biochemistry* **44**, 8898–8907 (2005).
22. Chafekar, S. M. *et al.* Branched KLVFF tetramers strongly potentiate inhibition of β -amyloid aggregation. *ChemBioChem* **8**, 1857–1864 (2007).
23. Findeis, M. A. *et al.* Modified-peptide inhibitors of amyloid β -peptide polymerization. *Biochemistry* **38**, 6791–6800 (1999).
24. Wei, C. W. *et al.* Synthesis and evaluation of ferrocenylpentapeptide (Fc-KLVFF). *Bioorg. Med. Chem. Lett.* **21**, 5818–5821 (2011).
25. Gordon, D. J., Tappe, R. & Meredith, S. C. Design and characterization of a membrane permeable N-methyl amino acid-containing peptide that inhibits A β 1–40 fibrillogenesis. *J. Peptide Res.* **60**, 37–55 (2002).
26. Kapurniotu, A., Schmauder, A. & Tenidis, K. Structure-based design and study of non-amyloidogenic, double N-methylated IAPP amyloid core sequences as inhibitors of IAPP amyloid formation and cytotoxicity. *J. Mol. Biol.* **315**, 339–350 (2002).
27. Amijee, H. *et al.* The N-methylated peptide SEN304 powerfully inhibits A β (1–42) toxicity by perturbing oligomer formation. *Biochemistry* **51**, 8338–8352 (2010).
28. Kokkoni, N., Stott, K., Amijee, H., Mason, J. M. & Doig, A. J. N-Methylated peptide inhibitors of β -amyloid aggregation and toxicity. Optimization of the inhibitor structure. *Biochemistry* **45**, 9906–9918 (2006).
29. Gordon, D. J., Sciarretta, K. L. & Meredith, S. C. Inhibition of β -amyloid(40) fibrillogenesis and disassembly of β -amyloid (40) fibrils by short β -amyloid congeners containing N-methyl amino acids at alternate residues. *Biochemistry* **40**, 8237–8245 (2001).
30. Turner, J. P. *et al.* Rationally designed peptoids modulate aggregation of amyloid-beta 40. *ACS Chem. Neurosci.* **5**, 552–558 (2014).
31. Manjithaya, R. & Subramani, S. Autophagy: A broad role in unconventional protein secretion? *Trends Cell Biol.* **21**, 67–73 (2011).
32. Rajasekhar, K. *et al.* Synthesis of hybrid cyclic peptoids and identification of autophagy enhancer. *ChemPlusChem.* **79**, 25–30 (2014).
33. Matlack, K. E. S. *et al.* Clioquinol promotes the degradation of metal-dependent amyloid- β (A β) oligomers to restore endocytosis and ameliorate A β toxicity. *Proc. Natl. Acad. Sci. USA* **111**, 4013–4018 (2014).
34. Smith, M. G. & Snyder, N. Yeast as a Model for Human Disease. *Current Protocols in Human Genetics*. (John Wiley & Sons, Inc. 2006).
35. Khurana, V. & Lindquist, S. Modelling neurodegeneration in *Saccharomyces cerevisiae*: why cook with baker's yeast? *Nat. Rev. Neurosci.* **11**, 436–449 (2010).
36. Treusch, S. *et al.* Functional links between A β toxicity, endocytic trafficking, and Alzheimer's disease risk factors in Yeast. *Science* **334**, 1241–1245 (2011).
37. Gilead, S. & Gazit, E. Inhibition of amyloid fibril formation by peptide analogues modified with alpha- aminoisobutyric acid. *Angew. Chem. Int. Ed.* **43**, 4041–4044 (2004).
38. Hochdrffer, K. *et al.* Rational design of β -sheet ligands against A β 42-induced toxicity. *J. Am. Chem. Soc.* **133**, 4348–4358 (2011).
39. De Bona, P. *et al.* Design and synthesis of new trehalose-conjugated pentapeptides as inhibitors of A β (1–42) fibrillogenesis and toxicity. *J. Pept. Sci.* **15**, 220–228 (2009).
40. Etienne, M. A., Aucoin, J. P., Fu, Y., McCarley, R. L. & Hammer, R. P. Stoichiometric Inhibition of Amyloid β -Protein Aggregation with Peptides Containing Alternating α,α -Disubstituted Amino Acids. *J. Am. Chem. Soc.* **128**, 3522–3523 (2006).
41. Hong, H. S. *et al.* Inhibition of Alzheimer's amyloid toxicity with a tricyclic pyrone molecule in vitro and in vivo. *J. Neurochem.* **108**, 1097–1108 (2009).
42. Hung, S. Y., Huang, W. P., Liou, H. C. & Fu, W. M. Autophagy protects neuron from A β -induced cytotoxicity. *Autophagy* **5**, 502–510 (2009).
43. Overbye, A., Brinckmann, M. F. & Seglen, P. O. Proteomic analysis of membrane-associated proteins from rat liver autophagosomes. *Autophagy* **3**, 300–322 (2007).
44. Jan, A., Hartley, D. M. & Lashuel, H. A. Preparation and characterization of toxic A β aggregates for structural and functional studies in Alzheimer's disease research. *Nat. Protoc.* **5**, 1186–1209 (2010).
45. Halai, R. *et al.* Effects of cyclization on stability, structure, and activity of α -conotoxinria at the $\alpha 9\alpha 10$ nicotinic acetylcholine receptor and GABA β receptor. *J. Med. Chem.* **54**, 6984–6992 (2011).
46. Lovelace, E. S. *et al.* Cyclic Mr1A: A stable and potent cyclic conotoxin with a novel topological fold that targets the norepinephrine transporter. *J. Med. Chem.* **49**, 6561–6568 (2006).
47. Dominik, M., Rolf, M. & Martin, F. Yeast vectors for controlled expression of heterologous proteins in different genetic backgrounds. *Gene* **156**, 119–122 (1995).
48. Caine, J. *et al.* Alzheimer's A β fused to green fluorescent protein induces growth stress and a heat shock response. *FEMS Yeast Res.* **7**, 1230–1236 (2007).

Acknowledgments

We thank Prof. C. N. R. Rao FRS for constant support, JNCASR, Science and Engineering Research Board (SERB) [Research grant: SB/S1/OC-47/2103] and the Department of Science and Technology (DST), Government of India and Wellcome-DBT India Alliance for financial support.

Author contributions

K.R. and T.G. designed the project. K.R. undertook the synthesis, photophysical studies and *in vitro* studies of the modulators, S.N.S. and R.M. designed *in vivo* studies. All authors contributed to writing the manuscript.

Additional information

Supplementary information accompanies this paper at <http://www.nature.com/scientificreports>

Competing financial interests: The authors have no competing interests as defined by Nature Publishing Group, or other interests that might be perceived to influence the results and/or discussion reported in this paper.

How to cite this article: Rajasekhar, K., Suresh, S.N., Manjithaya, R. & Govindaraju, T. Rationally Designed Peptidomimetic Modulators of A β Toxicity in Alzheimer's Disease. *Sci. Rep.* **5**, 8139; DOI:10.1038/srep08139 (2015).



This work is licensed under a Creative Commons Attribution 4.0 International License. The images or other third party material in this article are included in the article's Creative Commons license, unless indicated otherwise in the credit line; if the material is not included under the Creative Commons license, users will need to obtain permission from the license holder in order to reproduce the material. To view a copy of this license, visit <http://creativecommons.org/licenses/by/4.0/>

DOI: 10.1002/cplu.201300343



Synthesis of Hybrid Cyclic Peptoids and Identification of Autophagy Enhancer

Kolla Rajasekhar,^[a] Nagarjun Narayanaswamy,^[a] Piyush Mishra,^[b] S. N. Suresh,^[b]
Ravi Manjithaya,^[b] and T. Govindaraju^{*[a]}

Cyclic peptoids are potential candidates for diverse biological activities. However, applications of cyclic peptoids are limited by the synthetic difficulties, conformational flexibility of large cyclic peptoids, and lack of secondary amide in the backbone. Herein, an elegant methodology for the synthesis of small and medium-size cyclic hybrid peptoids is developed. ¹⁵N-Alkyl and ¹⁵N-acyl substituents in *N*-(2-aminoethyl)glycine monomers enforce intra- and intermolecular cyclization to form stable six- and 12-membered cyclic products, respectively. NMR studies show inter- and intramolecular hydrogen bonding in six- and 12-membered cyclic peptoids, respectively. Screening of a cyclic peptoid library resulted in the identification of a potential candidate that enhanced autophagic degradation of cargo in a live cell model. Such upregulation of autophagy using small molecules is a promising approach for elimination of intracellular pathogens and neurodegenerative protein aggregates.

Peptides have emerged as promising therapeutic agents in recent years owing to their inexpensive synthesis, efficacy, specificity, and low toxicity. However, high susceptibility to proteolysis, flexibility, short half-life, denaturation, and poor target delivery and bioavailability make peptides practically less viable candidates for therapeutics. The deficiencies of linear peptides can be addressed by macrocyclization and crosslinking, which provide proper conformational stability.^[1] Although cyclic peptides offer relative stability and cell penetration efficiency, they also suffer from low *in vivo* stability and bioavailability. To address the inherent drawbacks of natural peptides, promising peptidomimetics have been developed.^[2] In particular peptoids, oligomers of *N*-substituted glycine with distinct

unnatural structure, possess numerous advantages. Peptoids have long half-lives owing to proteolytic resistance and good cell permeability resulting in greater bioavailability.^[3] However, major limitations of peptoids are their conformational flexibility and lack of secondary interactions, which can reduce the selectivity and sensitivity. Yet again, the macrocyclization of peptoids has been pursued to restrict conformational flexibility.^[4] Applications of cyclic peptoids are limited by the synthetic procedures and lack of secondary amide in the backbone. The most challenging aspect of cyclic peptidomimetics synthesis is the ring-closure event.^[5] The yields obtained in cyclization of longer oligomers are very moderate and the cyclization of short oligomers suffers from poor yields.^[1] An increase in ring size of cyclic peptidomimetics reduces bioactivity as a result of enhanced flexibility. This reiterates the importance of small/medium-size cyclic peptoids.


The linear and cyclic peptidomimetics have been studied for antimicrobial activity, DNA interaction, and autophagy modulation.^[6] Autophagy is a key mechanism for long-lived protein degradation and organelle turnover, and serves as a critical adaptive response that recycles energy and nutrients during starvation or stress. Small molecules have been utilized as probes to understand mechanisms as well as the relationship between autophagy and disease.^[7]


Herein, we report coupling-reagent-free differential cyclization of *N*-(2-aminoethyl)glycine (*aeg*) hybrid peptoid monomer into six- and 12-membered cyclic peptoids. In the literature, *aeg* has been used extensively as a backbone unit for the synthesis of peptide nucleic acids.^[8] Our choice of *aeg* monomer stemmed from the fact that among other advantages, small and medium-size hybrid cyclic peptoids are formed with secondary amide bonds and stable conformation. Further, we employed a simple design strategy wherein ¹⁵N-alkyl substituents keep the flexibility intact, whereas ¹⁵N-acyl substituents introduce rigidity and restricted bond rotation in the *aeg* backbone. Thus, *aeg* monomers with distinct ¹⁵N substituents and conformational features are expected to follow different modes of cyclization. To the best of our knowledge, this is the first report wherein *aeg* monomer has been used for direct synthesis of six- and 12-membered hybrid cyclic peptoids under coupling-reagent-free conditions. This cyclic peptoid library was screened to identify modulators of the autophagy process.

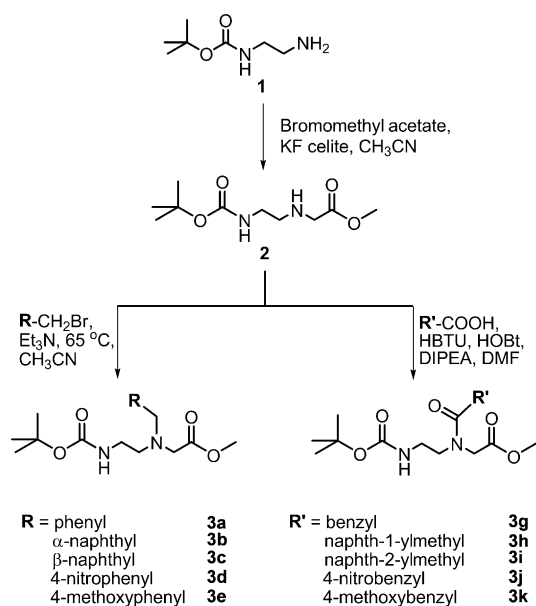
The *aeg* backbone was synthesized from mono *tert*-butoxycarbonyl (Boc)-protected ethylenediamine **1** (Scheme 1). The amine **1** was subjected to controlled mono-¹⁵N-alkylation by treatment with bromomethyl acetate using KF celite to obtain Boc-protected *aeg* methyl ester **2**. Then, the second ¹⁵N-alkyla-

[a] K. Rajasekhar, N. Narayanaswamy, Dr. T. Govindaraju
Bioorganic Chemistry Laboratory
New Chemistry Unit
Jawaharlal Nehru Centre for Advanced Scientific Research
Jakkur P.O., Bangalore 560064 (India)
Fax: (+91) 80-2208-2627
E-mail: tgraju@jncasr.ac.in
Homepage: <http://www.jncasr.ac.in/tgraju/>

[b] P. Mishra, S. N. Suresh, Dr. R. Manjithaya
Molecular Biology and Genetics Unit
Jawaharlal Nehru Centre for Advanced Scientific Research
Jakkur P.O., Bangalore 560064 (India)

 Supporting information for this article is available on the WWW under <http://dx.doi.org/10.1002/cplu.201300343>.

 This article is part of the "Early Career Series". To view the complete series, visit: <http://chempluschem.org/earlycareer>.



Scheme 1. Synthesis of Boc-protected α -N-alkyl (**3a–e**) and α -N-acyl (**3g–k**) modified *aeg* methyl ester monomers. HBTU = 2-(1*H*-benzotriazole-1-yl)-1,1,3,3-tetramethyluronium hexafluorophosphate, HOBT = *N*-hydroxybenzotriazole, DIPEA = *N,N*-diisopropylethylamine, DMF = *N,N*-dimethylformamide.

tion of amine **2** was performed with bromomethyl derivatives using triethylamine as base to obtain excellent yields of methyl esters of Boc-protected α -N-alkyl-*aeg* monomers **3a–e** (Scheme 1). The amine **2** was coupled to acetic acid derivatives to yield methyl esters of Boc-protected α -N-acyl-*aeg* monomers **3g–k**. The Boc-protected α -N-benzyl-*aeg* methyl ester monomer (**3a**) was subjected to in situ Boc deprotection and subsequent cyclization at 110 °C in *sec*-butanol containing 1% acetic acid (Table 1).^[9] The monomer **3a** underwent intramolecular cyclization to form six-membered cyclic product **4a**. Interestingly, under similar conditions α -N-(2'-phenylacetyl)-*aeg* methyl ester (**3g**) gave a very good yield of 12-membered hybrid cyclic peptoid **4g** through intermolecular cyclization (Table 2). To ascertain the generality of this differential cyclization, we tested variable functionalities for α -N-alkyl and α -N-acyl substituents (Tables 1 and 2). All the monomers were subjected to in situ Boc deprotection and subsequent cyclization. The peptoid monomers with α - and β -naphthalene functionalities (α -N-alkyl: **3b**, **3c** and α -N-acyl: **3h**, **3i**, respectively) were chosen to demonstrate if ring cyclization is independent of the type of aromatic moiety and position of attachment. Monomers having electron-withdrawing (4-nitrophenyl, **3d** and **3j**) and -donating (4-methoxyphenyl, **3e** and **3k**) groups were selected to study the influence of electronic effects on cyclization. Interestingly, the propensity of differential cyclization was found to be general, as the α -N-alkyl- and α -N-acyl-substituted *aeg* monomers formed six- and 12-membered products (**4b–e** and **4h–k**), respectively. The monomer **3f** with ethyl linker in the α -N-alkyl substituent also gave six-membered product **4f** (Table 1). This further confirmed our assumption that the flexibility of α -N-alkyl-*aeg* favors intramolecular cyclization. In contrast, the carbonyl group of the α -N-acyl substituent of *aeg* not only re-

Table 1. Intermolecular cyclization of α -N-alkyl-*aeg* monomers to six-membered cyclic products.

Reactant	Product	Yield [%] ^[a]
3a	4a	73
3b	4b	69
3c	4c	71
3d	4d	79
3e	4e	80
3f	4f	43

[a] Yields reported are of purified products.

stricted its free rotation but also rigidified the molecular conformation, thus favoring intermolecular cyclization to form 12-membered products. To extend the scope of this methodology, we synthesized adenine- and thymine-functionalized 12-membered products **4l** and **4m** (Table 2).

NMR and high-resolution mass spectroscopy (HRMS) product analysis confirmed the α -N-alkyl- and α -N-acyl-enforced differential cyclization of *aeg* methyl ester monomers. The ¹H NMR spectra (in labeled dimethyl sulfoxide, [D₆]DMSO) of monomer units (e.g., **3d** and **3j**) showed singlets at 1.5 and 3.7 ppm corresponding to Boc and methyl ester (–OCH₃) groups, respectively. In addition to the expected disappearance of the proton peak for the Boc group in the respective spectra of products (**4d** and **4j**), peaks for free amine (–NH₂) and –OCH₃ were absent, which indicates the possible cyclization of monomers (Figure 1 a). The ¹H NMR spectrum of product from **3d** showed four peaks (2', 3', 5', and 7') in the region 2.4–4.0 ppm, a broad peak at 7.85 ppm, and two doublets at 7.51–7.49 and 8.18–8.15 ppm corresponding to four –CH₂ amide protons (H_a) and four aromatic protons, respectively, which confirmed a six-membered cyclo-*aeg* structure for product **4d** (HRMS, mass =

Table 2. Intermolecular cyclization of α -N-alkyl-aeg monomers to 12-membered cyclic products.

Reactant	Product	Yield [%] ^[a]
3g	4g	72
3h	4h	68
3i	4i	76
3j	4j	82
3k	4k	68
3l	4l	78
3m	4m	72

[a] Yields reported are of purified products.

236.1055, $[M+H]^+$). The spectrum of product from **3j** (Figure 1a) showed a completely different splitting pattern including two amide peaks at 8.05 and 8.12 ppm for H_b and H_c , respectively, which indicated the possible product as either a trimer or a cyclic dimer. The trimer was ruled out by HRMS analysis (549.1664, $[M+Na]^+$), thus confirming the 12-membered cyclic dimer (*aeg-aeg*) product **4j**. Surprisingly, seven peaks in the region 3.0–4.3 ppm (2, 3, 5, 9, 11, 14, and 20) corresponding to protons of eight $-CH_2$ groups revealed that **4j** exists as a nonsymmetrical cyclic homodimer. The nonsymmetrical structure of **4j** was further established by ^{13}C NMR and

^{13}C DEPT-135 (distortionless enhancement by polarization transfer) studies (Figure S1 in the Supporting Information).

Next, we investigated the hydrogen-bonding patterns in representative examples **4d** and **4j** by temperature- and concentration-dependent studies.^[10] 1H NMR study revealed the presence of intermolecular hydrogen-bonding interactions in **4d** (Figure S2). For **4j**, 1H NMR spectra showed an upfield shift of 0.33 and 0.39 ppm, respectively, for the amide protons H_b and H_c with increasing temperature from 25 to 95 °C, thus confirming strong hydrogen-bonding interactions (Figure 1b). The nature of hydrogen bonding in **4j** was validated by a concentration-dependent NMR study. 1H NMR spectra with a decrease in concentration (dilution) of **4j** (3.8, 1.9, 0.95, 0.47, and 0.23 mM) did not show change in the peak position of H_a and H_c , which is possible only in the case of intramolecular hydrogen-bonding interactions (Figure S3). Such intramolecular hydrogen bonding can guide the structural conformation of cyclic peptidomimetics similar to that observed in cyclic peptides.^[11]

Temperature coefficient ($\Delta\delta_{NH}/\Delta T$) values^[12] of H_b and H_c were found to be -4.46 and -5.7 ppb, respectively. Therefore the strength of hydrogen bonding is moderate and amide protons are less shielded from the $[D_6]DMSO$. 1H NMR spectra of **4j** in CD_3CN with increase in temperature showed an upfield shift of H_b and H_c (0.146 and 0.09 ppm) with temperature coefficient values -2.3 and -3.62 ppb, respectively (Figure S5). The higher values of the temperature coefficient suggest stronger hydrogen bonding and shielding of amide protons from the solvent (CD_3CN). Interestingly, the difference in upfield shifts of H_b and H_c and their corresponding temperature coefficient values suggest two hydrogen bonds with different bond length, which is evidence for a nonsymmetrical conformation of **4j**. Further, two sets of proton peaks of **4j** merge at higher temperature (>65 °C) to form one set, thereby demonstrating the transformation from nonsymmetrical to symmetrical conformation (Figure 1b).^[13] The 1H - ^{13}C HSQC spectrum obtained was remarkably well dispersed, indicative of a nonrepetitive folded conformation (Figure S6). The energy-minimized structure showed the *trans* conformation for amides, which allowed the conclusion that the molecule exists in a low-energy stable state (Figure 1c). The model structure also revealed two intramolecular hydrogen bonds between secondary amide protons and α -N-carbonyls (H_b and $C^{13}=O$ and H_c and $C^{19}=O$; Figure 1d). The two intramolecular hydrogen bonds in **4j** exhibit different bond lengths (1.96 and 2.01 Å for H_b and H_c , respectively), which supports the inference deduced from 1H NMR spectroscopy. The observed differential cyclization can be understood from the structural aspects of *aeg* monomers. The flexible α -N-alkyl-*aeg* methyl esters follow Baldwin rules of intramolecular cyclization (Figure S7).^[14] The terminal amine attacks the electrophilic methyl ester carbonyl group without

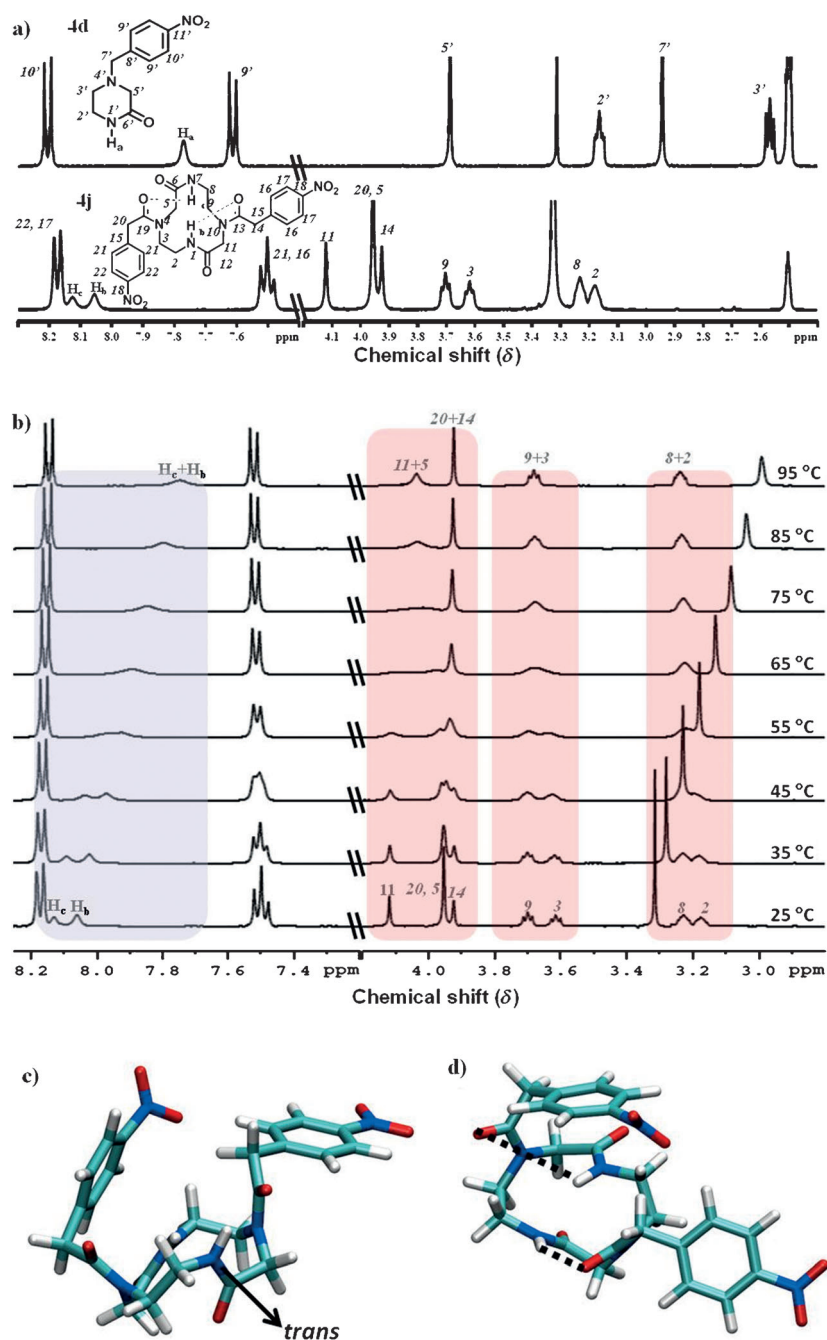


Figure 1. NMR studies and energy-minimized structure of **4j**. a) Comparative ¹H NMR spectra of cyclic products **4d** and **4j** ([D₆]DMSO). b) Variable-temperature ¹H NMR spectra of **4j** (in [D₆]DMSO). c, d) Energy-minimized model structure of **4j** showing *trans* amides and intramolecular hydrogen bonds (■■■■), respectively.

any hindrance to form six-membered products (**4a–e**), whereas in ^α*N*-acyl-aeg methyl esters, conformational rigidity prevents the intramolecular reaction. Alternatively, intermolecular nucleophilic attack of the free amine of one monomer onto the methyl ester carbonyl group of another monomer is energetically favored to form 12-membered products (**4g–m**).

The cyclic peptoids being amphipathic in nature, we envisaged them to be permeable to biological cell membranes.^[15] We wanted to test if these peptoids are bioactive against cellular phenomena such as cell viability, and whether they would

affect specific cellular processes such as autophagy. Cyclic peptoids (**4a–m**) were tested for their ability to affect autophagy, a biological process involved in the turnover of proteins and organelles. The degradation of a cargo marker indicative of selective autophagy was followed over time in the yeast *Pichia pastoris* (Figure 2a). Interestingly, **4a** increased the rate of degradation of the protein marker through autophagy significantly in a dose-dependent manner (Figure 2b). Furthermore, the growth characteristics suggest **4a** is not toxic to yeast cells (Figure 2c–e). Microscopy studies in *Saccharomyces cerevisiae* showed a faster rate of peroxisome (green fluorescent protein (GFP)-labeled) degradation through autophagy in the presence of **4a** (50 μM), as observed by the appearance of diffused GFP in the vacuole over time (arrowheads, Figure 2f,g). Strikingly, in the presence of **4a**, GFP appeared inside the vacuoles (Figure 2g, inset) at much earlier time points than for the untreated cells (Figure 2f, inset). To further confirm the activity of cyclic peptoid **4a**, GFP-autophagy-related protein 8 (GFP-Atg8) processing assay was performed. The cells were transferred to starvation conditions and free GFP released from GFP-Atg8 fusion protein was used as an indicator of autophagy flux. There were higher free GFP levels in cells treated with peptoid **4a**, which suggests an increase in autophagic flux (Figure 3). Thus, upregulation of autophagy by using

small molecules such as **4a** is a promising approach towards elimination of intracellular pathogens and neurodegenerative protein aggregates.^[7]

In summary, an elegant methodology for the synthesis of hybrid cyclic peptoids has been developed. The conformational flexibility and rigidity of the ^α*N*-alkyl- and ^α*N*-acyl-substituted *N*-(2-aminoethyl)glycine backbone enforce intra- and intermolecular cyclization, respectively, to form six- and 12-membered products. Unlike classical peptoids, our hybrid cyclic peptoids exhibit stable conformation and contain secondary amides

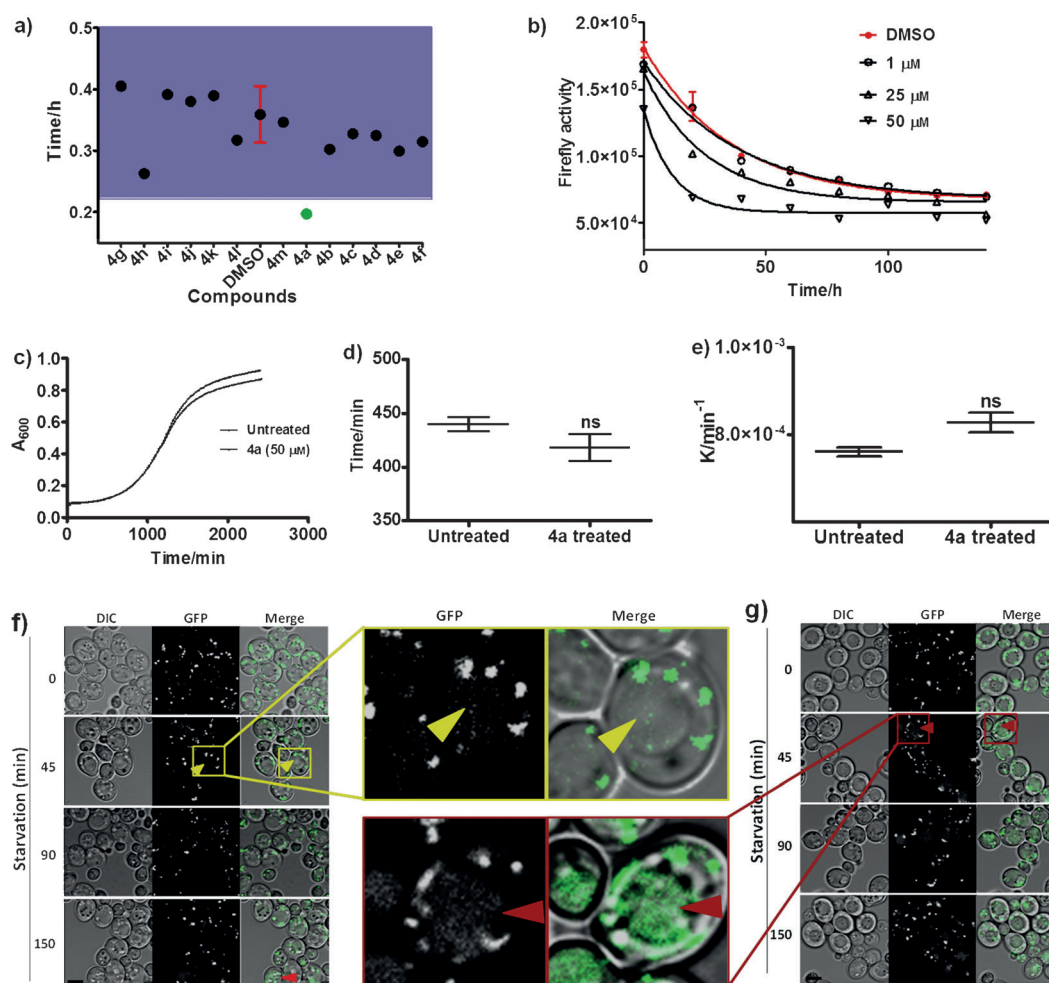


Figure 2. Autophagy studies in yeast. a) Time taken for a 50% decrease in cargo activity for the control (DMSO) and **4a–m** at 50 μM ; purple area denotes 3 standard deviation (SD) units. b) Dose response of **4a** (1, 25, and 50 μM) with time. Growth analysis of *Saccharomyces cerevisiae* in the presence and absence of **4a** was performed: c) growth curve, d) growth rate, e) doubling time were plotted using GraphPad Prism. f, g) Microscopy images showing degradation of peroxisomes (GFP) in the vacuole (arrowheads) in untreated (f) and **4a**-treated (g) cells. Scale bar: 4 μm . DIC = differential interference contrast, GFP = green fluorescent protein.

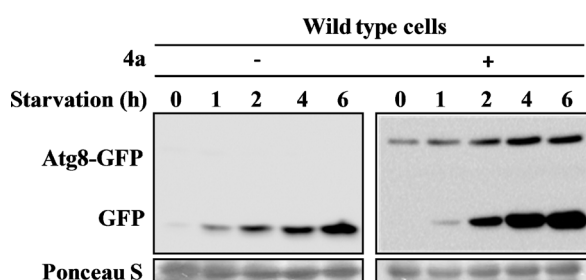


Figure 3. GFP-Atg8 processing assay. Peptoid **4a** increases GFP-Atg8 processing, as evident in later time points (at 4 and 6 h) relative to that of untreated cells. Atg8 = autophagy-related protein 8.

that may be useful for providing secondary interactions. Screening of a cyclic peptoids library gave an effective rate enhancer (**4a**) of autophagy. We are now working towards structure–activity relationships on **4a** as well as expanding our synthetic methodology to access the diverse hybrid cyclic peptoid library for numerous biological applications.

Experimental Section

General synthetic procedure for *N*-alkyl-^α*N*-(2-aminoethyl)glycine methyl ester monomers

Triethylamine (2 mmol) was added to a solution of **2** (1.1 mmol) in acetonitrile (15 mL) at room temperature under an argon atmosphere and the mixture was stirred for 15 min. Then bromomethyl derivatives were added and the reaction mixture was heated at reflux (81 °C) for 6–8 h. The reaction was monitored by TLC, and on completion of reaction, the solvent was evaporated and the crude product was purified by silica gel column chromatography.

General synthetic procedure for ^α*N*-acyl-*N*-(2-aminoethyl)glycine methyl ester monomers

2-(1*H*-Benzotriazole-1-yl)-1,1,3,3-tetramethyluronium hexafluorophosphate (HBTU, 1.2 mmol) was added to a solution of acetic acid derivatives (1 mmol) in DMF, followed by *N*-hydroxybenzotriazole (HOBT, 1.2 mmol) at ice-cooled temperature under an argon atmosphere. The reaction mixture was stirred until a clear solution was obtained, then compound **2** (1.1 mmol) followed by *N,N*-diisopro-

pylthyamine (DIPEA, 3 mmol) were added slowly in portions and the reaction mixture was stirred for 5–6 h at room temperature. The reaction was monitored by TLC, and on completion the reaction mixture was poured into water and extracted with CHCl_3 . The organic layer was dried over Na_2SO_4 , the solvent was evaporated, and the crude product was purified by silica gel column chromatography.

General synthetic procedure for cyclization

Trifluoroacetic acid (TFA) in dichloromethane (1:1, v/v; 5 mL) and a few drops of triisopropylsilane (TIPS) were added to a solution of Boc-protected $^{\text{N}}$ -alkyl- N -(2-aminoethyl)glycine or $^{\text{N}}$ -acyl- N -(2-aminoethyl)glycine monomers (200 mg) at ice-cooled temperature. The reaction mixture was stirred for 1 h, concentrated, and the obtained product was dissolved in *sec*-butanol (10 mL) and heated at reflux at 110 °C under an argon atmosphere for 10–12 h. Reaction was monitored by TLC, and on completion of the reaction, the solvent was evaporated and the crude product was purified by silica gel column chromatography.

Yeast culture and growth assay

S. cerevisiae (strain BY 4741) was inoculated into YPD (1% yeast extract, 2% peptone, and 2% dextrose) medium and incubated for 8 h (30 °C, 250 rpm). From this primary inoculum, the secondary culture was inoculated and incubated as above until the culture absorbance (600 nm) reached 0.8. High-throughput growth curve analysis in the presence and absence of **4a** (50 μM) was performed using a Varioskan Flash apparatus from Thermo Scientific by recording the absorbance (600 nm) after every 20 min in a 384-well plate. The autophagy assay was performed in the yeast *P. pastoris*, in which degradation of cargo was followed over time upon induction of autophagy. The time taken for a 50% decrease in cargo activity was plotted for untreated cells and the compounds at 50 μM concentration. Triplicate values for the control were plotted and a difference of 3 standard deviation (SD) units between the test and control was considered as significant. For the fluorescence microscopy assay, *S. cerevisiae* cells were checked for selective degradation of peroxisomes through autophagy with or without compound **4a**. Microscopic images were obtained using a Zeiss confocal microscope.

GFP-Atg8 processing assay

S. cerevisiae strain containing the GFP-Atg8 (pRS 416 vector backbone) plasmid was grown in synthetic complete medium lacking uracil (SC-URA) under appropriate conditions (30 °C, 250 rpm). From this, a secondary culture was inoculated at $A_{600}=0.2$ and grown as above until A_{600} reached 0.65. The cultures were transferred to SD-N (nitrogen starvation) medium at $A_{600}=3$, separately with and without **4a** (50 μM), and at time points (0, 1, 2, 4, and 6 h) were collected at A_{600} equivalent of 3. Proteins were precipitated using trichloroacetic acid and samples were resolved by sodium dodecyl sulfate–polyacrylamide gel electrophoresis (10%) followed

by immunoblotting and probing with anti-GFP primary antibody (1:3000) and anti-mouse secondary antibody (1:10000).

Acknowledgements

We thank Prof. C. N. R. Rao FRS for constant support, JNCASR, the Department of Biotechnology (DBT)–Innovative Young Biotechnology Award (IYBA, grant BT/03/IYBA/2010), the Department of Science and Technology (DST), and Wellcome-DBT India Alliance for financial support, and Arkamita for modeling studies.

Keywords: autophagy · cyclization · hydrogen bonds · peptoids · synthetic methods

- [1] a) C. J. White, A. K. Yudin, *Nat. Chem.* **2011**, *3*, 509–524; b) A. Thakkar, T. B. Trinh, D. Pei, *ACS Comb. Sci.* **2013**, *15*, 120–129; c) S. A. Fowler, D. M. Stacy, H. E. Blackwell, *Org. Lett.* **2008**, *10*, 2329–2332.
- [2] a) Y. D. Wu, S. Gellman, *Acc. Chem. Res.* **2008**, *41*, 1231–1242; b) R. M. J. Liskamp, D. T. S. Rijkers, J. A. W. Kruijtzter, J. Kemmink, *ChemBioChem* **2011**, *12*, 1626–1653.
- [3] a) S. A. Fowler, H. E. Blackwell, *Org. Biomol. Chem.* **2009**, *7*, 1508–1524; b) N. C. Tan, P. Yu, Y. U. Kwon, T. Kodadek, *Bioorg. Med. Chem.* **2008**, *16*, 5853–586; c) C. A. Olsen, *ChemBioChem* **2010**, *11*, 134–160; d) E. Nnanabu, K. Burgess, *Org. Lett.* **2006**, *8*, 1259–1262.
- [4] O. Ovadia, Y. Linde, C. Haskell-Luevano, M. L. Dirain, T. Sheynis, R. Jelinek, C. Gilon, A. Hoffman, *Bioorg. Med. Chem.* **2010**, *18*, 580–589.
- [5] a) S. B. Y. Shin, B. Yoo, L. Todaro, J. K. Kirshenbaum, *J. Am. Chem. Soc.* **2007**, *129*, 3218–3225; b) O. Roy, S. Faure, V. Thery, C. Didierjean, C. Taillefumier, *Org. Lett.* **2008**, *10*, 921–924.
- [6] a) T. Godballe, L. L. Nilsson, P. D. Petersen, H. Jenssen, *Chem. Biol. Drug Des.* **2011**, *77*, 107–116; < *lit* b > J. E. Murphy, T. Uno, J. D. Hamer, F. E. Cohen, V. Dwarki, R. Zuckermann, *Proc. Natl. Acad. Sci. USA* **1998**, *95*, 1517–1522; c) L. Zhang, J. Yu, H. Pan, P. Hu, Y. Hao, W. Cai, H. Zhu, A. D. Yu, X. Xie, D. Ma, J. Yuan, *Proc. Natl. Acad. Sci. USA* **2007**, *104*, 19023–19028.
- [7] T. Fleming, T. Noda, T. Yoshimori, D. C. Rubinsztein, *Nat. Chem. Biol.* **2011**, *7*, 9–17.
- [8] M. Egholm, P. E. Nielsen, O. Buchardt, R. H. Berg, *J. Am. Chem. Soc.* **1992**, *114*, 9677–9678.
- [9] N. Kaur, B. Zhou, F. Breitbeil, K. Hardy, K. S. Kraft, I. Trantcheva, O. Phanstiel IV, *Mol. Pharm.* **2008**, *5*, 294–315.
- [10] F. Cordier, S. Grzesiek, *J. Mol. Biol.* **2002**, *317*, 739–751.
- [11] T. R. White, C. M. Renzelman, A. C. Rand, T. Rezai, C. M. McEwen, V. M. Gelev, R. A. Turner, R. G. Linington, S. S. F. Leung, A. S. Kalgutkar, J. N. Bauman, Y. Z. Zhang, S. Liras, D. A. Price, A. M. Mathiowetz, M. P. Jacobson, R. S. Lokey, *Nat. Chem. Biol.* **2011**, *7*, 810–817.
- [12] T. Cierpicki, J. Otlewski, *J. Biomol. NMR* **2001**, *21*, 249–261.
- [13] N. Maulucci, I. Izzo, G. Bifulco, A. Aliberti, C. De Cola, D. Comegna, C. Gaeta, A. Napolitano, C. Pizza, C. Tedesco, D. Flot, F. De Riccardis, *Chem. Commun.* **2008**, 3927–3929.
- [14] J. E. Baldwin, *J. Chem. Soc. Chem. Commun.* **1976**, 734–736.
- [15] a) E. Santis, T. Hjelmgaard, S. Faure, O. Roy, C. Didierjean, B. Alexander, G. Siligardi, R. Hussain, T. Javorfi, A. Edwards, C. Taillefumier, *Amino Acids* **2011**, *41*, 663–672; b) Y.-U. Kwon, T. Kodadek, *J. Am. Chem. Soc.* **2007**, *129*, 1508–1509.

Received: October 7, 2013

Published online on December 11, 2013

Multifaceted Housekeeping Functions of Autophagy

Sarika Chinchwadkar, Sreedevi Padmanabhan, Piyush Mishra, Sunaina Singh, S. N. Suresh, Somya Vats, Gaurav Barve, Veena Ammanathan, et al.

Journal of the Indian Institute of Science

A Multidisciplinary Reviews Journal

ISSN 0970-4140

Volume 97

Number 1

J Indian Inst Sci (2017) 97:79-94

DOI 10.1007/s41745-016-0015-z



Your article is protected by copyright and all rights are held exclusively by Indian Institute of Science. This e-offprint is for personal use only and shall not be self-archived in electronic repositories. If you wish to self-archive your article, please use the accepted manuscript version for posting on your own website. You may further deposit the accepted manuscript version in any repository, provided it is only made publicly available 12 months after official publication or later and provided acknowledgement is given to the original source of publication and a link is inserted to the published article on Springer's website. The link must be accompanied by the following text: "The final publication is available at link.springer.com".



Multifaceted Housekeeping Functions of Autophagy

Sarika Chinchwadkar, Sreedevi Padmanabhan, Piyush Mishra, Sunaina Singh, S. N. Suresh, Somya Vats, Gaurav Barve, Veena Ammanathan and Ravi Manjithaya*

Abstract | Autophagy is an evolutionarily conserved intracellular degradation process in which cytoplasmic components are captured in double membrane vesicles called autophagosomes and delivered to lysosomes for degradation. This process has an indispensable role in maintaining cellular homeostasis. The rate at which the dynamic turnover of cellular components takes place via the process of autophagy is called autophagic flux. In this review, we discuss about the orchestrated events in the autophagy process, transcriptional regulation, role of autophagy in some major human diseases like cancer, neurodegeneration (aggrephagy), and pathogenesis (xenophagy). In addition, autophagy has non-canonical roles in protein secretion, thus demonstrating the multifaceted role of autophagy in intracellular processes.

1 Introduction

Autophagy, an intracellular evolutionarily conserved process, involves engulfment of unwanted proteins and organelles by double-membrane vesicles, called **autophagosomes**, which then fuse with the lysosomes/vacuole, and the engulfed cargo is subsequently degraded. It is a cell survival mechanism under stress conditions and it also play important roles in many other intra-cellular processes like protein and organelle turnover and transport of some of the vacuolar enzymes. This process can be divided into various steps, including autophagy induction, nucleation, autophagosome formation, maturation, fusion with the lysosomes/vacuole, degradation of the cargo, and recycling of the precursor molecules, such as amino acids, lipids, and nucleotides, back to the cytoplasm. Autophagy is a tightly regulated cellular mechanism and its flux varies depending on the cell type(s) of an organism. Autophagy is involved in various physiological roles, such as cellular homeostasis, embryonic development, antigen presentation, protein quality control, and maintenance of the amino-acid pool during starvation conditions. It is also implicated in various pathophysiological diseases, such as infection, cancer, diabetes, and neurodegeneration.

Although autophagy is predominantly a cytosolic event, the nucleus exerts a considerable control in the extent of autophagy response, especially during adverse conditions, such as starvation. Depending on the cargo it captures, autophagy is broadly classified as general and selective autophagy. For example, as a response to nutrient deprivation, general autophagy is triggered where it captures random portion of cytosol. In contrast, selective autophagy ensures specific capture of cytosolic cargo, such as damaged or superfluous organelles. When selective autophagy captures and degrades mitochondria, the process is termed as mitophagy. Similarly, autophagic degradation of peroxisomes (pexophagy), Golgi (golgiphagy), ER (ER-phagy), ribosomes (ribophagy), etc., have been documented.¹ The genes comprising the autophagy machinery are named as ATG (AuTophagy related gene).¹

2 Process of Autophagy

2.1 Autophagy Induction

The initial characterization of autophagy flux with respect to involvement of molecular players was carried out in yeast extensively. Although recycling of the cytoplasmic contents happens at

Autophagosomes: The “Pac-Man” like double membrane vesicles involved in macroautophagy.

Autophagy Laboratory,
Molecular Biology
and Genetics Unit,
Jawaharlal Nehru Centre
for Advanced Scientific
Research, Bengaluru 560
064, India
*ravim@jncasr.ac.in

Phagophore Assembly Site (PAS): The site inside cells that gives birth to autophagosomes.

steady state levels by basal autophagy, autophagy flux increases drastically when it is induced. Autophagy induction happens when the cells are under stress conditions, such as amino acid starvation¹ (Fig. 1). Alternatively, autophagy can also be induced using drugs, such as rapamycin,² which targets the TOR (Target of Rapamycin), a major serine-threonine kinase involved in nutrient sensing and cell growth regulation.³ Both amino-acid starvation and rapamycin inhibit TOR activity and induce autophagy. Under the nutrient rich conditions, TOR is active and it negatively regulates kinase activity of Atg1 by hyper-phosphorylating Atg13 and thus disturbing the Atg1–Atg13 association, required for downstream processes of autophagy.⁴ When autophagy is induced either by nutrient limitation or by rapamycin, TOR becomes inactive and does not phosphorylate Atg13 and thus increases affinity of Atg13 towards Atg1, further passing the signal for nucleation of different autophagy proteins (Fig. 1).

2.2 Nucleation of Autophagy Proteins

When autophagy is induced, nucleation of autophagy proteins takes place at a site called the pre-autophagosomal structure or **phagophore assembly site (PAS)** which is present near the vacuole. The very first autophagy-related protein (ATG) that is recruited at PAS is Atg17. Atg17 and Atg11 act as scaffold in general autophagy and selective autophagy, respectively.⁵ In general autophagy, Atg17 interacts with Atg31 which then interacts with Atg29 and thus forms a ternary complex. Atg17 also interacts with Atg13 and thus links the trimer to Atg1.^{6–8} Recent study showed that Atg1 tethers Atg9 vesicles at PAS.⁹ Atg9 is a transmembrane protein required for autophagy, and its transport from peripheral sources, such as mitochondria, ER, to PAS is believed to be important for providing a membrane source for the formation of autophagosomes.^{10, 11} Atg23 and Atg27 are involved in anterograde transport of Atg9, wherein Atg9 vesicles are brought to PAS.¹² Retrograde transport of Atg9 from PAS to peripheral

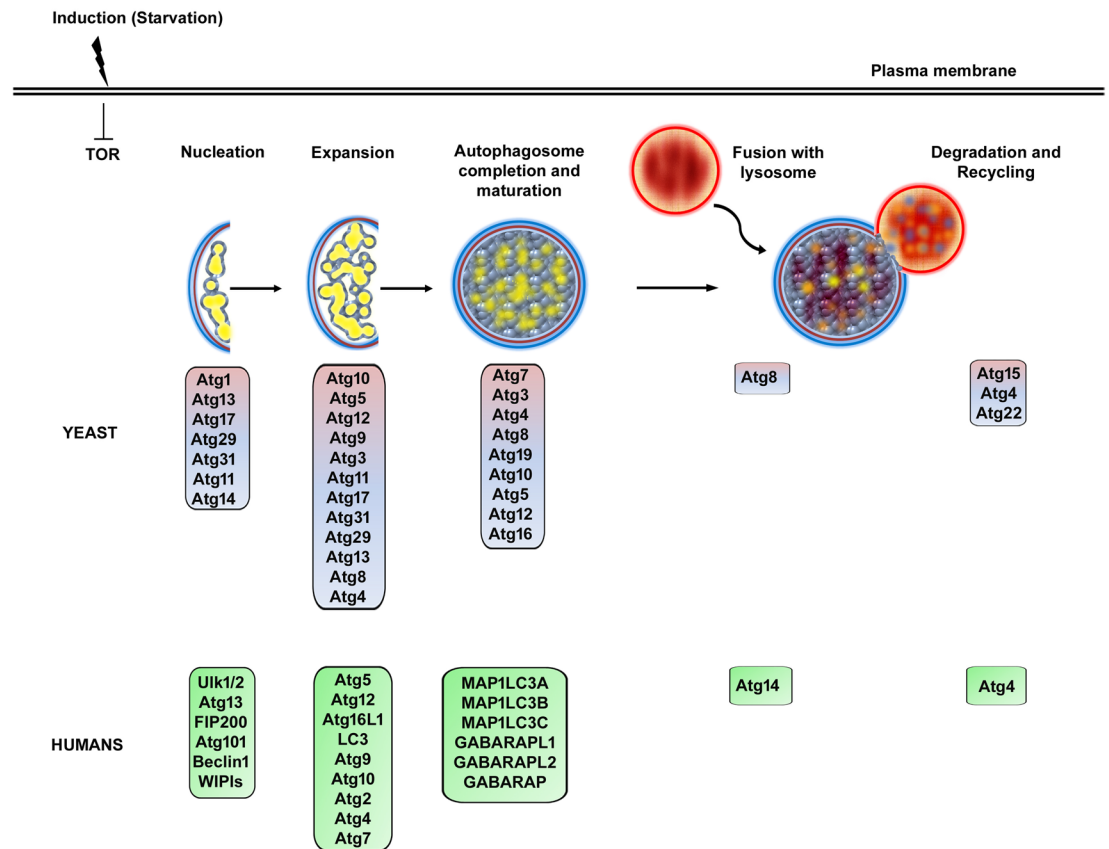


Figure 1: Schematic demonstrating the various steps in the autophagy process. The yeast and human autophagy proteins involved in nucleation, expansion, autophagosome maturation and completion, fusion, and degradation processes are mentioned.

membrane sources require Atg1, Atg2, and Atg18.¹³ Another complex important for PAS formation and initiation of autophagosomes is Class III PI3-K complex (VPS34, Atg6/VPS30, VPS15, and Atg14) which forms PI3P (Phosphatidylinositol-3-phosphate) that is present in the autophagosomal membranes.¹⁴ Graef et al. in 2013 also have shown that the PAS containing multiple Atg proteins are tethered to ER exit sites. Localization of all these ATG proteins and the hierarchy of the complexes they form at the PAS have been determined. These orchestrated signaling events lead to a double membrane vesicle formation called an autophagosome¹⁵ (Fig. 1).

2.3 Biogenesis, Maturation, and Completion of Autophagosomes

The initiation of the autophagosome biogenesis starts with formation of an **isolation membrane** at PAS. Atg8 is one of the important proteins that is present on the inner and outer membrane of the autophagosomes and it remains associated with the autophagosomes throughout the process of autophagy right from the formation of isolation membrane to the autophagosome degradation in the vacuole.¹⁶ Atg8 is inserted in the autophagosomal membranes in the form of Atg8-PE (Phosphatidylethanolamine). Two ubiquitin-like conjugation systems help in the formation of Atg8-PE, the first being the Atg7-Atg3-Atg10 conjugation system and the second Atg5-Atg12-Atg16.¹⁷ Atg4 is a cysteine protease that helps in conjugation of Atg8 with PE by cleaving the C-terminal Arg residue and exposes the Gly for conjugation. The recycling Atg8 from the Atg8-PE present at the outer membrane of the autophagosomes also requires Atg4 for the cleavage of PE from Atg8. Thus, Atg4 plays dual role of conjugation and recycling of Atg8.¹⁸ As explained earlier, the membrane source for autophagosome formation is further contributed by transport of Atg9 vesicles along with Atg41.¹⁹ Thus, Atg8, along with Atg4, Atg7-Atg3-Atg10 complex, and Atg5-Atg12-Atg16 help in autophagosome formation and maturation (Fig. 1). An important protein required for autophagosome completion is a PI3P phosphatase, Ymr1 in the absence of which recycling of the Atg proteins from the autophagosomal membrane is blocked and the Atg proteins remain associated with autophagosomes inside the cytoplasm.²⁰ Once the autophagosomes are completely formed, they are transported to the vacuole and are fused with the vacuole.

2.4 Fusion of Autophagosomes

As in the case of any vesicle destined to fuse with a membrane, autophagosomes also involve three major conditions for fusion with the vacuole— (1) interaction of Rab like GTPase, (2) tethering to the vacuole, and (3) **SNARE**-pair interactions leading to membrane fusion.

Ypt7, an yeast Rab GTPase, was shown to be involved in the homotypic vacuolar fusion along with Sec17 and Sec18.^{21–23} Tethering of the vesicles is mediated by a complex called as the class C VPS complex or the Homotypic fusion and Vacuolar Protein Sorting complex also known as HOPS. HOPS consists of six subunits Vps18, Vps11, Vps16, Vps33, Vps39, and Vps41.^{24–26} **HOPS** complex functions as an effector for Ypt7.²⁵

A number of SNARE proteins also mediate the process of membrane fusion. Vam3 is a v-SNARE (also a syntaxin homologue) that localizes to the vacuolar membrane and has been shown to be important for both cytoplasm to vacuole delivery of Ape1 and for the fusion of autophagosomes to the vacuole.²⁷ Vam7 was later shown to be functioning together with Vam3 in vacuolar fusion.²⁸ Another v-SNARE Vti1 was reported to interact with Vam3 in both alkaline phosphatase pathway (Golgi-vacuole) and **CVT pathway** (one of the selective autophagy pathways). Along with these two other proteins which form a complex and function in the fusion step are Ccz1 and Mon1 which were identified in a screen of mutants defective in autophagy and CVT pathways.²⁹

The fusion of outer membrane of the autophagosomes leads to the delivery of single membrane **autophagic bodies** into the vacuolar lumen which is then degraded.

2.5 Degradation of Autophagosomes and Its Contents

Takeshige et al. reported that yeast strain which was defective in vacuolar proteinases showed accumulation of autophagic bodies inside the vacuole.² Pep4 and Prb1 were the two mutants that accumulated autophagic bodies post starvation. Aut5/Cvt17 was identified to be an important component of the degradation machinery owing to its lipase activity.³⁰ Cvt17 was shown to be the lipase which degrades the membrane of the autophagic body in the vacuole.³¹ Moreover, acidification of the yeast vacuoles was shown to be important for the degradation per se.³²

SNAREs: Proteins involved in fusion of cytoplasmic vesicles.

Tethering complexes-HOPS: Tethering complexes-HOPS-Multi subunit protein complex that help anchoring autophagosomes and lysosomes.

Phagophore/isolation membrane: The beginning structure that grows into an autophagosome.

CVT pathway: Cytoplasm-to-Vacuole pathway that delivers proteins from cytoplasm to the vacuole.

Autophagic bodies: Single membrane vesicles inside yeast vacuoles as a result of autophagosome vacuole fusion.

2.6 Recycling of Degradation Products

One of the major roles of autophagy is to provide nutrients to the cell during nutrient limiting conditions. This requires not only degradation of part of cytoplasm but also effective recycling of the breakdown products to the cytoplasm. Aut4 which was later named as Atg22 was first identified to be involved in the degradation step as the mutants of Aut4 accumulated autophagic bodies in the vacuole.³³

3 Autophagy in Higher Eukaryotes

The highly conserved nature of autophagy assisted in the identification of orthologs of yeast autophagy genes in mammals. As in yeast, autophagy in mammals is responsible for cellular homeostasis and quality control. Basal levels of autophagy in the cell remove misfolded proteins and damaged organelles. Induced autophagy, on the other hand, combats nutrient starvation, intracellular bacterial infection, oxidative stress, genomic damage, or accumulation of toxic protein aggregates (Fig. 2). The process of autophagy begins with the assimilation of tetrameric ULK1 complex comprising of ULK1, FIP200, Atg101, and Atg13 at the membrane nucleation site or 'Phagophore assembly site' (PAS). The ULK1 kinase activity is necessary for recruiting the Class III PI3-K complex I kinase, Vps34 along with regulatory subunits Beclin1, p150, Atg14L, and AMBRA1 at the PAS. The PI3P produced by Vps34 activity brings FYVE domain containing proteins, such as WIPI2 and DFCP1, to the nucleation site.^{34, 35} Expansion of the phagophore is facilitated by Atg9 which brings membrane from various cellular organelles as well as the two conjugation systems; Atg5–Atg12–Atg16L and LC3.^{36, 37} Ubiquitin like protein Atg12 is activated by E1 ligase Atg7, transferred to E2 ligase Atg10 and eventually conjugates with Atg5. The Atg5–Atg12 non-covalently binds to Atg16L and forms an Atg5–Atg12/Atg16L complex which is targeted to the PAS. The second conjugation system involves LC3, an ubiquitin like protein, which is generally present in the cytoplasm. It is cleaved by protease Atg4 to expose a C-terminal glycine which gets conjugated to phosphatidylethanolamine (PE) with the help of Atg7 and Atg3 which are E1 and E2 ligases, respectively. The PE conjugated LC3 binds to the inner and outer membranes of the expanding autophagosome.^{38–40} The autophagosome cargo recognition and capture are facilitated by ubiquitin-binding adaptor proteins like p62/SQSTM1 which bind to polyubiquitinated cargo

on one end and LC3 through the LC3 interacting region (LIR) on the other end.⁴¹ Isolation membrane nucleation and elongation, cargo recognition and capture, and eventual closure result in the completion of double-membrane autophagosomes. Once completed, autophagosomes move along microtubules assisted by cytoskeletal motor proteins dynein and dynactin to fuse with lysosomes. The fusion of autophagosomes with lysosomes is mediated by small GTPases Rab7, autophagosomal SNARE Syntaxin17 (Stx17), lysosomal SNARE VAMP8, and tethering proteins of HOPS complex. Proper lysosomal function is important for autophagosome-lysosome fusion as autophagy inhibitors BafilomycinA1 and Chloroquine (CQ) inhibit fusion by affecting lysosomal pH. The end function of autophagic process is the degradation of cargo inside lysosomes by hydrolases like CathepsinB/D and recycling of biomolecules.^{37, 42, 43}

4 Signaling Regulation of Autophagy

The highly conserved serine/threonine kinase mTOR (mammalian Target Of Rapamycin) senses nutrient signals in a cell and regulates its growth and division. Two complexes of mTOR, mTORC1, and mTORC2 are localized to different subcellular compartments. In the presence of amino acids and growth factors like Insulin-like growth factor (IGF), protein kinase B (PKB/Akt) is activated by phosphoinositide-dependent kinase-1 (PDK1). Akt phosphorylates TSC1 which blocks its interaction with TSC2, and hence, TSC1/2 complex is not formed which allows small GTPase Rheb to remain active. The mTORC1 complex is targeted to the lysosome by Regulator-Rag complex where it is activated by Rheb and the active mTORC1, in turn, negatively regulates autophagy by inhibitory phosphorylation of ULK1 hence preventing ULK1 complex formation. During nutrient and metabolic stresses, the low levels of ATP in cells are sensed by AMPK which phosphorylates and activates TSC1/2 complex thereby inactivating Rheb and further mTORC1, hence allowing autophagy upregulation. AMPK also directly regulates autophagy independent of mTOR by phosphorylating and activating ULK1 independent of mTOR.^{44, 45}

5 Transcriptional Regulation of Autophagy

Understanding the process of autophagy in an unabridged manner requires study of nuclear events that control autophagy along

mTOR: A protein that negatively controls autophagy.

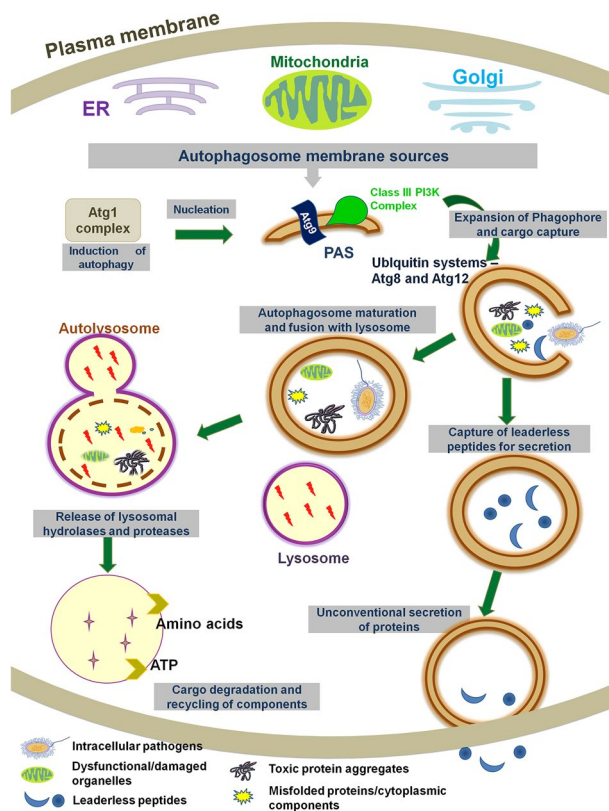


Figure 2: Canonical and non-canonical autophagy flux: under basal levels, autophagy helps in maintaining the cellular homeostasis by getting rid of cellular waste and superfluous components. Stimulation through several factors, such as starvation, stress, or chemicals, leads to induction of autophagy. The initiation complex comprising of Atg1 complex and Class III PI3K complex along with several accessory proteins helps in nucleation at the site of autophagosome biogenesis also referred to as Pre-autophagosomal structure (PAS). Addition of membrane from several different sources leads to the expansion of autophagosomal membrane (phagophore). Atg9 along with accessory proteins is known to provide membrane to the developing phagophore from different sources, such as plasma membrane, endoplasmic reticulum, mitochondria, and Golgi. A ubiquitin ligase like system delivers Atg8 to the developing membrane and leads to the autophagosome expansion around the cargo and finally captures of the cargo. The cargo could be: (1) destined for degradation inside the lysosome through the canonical form of autophagy or; (2) could be secreted out of the cell through non-canonical function of autophagy referred to as unconventional protein secretion. (1) The cargo destined for degradation could comprise of cytoplasmic components like misfolded proteins, dysfunctional or damaged organelles or superfluous components under the basal levels of autophagy. However, autophagy also serves a cytoprotective role by getting rid of any intracellular pathogen or protein aggregates. The mature autophagosome along with its constituents fuses with the lysosome. Lysosomal enzymes act upon the cargo and degrade it into simpler building blocks like amino acids and ATP that are eventually pumped back into the cytosol to be reused by the cell. (2) Many newly synthesized or processed peptides could also be taken up by the autophagy machinery and delivered to the plasma membrane for secretion out of the cell. Such phenomenon of unconventional protein secretion through autophagy has been observed for several peptides that lack any conventional leader sequences for secretion.

with cytoplasmic process that unfold during autophagy. Nuclear regulation of autophagy is mediated by transcription factors, miRNAs, epigenetic marks, and histone modifications. These factors regulate both rapid and long-term responses to autophagy. More than about 20 transcription factors are now known to regulate autophagy.⁴⁶ Transcriptional regulation of

autophagy can be via both mTOR-dependent and independent mechanisms. The first clue to the transcriptional regulation of autophagy came when in the yeast cells; Atg8 was found to be transcriptionally up-regulated via inactivation of the TOR signaling cascade.¹⁶

Studies by Settembre et al. gave new impetus to transcriptional regulation of autophagy. They

identified TFEB as the master positive regulator of autophagy. The two extensively studied major regulators of autophagy are TFEB and ZKSCAN3.^{47, 48} TFEB is a basic-helix-loop-helix-leucine zipper transcription factor which is a master positive regulator of autophagy. It controls expression from nexus of genes involved in lysosome biogenesis (and function) and autophagy. It regulates the expression of genes that contain Coordinated Lysosomal Expression and Regulation (CLEAR) DNA sequences.⁴⁷ ZKSCAN3 is a zinc finger family protein that contains KRAB (KRuppel-Associated Box) and SCAN domains. Silencing of ZKSCAN3 shows induction in autophagy and lysosome biogenesis, while their presence down-regulates the expression of large array of genes involved in autophagy and lysosome biogenesis.^{47, 48} TFEB and ZKSCAN3 play antagonistic role to each other in regulating expression of autophagy genes. Under nutrient rich conditions, mTORC1 in its active state phosphorylates TFEB on the lysosome membrane preventing it from entering the nucleus. This, in turn, prevents the activation of the genes harboring CLEAR DNA sequences. On the contrary, ZKSCAN3 has an antagonistic role. It is present in the nucleus where it down-regulates the expression of multitude of genes involved in autophagy and lysosome biogenesis. During starvation conditions, calcineurin dephosphorylates TFEB allowing it to enter the nucleus and positively regulate the expression of genes involved in autophagy and lysosome biogenesis. Concomitant to TFEB translocation to the nucleus, ZKSCAN3 is relocated to the cytoplasm releasing the negative control on the expression genes of autophagy and lysosome biogenesis.⁴⁹ Core autophagy genes transcriptionally regulated by TFEB are ATG4, ATG9, BCL2, LC3, SQSTM1, UVRAG, WIPI, and by ZKSCAN3 are ULK1 and WIPI, respectively.

Similarly there are other TFs, such as hypoxia inducing factor (HIF-1),⁵⁰ FOXO,⁵¹ p53,⁵² NF- κ B,⁵³ and many others, that play a direct or indirect role in autophagy under different environmental stress conditions.

Transcriptional regulation of autophagy has also been addressed in the yeast model. Here, Ume6, Pho23, and Rph1/KDM4 are the three master transcriptional repressors of autophagy related genes in yeast.^{54–56} Ume6 is associated with histone deacetylase complex which includes Sin3 and Rpd3, and negatively regulates the transcription of Atg8. Under nutrient replete conditions, the absence of any of these three

components leads to an increase in Atg8, and consequently, autophagic activity is augmented. During autophagy, a protein kinase named Rim15 is responsible for phosphorylating Ume6, thereby dissociating it from Sin3 and Rpd3. The absence of Rim15 from cells leads to reduction in the synthesis of Atg8 at basal level. The authors have demonstrated Rim15 as a positive regulator of autophagy that acts upstream of Ume6 to regulate Atg8 synthesis.⁵⁴ Pho23 is another transcriptional repressor of autophagy that negatively regulates ATG9 and thus controls the frequency of autophagosome formation. It also down-regulates the expression of other autophagy-related genes, such as ATG7, ATG14, and ATG29. Studies show that deletion of PHO23 in yeast cells leads to an increase in the autophagosome formation and the number of autophagic bodies. This increase is possibly due to an increase in the levels of Atg9.⁵⁵ Rph1/KDM4 is a histone demethylase that negatively regulates the expression of ATG7, ATG8, ATG9, ATG14, and ATG29. It regulates autophagy in histone demethylase independent manner. In nutrient rich conditions, Rph1 keeps autophagy induction under check. However, under starvation, Rph1 phosphorylation by Rim15 causes partial degradation of this protein, thereby leading to induction of autophagy.⁵⁶ Thus, as in mammalian cells, yeast too has transcriptional machinery devoted to control expression of autophagy genes.

In many genetic and neurodegenerative diseases, autophagy becomes dysfunctional. Mechanisms that promote autophagy and mediate cellular clearance of toxic protein aggregates are being identified that serve as the novel therapeutic targets. For example, over expression of TFEB rescues cytotoxicity of α -synuclein in rat model of Parkinson's disease⁵⁷ and also clears the polyQ Huntingtin protein.⁵⁸ Recently, HEP14 and HEP15 (small molecules) have been shown to increase biogenesis of lysosomes by activating TFEB. This increases the clearance of the cytotoxic aggregates from the cell and also increases the degradation of lipid droplets.⁴⁹ Thus, modulating the expression of TFs can help enhance autophagy which may be beneficial in alleviating disease conditions.

6 Autophagy in Disease

Dysfunctional autophagy is implicated in various diseases and disorders, such as cancer, intracellular infections, and neurodegeneration.

7 Cancer

The role of autophagy in maintaining cellular homeostasis is undeniably important and any perturbations in this can accumulate damaged organelles, oxidative stress, and misfolded proteins in a cell leading to genomic damage and even tumorigenesis. This concept was very elegantly proven in experiments with mice having deletion of essential autophagy genes like BECLIN, *ATG5*, and *ATG7* which made them prone to spontaneous tumors.⁵⁹ Beclin1 deletions were also identified in human breast, prostate, and ovarian cancer samples.⁶⁰ However, understanding the role of autophagy in cancer is not as simple as that. Autophagy can also provide survival advantage to tumor cells in a solid tumor which are facing nutrient limitation and hypoxia. Cancers, such as pancreatic and lung cancer, have been shown to have high basal levels of autophagy. On gene deletion of essential autophagy genes, tumor regression occurred in these cells. Hence, the role of autophagy in cancer is complex and requires an understanding of the stage and type of cancer. It definitely prevents the onset of tumorigenesis by limiting genomic damage but may be pro-cancer in established tumors.^{61–63}

8 Xenophagy

Autophagy, apart from serving as a metabolic pathway providing building blocks like amino acids during conditions of nutritional stress, is also involved in degrading intracellular pathogens. The process of capturing and eliminating intracellular pathogens by autophagy is called as xenophagy. The process of xenophagy provides a broad spectrum of defense mechanism to capture bacterial, viral, and protozoan pathogens. Plethora of studies in recent times has shown that xenophagy acts as a part of innate immune system against huge number of intracellular pathogens in both phagocytic and non-phagocytic cells.

Although the conventional autophagy was discovered in 1963 by de Duve,⁶⁴ xenophagy remained unknown until electron micrographs of guinea pig polymorphonuclear leukocytes (PMNs) infected with *Rickettsiae* (Gram-negative pleomorphic bacteria) showed autophagosome like structures containing bacteria.⁶⁵ Following this, notable discoveries on xenophagy in Group A *Streptococcus*,⁶⁶ *Mycobacterium*,⁶⁷ *Salmonella*,⁶⁸ *Shigella*,⁶⁹ HIV,⁷⁰ Sindbis virus,⁷¹ *Toxoplasma*⁷² showed that xenophagy is a conventional defense mechanism of host against various pathogen types.

8.1 Pathogen Capture by Xenophagy

Post entry, some pathogens escape into cytosol to prevent fusion with lysosomes. This also provides them with sufficient nutrition from the cytosol to replicate efficiently.⁷³ These cytosolic pathogens are targeted by xenophagy machinery that captures them in double membrane vesicles (xenophagosomes) and delivers them to the lysosomes.⁷⁴

Recognition of cargo for xenophagic capture occurs via ubiquitination of the pathogens which, in turn, is recognized by autophagy adaptor proteins like p62, NDP52, Optineurin, and NBR1. These adaptors bridge interactions with the ubiquitin and the autophagy machinery by interacting with LC3. This enables autophagosome formation around the pathogen.⁷⁵ Pathogen-specific adaptor proteins like septins (in case of *Shigella* and *Listeria*) and Tecpr1 (in case of *Shigella*) are also shown to recruit autophagy machinery to the pathogens.^{76,77}

Salmonella enterica serovar Typhimurium is a well-studied pathogen that gets restricted by xenophagy. Inside the host cells, *Salmonella* can reside either inside membrane bound endosomes or enter into cytosol by rupturing the endosomes. There are temporal changes in the intracellular *Salmonella* replicating niche in terms of morphology and recruitment of host factors. At later time points (6–8 h p.i), membrane bound endosomes develop into replicative vesicles for salmonella called as Salmonella Containing Vacuole (SCVs) which is characterized by its tubular structure. Adaptors like p62, NDP52, and optineurin recognize ubiquitin positive *Salmonella*, and NDP52 also recognizes galectin that are bound to damaged *Salmonella* containing endosomes. In a ubiquitin independent pathway, *Salmonella* gets captured to autophagosomes through diacylglycerol present on SCVs. Almost 25–30% of intracellular bacteria are shown to be captured by autophagosomes at early time points like 1 h post infection and the recruitment drastically falls at later points.⁶⁸ One of the speculated reasons for surpassing xenophagy is translocation of *Salmonella* virulence effectors, especially sseL which has deubiquitinase activity that could essentially prevent the ubiquitination of the pathogen. Another reason being repression of autophagy by *Salmonella* at later time points through mTOR activation.^{78,79}

The mechanism of subversion differs between pathogens. Another example is in the case of *Shigella flexneri* which causes shigellosis can escape from the phagosome/endosome and move within the host cells by directing actin polymerization

using its *virG* gene. VirG is an outer membrane protein that accumulates on one end of the bacterium and mediates bacteria's polar movement. It is also known to be the target of autophagy machinery via interaction with Atg5. Recent studies have shown that an effector protein of *Shigella*, IcsB, acts as anti-Atg5-binding protein, by having a strong affinity for the same binding region on VirG as that of Atg5. Hence, mutants of *icsB* are captured by autophagosomes more rapidly.⁶⁹ Thus, although xenophagy exists, it is suppressed/subverted by most pathogens to evade detection and capture.

Impairment of xenophagy is also known to play role in the chronic infection of Crohn's disease. Genome Wide Association Studies (GWAS) have provided evidence for the contribution of two autophagy genes, ATG16L1,⁸⁰ and immunity-related GTPase M (IRGM) in the disease pathogenesis.⁸¹ Subsequent studies show that single-nucleotide polymorphism occurring at ATG16L1 (T300A) does not impair the general autophagy process but show deficits in intracellular bacterial clearance.⁸²

8.2 Signaling Pathways of Xenophagy

Recent studies have shed light on signaling pathways that lead to xenophagy activation even prior to ubiquitination of pathogens. Pattern recognition receptors are host proteins of immune system that recognize pathogen products initiating anti-microbial signals. These receptors could be either membrane bound (e.g., Toll-like receptors) or cytoplasmic (e.g., NOD-like receptors). Both are shown to play role in inducing xenophagy.^{83, 84} IRGM is human gene shown to interact with NOD2 during infection, and together, they recruit Ulk1 and Beclin1 to initiate autophagy.⁸⁵ Similarly, membrane bound TLR4 has been shown to be involved in LPS-induced xenophagy. This activation also facilitates incorporation of VPS34 to autophagy vesicle formation.

Among other genetic factors that regulate xenophagy, TFEB, a mammalian transcription factor whose role is well studied in lysosomal biogenesis gets activated during *Staphylococcus aureus* infection in a pathogen-specific manner, while a similar effect is not seen in *E.coli* infection. In addition to lysosomes biogenesis, HLH30 (*Caenorhabditis elegans* homolog of TFEB) is also shown to induce number of autophagy genes, such as Atg2, Atg16, ULK1, among others. TFEB activation also seems to increase the tolerance to

bacterial infection by prolonging the life span of infected *C.elegans* in comparison to autophagy mutants.⁸⁶

In addition to the immediate innate response that xenophagy elicits, considerable research has been done to find its contribution to adaptive immunity in macrophages and antigen presenting cells. Atg5-deficient dendritic cells show reduced MHC class II representation of antimicrobial peptides and this, in turn, also affects the T-cell priming.⁸⁷ These cells also show reduced IL2 and interferon gamma production in response to viral infections.

These studies suggest that xenophagy is a conserved innate immunity pathway that pathogens evade to establish infection. Thus, enhancing xenophagy that rescind the block imposed by the pathogens would enhance the host immunity to fight against infectious agents. In this direction, screening for compounds that could enhance clearance of intracellular pathogens by xenophagy has been done for pathogens like *Toxoplasma* and *Mycobacterium*.^{88, 89}

9 Aggrephagy

One of the hallmarks of life threatening neurodegenerative diseases is neuronal death caused by accumulation of misfolded toxic protein aggregates, such as α -synuclein, β -amyloid, huntingtin polyQ repeats, FUS, and TDP43. Cellular proteostasis involving the clearance of superfluous cellular organelles and other cargos, including toxic proteins, is maintained through the chaperones, the Ubiquitin-Proteasome System (UPS), and the autophagy pathways.⁹⁰ Chaperone and UPS functions are choked by the misfolded protein aggregates. Misfolded proteins are substrates for autophagy.⁹¹ A selective autophagy pathway, aggrephagy, is a cellular degradation mechanism to clear the toxic, misfolded proteins. Recent studies highlight the importance of autophagy in maintaining organismal homeostasis. Brain-specific autophagy knockout mice (Atg5) accumulate p62 protein aggregates in neurons, and subsequently manifest neurodegenerative phenotypes, illustrating the vital role of basal autophagy for aggregate clearance.⁹²

Autophagy is dysfunctional in neurodegenerative disease pathologies.⁹¹ Thus, restoring autophagy through pharmacological approaches using small molecules has been reported to have beneficial neuroprotective effects.⁹³⁻⁹⁵

10 Non-canonical Roles of Autophagy

Besides the canonical role of cellular homeostasis and degradation, autophagy process also has some moonlighting functions which are underexplored. Involvement of autophagy machinery is seen in several contexts which do not involve capture and delivery of the cargo to the lysosome for degradation via a double membraned autophagosome. Such **non-canonical autophagy** processes include LC3-Associated Phagocytosis (LAP) and autophagy mediated unconventional protein secretion are two such examples. These non-canonical functions were explicitly put forth in a recent review by the pioneers in the field.⁹⁶ Some of the pleiotropic functions of autophagy include their role in cell survival and apoptosis, cellular transport, secretion, signaling, transcriptional and translational responses, membrane organization, and microbial pathogenesis.

The non-canonical roles can be looked upon from two diverse perspectives:

1. As **macroautophagy** involves formation of vesicles and membranous structures, these could be harnessed by other cellular and non-cellular processes.
2. Moonlighting functions of Atg proteins.

10.1 Harnessing Autophagy Machinery for Other Cellular Processes

The prime role of autophagy is turnover and is accompanied by the process of dynamic membrane biogenesis.^{97, 98} The double layered autophagosome membrane formation to entrap cargoes is an orchestrated, dynamic process with the involvement of several Atg proteins and requires PI3-K activity. This property has been elegantly exploited by the pathogens that infect mammalian cells. Virus and bacteria have evolved mechanisms not only to evade the degradative action of autophagy but also to hijack the host autophagy machinery for their multiplication. In this section, we will focus only on the non-canonical role of autophagy proteins in microbial pathogenesis. LC3 in mammals mediates the recruitment of the substrates onto the autophagosomes via their LC3-interacting regions (LIR). Some of the examples that utilize the Atg proteins besides their degradative functions are discussed below:

1. Influenza A virus redirects LC3-conjugated membranes meant for autophagy to the cell surface for budding of stable viruses.⁹⁹ The ion-channel matrix protein of the virus

(M2) recruits the central player of autophagosomal membrane or the landing pad of cargo receptor, LC3, inhibiting the fusion to lysosomes, thereby aiding in the transport of **virions** to the plasma membrane.¹⁰⁰

2. In *Mycobacterium tuberculosis* infection, Atg5 is found to play a unique role of protection by preventing PMN-mediated immunopathology. Knockout studies support an additional, ATG16L1 independent role of ATG5 in protecting the mice from *M. tuberculosis* infection.¹⁰¹
3. Another study from an unbiased siRNA screen has indicated the involvement of ATG13 and FIP200 in the picornavirus replication that is independent of their canonical autophagy functions.¹⁰² The host and the viruses exploit the autophagy machinery along with the autophagy-related membranous structures to either restrict or enhance viral replication that is non-canonical of the autophagy functions. Autophagy proteins, including Beclin1, LC3, Atg4B, Atg5, Atg7, and Atg12, positively regulate the Hepatitis C viral replication,¹⁰³ whereas in murine norovirus, some of the autophagy proteins are required by the IFN- γ activated macrophages to inhibit viral replication complex.¹⁰⁴ Non-involvement of ULK complex distinguishes the non-canonical from canonical autophagy.¹⁰⁵ There is a general notion that a single ATG gene deletion leads to specific block in the autophagy process, but the above-mentioned examples provide evidence that the Atg proteins also exhibit many of the non-canonical roles during viral infection.¹⁰⁶
4. In Mouse Hepatitis Virus (MHV) infection, as unlipidated LC3 (LC3-I) promotes viral replication in Double-Membrane Vesicles (DMVs) without utilizing ATG5¹⁰⁷ and LC3-II,¹⁰⁸ it suggests that the canonical autophagy is not involved. Detailed analysis of the vesicles indicates that the DMVs are another LC3-presenting membrane that is distinct from the canonical double membrane autophagosomes.
5. Zikavirus, a member of the Flaviviridae family, causes microcephaly affecting the central nervous system.¹⁰⁹ This virus produces a variety of intracytoplasmic inclusions termed as "virus factories" in the infected cells. The zika virus infected skin fibroblasts demonstrate that the virus not only blocks the autophagic flux but also hijacks the

Virions: Virus particles.

Non-canonical autophagy: Moonlighting functions of autophagy such as those involved in protein secretion.

Macroautophagy: An intracellular mechanism to capture, degrade and recycle unwanted, damaged or surplus cytoplasmic materials. Commonly referred as autophagy.

autophagic machinery for its own replication.^{110, 111}

In all the above examples, we see that the ability to form membrane structures of the autophagy proteins is being exploited by the virions to promote their viral budding and replication, thereby aiding in their survival and infection.

10.2 Moonlighting Functions of Atg proteins

(i) Role in Unconventional Protein Secretion

Beyond its role of cellular self-eating and homeostasis, autophagy proteins also play an important role in unconventional protein secretion whose mechanism is not well elucidated.

The conventional secretory proteins enter endoplasmic reticulum via signal peptides, whereas the unconventional secretory proteins destined for secretion follow an alternate trafficking route. The process by which proteins that are devoid of canonical leader sequence still get secreted is termed as unconventional protein secretion.

Extensive studies of two main cargoes studied till this date have provided us clues on autophagy-mediated unconventional protein secretion.

1. First, the secretion of mature cytokine, IL1- β , is found to be controlled by the process of autophagy.¹¹² Its secretion is presumed to involve Rab proteins and MVBs.¹¹³ The matured form of the IL1- β is released outside the cell after cleavage from its precursor form. Although Caspase-1 mediated IL1- β release is reported, elegant studies by Zhang et al, 2015 have demonstrated that the translocation of the unconventional secretory protein, IL1- β into a secretory vesicle, is mediated by autophagy, multivesicular bodies (MVBs), and Golgi-associated proteins (Golgi Reassembly Stacking Protein-GRASPs).
2. The second cargo is the Acyl-CoA-binding protein (Acb1) that gets secreted outside the cell by unconventional protein secretion upon starvation in yeast. Genetic studies in yeast¹¹⁴ have demonstrated that Acb1 is unconventionally secreted via vesicles and are captured in a new compartment called CUPS (Compartment for Unconventional Protein Secretion).¹¹⁵ These studies in yeast have revealed that the core autophagy machinery is a necessary requi-

site for autophagosome construction, suggesting that secretory autophagosomes must be formed. This secretion is found to be GRASP-dependent and autophagy-mediated, and plays an important role in peroxisome biogenesis providing some clues on membrane source for autophagosome biogenesis.¹¹⁶

Multiple lines of evidence demonstrate the interplay of autophagy and unconventional protein secretion in the clinical and pathophysiological context.

1. The GRASP-dependent unconventional secretion of CFTR, the Cystic Fibrosis Transmembrane conductance Regulator, demonstrates a physiological relevance of unconventional protein secretion in the cystic fibrosis disease. Autophagy-mediated trafficking of CFTR leads to proper insertion of the protein to the plasma membrane, whereas the transgenic overexpression of GRASP rescued the phenotype of the Δ F508-CFTR mice.¹¹⁷
2. Autophagy plays a significant role in polarized secretion of lysosomal contents in osteoclastic bone resorption.¹¹⁸
3. Impairment of autophagosome-lysosome fusion promotes tubulin polymerization-promoting protein (TPPP/p25 α) to secrete α -synuclein, the hallmark protein of Parkinson's disease, in an unconventional manner.¹¹⁹
4. Another unconventionally secreted protein, Insulin Degrading Enzyme (IDE), was found to be mediated through autophagy-based unconventional secretion upon statin induction¹²⁰ and also has disease relevance in Alzheimer's disease.¹²¹
5. Secretion of β -amyloid aggregates formed in the Alzheimer's disease is also mediated by autophagy. Knockout studies in mice neuronal Atg7 was found to influence the β -amyloid secretion thereby affecting the plaque formation, a pathological hallmark of AD.¹²²
6. Atg16L1 not only regulates cellular autophagy but also acts as Rab33A effector by secreting the hormone from the dense core vesicles of the neuroendocrine PC12 cells.¹²³ Another example of the combined role of Atg5, Atg7, Atg4B, and LC3 is observed in the polarized secretion of lysosomal contents (cathepsin) in the osteo-

clasts.¹¹⁸ Defects in Atg4B and Atg5 in mice are found to manifest balance related disorders due to deficient secretion of otoconins by vestibular sensory cells in the inner ear.^{124, 125}

(ii) Role in cell division:

The non-canonical role of autophagy proteins has gained significance, especially in microbial pathogenesis. The functional importance of localization of PfAtg8 to apicoplast, a four membrane-bound non-photosynthetic plastid, provides clue for non-canonical function of autophagy in *Plasmodium falciparum*.¹²⁶ In the apicomplexan parasite *Toxoplasma gondii*, TgATG8 is vital for normal replication of the parasite inside the host cell. Recent studies have demonstrated that another key role of apicoplasts bound TgATG8 is involved in centrosome-driven inheritance of the organelle during cell division.¹²⁷

In the Zika virus infected patients, microcephaly is brought about by the abnormal function of centrosomes affecting neural brain development.^{128, 129} As this process is coupled with hijacked autophagy machinery, it is presumed that autophagy proteins are probably involved in cell division too.

(iii) Role in inflammatory disease control:

The LC3-Associated Phagocytosis (LAP) is one of the prime non-canonical functions of autophagy that is required for effective clearance of apoptotic cells.¹³⁰ In canonical autophagy, LC3 conjugates to the autophagosomal membranes facilitating maturation upon fusion with lysosomes. Rubicon, a Beclin-1-binding protein, is found to be required for LAP but not for canonical autophagy.¹³¹ In Systemic Lupus Erythematosus (SLE), the pathogenesis is brought about by the defects in clearance of dying cells. LAP is found to inhibit autoinflammatory responses caused by dying cells implicating its link in inflammatory disease control of SLE.¹⁰⁵ Even in viral RNA-mediated infection, the immunostimulatory RNA (isRNA)-mediated type I interferon production is negatively regulated by the Atg12–Atg5 conjugate^{132, 133} demonstrating its suppressor activity in the innate antiviral immune signaling aiding cell survival.

Studies reveal interplay between inflammasomes (multiprotein complex that activates caspase-1) and autophagy. While autophagy negatively regulates inflammasome activation, autophagy induction is dependent on the

presence of specific inflammasome sensors. Autophagosomes degrade inflammasomes via the selective autophagic receptor p62 and autophagy plays a role in the biogenesis and secretion of the proinflammatory cytokine IL-1 β .^{134–138}

The involvement of the adaptor protein, ATG16L1, in the inflammatory bowel disease (Crohn's disease) is characterized by dramatic increase in commensal bacteria.¹³⁹ Deletion studies in ATG16L1-WD repeat domain and T300A mutant of mouse embryonic fibroblasts did not affect xenophagy or the normal autophagic function indicating its differential role in Crohn's disease.¹⁴⁰

(iv) Role in lipidogenesis and development:

Lipid droplet formation in mammalian white adipocytes involves massive cytoplasmic remodeling within the cells. Besides the conventional roles in autophagy, several autophagy genes have been implicated to have “non-autophagy roles”. For example, Atg2 and LC3 are also involved in lipid droplet biogenesis in mouse hepatocytes and cardiac myocytes,^{141, 142} while knockout studies in mice for Atg5 and Atg7 have revealed their additional roles in adipogenesis.^{143, 144} The mice fed with high fat diet in the Atg12 lacking pro-opiomelanocortin expressing neurons exhibited aggravated obesity which demonstrates an auxiliary function of Atg12 in diet-induced obesity.¹⁴⁵ In addition, Atg5-independent non-canonical autophagy generates autophagosomes in a Rab9-dependent manner. Such Atg5-independent autophagy is found to be required for iPSC reprogramming that mediates mitochondrial clearance.¹⁴⁶

The versatility of the autophagy proteins in all the cellular processes opens new avenues to explore its moonlighting functions. It is imperative to understand the discrete functions of the autophagy proteins besides their central role in degradation and cellular homeostasis.

10.3 Open Questions in Autophagy

Although the field has garnered much interest now with the award of the Nobel Prize to Prof. Yoshinori Ohsumi for his contributions to understanding the mechanism of autophagy, several autophagy-related frontiers remain unchallenged. Questions pertaining to understanding basal autophagy and the mechanisms that regulate it are still open. How various intracellular membrane sources contribute to autophagosome biogenesis and the factors that

govern autophagosome size and number is still an active area of research. In spite of identification of a conserved set of core autophagy proteins, their actual roles in autophagosome construction and mechanisms regulating autophagosome-lysosome fusion are not clear. The contribution of autophagy in cell death is controversial and the case of “cell death by over eating oneself” is highly debatable.^{147, 148} Finally, restoration of impaired autophagy in several disease states via small molecule autophagy modulators has been shown to be promising in many cases, but bona-fide and exclusive modulators are still elusive. Discovery of such small molecules will not only further our understanding of autophagy flux but will also fuel the tremendous therapeutic potential autophagy holds.

Received: 16 October 2016. Accepted: 15 November 2016
Published online: 28 February 2017

References

- Mizushima N, Yoshimori T, Ohsumi Y (2011) The role of Atg proteins in autophagosome formation. *Annu Rev Cell Dev Biol* 27:107–132
- Takehige K, Baba M, Tsuboi S, Noda T, Ohsumi Y (1992) Autophagy in yeast demonstrated with proteinase-deficient mutants and conditions for its induction. *J Cell Biol* 119:301–311
- Noda T, Ohsumi Y (1998) Tor, a phosphatidylinositol kinase homologue, controls autophagy in yeast. *J Biol Chem* 273:3963–3966
- Kamada Y et al (2000) Tor-mediated induction of autophagy via an Apg1 protein kinase complex. *J Cell Biol* 150:1507–1513
- Suzuki K, Kubota Y, Sekito T, Ohsumi Y (2007) Hierarchy of Atg proteins in pre-autophagosomal structure organization. *Genes Cells* 12:209–218
- Yamamoto H et al (2016) The intrinsically disordered protein Atg13 mediates supramolecular assembly of autophagy initiation complexes. *Dev Cell* 38:86–99
- Ragusa MJ, Stanley RE, Hurley JH (2012) Architecture of the Atg17 complex as a scaffold for autophagosome biogenesis. *Cell* 151:1501–1512
- Reggiori F, Ungermann C (2012) A dimer to bridge early autophagosomal membranes. *Cell* 151:1403–1405
- Rao Y, Perna MG, Hofmann B, Beier V, Wollert T (2016) The Atg1-kinase complex tethers Atg9-vesicles to initiate autophagy. *Nat Commun* 7:10338
- He C et al (2006) Recruitment of Atg9 to the preautophagosomal structure by Atg11 is essential for selective autophagy in budding yeast. *J Cell Biol* 175:925–935
- Reggiori F, Shintani T, Nair U, Klionsky DJ (2005) Atg9 cycles between mitochondria and the pre-autophagosomal structure in yeasts. *Autophagy* 1:101–109
- Backues SK et al (2015) Atg23 and Atg27 act at the early stages of Atg9 trafficking in *S. cerevisiae*. *Traffic* 16:172–190
- Reggiori F, Tucker KA, Stromhaug PE, Klionsky DJ (2004) The Atg1–Atg13 complex regulates Atg9 and Atg23 retrieval transport from the pre-autophagosomal structure. *Dev Cell* 6:79–90
- Obara K, Sekito T, Niimi K, Ohsumi Y (2008) The Atg18–Atg2 complex is recruited to autophagic membranes via phosphatidylinositol 3-phosphate and exerts an essential function. *J Biol Chem* 283:23972–23980
- Graef M, Friedman JR, Graham C, Babu M, Nunnari J (2013) ER exit sites are physical and functional core autophagosome biogenesis components. *Mol Biol Cell* 24:2918–2931
- Kirisako T et al (1999) Formation process of autophagosome is traced with Apg8/Aut7p in yeast. *J Cell Biol* 147:435–446
- Reggiori F, Klionsky DJ (2013) Autophagic processes in yeast: mechanism, machinery and regulation. *Genetics* 194:341–361
- Nakatogawa H, Ichimura Y, Ohsumi Y (2007) Atg8, a ubiquitin-like protein required for autophagosome formation, mediates membrane tethering and hemifusion. *Cell* 130:165–178
- Yao Z, Delorme-Axford E, Backues SK, Klionsky DJ (2015) Atg41/Icy2 regulates autophagosome formation. *Autophagy* 11:2288–2299
- Cebollero E et al (2012) Phosphatidylinositol-3-phosphate clearance plays a key role in autophagosome completion. *Curr Biol* 22:1545–1553
- Haas A, Scheglmann D, Lazar T, Gallwitz D, Wickner W (1995) The GTPase Ypt7p of *Saccharomyces cerevisiae* is required on both partner vacuoles for the homotypic fusion step of vacuole inheritance. *EMBO J* 14:5258–5270
- Mayer A, Wickner W (1997) Docking of yeast vacuoles is catalyzed by the Ras-like GTPase Ypt7p after symmetric priming by Sec18p (NSF). *J Cell Biol* 136:307–317
- Haas A, Wickner W (1996) Homotypic vacuole fusion requires Sec17p (yeast alpha-SNAP) and Sec18p (yeast NSF). *EMBO J* 15:3296–3305
- Rieder SE, Emr SD (1997) A novel RING finger protein complex essential for a late step in protein transport to the yeast vacuole. *Mol Biol Cell* 8:2307–2327
- Seals DF, Eitzen G, Margolis N, Wickner WT, Price A (2000) A Ypt/Rab effector complex containing the Sec1 homolog Vps33p is required for homotypic vacuole fusion. *Proc Natl Acad Sci USA* 97:9402–9407
- Wurmser AE, Sato TK, Emr SD (2000) New component of the vacuolar class C-Vps complex couples nucleotide exchange on the Ypt7 GTPase to SNARE-dependent docking and fusion. *J Cell Biol* 151:551–562
- Darsow T, Rieder SE, Emr SD (1997) A multispecificity syntaxin homologue, Vam3p, essential for autophagic

- and biosynthetic protein transport to the vacuole. *J Cell Biol* 138:517–529
28. Sato TK, Darsow T, Emr SD (1998) Vam7p, a SNAP-25-like molecule, and Vam3p, a syntaxin homolog, function together in yeast vacuolar protein trafficking. *Mol Cell Biol* 18:5308–5319
 29. Wang CW, Stromhaug PE, Shima J, Klionsky DJ (2002) The Ccz1-Mon1 protein complex is required for the late step of multiple vacuole delivery pathways. *J Biol Chem* 277:47917–47927
 30. Epple UD, Suriapranata I, Eskelinen EL, Thumm M (2001) Aut5/Cvt17p, a putative lipase essential for disintegration of autophagic bodies inside the vacuole. *J Bacteriol* 183:5942–5955
 31. Teter SA et al (2001) Degradation of lipid vesicles in the yeast vacuole requires function of Cvt17, a putative lipase. *J Biol Chem* 276:2083–2087
 32. Nakamura N, Matsuura A, Wada Y, Ohsumi Y (1997) Acidification of vacuoles is required for autophagic degradation in the yeast, *Saccharomyces cerevisiae*. *J Biochem* 121:338–344
 33. Suriapranata I et al (2000) The breakdown of autophagic vesicles inside the vacuole depends on Aut4p. *J Cell Sci* 113(Pt 22):4025–4033
 34. Tooze SA, Yoshimori T (2010) The origin of the autophagosomal membrane. *Nat Cell Biol* 12:831–835
 35. Bento CF et al (2016) Mammalian autophagy: how does it work? *Annu Rev Biochem* 85:685–713
 36. Yamamoto H et al (2012) Atg9 vesicles are an important membrane source during early steps of autophagosome formation. *J Cell Biol* 198:219–233
 37. Mizushima N, Yoshimori T, Levine B (2010) Methods in mammalian autophagy research. *Cell* 140:313–326
 38. Walczak M, Martens S (2013) Dissecting the role of the Atg12–Atg5–Atg16 complex during autophagosome formation. *Autophagy* 9:424–425
 39. Mizushima N et al (1998) A protein conjugation system essential for autophagy. *Nature* 395:395–398
 40. Tanida I, Ueno T, Kominami E (2004) LC3 conjugation system in mammalian autophagy. *Int J Biochem Cell Biol* 36:2503–2518
 41. Pankiv S et al (2007) p62/SQSTM1 binds directly to Atg8/LC3 to facilitate degradation of ubiquitinated protein aggregates by autophagy. *J Biol Chem* 282:24131–24145
 42. Itakura E, Kishi-Itakura C, Mizushima N (2012) The hairpin-type tail-anchored SNARE syntaxin 17 targets to autophagosomes for fusion with endosomes/lysosomes. *Cell* 151:1256–1269
 43. Jiang P et al (2014) The HOPS complex mediates autophagosome–lysosome fusion through interaction with syntaxin 17. *Mol Biol Cell* 25:1327–1337
 44. Yang Z, Klionsky DJ (2010) Mammalian autophagy: core molecular machinery and signaling regulation. *Curr Opin Cell Biol* 22:124–131
 45. He C, Klionsky DJ (2009) Regulation mechanisms and signaling pathways of autophagy. *Annu Rev Genet* 43:67–93
 46. Fullgrabe J, Klionsky DJ, Joseph B (2014) The return of the nucleus: transcriptional and epigenetic control of autophagy. *Nat Rev Mol Cell Biol* 15:65–74
 47. Settembre C et al (2011) TFEB links autophagy to lysosomal biogenesis. *Science* 332:1429–1433
 48. Chauhan S et al (2013) ZKSCAN3 is a master transcriptional repressor of autophagy. *Mol Cell* 50:16–28
 49. Li Y et al (2016) Protein kinase C controls lysosome biogenesis independently of mTORC1. *Nat Cell Biol* 18:1065–1077
 50. Wilkinson S, O'Prey J, Fricker M, Ryan KM (2009) Hypoxia-selective macroautophagy and cell survival signaled by autocrine PDGFR activity. *Genes Dev* 23:1283–1288
 51. Zhao Y et al (2010) Cytosolic FoxO1 is essential for the induction of autophagy and tumour suppressor activity. *Nat Cell Biol* 12:665–675
 52. Levine B, Abrams J (2008) p53: The Janus of autophagy? *Nat Cell Biol* 10:637–639
 53. Copetti T, Bertoli C, Dalla E, Demarchi F, Schneider C (2009) p65/RelA modulates BECN1 transcription and autophagy. *Mol Cell Biol* 29:2594–2608
 54. Bartholomew CR et al (2012) Ume6 transcription factor is part of a signaling cascade that regulates autophagy. *Proc Natl Acad Sci USA* 109:11206–11210
 55. Jin M et al (2014) Transcriptional regulation by Pho23 modulates the frequency of autophagosome formation. *Curr Biol* 24:1314–1322
 56. Bernard A et al (2015) Rph1/KDM4 mediates nutrient-limitation signaling that leads to the transcriptional induction of autophagy. *Curr Biol* 25:546–555
 57. Decressac M et al (2013) TFEB-mediated autophagy rescues midbrain dopamine neurons from alpha-synuclein toxicity. *Proc Natl Acad Sci USA* 110:E1817–E1826
 58. Tsunemi T et al (2012) PGC-1alpha rescues Huntington's disease proteotoxicity by preventing oxidative stress and promoting TFEB function. *Sci Transl Med* 4:142ra197
 59. Liang XH et al (1999) Induction of autophagy and inhibition of tumorigenesis by beclin 1. *Nature* 402:672–676
 60. Takamura A et al (2011) Autophagy-deficient mice develop multiple liver tumors. *Genes Dev* 25:795–800
 61. White E (2012) Deconvoluting the context-dependent role for autophagy in cancer. *Nat Rev Cancer* 12:401–410
 62. Guo JY et al (2013) Autophagy suppresses progression of K-ras-induced lung tumors to oncocytomas and maintains lipid homeostasis. *Genes Dev* 27:1447–1461
 63. Yang S et al (2011) Pancreatic cancers require autophagy for tumor growth. *Genes Dev* 25:717–729
 64. De Duve C, Wattiaux R (1966) Functions of lysosomes. *Annu Rev Physiol* 28:435–492
 65. Rikihisa Y (1984) Glycogen autophagosomes in polymorphonuclear leukocytes induced by rickettsiae. *Anat Rec* 208:319–327

66. Nakagawa I et al (2004) Autophagy defends cells against invading group A *Streptococcus*. *Science* 306:1037–1040
67. Gutierrez MG et al (2004) Autophagy is a defense mechanism inhibiting BCG and *Mycobacterium tuberculosis* survival in infected macrophages. *Cell* 119:753–766
68. Birmingham CL, Smith AC, Bakowski MA, Yoshimori T, Brumell JH (2006) Autophagy controls *Salmonella* infection in response to damage to the Salmonella-containing vacuole. *J Biol Chem* 281:11374–11383
69. Ogawa M et al (2005) Escape of intracellular Shigella from autophagy. *Science* 307:727–731
70. Levine B, Sodora DL (2006) HIV and CXCR4 in a kiss of autophagic death. *J Clin Invest* 116:2078–2080
71. Orvedahl A et al (2010) Autophagy protects against Sindbis virus infection of the central nervous system. *Cell Host Microbe* 7:115–127
72. Ling YM et al (2006) Vacuolar and plasma membrane stripping and autophagic elimination of *Toxoplasma gondii* in primed effector macrophages. *J Exp Med* 203:2063–2071
73. Friedrich N, Hagedorn M, Soldati-Favre D, Soldati T (2012) Prison break: pathogens' strategies to egress from host cells. *Microbiol Mol Biol Rev* 76:707–720
74. Rich KA, Burkett C, Webster P (2003) Cytoplasmic bacteria can be targets for autophagy. *Cell Microbiol* 5:455–468
75. Cemama M, Kim PK, Brumell JH (2011) The ubiquitin-binding adaptor proteins p62/SQSTM1 and NDP52 are recruited independently to bacteria-associated microdomains to target Salmonella to the autophagy pathway. *Autophagy* 7:341–345
76. Mostowy S et al (2010) Entrapment of intracytosolic bacteria by septin cage-like structures. *Cell Host Microbe* 8:433–444
77. Ogawa M et al (2011) A Tecpr1-dependent selective autophagy pathway targets bacterial pathogens. *Cell Host Microbe* 9:376–389
78. Mesquita FS et al (2012) The Salmonella deubiquitinase SseL inhibits selective autophagy of cytosolic aggregates. *PLoS Pathog* 8:e1002743
79. Tattoli I et al (2012) Amino acid starvation induced by invasive bacterial pathogens triggers an innate host defense program. *Cell Host Microbe* 11:563–575
80. Hampe J et al (2007) A genome-wide association scan of nonsynonymous SNPs identifies a susceptibility variant for Crohn disease in ATG16L1. *Nat Genet* 39:207–211
81. Massey DC, Parkes M (2007) Genome-wide association scanning highlights two autophagy genes, ATG16L1 and IRGM, as being significantly associated with Crohn's disease. *Autophagy* 3:649–651
82. Scolaro BL et al (2014) T300A genetic polymorphism: a susceptibility factor for Crohn's disease? *Arq Gastroenterol* 51:97–101
83. Xu Y et al (2007) Toll-like receptor 4 is a sensor for autophagy associated with innate immunity. *Immunity* 27:135–144
84. Negroni A et al (2016) NOD2 induces autophagy to control AIEC bacteria infectiveness in intestinal epithelial cells. *Inflamm Res* 65:803–813
85. Chauhan S, Mandell MA, Deretic V (2015) IRGM governs the core autophagy machinery to conduct antimicrobial defense. *Mol Cell* 58:507–521
86. Visvikis O et al (2014) Innate host defense requires TFEB-mediated transcription of cytoprotective and antimicrobial genes. *Immunity* 40:896–909
87. Lee HK et al (2010) In vivo requirement for Atg5 in antigen presentation by dendritic cells. *Immunity* 32:227–239
88. Dittmar AJ, Drozda AA, Blader IJ (2016) Drug repurposing screening identifies novel compounds that effectively inhibit toxoplasma gondii growth. *mSphere* 1:e00042-15
89. Shu CW, Liu PF, Huang CM (2012) High throughput screening for drug discovery of autophagy modulators. *Comb Chem High Throughput Screen* 15:721–729
90. Hipp MS, Park SH, Hartl FU (2014) Proteostasis impairment in protein-misfolding and -aggregation diseases. *Trends Cell Biol* 24:506–514
91. Nixon RA (2013) The role of autophagy in neurodegenerative disease. *Nat Med* 19:983–997
92. Hara T et al (2006) Suppression of basal autophagy in neural cells causes neurodegenerative disease in mice. *Nature* 441:885–889
93. Khurana V, Lindquist S (2010) Modelling neurodegeneration in *Saccharomyces cerevisiae*: why cook with baker's yeast? *Nat Rev Neurosci* 11:436–449
94. Rajasekhar K, Suresh SN, Manjithaya R, Govindaraju T (2015) Rationally designed peptidomimetic modulators of A β toxicity in Alzheimer's disease. *Sci Rep* 5:8139
95. Sarkar S et al (2007) Small molecules enhance autophagy and reduce toxicity in Huntington's disease models. *Nat Chem Biol* 3:331–338
96. Subramani S, Malhotra V (2013) Non-autophagic roles of autophagy-related proteins. *EMBO Rep* 14:143–151
97. Xie Z, Klionsky DJ (2007) Autophagosome formation: core machinery and adaptations. *Nat Cell Biol* 9:1102–1109
98. Mizushima N (2007) Autophagy: process and function. *Genes Dev* 21:2861–2873
99. Munz C (2014) Influenza A virus lures autophagic protein LC3 to budding sites. *Cell Host Microbe* 15:130–131
100. Beale R et al (2014) A LC3-interacting motif in the influenza A virus M2 protein is required to subvert autophagy and maintain virion stability. *Cell Host Microbe* 15:239–247
101. Kimmey JM et al (2015) Unique role for ATG5 in neutrophil-mediated immunopathology during *M. tuberculosis* infection. *Nature* 528:565–569

102. Mauthe M et al (2016) An siRNA screen for ATG protein depletion reveals the extent of the unconventional functions of the autophagy proteome in virus replication. *J Cell Biol* 214:619–635
103. Dreux M, Chisari FV (2011) Impact of the autophagy machinery on hepatitis C virus infection. *Viruses* 3:1342–1357
104. Hwang S et al (2012) Nondegradative role of Atg5–Atg12/Atg16L1 autophagy protein complex in antiviral activity of interferon gamma. *Cell Host Microbe* 11:397–409
105. Martinez J et al (2016) Noncanonical autophagy inhibits the autoinflammatory, lupus-like response to dying cells. *Nature* 533:115–119
106. Solvik T, Debnath J (2016) At the crossroads of autophagy and infection: noncanonical roles for ATG proteins in viral replication. *J Cell Biol* 214:503–505
107. Zhao Z et al (2007) Coronavirus replication does not require the autophagy gene ATG5. *Autophagy* 3:581–585
108. Reggiori F et al (2010) Coronaviruses Hijack the LC3-I-positive EDEMosomes, ER-derived vesicles exporting short-lived ERAD regulators, for replication. *Cell Host Microbe* 7:500–508
109. Bell TM, Field EJ, Narang HK (1971) Zika virus infection of the central nervous system of mice. *Arch Gesamte Virusforsch* 35:183–193
110. Jheng JR, Ho JY, Horng JT (2014) ER stress, autophagy, and RNA viruses. *Front Microbiol* 5:388
111. Hamel R et al (2015) Biology of Zika virus infection in human skin cells. *J Virol* 89:8880–8896
112. Harris J et al (2011) Autophagy controls IL-1beta secretion by targeting pro-IL-1 β for degradation. *J Biol Chem* 286:9587–9597
113. Zhang M, Kenny SJ, Ge L, Xu K, Schekman R (2015) Translocation of interleukin-1 β into a vesicle intermediate in autophagy-mediated secretion. *Elife* 4:e11205
114. Duran JM, Anjard C, Stefan C, Loomis WF, Malhotra V (2010) Unconventional secretion of Acb1 is mediated by autophagosomes. *J Cell Biol* 188:527–536
115. Malhotra V (2013) Unconventional protein secretion: an evolving mechanism. *EMBO J* 32:1660–1664
116. Manjithaya R, Subramani S (2010) Role of autophagy in unconventional protein secretion. *Autophagy* 6:650–651
117. Gee HY, Noh SH, Tang BL, Kim KH, Lee MG (2011) Rescue of Δ F508-CFTR trafficking via a GRASP-dependent unconventional secretion pathway. *Cell* 146:746–760
118. DeSelm CJ et al (2011) Autophagy proteins regulate the secretory component of osteoclastic bone resorption. *Dev Cell* 21:966–974
119. Ejlerskov P et al (2013) Tubulin polymerization-promoting protein (TPPP/p25 α) promotes unconventional secretion of α -synuclein through exophagy by impairing autophagosome–lysosome fusion. *J Biol Chem* 288:17313–17335
120. Son SM, Kang S, Choi H, Mook-Jung I (2015) Statins induce insulin-degrading enzyme secretion from astrocytes via an autophagy-based unconventional secretory pathway. *Mol Neurodegener* 10:56
121. Son SM et al (2016) Insulin-degrading enzyme secretion from astrocytes is mediated by an autophagy-based unconventional secretory pathway in Alzheimer disease. *Autophagy* 12:784–800
122. Nilsson P et al (2013) Abeta secretion and plaque formation depend on autophagy. *Cell Rep* 5:61–69
123. Ishibashi K, Uemura T, Waguri S, Fukuda M (2012) Atg16L1, an essential factor for canonical autophagy, participates in hormone secretion from PC12 cells independently of autophagic activity. *Mol Biol Cell* 23:3193–3202
124. Cabrera S, Marino G, Fernandez AF, Lopez-Otin C (2010) Autophagy, proteases and the sense of balance. *Autophagy* 6:961–963
125. Marino G et al (2010) Autophagy is essential for mouse sense of balance. *J Clin Invest* 120:2331–2344
126. Kitamura K et al (2012) Autophagy-related Atg8 localizes to the apicoplast of the human malaria parasite *Plasmodium falciparum*. *PLoS One* 7:e42977
127. Leveque MF et al (2015) Autophagy-related protein ATG8 has a noncanonical function for apicoplast inheritance in *Toxoplasma gondii*. *MBio* 6:e01446–15
128. Thornton GK, Woods CG (2009) Primary microcephaly: do all roads lead to Rome? *Trends Genet* 25:501–510
129. Marthiens V et al (2013) Centrosome amplification causes microcephaly. *Nat Cell Biol* 15:731–740
130. Simon AK, Clarke AJ (2016) Non-canonical autophagy LAPs lupus. *Cell Death Differ* 23:1267–1268
131. Martinez J et al (2015) Molecular characterization of LC3-associated phagocytosis reveals distinct roles for Rubicon, NOX2 and autophagy proteins. *Nat Cell Biol* 17:893–906
132. Takeshita F, Kobiyama K, Miyawaki A, Jounai N, Okuda K (2008) The non-canonical role of Atg family members as suppressors of innate antiviral immune signaling. *Autophagy* 4:67–69
133. Jounai N et al (2007) The Atg5 Atg12 conjugate associates with innate antiviral immune responses. *Proc Natl Acad Sci USA* 104:14050–14055
134. Deretic V (2012) Autophagy: an emerging immunological paradigm. *J Immunol* 189:15–20
135. Dupont N et al (2011) Autophagy-based unconventional secretory pathway for extracellular delivery of IL-1 β . *EMBO J* 30:4701–4711
136. Levine B, Mizushima N, Virgin HW (2011) Autophagy in immunity and inflammation. *Nature* 469:323–335
137. Shi CS et al (2012) Activation of autophagy by inflammatory signals limits IL-1beta production by targeting

- ubiquitinated inflammasomes for destruction. *Nat Immunol* 13:255–263
138. Zhou R, Yazdi AS, Menu P, Tschopp J (2011) A role for mitochondria in NLRP3 inflammasome activation. *Nature* 469:221–225
 139. Xavier RJ, Podolsky DK (2007) Unravelling the pathogenesis of inflammatory bowel disease. *Nature* 448:427–434
 140. Fujita N et al (2009) Differential involvement of Atg16L1 in Crohn disease and canonical autophagy: analysis of the organization of the Atg16L1 complex in fibroblasts. *J Biol Chem* 284:32602–32609
 141. Shibata M et al (2010) LC3, a microtubule-associated protein1A/B light chain3, is involved in cytoplasmic lipid droplet formation. *Biochem Biophys Res Commun* 393:274–279
 142. Velikkakath AK, Nishimura T, Oita E, Ishihara N, Mizushima N (2012) Mammalian Atg2 proteins are essential for autophagosome formation and important for regulation of size and distribution of lipid droplets. *Mol Biol Cell* 23:896–909
 143. Baerga R, Zhang Y, Chen PH, Goldman S, Jin S (2009) Targeted deletion of autophagy-related 5 (atg5) impairs adipogenesis in a cellular model and in mice. *Autophagy* 5:1118–1130
 144. Zhang Y et al (2009) Adipose-specific deletion of autophagy-related gene 7 (atg7) in mice reveals a role in adipogenesis. *Proc Natl Acad Sci USA* 106:19860–19865
 145. Malhotra R, Warne JP, Salas E, Xu AW, Debnath J (2015) Loss of Atg12, but not Atg5, in pro-opiomelanocortin neurons exacerbates diet-induced obesity. *Autophagy* 11:145–154
 146. Ma T et al (2015) Atg5-independent autophagy regulates mitochondrial clearance and is essential for iPSC reprogramming. *Nat Cell Biol* 17:1379–1387
 147. Tsujimoto Y, Shimizu S (2005) Another way to die: autophagic programmed cell death. *Cell Death Differ* 12(Suppl 2):1528–1534
 148. Kroemer G, Levine B (2008) Autophagic cell death: the story of a misnomer. *Nat Rev Mol Cell Biol* 9:1004–1010



Sarika Chinchwadkar is an IntPhD student doing her Masters thesis on novel genes involved in autophagy.



Sreedevi Padmanabhan is currently working as a SERB-National Post-Doctoral Fellow at the Autophagy Laboratory working on unconventional secretion.



Piyush Mishra did his M.Sc. in biomedical sciences from ACBR, Delhi University. Piyush is developing assays to study autophagy-related pathways and wants to apply them to discover new drugs (small molecules).



Sunaina Singh is an IntPhD student. Currently, she is working on the moonlighting functions of vesicular trafficking pathways in autophagy in yeast.



S. N. Suresh is an IntPhD student. His interests include studying neurodegenerative diseases using yeast as model organism.



Somya Vats is an IntPhD student interested in using small molecules as probes to understand autophagy flux.



Gaurav Barve completed his M.Sc. in microbiology from the Department of Microbiology, University of Pune. His interest lies in studying involvement of cytoskeletal elements in autophagy.



Veena Ammanathan is an IntPhD student studying xenophagy.



Dr. Ravi Manjithaya received his Ph.D. degree in posttranscriptional gene regulation from the Indian Institute of Science (Advisor: Prof. Rajan Dighe). He did his postdoctoral training in the autophagy-related pathways at the University of California, San Diego (Mentor: Prof. Suresh Subramani) before joining JNCASR as a Faculty Fellow in 2011. He was a Wellcome Trust-DBT Intermediate fellow (2011–16).

Dear Dr. Suresh,

As an editor-in-chief of BMB Reports,

I give you permission to reproduce the following article:

Therapeutic implication of autophagy in neurodegenerative diseases

Md. Ataur Rahman and Hyewhon Rhim

BMB Rep. Vol. 50, No. 7, pp. 345-354

The article including figures and contents will be reproduced in Suresh's article entitled Investigating mechanisms of aggrephagy flux using small molecules: Potential implications in neurodegeneration at JNCASR. However, you should rephrase contents of the article, not directly copy and paste from the article.

Sincerely,



Editor-in-Chief
BMB Reports

Korean Society for Biochemistry and Molecular Biology
BMB Reports
Room 801 The Korea Science and Technology Center
22, 7Gil Teheranro-ro, Gangnam-gu, Seoul 06130, Korea.
Tel: 82-2-508-7434~6, Fax: 82-2-508-7578
E-mail: bmbreports@bmbreports.org
Homepage: <http://submit.bmbreports.org>



KSBMB
Korean Society for Biochemistry and Molecular Biology